Ab-initio modeling of ultrafast demagnetization after laser irradiation in nickel, iron and cobalt

Von der Fakultät Mathematik und Physik der Universität Stuttgart
zur Erlangung der Würde eines Doktors der
Naturwissenschaften (Dr. rer. nat.) genehmigte Abhandlung

Vorgelegt von

Christian Michael Illg

aus Waiblingen

Hauptberichter:	Prof. Dr. Manfred Fähnle
Mitberichter:	Prof. Dr. Günter Wunner
Tag der mündlichen Prüfung:	17.12.2013

Max - Planck - Institut für Intelligente Systeme, Stuttgart

2013

Ehrenwörtliche Erklärung

Ich erkläre, dass ich diese Arbeit selbstständig verfasst und keine anderen als die angegebenen Quellen und Hilfsmittel benutzt habe.

Stuttgart, im September 2013

Christian Michael Illg

Contents

1 Introduction

1.1 Motivation and background

Computers consist of several technical parts. One important part is the hard disk drive which developed enormously in the last decades. A hard disk drive is a magnetic disk where the bits "0" and "1" are saved in magnetic regions. The magnetic regions are magnetized in two directions whereas one direction is interpreted as bit "0" and the other direction is interpreted as bit "1". A very small head which is an electromagnet can be positioned directly above any magnetic region and is able to change the direction of the bit by an electromagnetic field. Of course it is desirable to increase the data storage density by miniaturizing the components or to increase the write speed. From a researching point of view it is therefore interesting to study the miniaturization of components or to study new ways of manipulating a magnetization apart from applying an external magnetic field. The latter is addressed in this thesis.

It is known for a long time that a magnetization can be changed by an external magnetic field. Another way of changing the magnetization is the irradiation with a short laser pulse (without external magnetic field) which is the topic of the present thesis. One can distinguish two effects depending on the material and several other parameters: The first effect is called "ultrafast demagnetization" and the second is called "all-optical switching". The former is interesting for research, the latter is also interesting for application as non-volatile data storage. First of all I want to explain the ultrafast demagnetization.

In 1996 Beaurepaire and coworkers discovered for the first time that a thin ferromagnetic Ni film with in-plane magnetization can be demagnetized by about 40% within 1 ps after irradiating the Ni film with a short (60 fs) optical linearly polarized laser pulse [1]. Fig. 1.1 (a) shows schematically a laser pulse which is shot on a Ni film with in-plane magnetization (on a substrate) and fig. 1.1 (b) shows schematically the nor-

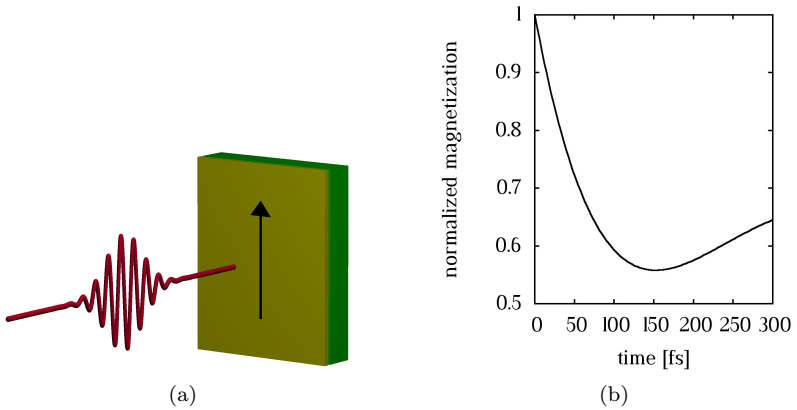

(a) (b)

Figure 1.1: (a) A fs optical laser pulse is shot on a thin Ni sample with in-plane magnetization (schematic). (b) Normalized magnetization as function of time (schematic).

malized magnetization as function of time. One can observe a sharp drop of the magnetization within some few hundreds of fs and thereafter a slow recovery. On a longer timescale (not shown in the figure) one would see that the magnetization recovers to its original value (before laser irradiation). In fact, there were earlier demagnetization experiments after laser pulse irradiation, see, e.g., ref. [2] for Ni in 1984 or refs. [3, 4] for Fe and Gd in 1991 and 1992, but these authors estimated a demagnetization time in the ns- and 100 ps-range, respectively. The novelty of the experiment by Beaurepaire and coworkers was the much faster timescale of about 1 ps which was the fastest manipulation of a magnetization so far known. Due to this fact they called this dynamics “ultrafast”.

There was a worldwide intensive research activity to study and explain the ultrafast demagnetization experiments. Until now the experiments could not be explained in every respect. An overview about current models and explanations is given in chapter 4.

The second above-mentioned effect is the so-called “all-optical switching” which was experimentally first shown by Stanciu and coworkers in 2007 [5]. A thin ferrimagnetic GdFeCo film with out-of-plane magneti-

zation was irradiated by a circularly polarized laser pulse. The authors showed that it is possible to switch the magnetization without magnetic field depending on the helicity of the laser pulse. The switching time is in the ps-range. The material composition and the laser parameters are crucial for the switching. Some years later it was shown by Radu et al. that it is even possible to switch the magnetization of a ferrimagnetic GdFeCo sample by linearly polarized light [6]. The underlying mechanisms for all-optical switching are currently a hot topic of research and could not be clarified yet.

The two effects, ultrafast demagnetization and all-optical switching, are related with each other but only the ultrafast demagnetization is discussed in this thesis. The studied materials in this thesis are Ni, Fe and Co but ultrafast demagnetization can also be observed for other materials, e.g., Gd [7].

1.2 Goal and organization of the thesis

Several mechanisms have been proposed to explain the ultrafast demagnetization experiments, see, e.g., ref. [8] for a review. A detailed discussion is given in chapter 4. A very promising candidate to explain the experiments is the scattering of electrons at phonons (which are the quantized oscillations of the atoms in a solid). The scope of this thesis is to examine by ab-initio methods and modeling whether the spin-flip electron-phonon scattering can explain the ultrafast demagnetization. Thereby the electronic states and the phononic states are calculated ab-initio. The electron-phonon scattering matrix elements are derived, calculated and implemented using the rigid-ion approximation. The transition rates are represented with Fermi's golden rule and Boltzmann rate equations. Finally, the relaxation time and demagnetization rate for Ni and Fe as well as the maximum possible demagnetization for Ni, Fe and Co are modeled and calculated within the Elliott-Yafet theory for ferromagnets. The results are discussed in comparison with experiments and other publications.

The thesis is organized as follows:

- In chapter 2 the basics are given. First, the density-functional theory and their implementation with the linear-muffin-tin-orbital method and with the pseudopotential method are explained. Second, some

important physical properties of Ni, Fe, Co and Al are given. Third, lattice dynamics is briefly introduced.

- In chapter 3 the phonon frequencies and polarization vectors are calculated on the one hand by using experimentally fitted force constants and on the other hand by using ab-initio force constants. Finally, the corresponding phonon frequencies and polarization vectors obtained by the two approaches are compared with each other.

- In chapter 4 the present knowledge about ultrafast demagnetization is presented. Both old and new publications are discussed. Some further contributions to the angular momentum conservation are made.

- The fundamental equations for calculating the relaxation time, the demagnetization rate and the maximum possible demagnetization within the Elliott-Yafet theory are derived in chapter 5 and are discussed critically. Thereby Fermi's golden rule and Boltzmann rate equations are used.

- The implementation of the equations given in chapter 5 is explained in chapter 6. The implementation uses the rigid-ion approximation, and the consequences of this approximation with respect to screening are discussed.

- The numerical results for the relaxation time, the demagnetization rate and the maximum possible demagnetization can finally be found in chapter 7. The results are shown for the ground-state atomic magnetic moment and reduced atomic magnetic moments and are compared with those of other publications.

- Chapter 8 summarizes the thesis in English and German.

1.3 Notation, symbols and units

The notation is usually explained in the text and if possible the standard notation is used. Here are some commonly used notations:

- Vectors are written in bold letters, e.g., $\mathbf{r}$.

- Tensors are twice underlined, e.g., $\underline{\underline{V}}$.
- Operators have a circumflex, e.g., $\widehat{H}$.
- Einstein's sum convention is not used. All sums are given in the equations.
- Dirac's bra- and ket-notation is used.

Some symbols are usually reserved and generally used in physics. I use the following symbols without explaining in the text:

- μ_B: Bohr's magneton
- $\hbar$: Planck's constant divided by 2π
- m_e: mass of the electron
- e: elementary charge
- V: volume
- $\mathbf{r}$: position vector
- $\mathbf{k}$: wavevector
- ε: energy
- ε_F: Fermi energy
- t: time
- $Z(\varepsilon)$: density of states
- occ.: occupied states
- BZ: first Brillouin zone

Rydberg units are used in the implementation of the density functional theory and therefore Rydberg units are used in this thesis. In the Rydberg unit system the following definitions are made: $\hbar \equiv 1$, $m_e \equiv \frac{1}{2}$, $e \equiv \sqrt{2}$. With these definitions all other units can be derived. Especially important are the following:

- length: 1 Ry-length unit = 0.52917725$\mathring{A}$ (Bohr's radius)
- energy: 1 Ry-energy unit = 1 Ry = 13.60569253 eV
- mass: 1 Ry-mass unit = $1.8218779 \cdot 10^{-30}$ kg
- time: 1 Ry-time unit = $4.8377687 \cdot 10^{-17}$s $\approx 1/20$ fs
- frequency: 1 Ry-frequency unit = $2.0670687 \cdot 10^{16}$ Hz

2 Basics

2.1 Density functional theory

There are several good and elaborate introductions to non-relativistic and relativistic density functional theory and its implementation. For reference I recommend the doctoral theses of Olaf Grotheer [9], Claude Ederer [10] and Bernd Meyer [11]. Nevertheless, a short introduction with the most important results is necessary because the density functional theory and its implementation with the linear-muffin-tin-orbital (LMTO) method and the pseudopotential method will be used later on in this thesis. All numerical calculations are obtained with the LMTO or the pseudopotential method. This section is very similar to the section 2.2 in my diploma thesis [12] which is a summary of the corresponding chapters in the theses of Grotheer [9] and Ederer [10]. The original references are not given here but can be found in the latter-mentioned theses.

The goal of the density functional theory is to determine the properties of the ground state of an interacting (non-relativistic or relativistic) electron system of N electrons. Electrons are identical and cannot be distinguished. The Schrödinger equation of the system reads

$$\widehat{H}\Psi(\mathbf{r}_1,...,\mathbf{r}_\mathrm{N}) = E\ \Psi(\mathbf{r}_1,...,\mathbf{r}_\mathrm{N}) \tag{2.1}$$

with the Hamiltonian $\widehat{H}$ of the system (in Born-Oppenheimer approximation)

$$\begin{aligned}\widehat{H} &= \widehat{T} + \widehat{U} + \widehat{W} \\ &= \underbrace{\sum_{n=1}^{N} \frac{-\hbar^2}{2m_e}\Delta_n \underline{\underline{1}}}_{\widehat{T}} + \underbrace{\frac{1}{2}\sum_{\substack{n,j=1\\ n\neq j}}^{N} \frac{e^2}{|\mathbf{r}_n - \mathbf{r}_j|}\underline{\underline{1}}}_{\widehat{U}} + \underbrace{\sum_{n=1}^{N}\left[\underline{\underline{\widehat{W}}}_{\mathrm{ext}}(\mathbf{r}_n) - \sum_{\mathbf{R}} \frac{Z_\mathbf{R} e^2}{|\mathbf{r}_n - \mathbf{R}|}\underline{\underline{1}}\right]}_{\widehat{W}}\end{aligned} \tag{2.2}$$

where $\widehat{T}$ is the kinetic energy of the electrons, $\widehat{U}$ is the mutual interaction energy of the electrons and $\widehat{W}$ is the potential matrix containing the external potential and the Coulomb interaction between nuclei and electrons ($\mathbf{r}_n$: coordinate of the electron with index n, $\mathbf{R}$: coordinate of the nucleus, $Z_{\mathbf{R}}$: atomic number). $\Psi(\mathbf{r}_1, ..., \mathbf{r}_\mathrm{N})$ is the many particle wavefunction.

In the theory of Kohn and Sham (see subsection 2.1.2) the problem of calculating the ground-state properties of the system of interacting electrons is reduced to the problem of calculating these properties via a hypothetical system of non-interacting electrons in an effective potential W_{eff}. With the respective single-electron wavefunctions $\psi_i(\mathbf{r}) = \begin{pmatrix} \psi_i^{\uparrow}(\mathbf{r}) \\ \psi_i^{\downarrow}(\mathbf{r}) \end{pmatrix}$ the spin-density matrix $\underline{\underline{\rho}}$ with components

$$\rho_{\alpha,\alpha'} = \sum_{\substack{i=1 \\ \mathrm{occ.}}}^{N} \psi_i^{\alpha}(\mathbf{r}) \left(\psi_i^{\alpha'}(\mathbf{r})\right)^* \qquad \text{with} \qquad \alpha = \uparrow, \downarrow \tag{2.3}$$

can be defined. It is useful to introduce the particle density as well

$$n(\mathbf{r}) = \sum_{\substack{i=1 \\ \mathrm{occ.}}}^{N} \left(|\psi_i^{\uparrow}(\mathbf{r})|^2 + |\psi_i^{\downarrow}(\mathbf{r})|^2 \right). \tag{2.4}$$

For details see ref. [9].

2.1.1 Theorems of Hohenberg and Kohn

First theorem of Hohenberg and Kohn

In principle, all properties of the ground state can be expressed as functionals of the ground state spin density matrix $\underline{\underline{\rho_0}}$.

One can prove that the ground state spin density matrix $\underline{\underline{\rho_0}}$ determines unambiguously (except for an unimportant additive constant) the expectation value $W(\mathbf{r}) = \langle\Psi|\widehat{W}|\Psi\rangle$, i. e., this expectation value is a unique functional of $\underline{\underline{\rho_0}}$: $W[\underline{\underline{\rho_0}}]$. Vice versa, $W[\underline{\underline{\rho_0}}]$ determines the Hamiltonian. Therefore the ground state wavefunction Ψ_0 (which can be determined by

minimizing the energy functional $E[\Psi] = \langle\Psi|\widehat{H}|\Psi\rangle$) is a unique functional of $\underline{\underline{\rho_0}}$: $\Psi_0[\underline{\underline{\rho_0}}]$. Using $\Psi_0[\underline{\underline{\rho_0}}]$ one can determine all properties by calculating $\langle\widehat{O}\rangle[\underline{\underline{\rho_0}}] = \langle\Psi_0[\underline{\underline{\rho_0}}]|\widehat{O}|\Psi_0[\underline{\underline{\rho_0}}]\rangle$ where $\widehat{O}$ is an arbitrary operator. This is in particular true for the ground state energy $E[\underline{\underline{\rho_0}}]$ or the expectation value of the kinetic energy $\langle\widehat{T}\rangle[\underline{\underline{\rho_0}}]$ or for the interaction energy of the electrons $\langle\widehat{U}\rangle[\underline{\underline{\rho_0}}]$. Hence the ground state properties are functionals of the ground state spin density matrix which simplifies the problem because $\underline{\underline{\rho_0}}(\mathbf{r})$ has only three variables compared to the wavefunction with $3N$ variables.

In the following the double underline of the spin density matrix is omitted.

Second theorem of Hohenberg and Kohn

We define the following functional of the spin density matrix ρ

$$F[\rho] \equiv \min\, \langle\Psi|\widehat{T}[\rho] + \widehat{U}[\rho]|\Psi\rangle. \tag{2.5}$$

The minimum is with respect to the wavefunction Ψ but for a given spin density matrix ρ only those wavefunctions are valid which build ρ. The functional of the total energy is

$$E[\rho] \equiv F[\rho] + \int \mathrm{tr}(\rho(\mathbf{r})W[\rho(\mathbf{r})])\ \mathrm{d}^3r. \tag{2.6}$$

For a given potential matrix W, minimizing eq. (2.6) *yields the ground state energy E_0 and the ground state spin density matrix ρ_0.*

If $F[\rho]$ was known, the problem was just a minimization problem for ρ which has three variables. With Ritz' variation principle one needs $3N$ variables to determine the ground state energy E_0.

2.1.2 Kohn-Sham equations

Kohn and Sham use a model system (subscript s) where N mutually non-interacting particles are in an effective potential (matrix) W_{eff}. The effective Schrödinger equation reads

$$\left[-\frac{\hbar^2}{2m_e}\Delta + W_{\mathrm{eff}}[\rho(\mathbf{r})]\right]\psi_i(\mathbf{r}) = \varepsilon_i\psi_i(\mathbf{r}). \tag{2.7}$$

The spin density matrix of the model system can be calculated according to eq. (2.3)

$$\rho_\mathrm{s}(\mathbf{r}) = \sum_{\substack{i=1 \\ \text{occ.}}}^{N} \psi_i(\mathbf{r})\psi_i^\dagger(\mathbf{r}) \tag{2.8}$$

and it is demanded that the spin density matrix of the model system equals the ground state spin density matrix of the original system, i. e., $\rho_\mathrm{s} = \rho_0$. For the original system an ansatz for the functional $E[\rho]$ of eq. (2.6) is used,

$$E[\rho] = T_\mathrm{s}[\rho] + E_\mathrm{H}[n] + E_\mathrm{xc}[\rho] + \int \mathrm{tr}(\rho(\mathbf{r})W[\rho(\mathbf{r})])\ \mathrm{d}^3r. \tag{2.9}$$

$T_\mathrm{s}[\rho]$ is the kinetic energy of the model system

$$T_\mathrm{s}[\rho] = \min\left(\sum_{\substack{i=1 \\ \text{occ.}}}^{N} \langle\psi_i| - \frac{\hbar^2}{2m_e}\Delta\underline{\underline{1}}\ |\psi_i\rangle\right), \tag{2.10}$$

$E_\mathrm{H}[n]$ is the Hartree energy

$$E_\mathrm{H}[n] = \frac{e^2}{2}\int\int \frac{n(\mathbf{r})n(\mathbf{r}')}{|\mathbf{r}-\mathbf{r}'|}\ \mathrm{d}^3r\ \mathrm{d}^3r' \tag{2.11}$$

and $E_\mathrm{xc}[\rho]$ contains by definition everything which has been "forgotten" in the other terms and is called exchange-correlation energy. The energy functional of the model system is simply

$$E_\mathrm{s}[\rho] = T_\mathrm{s}[\rho] + \int \mathrm{tr}(\rho(\mathbf{r})W_\mathrm{eff}[\rho(\mathbf{r})])\ \mathrm{d}^3r. \tag{2.12}$$

For ρ_0 the variation of eq. (2.9) and (2.12) (under the constraint of given number of electrons) has to vanish (second theorem of Hohenberg and Kohn) and therewith one obtains the effective potential

$$\begin{aligned} &W_\mathrm{eff}[\rho(\mathbf{r})] = W[\rho(\mathbf{r})] + V_\mathrm{H}(\mathbf{r})\ \underline{\underline{1}} + W_\mathrm{xc}(\mathbf{r}) \quad \text{with} \\ &V_\mathrm{H}(\mathbf{r}) = e^2\int \frac{n(\mathbf{r}')}{|\mathbf{r}-\mathbf{r}'|}\ \mathrm{d}^3r', \qquad W_\mathrm{xc}(\mathbf{r}) = \frac{\delta E_\mathrm{xc}}{\delta\rho(\mathbf{r})} = \begin{pmatrix} V_\mathrm{xc}^\uparrow(\mathbf{r}) & 0 \\ 0 & V_\mathrm{xc}^\downarrow(\mathbf{r}) \end{pmatrix} \end{aligned} \tag{2.13}$$

for collinear spin systems. The Kohn-Sham equations (2.7), (2.8) and (2.13) have to be solved self consistently, i. e., one has to find a correct effective potential $W_{\text{eff}}(\mathbf{r})$ to solve the effective Schrödinger equation for the wavefunctions ψ_i to get the corresponding spin density matrix ρ_{s}.

The question arises how to treat the exchange-correlation energy $E_{\text{xc}}[\rho]$. Since it should be rather small compared to the other terms, an approximation is reasonable. The local spin density approximation (LSDA) reads

$$E_{\text{xc}}[\rho] = \int n(\mathbf{r})\varepsilon_{\text{xc}}(\rho(\mathbf{r}))\ \mathrm{d}^3r, \tag{2.14}$$

i. e., the exchange-correlation energy density $\varepsilon_{\text{xc}}(\rho(\mathbf{r}))$ (exchange-correlation energy per electron) depends only on the local spin density matrix. The next idea is to replace the exchange-correlation energy density of an inhomogeneous electron gas with the known exchange-correlation energy density of a homogeneous (interacting) electron gas with the spin density matrix ρ. Hence the ansatz is quite good for slowly varying spin density matrices.

It is well known that the LSDA fails for fast varying spin density matrices and for strong correlations between electrons. Therefore, one can make a more suitable ansatz for this system, the generalized gradient approximation (GGA) [13]: The exchange-correlation energy density is not only a function of the spin-density matrix $\varepsilon_{\text{xc}}(\rho(\mathbf{r}))$ but also of the gradient of the spin-density matrix $\varepsilon_{\text{xc}}(\rho(\mathbf{r}), \nabla\rho(\mathbf{r}))$. Hence, it depends on the system which ansatz is appropriate.

After the solution of the Kohn-Sham equations the total energy can be calculated when the spin density matrix ρ_0 is inserted into eq. (2.9).

2.1.3 Density functional theory in solids

Now we do not consider only N electrons but a solid which shall be infinite in every dimension and which is lattice periodic. Then N is the number of electrons in the unit cell considered in the calculation and all quantities are related to the unit cell, in particular the energy. The symbol $\mathbf{R}$ denotes the coordinates of the nuclei in the unit cell and all other nuclei can be reached with the translational vector $\mathbf{T}$. The functional of the crystal energy which is the sum of the electronic energy $E[\rho]$ of eq. (2.9) and the

nucleus-nucleus interaction energy may be rewritten in the form [9]

$$E[\rho] = T_\mathrm{s}[\rho] + E_\mathrm{elstat}[n] + E_\mathrm{xc}[\rho] + \int \mathrm{tr}(\rho(\mathbf{r})W_\mathrm{ext})\ \mathrm{d}^3r \tag{2.15}$$

where E_elstat is composed of the electron energy and the nucleus energy in the total electrostatic potential ($V_\mathrm{H}[n]$, electron-nucleus interaction

$$E_\text{e-nuc} = -e^2 \sum_\mathbf{T} \sum_\mathbf{R} \frac{Z_\mathbf{R}}{|\mathbf{r} - \mathbf{R} - \mathbf{T}|} \tag{2.16}$$

and nucleus-nucleus interaction).

Furthermore all sums $\sum_{i=1}^{N} f(\varepsilon_i, \varepsilon_\mathrm{F}^0)$... have to be replaced by integrals over the Brillouin zone (BZ)

$$\sum_j \frac{1}{\Omega_\mathrm{BZ}} \int_\mathrm{BZ} f(\varepsilon_{j\mathbf{k}}, \varepsilon_\mathrm{F}^0)\ \ldots\ \mathrm{d}^3k. \tag{2.17}$$

f is the Fermi distribution function for temperature $T = 0$ K, ε_F^0 is the Fermi energy, j is the band index and Ω_BZ is the volume of the Brillouin zone. The task is often to calculate expectation values of an arbitrary operator $\widehat{O}$

$$\langle\widehat{O}\rangle = \sum_j \frac{1}{\Omega_\mathrm{BZ}} \int_\mathrm{BZ} f(\varepsilon_{j\mathbf{k}}, \varepsilon_\mathrm{F}^0)\ \langle\psi_{j\mathbf{k}}|\widehat{O}|\psi_{j\mathbf{k}}\rangle\ \mathrm{d}^3k. \tag{2.18}$$

Of course the k-points cannot be chosen continuously. Usually one has a finite k-grid with discrete k-points k_ν. Then the above equation (2.18) can be approximated by

$$\langle\widehat{O}\rangle = \sum_\nu \frac{\Omega_\nu}{\Omega_\mathrm{BZ}} \sum_j \widetilde{f}(\varepsilon_{j\mathbf{k}_\nu}, \varepsilon_\mathrm{F}^0)\ \langle\psi_{j\mathbf{k}_\nu}|\widehat{O}|\psi_{j\mathbf{k}_\nu}\rangle \tag{2.19}$$

where $\widetilde{f}(\varepsilon_{j\mathbf{k}_\nu}, \varepsilon_\mathrm{F}^0)$ is the smeared Fermi distribution function (Gaussian or Fermi-Dirac smearing) and $\Omega_\nu/\Omega_\mathrm{BZ}$ represents the weight of the wavevector $\mathbf{k}_\nu$ [9].

2.1.4 The linear-muffin-tin-orbital (LMTO) method and the atomic-sphere approximation (ASA)

The basic task is to solve the Kohn-Sham equation (2.7)

$$\left[\underbrace{-\frac{\hbar^2}{2m_e}\Delta + W_{\text{eff}}[\rho(\mathbf{r})]}_{\widehat{H}} - \varepsilon_{j\mathbf{k}}\right] \psi_{j\mathbf{k}}(\mathbf{r}) = 0 \tag{2.20}$$

where $\psi_{j\mathbf{k}}$ is the one electron Bloch wavefunction. The natural approach is to expand $\psi_{j\mathbf{k}}(\mathbf{r})$ in some complete basis

$$|\psi_{j\mathbf{k}}(\mathbf{r})\rangle = \sum_{\beta} b_{\beta}^{j\mathbf{k}} |B_{\beta}^{\mathbf{k}}\rangle \tag{2.21}$$

where $b_{\beta}^{j\mathbf{k}}$ are the expansion coefficients and $|B_{\beta}^{\mathbf{k}}\rangle$ are the basis functions which have to satisfy Bloch's theorem[1]. Then we end up with an eigenvalue equation

$$\sum_{\beta} \left(\langle B_{\gamma}^{\mathbf{k}} | \widehat{H} | B_{\beta}^{\mathbf{k}} \rangle - \varepsilon_{j\mathbf{k}} \langle B_{\gamma}^{\mathbf{k}} | B_{\beta}^{\mathbf{k}} \rangle \right) b_{\beta}^{j\mathbf{k}} = 0 \tag{2.22}$$

where $\langle B_{\gamma}^{\mathbf{k}} | \widehat{H} | B_{\beta}^{\mathbf{k}} \rangle$ is called Hamiltonian matrix and $\langle B_{\gamma}^{\mathbf{k}} | B_{\beta}^{\mathbf{k}} \rangle$ is called overlap matrix. In the LMTO method the basis functions are linear combinations of local orbitals $|B_{\beta}^{\mathbf{k}}\rangle = \sum_{\mathbf{T}} \exp(i\mathbf{k}\mathbf{T})\, |B_{\beta}(\mathbf{r}_{\mathbf{R}} - \mathbf{T})\rangle$ with $\mathbf{r}_{\mathbf{R}} = \mathbf{r} - \mathbf{R}$. One uses basis functions that are almost crystal wavefunctions. On the one hand only few of them are needed but on the other hand they (and therefore all matrix elements) are quite complicated.

In the muffin-tin construction the real crystal is partitioned into spheres around the nuclei that do not overlap and into interstitial regions. The potential is assumed to be spherically symmetric inside the sphere and constant outside. This approximation is quite good for the bulk. The solution of eq. (2.20) outside the spheres are the plane waves (linear augmented plane waves (LAPW) method) or the Hankel functions (LMTO

[1] Actually, the notation $|\psi_{j\mathbf{k}}(\mathbf{r})\rangle$ is not good because the ket denotes a state and $\psi_{j\mathbf{k}}(\mathbf{r})$ denotes already a representation in a specific basis but I use the notation anyway.

method). Inside the sphere the solutions can be written as atomic functions $|\Phi_{\mathbf{R}lms}(\mathbf{r})\rangle$ which are only defined inside the corresponding sphere

$$|\Phi_{\mathbf{R}lm\alpha}(\mathbf{r})\rangle = \phi_{\mathbf{R}l\alpha}(r_{\mathbf{R}}) Z_{lm}(\widehat{\mathbf{r}}_{\mathbf{R}}) |\chi_{\mathbf{R}\alpha}\rangle \tag{2.23}$$

where $\mathbf{R}$ is the center of the sphere, l, m and α are the angular momentum, magnetic and spin quantum numbers, $r_{\mathbf{R}} = |\mathbf{r} - \mathbf{R}|$, $\widehat{\mathbf{r}}_{\mathbf{R}} = (\mathbf{r} - \mathbf{R})/r_{\mathbf{R}}$, $\phi_{\mathbf{R}l\alpha}$ is the radial function calculated for the (not yet known) energy $\varepsilon_{j\mathbf{k}}$, Z_{lm} are the cubic harmonics and

$$|\chi_{\mathbf{R}\uparrow}\rangle = \begin{pmatrix} 1 \\ 0 \end{pmatrix}, \quad |\chi_{\mathbf{R}\downarrow}\rangle = \begin{pmatrix} 0 \\ 1 \end{pmatrix} \tag{2.24}$$

are the spin eigenfunctions. The atomic functions are normalized and orthogonal: $\langle \Phi_{\mathbf{R}lm\alpha} | \Phi_{\mathbf{R}'l'm'\alpha'} \rangle = \delta_{\mathbf{R}\mathbf{R}'} \delta_{ll'} \delta_{mm'} \delta_{\alpha\alpha'}$. The solution in the sphere ("head" of the "muffin tin orbital") can be continuously and continuously differentiably connected to the solution in the interstitial regime ("tail" of the "muffin tin orbital"). To construct basis functions which make the calculation of the matrix elements as simple as possible, both the head and the tail of the muffin tin orbital are modified. Thereby the energy derivatives $\dot{\Phi}_{\mathbf{R}lm\alpha}(\mathbf{r})$ of the atomic functions play a central role, for which $\langle \Phi_{\mathbf{R}lm\alpha}(\mathbf{r}) | \dot{\Phi}_{\mathbf{R}'l'm'\alpha'}(\mathbf{r}) \rangle = 0$.

Furthermore, the atomic functions are not evaluated at the not yet known energy $\varepsilon_{j\mathbf{k}}$, but at a fixed and suitably defined energy $\varepsilon_{\mathbf{R}l\alpha}$. The consequence is that the eigenvalue problem defined by eq. (2.22) becomes a linear eigenvalue problem, and therefore the so-constructed basis orbitals are called "linear muffin tin orbitals". Finally, the atomic-sphere approximation is often used. In this approximation the spheres in the unit cell are blown up so that they overlap and that the sum of the volumes of all spheres is equal to the volume of the unit cell, and the contributions of remaining interstitial regimes to the matrix elements are neglected. Altogether, after the solution of eq. (2.22) the representation of the crystal wavefunction $\psi_{j\mathbf{k}}(\mathbf{r})$ in terms of linear muffin tin orbitals may be written in the form (for details see [9])

$$\begin{aligned} |\psi_{j\mathbf{k}}(\mathbf{r})\rangle = & \frac{1}{\sqrt{\widetilde{N}}} \sum_{\mathbf{T}} \exp(i\mathbf{k}\mathbf{T}) \cdot \\ & \left[\sum_{\mathbf{R}lm\alpha} c^{j\mathbf{k}}_{\mathbf{R}lm\alpha} |\Phi_{(\mathbf{R}+\mathbf{T})lm\alpha}(\mathbf{r})\rangle + d^{j\mathbf{k}}_{\mathbf{R}lm\alpha} |\dot{\Phi}_{(\mathbf{R}+\mathbf{T})lm\alpha}(\mathbf{r})\rangle \right]. \end{aligned} \tag{2.25}$$

In eq. (2.25) the quantities $\mathbf{T}$ denote the translation vectors of the unit cell of the crystal, the vectors $\mathbf{R}$ denote the positions of the basis atoms in the unit cell and $\widetilde{N}$ is the number of elementary unit cells in the considered unit cell of the calculation (the calculation in an infinitely large solid is reduced to a calculation in a supercell or in a unit cell). The expansion coefficients $c^{j\mathbf{k}}_{\mathbf{R}lm\alpha}$ and $d^{j\mathbf{k}}_{\mathbf{R}lm\alpha}$ are determined by the coefficients $b^{j\mathbf{k}}_{\mathbf{R}lm\alpha}$ via eq. (2.22), and by the requirement that the head and tail parts of the linear muffin tin orbital are connected to the original tail function (the Hankel function) in a continuous and continuously differentiable manner.

Please note that in atomic-sphere approximation matrix elements reduce to the integrals over the spheres

$$\langle \psi_{j'\mathbf{k}'} | \widehat{O} | \psi_{j\mathbf{k}} \rangle = \sum_{\mathbf{R}} \int_{\text{sphere}} \psi^*_{j'\mathbf{k}'}(\mathbf{r})\ \widehat{O}(\mathbf{r})\ \psi_{j\mathbf{k}}(\mathbf{r})\ \mathrm{d}^3 r. \tag{2.26}$$

Therefore the ASA simplifies and accelerates the calculations. This approximation is reasonable for close-packed structures.

2.1.5 Relativistic density functional theory

The spin-orbit coupling which is a relativistic effect is indispensable for a correct treatment. In the non-relativistic density functional theory it turned out that the spin density or the particle density is the central variable. For the relativistic case the four-vector of current density is the central variable [10]. Therefore the relativistic density functional theory is called "current-density-functional-theory".

Similarly to the non-relativistic case one can find the generalization of the theorems of Hohenberg and Kohn in the relativistic case. A further generalization of the Kohn-Sham equations can be derived as well and the derivation is more or less analogous to the non-relativistic case. The difficult part is to find a functional for the exchange-correlation energy. In the present thesis therefore the "spin-only approximation" is adopted where the contribution of orbital currents to the total current density is neglected and only the spin current density is taken into account, and where the conventional local-spin-density approximation is used for the spin-only exchange correlation energy. Finally, one ends up with the one-particle Dirac equation with an effective potential V_{eff} and an effective magnetic field B_{eff} that only affects the spins of the electrons. Let the

effective potential and magnetic field be spherically symmetric with respect to a center and let the effective magnetic field be collinear and in z-direction. The one-particle Dirac equation then reads

$$\underbrace{\left(c\sum_i \underline{\underline{\alpha}}_i \widehat{p}_i + (\underline{\underline{\beta}} - \underline{\underline{1}})m_e c^2 + V_{\text{eff}}(r)\underline{\underline{1}} + \mu_{\text{B}}\underline{\underline{\beta}} \begin{pmatrix} \underline{\underline{\sigma_z}} & 0 \\ 0 & \underline{\underline{\sigma_z}} \end{pmatrix} B_{\text{eff},z}(r) \right)}_{\widehat{H}_{\text{Dirac}}} \psi(\mathbf{r})$$

$$= \varepsilon\psi(\mathbf{r}) \tag{2.27}$$

with

$$V_{\text{eff}}(r) = V_{\text{ext}} + V_{\text{H}}(r) + V_{\text{xc}}(r), \quad B_{\text{eff},z} = B_{\text{ext},z} + B_{\text{xc},z} \tag{2.28}$$

where $\underline{\underline{\alpha}}$ and $\underline{\underline{\beta}}$ are the α- and β-matrices of the Dirac theory, $\widehat{p}_i$ is the i-th component of the momentum operator, $\underline{\underline{\widehat{\sigma}}}_z$ is the third Pauli matrix and $\varepsilon = E - m_e c^2$ is the energy without rest mass. ψ is a four-vector with a large component $\underline{\Phi}$ and a small component $\underline{\varphi}$: $\psi = \begin{pmatrix} \underline{\Phi} \\ \underline{\varphi} \end{pmatrix}$. For simplification the indices "eff" and "eff,z" are omitted in the following.

The Dirac equation is not easy to solve because of the spin-polarized potential ($B(r) \neq 0$). Instead of an exact solution the scalar-relativistic approximation is used, i. e., one tries to solve the Dirac equation approximately with use of the angular momentum eigenfunctions $|l,\ m_l,\ s = 1/2,\ m_s = \alpha/2\rangle$ (with $\alpha = \pm 1$) to the operators $\widehat{\mathbf{L}}^2, \widehat{L}_z, \widehat{\mathbf{S}}^2, \widehat{S}_z$. This is advantageous in many respects but it is only an approximation. It turns out that the scalar-relativistic approximation includes all relativistic effects except for the spin-orbit coupling. In the LMTO program the valence electrons are treated scalar-relativistically in the atomic calculation but the spin-orbit coupling is considered in the band calculation so that it is included in part implicitly in the atomic calculation [10]. The differences between a fully relativistic treatment and a scalar-relativistic treatment for the valence electrons are negligible. The core electrons are treated fully relativistically. The atomic function (see eq. (2.23)) and the energy derivative in scalar-relativistic representation are

$|\Phi_{\mathbf{R}lm\alpha}(\mathbf{r})\rangle =$

$$\begin{pmatrix} \phi_{\mathbf{R}l\alpha}(r_{\mathbf{R}}) Z_{lm}(\widehat{r}_{\mathbf{R}})|\chi_{\mathbf{R}\alpha}\rangle \\ i\underline{\underline{\widehat{\sigma}}}_{r_{\mathbf{R}}} \left(-\gamma_{\mathbf{R}l\alpha}(r_{\mathbf{R}}) + \frac{\phi_{\mathbf{R}l\alpha}(r_{\mathbf{R}})}{2M_{\mathbf{R}l\alpha}(r_{\mathbf{R}})cr_{\mathbf{R}}} \sum_i \underline{\underline{\widehat{\sigma}}}_{\mathbf{R}i} \widehat{L}_{\mathbf{R}i}\right) Z_{lm}(\widehat{r}_{\mathbf{R}})|\chi_{\mathbf{R}\alpha}\rangle \end{pmatrix} \tag{2.29}$$

and

$$|\dot{\Phi}_{\mathbf{R}lm\alpha}(\mathbf{r})\rangle = \begin{pmatrix} \dot{\phi}_{\mathbf{R}l\alpha}(r_{\mathbf{R}}) Z_{lm}(\widehat{r}_{\mathbf{R}})|\chi_{\mathbf{R}\alpha}\rangle \\ i\underline{\underline{\widehat{\sigma}}}_{r_{\mathbf{R}}} \left(-\dot{\gamma}_{\mathbf{R}l\alpha}(r_{\mathbf{R}}) + \frac{\dot{\phi}_{\mathbf{R}l\alpha}(r_{\mathbf{R}})}{2M_{\mathbf{R}l\alpha}(r_{\mathbf{R}})cr_{\mathbf{R}}} \sum_i \underline{\underline{\widehat{\sigma}}}_{\mathbf{R}i} \widehat{L}_{\mathbf{R}i}\right) Z_{lm}(\widehat{r}_{\mathbf{R}})|\chi_{\mathbf{R}\alpha}\rangle \end{pmatrix}, \tag{2.30}$$

respectively[2]. $\phi_{\mathbf{R}l\alpha}(r_{\mathbf{R}})$ and $\gamma_{\mathbf{R}l\alpha}(r_{\mathbf{R}})$ are the radial functions of the large and small components and have to satisfy some equations [10]. $\underline{\underline{\widehat{\sigma}}}_{r_{\mathbf{R}}} = \frac{1}{r_{\mathbf{R}}} \sum_i r_{\mathbf{R}i} \underline{\underline{\widehat{\sigma}}}_i$ is the radial Pauli matrix, $M_{\mathbf{R}l\alpha}(r_{\mathbf{R}}) = m_e + \frac{1}{2c^2}(\varepsilon_{\mathbf{R}l\alpha} - V^{\alpha}(r_{\mathbf{R}}))$ is the generalized relativistic mass with $V^{\alpha}(r_{\mathbf{R}}) = V(r_{\mathbf{R}}) + \alpha\mu_{\mathrm{B}}B(r_{\mathbf{R}})$ ($\alpha = 1$ for spin-up and $\alpha = -1$ for spin-down), and the energy dependence of $M_{\mathbf{R}l\alpha}(r_{\mathbf{R}})$ is neglected for the energy derivative. $\widehat{L}_{\mathbf{R}i}$ is the i-th component of the angular momentum operator. The scalar-relativistic wavefunction $\Phi_{\mathbf{R}lm\alpha}$ and energy derivative $\dot{\Phi}_{\mathbf{R}lm\alpha}$ are not orthonormal (in contrast to the non-relativistic case)!

According to ref. [10] the result of the application of the Dirac Hamiltonian on the atomic wavefunction is

$$\widehat{H}_{Dirac}|\Phi_{\mathbf{R}lm\alpha}\rangle = \varepsilon_{\mathbf{R}l\alpha}|\Phi_{\mathbf{R}lm\alpha}\rangle + \widehat{H}^{SOC}_{Dirac}|\Phi_{\mathbf{R}lm\alpha}\rangle. \tag{2.31}$$

If the term proportional to $B(r)$ is neglected in the small component, the spin-orbit coupling part reads

$$\widehat{H}^{SOC}_{Dirac}|\Phi_{\mathbf{R}lm\alpha}\rangle = \begin{pmatrix} \frac{\hbar}{4M^2_{\mathbf{R}l\alpha}(r_{\mathbf{R}})c^2 r_{\mathbf{R}}} \frac{dV^{\alpha}(r_{\mathbf{R}})}{dr_{\mathbf{R}}} \phi_{\mathbf{R}l\alpha}(r_{\mathbf{R}}) \sum_i \widehat{L}_{\mathbf{R}i} \underline{\underline{\widehat{\sigma}}}_{\mathbf{R}i} Z_{lm}(\widehat{r}_{\mathbf{R}})|\chi_{\mathbf{R}\alpha}\rangle \\ 0 \end{pmatrix}. \tag{2.32}$$

It is added in eq. (2.31) since $\Phi_{\mathbf{R}lm\alpha}$ is not an exact solution of the Dirac equation. If a Hermitian form of the spin-orbit part is needed

[2] Actually, the notation $|\Phi_{\mathbf{R}lm\alpha}(\mathbf{r})\rangle$ is not good because the ket denotes a state and $\Phi_{\mathbf{R}lm\alpha}(\mathbf{r})$ denotes already a representation in a specific basis but I use the notation anyway.

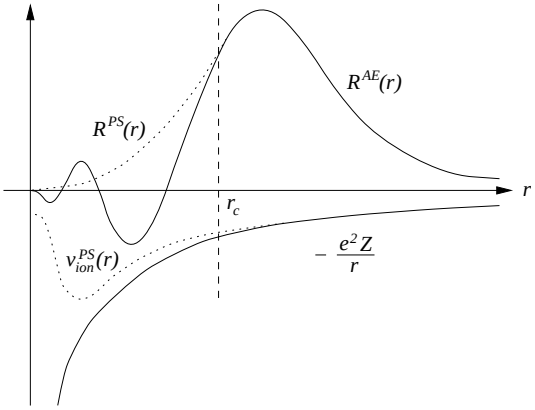

Figure 2.1: All-electron potential $-e^2Z/r$ and the corresponding radial wavefunction $R^{AE}(r)$ (solid lines) in comparison with the pseudopotential $v_{ion}^{PS}(r)$ and the corresponding radial wavefunction $R^{PS}(r)$ (dashed lines). From ref. [11]. Copyright by the Cuvillier publishing company, Göttingen.

(this is the case for the Hamiltonian matrix in the relativistic LMTO program), one replaces V^α and $M_{\mathbf{R}l\alpha}$ by $V^{\alpha\alpha'} = \frac{1}{2}(V^\alpha + V^{\alpha'})$ and $M_{\mathbf{R}l\alpha,\mathbf{R}'l'\alpha'} = \frac{1}{2}(M_{\mathbf{R}l\alpha} + M_{\mathbf{R}'l'\alpha'})$ [10]. There is no need to distinguish between a definition with respect to a local or global spin quantization axis because only collinear systems are considered in this thesis ($\widehat{L}_{\mathbf{R}i} = \widehat{L}_i$, $\underline{\widehat{\sigma}}_{\mathbf{R}i} = \underline{\widehat{\sigma}}_i$).

2.1.6 Pseudopotential method and the PWscf code

In the previous subsections the LMTO method for the solution of the Kohn-Sham equations is explained. The advantage of the LMTO method is that the basis functions in eq. (2.21) are almost crystal wavefunctions. The disadvantage is that the basis functions are very complicated and therefore also the calculation of matrix elements is complicated. It would be nice to make an expansion with easier basis functions.

Plane waves are easy lattice-periodic basis functions but in general it is not possible to expand the crystal wavefunction in plane waves because of the strong oscillation near the cores (almost infinitely many plane waves

would be required). The pseudopotential method avoids the problem. It is explained very briefly in the following (based on ref. [11]):

One can subdivide the crystal into two types of electrons: the core electrons and the valence electrons. The valence electrons are important for the physical and chemical properties of a crystal whereas the core electrons are usually less interesting. In the pseudopotential method it is assumed that the core electrons do not change much and are more or less "frozen" (frozen-core approximation). The ground state density of a free atom is taken for the core electrons. Thus one solves the Kohn-Sham equations *only for the valence electrons* in the effective potential (core potential and core-electrons potential). This is a big simplification.

In order to make an expansion in plane waves possible one replaces the potential which an electron feels ($-e^2Z/r$ in fig. 2.1) with a pseudopotential ($v_{ion}^{PS}(r)$ in fig. 2.1). Thereby the pseudopotential is constructed in such a way that the wavefunction of the potential ($R^{AE}(r)$ in fig. 2.1) and the wavefunction of the pseudopotential ($R^{PS}(r)$ in fig. 2.1) are the same if the radius is larger than the cut-off radius $r > r_c$ and that $R^{PS}(r)$ is a smooth function, and that the energy eigenvalues are the same as in the all-electron (AE) calculation. Now, it is possible to expand $R^{PS}(r)$ in a small number of plane waves. One can show that a lot of physical and chemical properties can be calculated correctly with the pseudopotential method because of the correct description of the wavefunction for $r > r_c$.

The construction of the pseudopotential is not unique. Several methods exist. A very famous one is the ultrasoft pseudopotential method by Vanderbilt [14]. The ultrasoft pseudopotential is constructed to be even smoother (than the pseudopotential of former pseudopotential methods) and also the pseudopotential wavefunctions are even smoother (than the pseudopotential wavefunctions of former pseudopotential methods) which has the advantage that an even smaller amount of plane waves are needed for the expansion.

This is only the basic idea of the pseudopotential method sufficient for the purposes of this thesis. Details can be found in ref. [11].

A popular implementation of the ultrasoft pseudopotential method is the open-source plane-wave self-consistent-field (PWscf) code called Quantum ESPRESSO [15]. It is used to calculate the force constants in chapter 3.

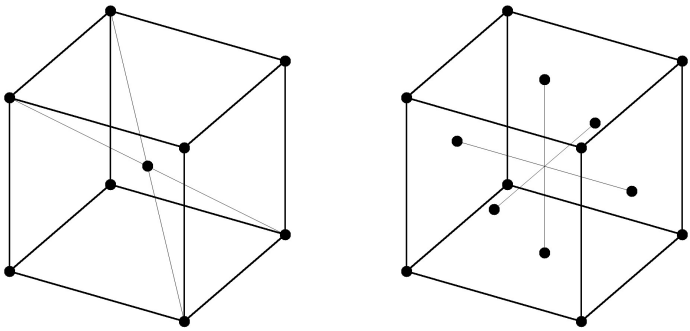

(a) bcc (b) fcc

Figure 2.2: Conventional unit cell for the bcc and fcc crystal structure.

2.2 Properties of Fe, Co, Ni and Al

The ultrafast demagnetization can be observed in elemental ferromagnets like Fe, Ni, Co, Gd and also in ferromagnetic alloys like $Co_{0.5}Pd_{0.5}$ [16, 17]. The fastest demagnetization can be observed in Fe, Co and Ni for which numerical calculations are presented in chapter 7. Gd or other materials are not a topic of this thesis.

Al is not interesting in the context of ultrafast demagnetization because it is not ferromagnetic but Al is used for a comparison of the results of different force-constant models for the materials Fe, Ni and Al.

The following subsections give some basic properties about Fe, Co, Ni and Al.

2.2.1 Physical properties

The lattice structure of the materials is body-centered cubic (bcc) for Fe and face-centered cubic (fcc) for both Ni and Al. The lattice structure of Co is hexagonal-close packed (hcp), however, in the ultrafast demagnetization experiments Co on MgO is used [18] where the Co film has an fcc structure. Fig. 2.2 shows the conventional unit cell of the bcc and the fcc crystal structure. The primitive lattice vectors for the bcc and the fcc

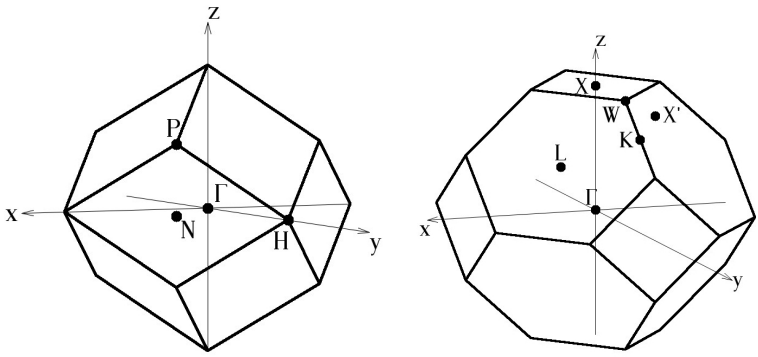

(a) bcc (b) fcc

Figure 2.3: Brillouin zones and special points in the Brillouin zone

structure read (a: lattice constant)

$$\mathbf{a}_1^{\text{bcc}} = \frac{a}{2}\begin{pmatrix} -1 \\ 1 \\ 1 \end{pmatrix}, \quad \mathbf{a}_2^{\text{bcc}} = \frac{a}{2}\begin{pmatrix} 1 \\ -1 \\ 1 \end{pmatrix}, \quad \mathbf{a}_3^{\text{bcc}} = \frac{a}{2}\begin{pmatrix} 1 \\ 1 \\ -1 \end{pmatrix}$$

$$\mathbf{a}_1^{\text{fcc}} = \frac{a}{2}\begin{pmatrix} 0 \\ 1 \\ 1 \end{pmatrix}, \quad \mathbf{a}_2^{\text{fcc}} = \frac{a}{2}\begin{pmatrix} 1 \\ 0 \\ 1 \end{pmatrix}, \quad \mathbf{a}_3^{\text{fcc}} = \frac{a}{2}\begin{pmatrix} 1 \\ 1 \\ 0 \end{pmatrix}. \tag{2.33}$$

Fig. 2.3 shows the bcc and the fcc Brillouin zone (BZ) with special points. The reciprocal lattice vectors read

$$\mathbf{b}_1^{\text{bcc}} = \frac{2\pi}{a}\begin{pmatrix} 0 \\ 1 \\ 1 \end{pmatrix}, \quad \mathbf{b}_2^{\text{bcc}} = \frac{2\pi}{a}\begin{pmatrix} 1 \\ 0 \\ 1 \end{pmatrix}, \quad \mathbf{b}_3^{\text{bcc}} = \frac{2\pi}{a}\begin{pmatrix} 1 \\ 1 \\ 0 \end{pmatrix}$$

$$\mathbf{b}_1^{\text{fcc}} = \frac{2\pi}{a}\begin{pmatrix} -1 \\ 1 \\ 1 \end{pmatrix}, \quad \mathbf{b}_2^{\text{fcc}} = \frac{2\pi}{a}\begin{pmatrix} 1 \\ -1 \\ 1 \end{pmatrix}, \quad \mathbf{b}_3^{\text{fcc}} = \frac{2\pi}{a}\begin{pmatrix} 1 \\ 1 \\ -1 \end{pmatrix}. \tag{2.34}$$

The special points in the bcc BZ have the coordinates:

$$\Gamma = \frac{2\pi}{a}(0,0,0), \quad H = \frac{2\pi}{a}(0,1,0), \quad N = \frac{2\pi}{a}(0.5,0.5,0),$$

$$P = \frac{2\pi}{a}(0.5, 0.5, 0.5). \tag{2.35}$$

The special points in the fcc BZ have the coordinates:

$$\begin{aligned} &\Gamma = \frac{2\pi}{a}(0,0,0), \quad X = \frac{2\pi}{a}(0,0,1), \quad X' = \frac{2\pi}{a}(0,1,1), \\ &L = \frac{2\pi}{a}(0.5,0.5,0.5), \quad W = \frac{2\pi}{a}(0,0.5,1), \quad K = \frac{2\pi}{a}(0,0.75,0.75). \end{aligned} \tag{2.36}$$

Table 2.1 gives the most important properties which are necessary for the numerical calculations.

	Al	**Fe**	**Co**	**Ni**
atomic number	13	26	27	28
group	IIIa / 13	VIIIb / 8	VIIIb / 9	VIIIb / 10
configuration	[Ne]$3s^2 3p^1$	[Ar]$3d^6 4s^2$	[Ar]$3d^7 4s^2$	[Ar]$3d^8 4s^2$
affiliation	metal	3d transition metal		
crystal structure	fcc	bcc	fcc*	fcc
latt.const. (RT)	4.050 $\mathring{A}$	2.870$\mathring{A}$	3.544$\mathring{A}$*	3.5200$\mathring{A}$
latt.const. (0K)	4.032 $\mathring{A}$	2.860$\mathring{A}$	-	3.5155$\mathring{A}$
magnetism (RT)	paramag.	ferromagnetic		
Curie temp.	-	1043 K	1388 K	627 K
easy axis (RT)	-	[001]	[111]*	[111]

Table 2.1: Important properties at room temperature (RT) of Al, Fe, Co (*fcc structure only for temperatures above 723 K or for a Co film on MgO) and Ni [19, 20, 21]

For Ni and fcc Co it is convenient for the LMTO-ASA calculation not to use the primitive lattice vectors of eq. (2.33) but to use rotated lattice vectors so that the easy axis coincides with the z-axis. This has been done by applying a rotation matrix on the primitive lattice vectors. For Fe the easy axis already coincides with the z-axis.

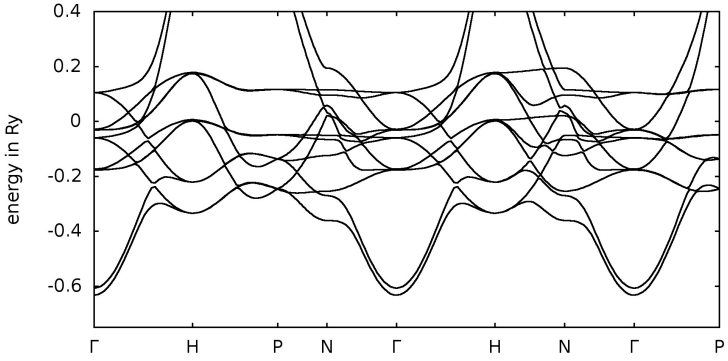

Figure 2.4: Band structure of bcc Fe with spin-orbit coupling along high-symmetry directions (calculated with the LMTO-ASA code).

2.2.2 Band structure

The main task of the LMTO-ASA program is to solve the effective one-particle Kohn-Sham equation (2.7)

$$\underbrace{\left[-\frac{\hbar^2}{2m_e}\Delta + W_{\text{eff}}[\rho(\mathbf{r})]\right]}_{\widehat{H}} \psi_{j\mathbf{k}}(\mathbf{r}) = \varepsilon_{j\mathbf{k}}\psi_{j\mathbf{k}}(\mathbf{r}). \tag{2.37}$$

An important output is the band structure $\varepsilon_{j\mathbf{k}}$ which gives the energy as function of the wavevector $\mathbf{k}$ for different band indices j. A band structure calculation with spin-orbit coupling using the LMTO-ASA code is shown in fig. 2.4 for bcc Fe and in fig. 2.5 for fcc Ni. The energy is calculated along the high-symmetry directions (see fig. 2.3) and the Fermi energy is set to zero. The calculation is in very good agreement with other band structure calculations (see, e.g., ref. [21]). Because of its chaotic look the band structure is often called "spaghetti".

2.2.3 Spin-mixing

Spin-orbit coupling is very crucial for electron-phonon scattering. The reason is explained in chapter 5. Let us first discuss the situation without

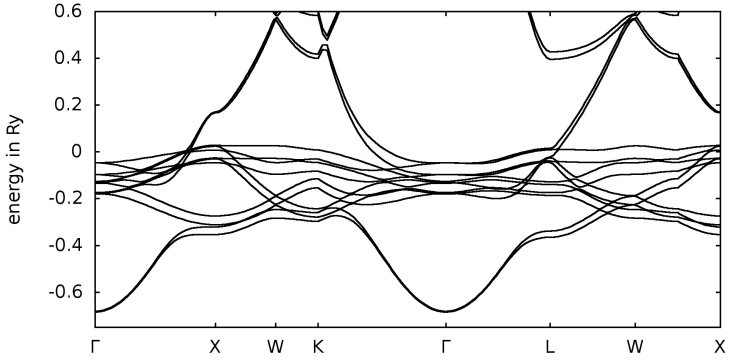

Figure 2.5: Band structure of fcc Ni with spin-orbit coupling along high-symmetry directions (calculated with the LMTO-ASA code).

spin-orbit coupling:

In a system without spin-orbit coupling the commutator of the Hamiltonian with the Pauli matrix σ_z is zero:

$$[\widehat{H}, \sigma_z] = 0. \tag{2.38}$$

For a collinear orientation the eigenstates are pure spin-states

$$\begin{aligned} \psi^{\uparrow}_{j\mathbf{k}} &= a_{j\mathbf{k}}(\mathbf{r}) e^{i\mathbf{kr}} |\chi_{\uparrow}\rangle \\ \psi^{\downarrow}_{j\mathbf{k}} &= b_{j\mathbf{k}}(\mathbf{r}) e^{i\mathbf{kr}} |\chi_{\downarrow}\rangle. \end{aligned} \tag{2.39}$$

$a_{j\mathbf{k}}(\mathbf{r})$ and $b_{j\mathbf{k}}(\mathbf{r})$ are the lattice-periodic functions according to Bloch's theorem.

In a system with spin-orbit coupling eq. (2.38) does not hold

$$[\widehat{H}, \sigma_z] \neq 0 \tag{2.40}$$

and the eigenstates are spin-mixed

$$\psi_{j\mathbf{k}} = [\ a_{j\mathbf{k}}(\mathbf{r}) |\chi_{\uparrow}\rangle + b_{j\mathbf{k}}(\mathbf{r}) |\chi_{\downarrow}\rangle\ ]\, e^{i\mathbf{kr}}. \tag{2.41}$$

The probability to find $\psi_{j\mathbf{k}}$ in spin-up or spin-down, respectively, is

$$p^{\uparrow}_{j\mathbf{k}} = \langle \psi_{j\mathbf{k}} | \chi_{\uparrow} \rangle \langle \chi_{\uparrow} | \psi_{j\mathbf{k}} \rangle, \quad p^{\downarrow}_{j\mathbf{k}} = \langle \psi_{j\mathbf{k}} | \chi_{\downarrow} \rangle \langle \chi_{\downarrow} | \psi_{j\mathbf{k}} \rangle \tag{2.42}$$

with the normalization

$$1 = p^{\uparrow}_{j\mathbf{k}} + p^{\downarrow}_{j\mathbf{k}} = \langle \psi_{j\mathbf{k}} | \psi_{j\mathbf{k}} \rangle. \tag{2.43}$$

It is now possible to distinguish two cases: The wavefunction can either be "dominant-up" if $p^{\uparrow}_{j\mathbf{k}} > p^{\downarrow}_{j\mathbf{k}}$ or "dominant-down" if $p^{\uparrow}_{j\mathbf{k}} < p^{\downarrow}_{j\mathbf{k}}$. It is useful to introduce a new notation in order not to mix up the expressions pure-up (pure-down) and dominant-up (dominant-down)

$$\begin{aligned} \psi^{\uparrow}_{j\mathbf{k}} &= \left[\, a^{\uparrow}_{j\mathbf{k}}(\mathbf{r}) |\chi_{\uparrow}\rangle + b^{\uparrow}_{j\mathbf{k}}(\mathbf{r}) |\chi_{\downarrow}\rangle \, \right] e^{i\mathbf{kr}} \qquad \text{if} \qquad p^{\uparrow}_{j\mathbf{k}} > p^{\downarrow}_{j\mathbf{k}} \\ \psi^{\downarrow}_{j\mathbf{k}} &= \left[\, b^{\downarrow}_{j\mathbf{k}}(\mathbf{r}) |\chi_{\uparrow}\rangle + a^{\downarrow}_{j\mathbf{k}}(\mathbf{r}) |\chi_{\downarrow}\rangle \, \right] e^{i\mathbf{kr}} \qquad \text{if} \qquad p^{\uparrow}_{j\mathbf{k}} < p^{\downarrow}_{j\mathbf{k}} \, . \end{aligned} \tag{2.44}$$

One can show that normally most of the states $\psi_{j\mathbf{k}}$ are almost pure spin-states and only few states have a strong spin-mixing factor $|b_{j\mathbf{k}}|^2$ [22] which is defined by

$$|b_{j\mathbf{k}}|^2 = \min(p^{\uparrow}_{j\mathbf{k}}, p^{\downarrow}_{j\mathbf{k}}). \tag{2.45}$$

The averaged spin-mixing factor is calculated by an average over all states on the Fermi surface

$$b^2 = \left\langle |b_{j\mathbf{k}}|^2 \right\rangle_{\text{Fermi}} = \frac{\sum_j \int_{\text{BZ}} \mathrm{d}^3k \;\; |b_{j\mathbf{k}}|^2 \;\; \delta(\varepsilon_{j\mathbf{k}} - \varepsilon_{\text{F}})}{\sum_j \int_{\text{BZ}} \mathrm{d}^3k \;\; \delta(\varepsilon_{j\mathbf{k}} - \varepsilon_{\text{F}})}. \tag{2.46}$$

The spin-mixing factors $|b_{j\mathbf{k}}|^2$ and b^2 can be calculated with the LMTO-ASA code. Thereby, one has to use a Gaussian smearing instead of the delta function. The averaged spin-mixing factor is $b^2 = 0.024$ for Fe and $b^2 = 0.025$ for Ni if a thermal smearing of 25 meV is used [22, 23].

2.2.4 Density of states

The density of states $Z(\varepsilon)$ is calculated in the LMTO-ASA code with the following equation

$$Z(\varepsilon) = \frac{1}{\Omega_{\text{BZ}}} \sum_j \int_{\text{BZ}} \mathrm{d}^3k \;\; \delta(\varepsilon - \varepsilon_{j\mathbf{k}}). \tag{2.47}$$

The spin-resolved density of states $Z^{\uparrow,\downarrow}(\varepsilon)$ is obtained when using the normalization $1 = p^{\uparrow}_{j\mathbf{k}} + p^{\downarrow}_{j\mathbf{k}}$

$$\begin{aligned} Z(\varepsilon) &= \frac{1}{\Omega_{\mathrm{BZ}}} \sum_j \int_{\mathrm{BZ}} \mathrm{d}^3k \; (p^{\uparrow}_{j\mathbf{k}} + p^{\downarrow}_{j\mathbf{k}}) \; \delta(\varepsilon - \varepsilon_{j\mathbf{k}}) \\ &= \underbrace{\frac{1}{\Omega_{\mathrm{BZ}}} \sum_j \int_{\mathrm{BZ}} \mathrm{d}^3k \; p^{\uparrow}_{j\mathbf{k}} \; \delta(\varepsilon - \varepsilon_{j\mathbf{k}})}_{Z^{\uparrow}(\varepsilon)} + \underbrace{\frac{1}{\Omega_{\mathrm{BZ}}} \sum_j \int_{\mathrm{BZ}} \mathrm{d}^3k \; p^{\downarrow}_{j\mathbf{k}} \; \delta(\varepsilon - \varepsilon_{j\mathbf{k}})}_{Z^{\downarrow}(\varepsilon)} \\ &= Z^{\uparrow}(\varepsilon) + Z^{\downarrow}(\varepsilon). \end{aligned} \tag{2.48}$$

Similarly, one can define the dominant-up and dominant-down density of states $Z^{\uparrow,\downarrow}(\varepsilon)$. Thereby, one has to specify which states are called dominant-up or dominant-down. The usual definition is that a state is called dominant-up if $p^{\uparrow}_{j\mathbf{k}} > 0.5$ and dominant-down if $p^{\downarrow}_{j\mathbf{k}} > 0.5$. There are good reasons to choose a different definition (this is discussed in subsection 7.1.1). In general a threshold S (where $0.5 < S < 1$) has to be specified with dominant-up for $p^{\uparrow}_{j\mathbf{k}} > S$ and dominant-down for $p^{\downarrow}_{j\mathbf{k}} > S$. Therefore, the dominant-up and dominant-down density of states can be calculated with

$$\begin{aligned} Z^{\uparrow}(\varepsilon) &= \frac{1}{\Omega_{\mathrm{BZ}}} \sum_j \int_{\mathrm{BZ}} \mathrm{d}^3k \; n^{\uparrow}_{j\mathbf{k}} \; \delta(\varepsilon - \varepsilon_{j\mathbf{k}}), \qquad n^{\uparrow}_{j\mathbf{k}} = \begin{cases} 1 & \text{if } p^{\uparrow}_{j\mathbf{k}} > S \\ 0 & \text{otherwise} \end{cases} \\ Z^{\downarrow}(\varepsilon) &= \frac{1}{\Omega_{\mathrm{BZ}}} \sum_j \int_{\mathrm{BZ}} \mathrm{d}^3k \; n^{\downarrow}_{j\mathbf{k}} \; \delta(\varepsilon - \varepsilon_{j\mathbf{k}}), \qquad n^{\downarrow}_{j\mathbf{k}} = \begin{cases} 1 & \text{if } p^{\downarrow}_{j\mathbf{k}} > S \\ 0 & \text{otherwise} \end{cases} . \end{aligned} \tag{2.49}$$

Gaussian smearing is used for the numerical integration and it turns out that the density of states does not depend strongly on the chosen smearing parameter. Fig. 2.6 and 2.7 show the dominant-up and dominant-down density of states for bcc Fe and fcc Ni, respectively, for different threshold values S. The Fermi energy is set to zero. The different threshold values do not have a big impact on the behavior of the density of states except for the value $S = 0.95$ and $S = 0.995$ which are extreme definitions. This is a hint that most of the states have a low spin-mixing and that only few states have a strong spin-mixing. The spin-resolved density of states $Z^{\uparrow,\downarrow}$ and the dominant-up/dominant-down density of states $Z^{\uparrow,\downarrow}$ for $S = 0.5$ coincide (not shown in the figures).

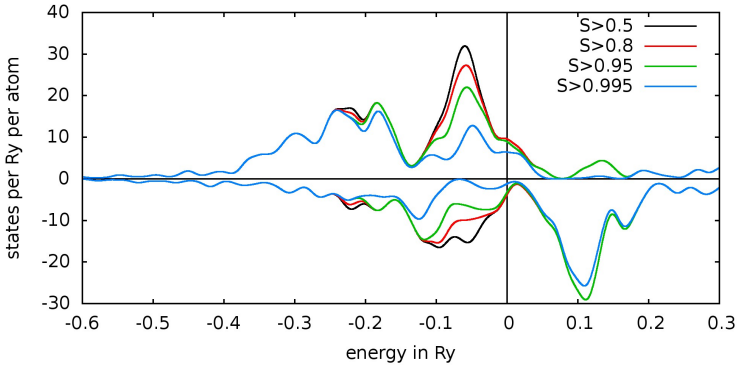

Figure 2.6: Density of states $Z^{\uparrow,\downarrow}(\varepsilon)$ for bcc Fe for different definitions of dominant-up/dominant-down (calculated with the LMTO-ASA code). The Fermi energy is set to zero. Positive values denote dominant-up and negative values denote dominant-down.

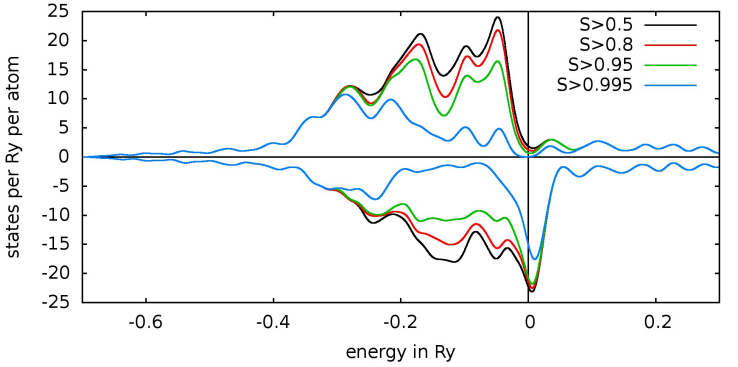

Figure 2.7: Density of states $Z^{\uparrow,\downarrow}(\varepsilon)$ for fcc Ni for different definitions of dominant-up/dominant-down (calculated with the LMTO-ASA code). The Fermi energy is set to zero. Positive values denote dominant-up and negative values denote dominant-down.

2.3 Lattice dynamics

Only a very short introduction into lattice dynamics is given in this section. In the following solids with one atom in the unit cell are considered. The extension for solids with more than one atom in the unit cell is straightforward but not necessary for Al, Fe and Ni. Details can be found in refs. [19, 24], e.g.

Atoms in a solid vibrate around their equilibrium positions due to thermal fluctuations. The displacement $\mathbf{u}(\mathbf{T})$ of an atom in the unit cell $\mathbf{T}$ is rather small. Therefore, a harmonic approximation is reasonable. In the harmonic approximation the forces $\mathbf{F}$ are proportional to the (small) displacements $\mathbf{u}$. The force on an atom in unit cell $\mathbf{T}$ is given by the sum of all the forces when the atoms in unit cells $\mathbf{T'}$ are displaced by $\mathbf{u}(\mathbf{T'})$:

$$\mathbf{F}(\mathbf{T}) = -\sum_{\mathbf{T'}} \underline{\underline{\phi}}(\mathbf{T}, \mathbf{T'})\mathbf{u}(\mathbf{T'}). \tag{2.50}$$

$\underline{\underline{\phi}}(\mathbf{T}, \mathbf{T'})$ is the force-constant matrix and the components are defined by

$$\phi_{ij}(\mathbf{T}, \mathbf{T'}) = -\left.\frac{\partial F_j(\mathbf{T'})}{\partial u_i(\mathbf{T})}\right|_{u_i=0} = -\lim_{u_i \to 0} \frac{F_j(\mathbf{T'})}{u_i(\mathbf{T})}. \tag{2.51}$$

Newton's equation of motion reads

$$M\frac{\partial^2 \mathbf{u}(\mathbf{T})}{\partial t^2} = -\sum_{\mathbf{T'}} \underline{\underline{\phi}}(\mathbf{T}, \mathbf{T'})\mathbf{u}(\mathbf{T'}) \tag{2.52}$$

where M is the mass of the atoms. The plane wave ansatz

$$\mathbf{u}(\mathbf{T}) = \frac{u_0}{\sqrt{M}}\mathbf{e}(\mathbf{q}) \exp(i(\mathbf{qT} - \omega(\mathbf{q})t)) \tag{2.53}$$

is a solution of Newton's equation of motion. u_0 is the amplitude of the displacement and $\mathbf{e}(\mathbf{q})$ is the polarization vector of the displacement with wavevector $\mathbf{q}$. Using the plane wave ansatz in eq. (2.52) yields the eigenvalue equation

$$\underline{\underline{D}}(\mathbf{q})\mathbf{e}(\mathbf{q}) = \omega^2(\mathbf{q})\mathbf{e}(\mathbf{q}) \tag{2.54}$$

with

$$\begin{aligned}\underline{\underline{D}}(\mathbf{q}) &= \frac{1}{M}\sum_{\mathbf{T}'}\underline{\underline{\phi}}(\mathbf{T},\mathbf{T}')\exp(i\mathbf{q}(\mathbf{T}'-\mathbf{T})) \\ &= \frac{1}{M}\sum_{\mathbf{T}'}\underline{\underline{\phi}}(0,\mathbf{T}')\exp(i\mathbf{q}\mathbf{T}'). \end{aligned} \tag{2.55}$$

$\underline{\underline{D}}$ is the Fourier transformation of the force-constant matrix $\underline{\underline{\phi}}$ and is called dynamical matrix. It is a real symmetric 3×3-matrix in case of a crystal with only one atom in the unit cell. In general the eigenvalue equation has three different solutions $\omega_\lambda^2(\mathbf{q})$, $\mathbf{e}_\lambda(\mathbf{q})$ with $\lambda = 1,2,3$ for every $\mathbf{q}$ but the eigenvalues might be degenerate. If the vibrations are quantized, the modes are called phonons (quasiparticle picture). The eigenvalues are the squared phonon frequencies and the eigenvectors are the polarization vectors of the phonons. For high-symmetry directions the polarization vectors are longitudinal ($\mathbf{e}(\mathbf{q}) \parallel \mathbf{q}$) and transverse ($\mathbf{e}(\mathbf{q}) \perp \mathbf{q}$). For non-high-symmetry directions the polarization vectors are pseudo-longitudinal and pseudo-transverse.

In summary one needs the force constants $\phi_{ij}(0,\mathbf{T}')$ and the crystal symmetry in order to determine all the phonon frequencies and all the phonon polarization vectors. Of course it is not possible to determine the force constants for a very large number of nearest neighbors. That's why one takes only few nearest-neighbor interactions into account. Anyway, the interaction with far neighbors is only small.

For a calculation of the dynamical matrix it is convenient to use another expression for the dynamical matrix. The derivation can be found in ref. [19]:

$$\underline{\underline{D}}(\mathbf{q}) = -\frac{2}{M}\sum_{\mathbf{T}'}\underline{\underline{\phi}}(0,\mathbf{T}')\sin^2\left(\frac{\mathbf{q}\mathbf{T}'}{2}\right). \tag{2.56}$$

Eq. (2.56) shows that $\underline{\underline{D}}$ is a real matrix which is even in $\mathbf{q}$. The summation runs over all nearest neighbors $\mathbf{T}'$ taken into account (see above). It is a bit cumbersome to find all the positions of the nearest neighbors and to find the symmetries of the force-constant matrix $\underline{\underline{\phi}}$. As an example the positions and force-constant matrices of the first nearest neighbors of the

fcc lattice are given here:

$$
\begin{aligned}
\mathbf{T}'_1 &= \pm\frac{a}{2}\begin{pmatrix}1\\1\\0\end{pmatrix}, \quad \underset{=1}{\phi}(0,\mathbf{T}'_1) = \begin{pmatrix}\alpha & \gamma & 0\\ \gamma & \alpha & 0\\ 0 & 0 & \beta\end{pmatrix}\\
\mathbf{T}'_2 &= \pm\frac{a}{2}\begin{pmatrix}1\\0\\1\end{pmatrix}, \quad \underset{=2}{\phi}(0,\mathbf{T}'_2) = \begin{pmatrix}\alpha & 0 & \gamma\\ 0 & \beta & 0\\ \gamma & 0 & \alpha\end{pmatrix}\\
\mathbf{T}'_3 &= \pm\frac{a}{2}\begin{pmatrix}0\\1\\1\end{pmatrix}, \quad \underset{=3}{\phi}(0,\mathbf{T}'_3) = \begin{pmatrix}\beta & 0 & 0\\ 0 & \alpha & \gamma\\ 0 & \gamma & \alpha\end{pmatrix}\\
\mathbf{T}'_4 &= \pm\frac{a}{2}\begin{pmatrix}-1\\1\\0\end{pmatrix}, \quad \underset{=4}{\phi}(0,\mathbf{T}'_4) = \begin{pmatrix}\alpha & -\gamma & 0\\ -\gamma & \alpha & 0\\ 0 & 0 & \beta\end{pmatrix}\\
\mathbf{T}'_5 &= \pm\frac{a}{2}\begin{pmatrix}-1\\0\\1\end{pmatrix}, \quad \underset{=5}{\phi}(0,\mathbf{T}'_5) = \begin{pmatrix}\alpha & 0 & -\gamma\\ 0 & \beta & 0\\ -\gamma & 0 & \alpha\end{pmatrix}\\
\mathbf{T}'_6 &= \pm\frac{a}{2}\begin{pmatrix}0\\-1\\1\end{pmatrix}, \quad \underset{=6}{\phi}(0,\mathbf{T}'_6) = \begin{pmatrix}\beta & 0 & 0\\ 0 & \alpha & -\gamma\\ 0 & -\gamma & \alpha\end{pmatrix}
\end{aligned}
\tag{2.57}
$$

Squires has published a form of eq. (2.56) which already includes the fcc or bcc crystal symmetry, respectively. This avoids the cumbersome nearest neighbor and symmetry considerations. The equations can be found in ref. [25].

3 Calculation of the phonon frequencies and polarization vectors

In order to calculate the electron-phonon scattering matrix elements it is necessary to determine the phonon frequencies $\omega(\mathbf{q})$ and polarization vectors $\mathbf{e}(\mathbf{q})$ in the whole Brillouin zone for arbitrary wavevectors $\mathbf{q}$. It is not possible to determine the frequencies and polarization vectors in the whole Brillouin zone experimentally. Instead, the force-constant matrix is determined and with the eigenvalue equation (2.54) one can calculate the frequencies and polarization vectors in the whole Brillouin zone. There are several ways to determine the force constants: one can obtain them from experiments (see section 3.1), from ab-initio calculations (see section 3.2) or from phenomenological model calculations which is not discussed here. The results of the experimental method and of the ab-initio method are compared with each other in section 3.3.

This chapter is based on an earlier publication by Illg, Meyer and Fähnle [26]. The explanations given here go at some points beyond the explanations in the publications.

3.1 Experimental force-constant model

3.1.1 Experiments

Neutrons, x-rays or visible light are suitable to make scattering experiments at phonons because they do not possess an electric charge and therefore only interact very slightly with the electrons. The dominant interaction is with the nuclei. Normally, neutron scattering experiments are preferred because they are easier to interpret than x-ray or light scattering experiments [19]. The incident energy E and momentum $\mathbf{p}$ of the neutron

is known and the energy E' and momentum $\mathbf{p}'$ of the scattered neutron can be measured. Energy and momentum conservation holds and reads for the one-phonon scattering

$$\begin{aligned} E' &= E \pm \hbar\omega_\lambda(\mathbf{q}) \\ \mathbf{p}' &= \mathbf{p} \pm \hbar\mathbf{q} + \hbar\mathbf{G} \end{aligned} \tag{3.1}$$

where the plus-sign denotes an absorption and the minus-sign denotes an emission of a phonon. Therefore, the phonon frequency is $\pm\omega_\lambda(\mathbf{q}) = (E' - E)/\hbar$ and the phonon wavevector is $\pm\mathbf{q} = (\mathbf{p}' - \mathbf{p})/\hbar - \mathbf{G}$ where $\mathbf{G}$ is a reciprocal lattice vector. So, it is possible to measure the frequency spectrum of the whole Brillouin zone. Of course there are also zero-phonon and multiple-phonon scatterings which are discussed in ref. [19]. They have to be taken into account. Since it is quite cumbersome to measure the phonon frequencies in the whole Brillouin zone, usually only the phonon frequencies along high-symmetry directions are measured.

The case is more difficult for the phonon polarization vectors $\mathbf{e}(\mathbf{q})$. The scattered intensity is proportional to the square of the modulus of the dynamical structure factor. The polarization vectors $\mathbf{e}(\mathbf{q})$ enter the dynamical structure factor. In general it is not possible to determine $\mathbf{e}(\mathbf{q})$ from the scattered intensity, only in special cases where $\mathbf{q}$ is symmetric one can retrieve the polarization vector. Therefore, Kohl proposed to orient the crystal in a coherent inelastic neutron scattering experiment such that a Bragg peak is excited in order to gain more information about the polarization vector [27]. Experiments with this technique were done by Spalt et al. [28] and Zounek et al. [29] but in most publications very few attention is paid to the measurement of phonon polarization vectors.

3.1.2 Fitting procedure

Because the polarization vectors are normally unknown (except for high-symmetry $\mathbf{q}$), the force constants are determined from the frequencies only. To do this one "cuts" the nearest-neighbor interaction, e.g., only interactions from the first to the fifth nearest neighbors are taken into account. The force constants can then be determined by fitting (least-square method) the theoretical frequencies $\omega_j^2(\mathbf{q}; \{\underline{\underline{\phi}}(0, \mathbf{T}')\})$ to the measured frequencies along high-symmetry directions (for Ni see, e.g., ref. [30]) or to the measured density of states (for Ni see ref. [31]). The fitting procedure

is shown in ref. [32] in detail. However, it is also shown that it is not possible to determine the force constants unambiguously. To do so one would have to include the phonon polarization vectors which are very difficult to measure.

3.1.3 Ambiguity of force constants

Many publications point to the problem that the force constants are not unique if only information about the phonon frequencies enter [32, 33, 34]. An illustrative example was given by Leigh and coworkers [33] who applied a unitary transformation to the force constant matrix. They showed that the force constants and eigenvectors alter under a unitary transformation that respects the crystal symmetry while leaving the frequencies unchanged. Hence, different sets of force constants may give the same frequencies but different polarization vectors. Leigh et al. illustrated this behavior with an example for germanium [33], and also Cochran gave an example for a diatomic linear chain of masses m_1 and m_2 [34]. The knowledge of the eigenvectors would resolve the problem of ambiguity of the force constants.

3.2 Ab-initio force-constant model

Many authors have shown that ab-initio calculations are a good tool to study lattice dynamics [35]. Especially for Fe and Ni this has already been done by Dal Corso and de Gironcoli [36]. It is not the purpose to show this by further ab-initio calculations. The scope is to compare the ab-initio results with the results obtained from experimentally fitted force constants.

Force constants can be calculated ab-initio with the direct approach or the linear-response method. There are two types of direct approaches: first, the frozen-phonon method in which a phonon mode is imprinted in the supercell and second, the determination of forces by displacing an atom in the crystal. Here, the direct approach and the second method is chosen and explained in the following.

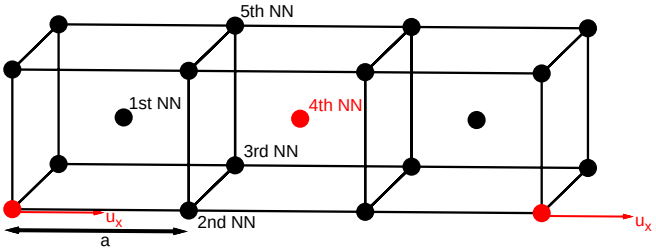

Figure 3.1: In a bcc $3 \times 3 \times 3$-supercell an atom is displaced in x-direction u_x. Because of the periodic array the atom with distance $3a$ is also displaced. NN is the abbreviation for nearest neighbor.

3.2.1 Supercell calculations

The basic idea can be explained with fig. 3.1 and with eq. (2.51)

$$\phi_{ij}(0, \mathbf{T}') = -\lim_{u_i \to 0} \frac{F_j(\mathbf{T}')}{u_i(0)}. \tag{3.2}$$

In fig. 3.1 a part of a bcc $3\times3\times3$-supercell is shown. The $3\times3\times3$-supercell contains 27 conventional unit cells, and because every conventional bcc unit cell contains two atoms, the $3 \times 3 \times 3$-supercell consists of 54 atoms. To determine the force constants one has to displace the atom in a cell (cell "0") in x-, y- and z-direction and determine the forces in x-, y- and z-direction in every cell $\mathbf{T}'$. In fig. 3.1 an atom in the supercell is displaced in x-direction u_x (red arrow) and the force F_x, F_y and F_z on the neighboring atoms can be calculated ab-initio. For a monatomic cubic crystal it can be shown that the displacement in only one Cartesian direction is sufficient to determine the full force-constant matrix [11].

For an ab-initio calculation a periodic continuation of the supercell is necessary. Hence, if the atom in cell 0 is displaced, also the atom with translation vector of the supercell $\mathbf{T}_{\text{sc}}$ is displaced. This is shown in fig. 3.1. This fact causes problems for the calculation of forces for the fourth nearest neighbor in fig. 3.1 (marked red) because it is the fourth nearest neighbor for the displaced atom on the left hand side and also the fourth nearest neighbor for the displaced atom on the right hand side. Therefore, the force in x-direction F_x is twice as large as the force which would act on the fourth nearest neighbor if only the atom in cell 0 was displaced, and the forces in y- and z-direction F_y, F_z are zero. This is

called "superposition effect". It is required to consider larger supercells and to see whether the force constants converge. However, one can show that the dynamical matrix is exact despite the superposition effects (and therefore the frequencies and polarization vectors are exact) for special $\mathbf{q}$-points if the condition $\mathbf{q} \cdot \mathbf{T}_{\mathrm{sc}} = 2\pi n, n \in \mathbb{Z}$ is fulfilled [37].

The ab-initio calculations were done for $u_i(0) = 0.1\mathring{A} \cdot f, f = 1, 2, ..., 6$ and a third-order polynomial was used for the fit of $F_j(\mathbf{T}')$ as function of $u_i(0)$. The derivative of the polynomial at $u_i(0) = 0$ is the force constant ϕ_{ij}.

3.2.2 Calculational details

The ab-initio calculations for Al, Fe and Ni were done with the pseudopotential method using the PWscf code (Quantum ESPRESSO) [15]. Thereby, Vanderbilt ultrasoft pseudopotentials [14], the generalized gradient approximation [13] and a Gaussian smearing of 136 meV were used (see subsection 2.1.6 and 2.1.2). The experimental lattice constants at 0 K given in table 2.1 were applied. The 3s and 3p states were treated as semicore states for Ni and as true core states for Fe and Al. After respective convergence tests the cutoffs for the plane waves were chosen to be 25 Ry for Al and 30 Ry for Fe and Ni. The cutoff for the electron density is 120 Ry for Al and 200 Ry for Fe and Ni. For Al a $24 \times 24 \times 24$ Monkhorst-Pack mesh in the Brillouin zone of the conventional unit cell was used for the k-point sampling [38]. For Fe a $20 \times 20 \times 20$ mesh and for Ni a $12 \times 12 \times 12$ mesh was used. The calculations were performed for different supercell sizes. The largest were a $4 \times 4 \times 4$ supercell of the conventional unit cell for Al and Ni and a $5 \times 5 \times 5$ supercell of the conventional unit cell for Fe.

3.3 Comparison of the experimental and ab-initio force-constant model

3.3.1 Comparison of force constants obtained from the experimental and from the ab-initio force-constant model

In table 3.1, 3.2 and 3.3 the results of the ab-initio calculations for fcc Ni, fcc Al and bcc Fe are presented. The neighbor position (NP) is given in units of $a_0/2$ (a_0: lattice constant at 0 K). The force constants (FC) $\phi_{n,ij}$ of the force-constant matrix $\underline{\underline{\phi}}(0, \mathbf{T}')$ are labeled with the index of the n-th nearest neighbor (up to the 28th nearest neighbor for the 4×4×4 fcc supercell and up to the 32nd nearest neighbor for the 5×5×5 bcc supercell) and with the Cartesian directions i and j. Note that the 15th, 16th, 19th and 21st up to the 27th neighbors are outside the 4×4×4 fcc supercell and that the 15th, 16th, 18th, 21st, 22nd, 23rd and 25th up to the 31st neighbors are outside the 5×5×5 bcc supercell. The unit of the force constants is N/m. The ab-initio force constants are compared with the force constants fitted to the experimentally determined phonon density of states by Kresch et al. [31, 39, 40] (up to the 5th nearest neighbor at T=10 K for fcc Ni, up to the 8th nearest neighbor at T=10 K for fcc Al, up to the 5th nearest neighbor at T=21 K for bcc Fe).

Even without calculating the phonon frequencies and polarization vectors we can already see two things: First, the agreement between ab-initio and fitted force constants is quite good for Ni and slightly worse for Al and Fe. One can see that there are deviations (see, e.g., $\phi_{1,xx}$ for Fe) but they are not altered totally as was argued by Leigh et al. [33] and Cochran [34]. Probably, the symmetry requirements for the unitary transformation sets limits. Second, the ab-initio force constants beyond the 5th nearest neighbors for Ni and Fe and beyond the 8th nearest neighbor for Al are not vanishingly small (see, e.g., $\phi_{9,xx}$ for Ni).

Certainly, the ab-initio force constants should be more reliable than the fitted force constants since the ab-initio force constants are parameter free. The frequencies and polarization vectors obtained from the ab-initio force constants are compared with the frequencies and polarization vectors obtained from the fitted force constants in the next subsection.

Table 3.1: Force constants (FC) for fcc Ni in N/m of the ab-initio calculations up to the 28th nearest neighbor (numerical uncertainty: about ±0.03 N/m) and force constants fitted to the experimentally determined phonon density of states at T=10 K by Kresch et al. [31] up to the 5th nearest neighbor. The neighbor position (NP) is given in units of $a_0/2$.

NP	FC	ab-initio	fit [31]	NP	FC	ab-initio
(1,1,0)	$\phi_{1,xx}$	17.02	17.584	(4,2,0)	$\phi_{11,xx}$	-0.02
	$\phi_{1,zz}$	-0.23	-0.391		$\phi_{11,yy}$	0.08
	$\phi_{1,xy}$	19.05	18.976		$\phi_{11,zz}$	0.00
(2,0,0)	$\phi_{2,xx}$	2.05	0.975		$\phi_{11,xy}$	0.00
	$\phi_{2,yy}$	-0.87	-0.610	(2,3,3)	$\phi_{12,xx}$	0.03
(2,1,1)	$\phi_{3,xx}$	1.22	0.593		$\phi_{12,yy}$	-0.02
	$\phi_{3,yy}$	0.44	0.302		$\phi_{12,xy}$	0.02
	$\phi_{3,xy}$	0.75	0.378		$\phi_{12,yz}$	0.03
	$\phi_{3,yz}$	0.04	-0.120	(4,2,2)	$\phi_{13,xx}$	0.05
(2,2,0)	$\phi_{4,xx}$	0.13	0.386		$\phi_{13,yy}$	-0.02
	$\phi_{4,zz}$	-0.15	-0.218		$\phi_{13,xy}$	0.00
	$\phi_{4,xy}$	0.15	0.517		$\phi_{13,yz}$	0.04
(3,1,0)	$\phi_{5,xx}$	-0.03	-0.085	(4,3,1)	$\phi_{14,xx}$	-0.07
	$\phi_{5,yy}$	-0.03	0.006		$\phi_{14,yy}$	-0.04
	$\phi_{5,zz}$	-0.12	0.014		$\phi_{14,zz}$	0.00
	$\phi_{5,xy}$	-0.07	-0.039		$\phi_{14,xy}$	0.00
(2,2,2)	$\phi_{6,xx}$	0.02			$\phi_{14,xz}$	0.00
	$\phi_{6,xy}$	0.07			$\phi_{14,yz}$	-0.04
(3,2,1)	$\phi_{7,xx}$	-0.16		(4,4,0)	$\phi_{17,xx}$	0.15
	$\phi_{7,yy}$	0.04			$\phi_{17,zz}$	0.04
	$\phi_{7,zz}$	-0.01			$\phi_{17,xy}$	0.00
	$\phi_{7,xy}$	-0.01		(4,3,3)	$\phi_{18,xx}$	-0.02
	$\phi_{7,xz}$	-0.14			$\phi_{18,yy}$	-0.01
	$\phi_{7,yz}$	-0.12			$\phi_{18,xy}$	0.00
(4,0,0)	$\phi_{8,xx}$	-0.09			$\phi_{18,yz}$	0.01
	$\phi_{8,yy}$	-0.05		(2,4,4)	$\phi_{20,xx}$	0.00
(3,3,0)	$\phi_{9,xx}$	0.42			$\phi_{20,yy}$	0.00
	$\phi_{9,zz}$	-0.02			$\phi_{20,xy}$	0.00
	$\phi_{9,xy}$	0.40			$\phi_{20,yz}$	0.00
(4,1,1)	$\phi_{10,xx}$	-0.01		(4,4,4)	$\phi_{28,xx}$	0.00
	$\phi_{10,yy}$	0.04			$\phi_{28,xy}$	0.00
	$\phi_{10,xy}$	0.00				
	$\phi_{10,yz}$	-0.04				

Table 3.2: Force constants for fcc Al in N/m of the ab-initio calculations up to the 28th nearest neighbor (numerical uncertainty: about ±0.02 N/m) and force constants fitted to the experimentally determined phonon density of states at T=10 K by Kresch et al. [39] up to the 8th nearest neighbor.

NP	FC	ab-initio	fit [39]	NP	FC	ab-initio
(1,1,0)	$\phi_{1,xx}$	10.62	10.112	(4,2,0)	$\phi_{11,xx}$	-0.06
	$\phi_{1,zz}$	-1.81	-1.356		$\phi_{11,yy}$	0.03
	$\phi_{1,xy}$	11.26	11.148		$\phi_{11,zz}$	0.01
(2,0,0)	$\phi_{2,xx}$	1.94	2.454		$\phi_{11,xy}$	0.00
	$\phi_{2,yy}$	-0.03	-0.532	(2,3,3)	$\phi_{12,xx}$	0.07
(2,1,1)	$\phi_{3,xx}$	-0.40	-0.634		$\phi_{12,yy}$	0.03
	$\phi_{3,yy}$	-0.09	-0.298		$\phi_{12,xy}$	0.03
	$\phi_{3,xy}$	-0.30	-0.185		$\phi_{12,yz}$	0.05
	$\phi_{3,yz}$	-0.08	-0.149	(4,2,2)	$\phi_{13,xx}$	0.04
(2,2,0)	$\phi_{4,xx}$	0.19	0.273		$\phi_{13,yy}$	0.01
	$\phi_{4,zz}$	-0.01	0.324		$\phi_{13,xy}$	0.00
	$\phi_{4,xy}$	0.31	-0.051		$\phi_{13,yz}$	0.01
(3,1,0)	$\phi_{5,xx}$	0.21	0.469	(4,3,1)	$\phi_{14,xx}$	-0.04
	$\phi_{5,yy}$	0.02	0.229		$\phi_{14,yy}$	-0.03
	$\phi_{5,zz}$	0.01	0.199		$\phi_{14,zz}$	0.01
	$\phi_{5,xy}$	-0.03	0.090		$\phi_{14,xy}$	0.00
(2,2,2)	$\phi_{6,xx}$	-0.11	0.144		$\phi_{14,xz}$	0.00
	$\phi_{6,xy}$	-0.18	-0.110		$\phi_{14,yz}$	-0.02
(3,2,1)	$\phi_{7,xx}$	0.07	-0.061	(4,4,0)	$\phi_{17,xx}$	0.02
	$\phi_{7,yy}$	0.03	-0.088		$\phi_{17,zz}$	-0.02
	$\phi_{7,zz}$	-0.02	-0.105		$\phi_{17,xy}$	0.00
	$\phi_{7,xy}$	0.05	0.032	(4,3,3)	$\phi_{18,xx}$	0.02
	$\phi_{7,xz}$	0.06	0.016		$\phi_{18,yy}$	-0.02
	$\phi_{7,yz}$	0.01	0.011		$\phi_{18,xy}$	0.00
(4,0,0)	$\phi_{8,xx}$	0.14	-0.536		$\phi_{18,yz}$	0.02
	$\phi_{8,yy}$	-0.03	-0.117	(2,4,4)	$\phi_{20,xx}$	-0.03
(3,3,0)	$\phi_{9,xx}$	-0.06			$\phi_{20,yy}$	-0.03
	$\phi_{9,zz}$	-0.01			$\phi_{20,xy}$	0.00
	$\phi_{9,xy}$	-0.05			$\phi_{20,yz}$	0.00
(4,1,1)	$\phi_{10,xx}$	-0.14		(4,4,4)	$\phi_{28,xx}$	-0.02
	$\phi_{10,yy}$	-0.01			$\phi_{28,xy}$	0.00
	$\phi_{10,xy}$	0.00				
	$\phi_{10,yz}$	0.01				

Table 3.3: Force constants for bcc Fe in N/m of the ab-initio calculations up to the 32nd nearest neighbor (numerical uncertainty: about ±0.03 N/m) and force constants fitted to the experimentally determined phonon density of states at T=21 K by Kresch [40] up to the 5th nearest neighbor.

NP	FC	ab-initio	fit [40]	NP	FC	ab-initio
(1,1,1)	$\phi_{1,xx}$	15.79	17.263	(4,4,0)	$\phi_{12,xx}$	0.17
	$\phi_{1,xy}$	12.32	14.910		$\phi_{12,zz}$	0.13
(2,0,0)	$\phi_{2,xx}$	15.29	15.314		$\phi_{12,xy}$	0.06
	$\phi_{2,yy}$	-0.10	0.115	(5,3,1)	$\phi_{13,xx}$	0.00
(2,2,0)	$\phi_{3,xx}$	1.24	1.020		$\phi_{13,yy}$	-0.01
	$\phi_{3,zz}$	-0.84	-0.393		$\phi_{13,zz}$	0.02
	$\phi_{3,xy}$	0.60	0.273		$\phi_{13,xy}$	0.00
(3,1,1)	$\phi_{4,xx}$	0.57	-0.286		$\phi_{13,xz}$	0.00
	$\phi_{4,yy}$	0.39	0.048		$\phi_{13,yz}$	-0.01
	$\phi_{4,xy}$	0.54	-0.067	(2,4,4)	$\phi_{14,xx}$	-0.01
	$\phi_{4,yz}$	0.47	0.566		$\phi_{14,yy}$	0.09
(2,2,2)	$\phi_{5,xx}$	-0.82	-0.382		$\phi_{14,xy}$	0.04
	$\phi_{5,xy}$	-0.25	0.090		$\phi_{14,yz}$	0.08
(4,0,0)	$\phi_{6,xx}$	0.44		(5,3,3)	$\phi_{17,xx}$	0.19
	$\phi_{6,yy}$	0.09			$\phi_{17,yy}$	-0.07
(1,3,3)	$\phi_{7,xx}$	0.04			$\phi_{17,xy}$	0.00
	$\phi_{7,yy}$	-0.21			$\phi_{17,yz}$	-0.05
	$\phi_{7,xy}$	-0.01		(4,4,4)	$\phi_{19,xx}$	-0.17
	$\phi_{7,yz}$	-0.09			$\phi_{19,xy}$	0.03
(4,2,0)	$\phi_{8,xx}$	-0.21		(1,5,5)	$\phi_{20,xx}$	-0.07
	$\phi_{8,yy}$	-0.17			$\phi_{20,yy}$	-0.03
	$\phi_{8,zz}$	0.00			$\phi_{20,xy}$	0.00
	$\phi_{8,xy}$	-0.23			$\phi_{20,yz}$	0.00
(4,2,2)	$\phi_{9,xx}$	-0.41		(3,5,5)	$\phi_{24,xx}$	0.01
	$\phi_{9,yy}$	-0.23			$\phi_{24,yy}$	0.00
	$\phi_{9,xy}$	-0.19			$\phi_{24,xy}$	0.00
	$\phi_{9,yz}$	-0.12			$\phi_{24,yz}$	0.00
(3,3,3)	$\phi_{10,xx}$	-0.03		(5,5,5)	$\phi_{32,xx}$	0.10
	$\phi_{10,xy}$	-0.20			$\phi_{32,xy}$	0.00
(5,1,1)	$\phi_{11,xx}$	-0.12				
	$\phi_{11,yy}$	0.09				
	$\phi_{11,xy}$	0.00				
	$\phi_{11,yz}$	0.06				

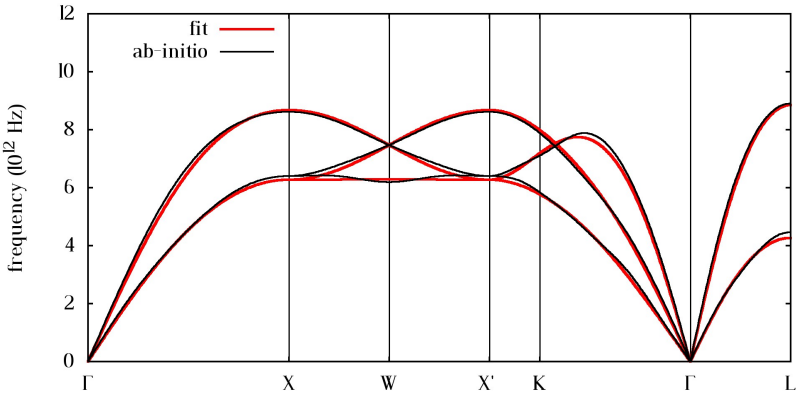

Figure 3.2: Phonon frequencies along high-symmetry directions obtained from fitted force constants (red line) and obtained from ab-initio force constants (black line) for fcc Ni.

3.3.2 Comparison of phonon frequencies and phonon polarization vectors obtained from the experimental and from the ab-initio force-constant model

The phonon frequencies obtained from ab-initio force constants and obtained from fitted force constants are compared with each other. First of all the frequencies are compared for the high-symmetry directions, then they are compared for the whole Brillouin zone.

The comparison of the frequencies along high-symmetry directions is shown in fig. 3.2 for Ni, in fig. 3.3 for Al and in fig. 3.4 for Fe. The agreement is nearly perfect for fcc Ni and only few deviations can be found. The agreement is a bit worse at the X-, X'- and W-point for fcc Al and at the N-point in bcc Fe. Certainly, a comparison for non-high-symmetry directions is more interesting since the fitted force constants are usually fitted to the high-symmetry directions or at least tested for the high-symmetry directions. Moreover, a comparison of phonon polarization vectors is even more interesting because it is not really clear how wrong the polarization vectors obtained from fitted force constants are (see subsection 3.1.3).

Therefore, I compare the phonon frequencies and polarization vectors

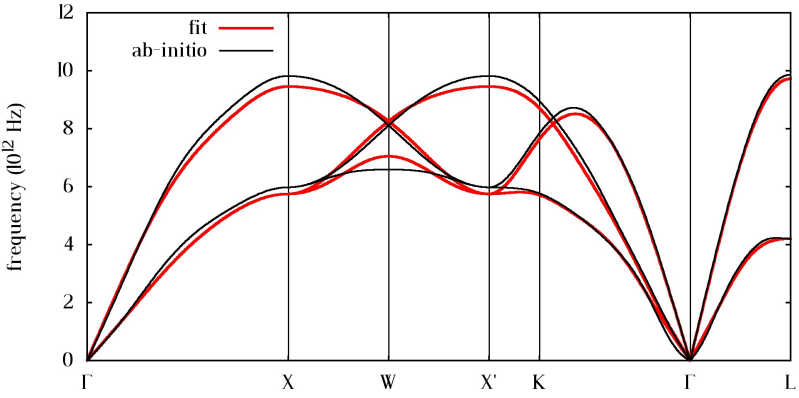

Figure 3.3: Phonon frequencies along high-symmetry directions obtained from fitted force constants (red line) and obtained from ab-initio force constants (black line) for fcc Al.

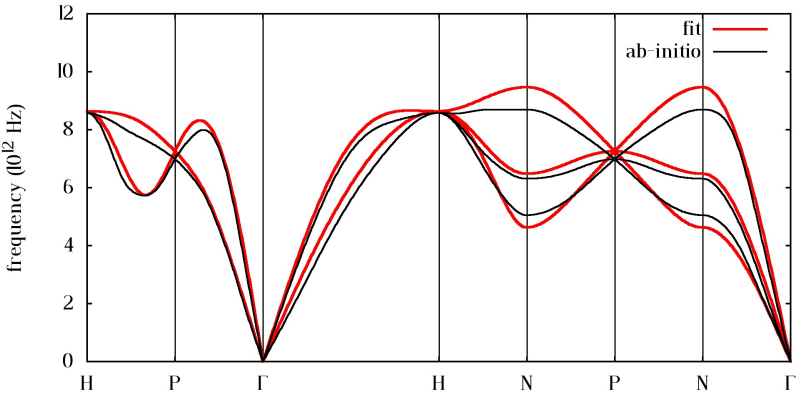

Figure 3.4: Phonon frequencies along high-symmetry directions obtained from fitted force constants (red line) and obtained from ab-initio force constants (black line) for bcc Fe.

in the whole phonon Brillouin zone. The procedure is described in the following: The set of fitted force constants yields three phonon frequencies $\omega^{\text{fit}}_{\mu\mathbf{q}}$, $\mu = 1,2,3$ and three polarization vectors $\mathbf{e}^{\text{fit}}_{\mu\mathbf{q}}$, $\mu = 1,2,3$ for every phonon wavevector $\mathbf{q}$. The same holds for the set of ab-initio force constants which yields $\omega^{\text{ab-initio}}_{\nu\mathbf{q}}$, $\nu = 1,2,3$ and $\mathbf{e}^{\text{ab-initio}}_{\nu\mathbf{q}}$, $\nu = 1,2,3$. It is not clear from the very beginning how to compare the frequencies and polarization vectors. There are in total six possibilities:

1. $\mu_1 = 1$ with $\nu_1 = 1$, $\mu_2 = 2$ with $\nu_2 = 2$, $\mu_3 = 3$ with $\nu_3 = 3$
2. $\mu_1 = 1$ with $\nu_1 = 1$, $\mu_2 = 2$ with $\nu_2 = 3$, $\mu_3 = 3$ with $\nu_3 = 2$
3. $\mu_1 = 1$ with $\nu_1 = 2$, $\mu_2 = 2$ with $\nu_2 = 1$, $\mu_3 = 3$ with $\nu_3 = 3$
4. $\mu_1 = 1$ with $\nu_1 = 2$, $\mu_2 = 2$ with $\nu_2 = 3$, $\mu_3 = 3$ with $\nu_3 = 1$
5. $\mu_1 = 1$ with $\nu_1 = 3$, $\mu_2 = 2$ with $\nu_2 = 2$, $\mu_3 = 3$ with $\nu_3 = 1$
6. $\mu_1 = 1$ with $\nu_1 = 3$, $\mu_2 = 2$ with $\nu_2 = 1$, $\mu_3 = 3$ with $\nu_3 = 2$.

To determine the correct possibility a combination of frequency and eigenvector argumentation is used.

1. Look at just one special q-point $\widetilde{\mathbf{q}}$ where the following condition is fulfilled: All three frequencies $\omega^{\text{fit}}_{\mu\widetilde{\mathbf{q}}}$ are clearly separated for $\mu = 1,2,3$, i.e., not degenerate or near a degeneracy, and all three frequencies $\omega^{\text{ab-initio}}_{\nu\widetilde{\mathbf{q}}}$ are clearly separated for $\nu = 1,2,3$. Then, it makes sense to compare the maximum frequency of the ab-initio force-constant model with the maximum frequency of the fitted force-constant model $|\omega^{\text{fit}}_{\mu_{\max}\widetilde{\mathbf{q}}} - \omega^{\text{ab-initio}}_{\nu_{\max}\widetilde{\mathbf{q}}}|$, and consequently the comparison of the minimum frequencies $|\omega^{\text{fit}}_{\mu_{\min}\widetilde{\mathbf{q}}} - \omega^{\text{ab-initio}}_{\nu_{\min}\widetilde{\mathbf{q}}}|$ and middle frequencies $|\omega^{\text{fit}}_{\mu_{\text{mid}}\widetilde{\mathbf{q}}} - \omega^{\text{ab-initio}}_{\nu_{\text{mid}}\widetilde{\mathbf{q}}}|$ makes sense. In principle, it could be possible that this choice is wrong but the calculation showed that this choice is in general correct. It is certainly wrong for q-points at or near a degeneracy.

2. The eigenvectors of neighboring q-points on the same branch μ or ν are almost perfectly parallel for dense q-point grids. The scalar product is almost 1, for example $\mathbf{e}^{\text{fit}}_{\mu\mathbf{q}_1} \cdot \mathbf{e}^{\text{fit}}_{\mu\mathbf{q}_2} \approx 1$, where $\mathbf{q}_1$ and $\mathbf{q}_2$ are neighboring q-points on a dense grid. This is wrong for q-points at or near degeneracies!

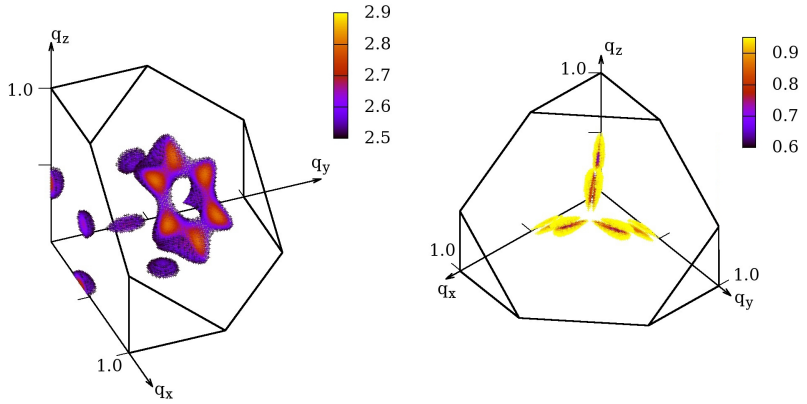

Figure 3.5: Differences between the calculation with ab-initio force constants and the calculation with fitted force constants [31] for fcc Ni. (a) relative phonon frequency deviation in percent (only greater than 2.5%), (b) modulus of the scalar product between the polarization vectors (only less than 0.95). From ref. [26]. Copyright by the American Physical Society.

3. For regions which are far away from a degeneracy point we can find the right comparison of branches with a combination of step 1. and step 2. For regions near or at a degeneracy point where the criterion of step 1. and step 2. fails, one cannot find the correct comparison. Therefore, these points are omitted for the comparison of eigenvectors but taken into account for the comparison of the frequencies because the frequencies are anyway almost the same even if one had chosen the wrong combination. Note that directly at the degeneracy point any linear combination of eigenvectors is again an eigenvector.

With this procedure at hand the comparison of phonon frequencies and polarization vectors obtained from ab-initio and from fitted force-constants can be made. Fig. 3.5, fig. 3.6 and fig. 3.7 show the difference of frequencies (see (a)) and polarization vectors (see (b)) for fcc Ni, fcc Al and bcc

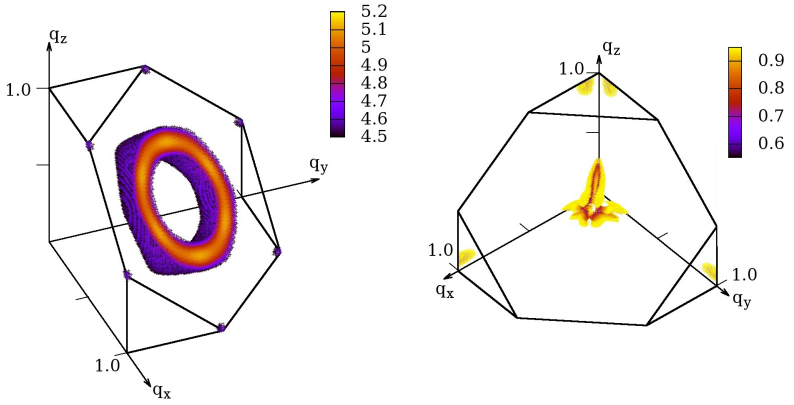

Figure 3.6: Differences between the calculation with ab-initio force constants and the calculation with fitted force constants [39] for fcc Al. (a) relative phonon frequency deviation in percent (only greater than 4.5%), (b) modulus of the scalar product between the polarization vectors (only less than 0.95). From ref. [26]. Copyright by the American Physical Society.

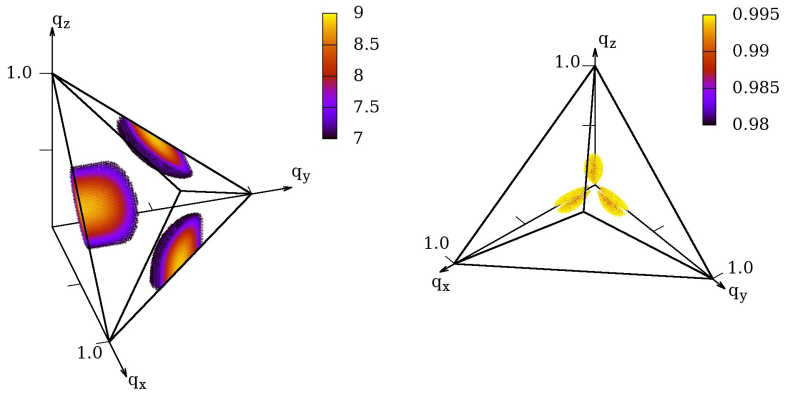

Figure 3.7: Differences between the calculation with ab-initio force constants and the calculation with fitted force constants [40] for bcc Fe. (a) relative phonon frequency deviation in percent (only greater than 7%), (b) modulus of the scalar product between the polarization vectors (only less than 0.995). From ref. [26]. Copyright by the American Physical Society.

Fe, respectively, for a 100×100×100-grid in the first octant of the first phonon Brillouin zone ($q_x, q_y, q_z \geq 0$).

The frequency difference is normalized by the maximum frequency in the Brillouin zone, $|\omega_{\mu\mathbf{q}}^{\text{fit}} - \omega_{\nu\mathbf{q}}^{\text{ab-initio}}|/\omega_{\max}$ and is given in percent. The deviation is up to 2.9% for Ni, up to 5.2% for Al and up to 9% for Fe and for all three materials only in small regions of the Brillouin zone whereas in most regions the deviations between the two results are very small.

The deviation of polarization vectors is given as modulus of the scalar product, $|\mathbf{e}_{\mu\mathbf{q}}^{\text{fit}} \cdot \mathbf{e}_{\nu\mathbf{q}}^{\text{ab-initio}}|$, i.e., $|\cos\phi|$ is given where ϕ is the angle between $\mathbf{e}_{\mu\mathbf{q}}^{\text{fit}}$ and $\mathbf{e}_{\nu\mathbf{q}}^{\text{ab-initio}}$. There are only small regions of the Brillouin zone for which the scalar products are smaller than 0.95 for Ni and Al and smaller than 0.995 for Fe, and in these regions the scalar products reach values down to 0.6 for Ni and Al and down to 0.98 for Fe. Obviously, the smallest deviations can be found for Fe although the frequency deviations are the largest of the three materials.

In summary, the investigations showed that there are indeed deviations between the frequencies and polarization vectors obtained from the ab-initio force constants and obtained from the fitted force constants. However, the deviations are not large and only small parts of the phonon Brillouin zone are affected. One can conclude that for a calculation for which reliable phonon frequencies and polarization vectors are necessary it is also possible to take force constants which were fitted to phonon frequencies only (without using polarization vectors). Probably, the symmetry requirements for the unitary transformation of the force-constant matrix is restrictive enough to give good results for both frequencies and polarization vectors. Probably, similar results can be obtained for other three-dimensional metals and it is concluded that time-consuming ab-initio calculations are not necessary to obtain reliable frequencies and polarization vectors in the whole phonon Brillouin zone.

4 Ultrafast demagnetization after laser pulse irradiation

As already explained in the introduction one can distinguish two main ultrafast demagnetization effects: the all-optical switching and the ultrafast demagnetization. They are closely related but only the latter is discussed in this thesis and fig. 1.1 shows a schematic picture of the typical experiment. In fig. 1.1 (a) a ferromagnetic material with in-plane magnetization (on a substrate) is irradiated by a fs laser pulse and in (b) one can see a sharp drop of the magnetization by about 40% within about 100 fs.

4.1 Basics

4.1.1 Experiments and models in the past

Pioneers in demagnetization experiments with laser pulses were Agranat et al. [2] in 1984 and Vaterlaus et al. [3, 4] in 1991 and 1992. Agranat et al. made experiments with Ni and measured demagnetization times in the ns timescale. Vaterlaus et al. used Fe and Gd and estimated a demagnetization time in the 100 ps timescale. In the pioneering experiments quite long laser pulses in the ps or ns range were used.

Beaurepaire and coworkers made a real breakthrough when they showed in 1996 that it is possible to demagnetize a thin Ni film in less than 1 ps after irradiation with a 60 fs laser pulse [1]. They used a 20 nm Ni film with a 100 nm MgF_2 coating as sample. The laser fluence was 7 mJ cm^{-2}. The magneto-optical Kerr effect (pump-probe) was used to measure the magnetization as function of time. The authors used the three-temperature model to explain the ultrafast demagnetization which is an extension of the earlier two-temperature model [41]. The three-temperature model is a phenomenological model in which the system is separated into three different subsystems: spinless electrons, spins and

lattice. Every subsystem has a temperature and a specific heat, and the three subsystems are coupled among each other with coupling constants.

Only one year later Scholl and coworkers also reported on an ultrafast demagnetization within about a ps in a thin Ni film grown on Au [42]. They measured the polarization of the photo-excited electrons in a two-photon photo spectroscopy. The time resolution in their experiment was a bit worse compared with Beaurepaire's experiment, and therefore the ultrafast demagnetization is not as clearly visible as in Beaurepaire's publication.

In 2000 Koopmans et al. raised the question whether the magneto-optical Kerr effect signal is really due to the demagnetization or whether there are artifacts [43]. They pinpointed it to the question "Ultrafast Magneto-Optics in Nickel: Magnetism or Optics?". Nowadays a lot of different experimental methods have been performed in order to measure the ultrafast demagnetization. These are mainly magneto-optical Kerr effect experiments, two-photon photo emission spectroscopy and XMCD (x-ray magnetic circular dichroism) measurements. All of them show a clear ultrafast demagnetization within about some few hundreds of fs, and nowadays it is not doubted anymore that the ultrafast demagnetization experiments show a real demagnetization (not an artifact).

A first theoretical model was published by Zhang and Hübner [44]. They suggested a direct interaction of laser photons with electrons via spin-orbit coupling. However, simple estimates by Koopmans et al. [45, 46] gave a photo-quenching of about 10^{-4} μ_B/atom for ferromagnetic Ni which is too small to explain the observed demagnetization (Ni has an atomic magnetic moment of 0.64 μ_B/atom). The issue of photo-quenching is discussed in subsection 4.2.1 with newer experiments.

4.1.2 Excitation and processes thereafter

Normally, the sample contains a ferromagnetic thin film on a substrate which can be insulating or conducting. To prevent the ferromagnetic film from oxidation it has a capping layer on top (e.g., Cu). In most experiments the laser penetration depth is as large as the sample thickness (but not larger) to avoid contributions from the substrate. The penetration depth δ is defined by Lambert-Beer's law $I(d) = I_0 \exp(-d/\delta)$ where I is the reduced intensity as function of the thickness d and I_0 is the full intensity. The pump laser spot size is usually smaller than the area of the

thin ferromagnetic film (pump laser spot size: 1.5×0.5 mm^2, area of the film: 5×5 mm^2 in refs. [47, 48]). The probe spot size is usually smaller or equal to the pump laser spot size (probe x-ray spot size: 0.5×0.1 mm^2 and pump laser spot size: 1.5×0.5 mm^2 in ref. [47]; probe x-ray spot size: 1.0×0.2 mm^2 and pump laser spot size: 1.5×0.5 mm^2 in ref. [48]; pump and probe laser spot diameter: 0.2 mm in ref. [42]). It is already mentioned here that any in-plane effects, e.g., in-plane propagating spin waves or majority electrons which reduce the measured magnetization because they are outside the probe spot, can be neglected for the following reason: Even if they propagate with the speed of light ($3 \cdot 10^8$ m/s), the distance they travel within 100 fs is only 0.03 mm which is very small compared with the probe spot size of about 0.2 mm. However, effects perpendicular to the plane can be possible since the sample is only about 20 nm thick (see subsection 4.2.6).

Fig. 4.1 shows schematically the occupation number of electronic states as function of energy for different stages. In fig. 4.1 (a) the situation before the laser action at 0 K is depicted. Fig. 4.1 (b) shows the occupation after laser irradiation. Some electrons below the Fermi energy are excited to higher (formerly unoccupied) levels above the Fermi energy. To a very good approximation the laser excitation does not flip the spin. The final state cannot be described by a Fermi-Dirac function, it is non-thermal. The electron-electron interaction is very strong and the excited electrons thermalize via electron-electron scattering into a thermal Fermi-Dirac distribution corresponding to an enhanced electron temperature shown in fig. 4.1 (c). The thermalization process takes less than 100 fs [18, 49]. The electrons are not yet in equilibrium with the lattice. Electron-phonon scattering leads to a further thermalization shown in fig. 4.1 (d). Electrons and lattice are in equilibrium now. This process takes some few ps [50, 51]. It is the slow lattice cooling that leads to a remagnetization. The process of remagnetization is quite complicated (heat transport with the non-irradiated parts of the sample, heat transport with environment) and is not explained further in this thesis. The dynamics of remagnetization can be found in refs. [52, 53]. After the remagnetization the system is again in the ground state (fig. 4.1 (a)).

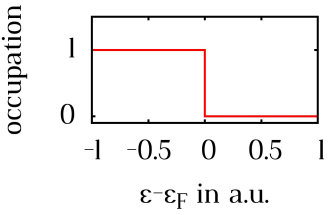

(a) before laser excitation

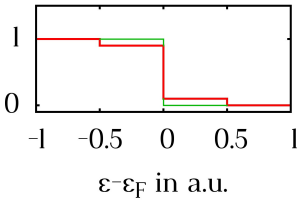

(b) after laser excitation

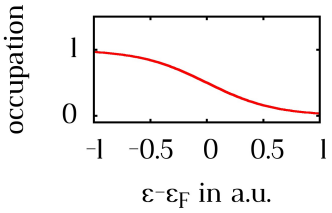

(c) after electron-electron scattering

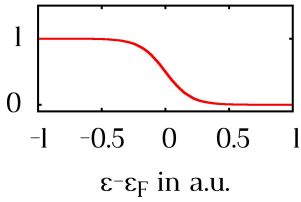

(d) after electron-phonon scattering

Figure 4.1: Occupation number as function of energy (a) before laser excitation (at 0 K), (b) after laser excitation (schematic), (c) after electron-electron scattering (schematic) and (d) after electron-phonon scattering (schematic).

4.2 Status quo

This section gives an overview of the current status quo of the research on ultrafast demagnetization.

4.2.1 Direct interaction with the laser light

As already mentioned in section 4.1.1 one of the first explanations of the ultrafast demagnetization was the direct interaction with the laser photons. Several models have been published, the most important ones are: Zhang and Hübner in 2000 [44], Bigot et al. in 2009 [54], Zhang et al. in 2009 [55], Si and Zhang in 2010 [56]. Easy estimates by Koopmans et al. [45, 46] showed that there are too few photons to explain the observed demagnetization. They estimated a demagnetization of about $10^{-4}\mu_B$/atom for ferromagnetic Ni if only photons are responsible for the demagnetization (Ni has an atomic magnetic moment of 0.64 μ_B/atom). There was also some controversy about the correctness of ref. [55] by Carva, Battiato and Oppeneer [57]. Experiments give strong evidence that the direct interaction with the laser photons only play a minor role. First, the largest part of the demagnetization occurs after the laser irradiation. Second, Dalla Longa et al. [58], Rhie et al. [50] and Eschenlohr et al. [59] give experimental proofs against a photo-quenching. In summary, a noticeable effect by the laser photons seems to be unlikely.

4.2.2 One-step and two-step demagnetization dynamics

In principle one can distinguish two different types of dynamics: the one-step demagnetization "type-I" (e.g., in Ni, Co and Fe) on a short timescale (hundred fs) as shown in fig. 1.1 (b) and the two-step demagnetization "type-II" (e.g., in Gd and Tb) on a longer timescale (several ps) with a subsequent second demagnetization on an even longer timescale. They can be described on the same footing within the microscopic three-temperature model [18] which is similar to the three-temperature model. Temperature and fluence dependent measurements were done for Ni, and the microscopic three-temperature model successfully predicted a change from type-I to type-II dynamics (however on a shorter timescale than in Gd or Tb) when increasing the temperature [60]. However, the microscopic three-temperature model depends on several parameters which are

not very well known and the underlying mechanisms remain hidden.

4.2.3 Light emission

Light is emitted during the demagnetization process since the magnetization changes with time. Measurements were done by Beaurepaire et al. [61] and by Hilton et al. [62]. The emitted light is in the THz range and linearly polarized. In principle the emission of linearly polarized light could lead to a demagnetization in a dichroic material (which Ni is), however, it is assumed to be a small effect and is usually not discussed. A further discussion of the light emission follows in subsection 4.3.2.

4.2.4 Spin and orbital angular momentum

The expectation value of the spin angular momentum $\langle\widehat{\mathbf{S}}\rangle$ and of the orbital angular momentum $\langle\widehat{\mathbf{L}}\rangle$ build the magnetization $\mathbf{M}$

$$\mathbf{M} = \mu_{\mathrm{B}} \left(\langle\widehat{\mathbf{L}}\rangle + g\langle\widehat{\mathbf{S}}\rangle \right) \tag{4.1}$$

where g is the g-factor. In transition metals the orbital angular momentum is almost completely quenched by the crystal field and therefore the spin angular momentum builds the magnetization to a good approximation. It is possible to measure the dynamics of $\langle\widehat{\mathbf{S}}\rangle$ and $\langle\widehat{\mathbf{L}}\rangle$ during the ultrafast demagnetization experiment with XMCD (x-ray magnetic circular dichroism). This was done by Stamm et al. in 2007 [47] for Ni and by Boeglin et al. in 2010 for CoPd [17]. The authors could exclude a flow of angular momentum from the spin angular momentum $\langle\widehat{\mathbf{S}}\rangle$ to the orbital angular momentum $\langle\widehat{\mathbf{L}}\rangle$. The experiments revealed a decrease of both $\langle\widehat{\mathbf{S}}\rangle$ and $\langle\widehat{\mathbf{L}}\rangle$. In CoPd the dynamics of the orbital angular momentum was a bit faster than the dynamics of the spin angular momentum.

4.2.5 Spin-flip processes

Spin-flip processes are very popular to explain the ultrafast demagnetization. The most important ones are electron-electron, electron-magnon and electron-phonon spin-flip scattering which are described in the following. In principle other scattering mechanisms are imaginable, e.g.,

electron-defect or electron-interface scattering, but these are assumed to be of minor importance [46].

1. Spin-flip scattering is often discussed in the simplified version of Elliott [63] and Yafet [64] where the matrix-elements and rate equations are not calculated directly. The spin-flip relaxation time T_1 is related with the non-spin-flip (Drude) relaxation time τ. The Elliott-Yafet relation reads

$$\frac{1}{T_1} = pb^2 \frac{1}{\tau} \tag{4.2}$$

where p is a material-dependent proportionality factor and b^2 is the spin-mixing factor explained in subsection 2.2.3. It was shown by Beuneu and Monod [65] that p is between 1 and 10 for most metals. The spin-mixing factor b^2 is calculated for several elements in refs. [22, 23]. It is 0.025 for Ni and 0.024 for Fe using a thermal smearing of 25 meV. Koopmans et al. showed that an Elliott-Yafet parameter pb^2 well below 1 can be sufficient to explain the demagnetization experiments [66]. The Elliott-Yafet parameter for Ni and Fe is approximately in the range between 0.02 and 0.3 (if $1 < p < 10$). Therefore it was concluded in ref. [23] that the demagnetization experiments could well be explained with the Elliott-Yafet mechanism. Though, the Elliott-Yafet relation does not say anything about the underlying scattering mechanism.

2. Electron-electron scattering was theoretically investigated by Krauß et al. [67]. A simple band structure and simplifying assumptions for the Coulomb and the dipole matrix elements were used. Within this model the demagnetization in Ni and Co could be explained by electron-electron spin-flip processes. However, some of the same authors admitted an overestimation of the energy deposited by the excitation pulse [68] and hence, the result is not on a firm footing.

   I want to make an important remark: If electron-electron spin-flip scattering is responsible for the demagnetization, one would have to explain where the spin angular momentum goes to. It can only stay in the electronic system, i.e., go to the orbital angular momentum which is a contradiction to Stamm's experiments [47]. The authors of ref. [67] implicitly assume that the lattice is a perfect sink of

angular momentum which would require electron-phonon scatterings in addition.

3. Electron-magnon scattering was first suggested by Carpene et al. [69]. Without spin-orbit coupling a magnon absorption or emission cannot change the magnetization because of the angular momentum conservation required for the single-scattering process. In the authors' mind an electron scatters with a magnon decreasing the spin angular momentum in the following way: Because of the spin-orbit coupling $\widehat{\mathbf{LS}} = \widehat{L}_z\widehat{S}_z + 1/2 \cdot (\widehat{L}^+\widehat{S}^- + \widehat{L}^-\widehat{S}^+)$ a decrease of the spin angular momentum $\widehat{S}^-$ creates an increase of the orbital angular momentum $\widehat{L}^+$ which is immediately quenched by the crystal field. It is claimed that the crystal field quenching (also called orbital quenching) is a very fast process. I want to note that the crystal field quenching is probably also mediated via electron-phonon scattering processes. Because of ref. [47] an increase of the orbital angular momentum can only occur on a very short timescale (smaller than the experimental resolution of ref. [47]), and therefore one had to assume that the orbital angular momentum is transferred to the lattice by electron-phonon scatterings in that extremely short time.

   Another publication showed experimentally [70] that magnon emission by hot electrons indeed occurs on the fs timescale in Fe.

4. Most promising is certainly the electron-phonon spin-flip scattering because the lattice is a possible sink for angular momentum whereas in electron-electron or electron-magnon scattering one has problems to argue where the spin angular momentum goes to. The microscopic three-temperature model showed that electron-phonon scattering combined with atomic spin-flips can explain the demagnetization experiments in principle [18]. However, several approximations enter the microscopic three-temperature model. Ab-initio calculations by Carva et al. [71, 72] and Essert et al. [68, 73] came to the conclusion that electron-phonon scattering within a fixed band structure cannot explain the experimentally observed demagnetization. Only few approximations entered the ab-initio calculations. It was suggested in ref. [68] that a dynamic band structure which respects a varying exchange splitting should be used in the calculation instead. A change in the band structure and especially in the ex-

change splitting was observed in experiments [48, 50, 74] and could in principle change the results. In ref. [74] Stamm et al. observed a reduction of the spin-orbit coupling of about 6%. Carva et al. [71] found out that a non-equilibrium electron distribution results in a higher demagnetization rate than a thermal electron distribution but still not enough to explain the experiments. This is in contradiction to Koopmans et al. [18] who claimed that the thermal electrons are responsible for the main demagnetization.

5. A very recent publication by Schellekens and Koopmans [75] suggests that single-electron spin-flips in combination with atomic spin-flips (using the microscopic three-temperature model) can explain the demagnetization whereas single-electron spin-flips in a rigid-band structure alone can never reproduce the experimental demagnetization rates because of a lack of driving force of demagnetization. The authors showed that the microscopic three-temperature model naturally explains the demagnetization by a thermal disorder of the atomic magnetic moments. So, they claim that one should not only look at the longitudinal reduction of the atomic magnetic moment (length reduction) but also on the transverse reduction (disorder)[3]. This is only possible if both magnons and phonons are taken into account. One can imagine several processes where phonons and magnons are involved:
   - Three-particle scattering processes between electron, magnon and phonon: Three-particle scattering processes are in general very unlikely. To the best of my knowledge it has never been discussed before in the literature of ultrafast demagnetization.
   - Phonon-magnon scattering processes: Phonon-magnon scattering is a very slow process in the order of 100 ps [76] (whereas electron-phonon scattering is in the order of 1 ps) and usually seen as irrelevant for Ni and Fe on a fs timescale [1, 18, 61].
   - Depletion/diffusion of magnons: Magnons could diffuse into the substrate so that they deplete in the sample. In principle this could be very similar to the dynamics suggested by Battiato et al. [77] discussed in subsection 4.2.6.

[3] It was always assumed that a disorder (transverse reduction) is too slow to explain a dynamics on the fs timescale since phonon-magnon scattering (which is necessary to explain Bloch's $T^{3/2}$-law) is a very slow process on the 100 ps timescale [76].

- Combined electron-phonon and electron-magnon scattering processes: Electron-phonon scattering and electron-magnon scattering could happen one after another. Spin-up and spin-down electrons can both absorb or emit phonons and flip their spin. However, only spin-down electrons can emit a magnon and flip their spin ($\downarrow \rightarrow \uparrow$ +magnon) and only spin-up electrons can absorb magnons and flip their spin ($\uparrow$ +magnon $\rightarrow \downarrow$) due to angular momentum conservation which is required in electron-magnon single-scattering processes. A combined electron-phonon and electron-magnon spin-flip scattering process could be:

  $$\begin{aligned} \uparrow + \text{phonon} &\rightarrow \downarrow \\ \downarrow &\rightarrow \uparrow + \text{magnon} \end{aligned} \tag{4.3}$$

  or effectively

  $$\uparrow + \text{phonon} \rightarrow \uparrow + \text{magnon}. \tag{4.4}$$

  The electron-phonon scattering transports the angular momentum to the lattice and the electron-magnon scattering changes the directions of the atomic magnetic moments which leads naturally to a demagnetization. It could well be that these combined electron-phonon and electron-magnon scattering processes are important, though, one has to check carefully how realistic this model is. Especially, one has to compare the electron-phonon and electron-magnon scattering rates (investigations on this line are under way in our group, see PhD thesis of Michael Haag and ref. [78]). They could be in the same order of magnitude or have a totally different order of magnitude. If the rates are different, the slower process determines the combined electron-phonon/electron-magnon scattering dynamics.

This list is certainly not complete and there are definitely even more possibilities involving phonons and magnons.

The ultrafast demagnetization process can also be described by a Landau-Lifshitz-Bloch equation [79] which is a generalized Gilbert equation including temperature and a longitudinal and transverse damping parameter. While the model includes nicely both longitudinal and transverse damping, the underlying microscopic mechanisms are not specified.

In summary, the electron-phonon spin-flip scattering is more promising to explain the ultrafast demagnetization than the electron-electron and electron-magnon scattering alone since the sink for angular momentum (the lattice) is clear for electron-phonon scattering. However, ab-initio results including the very accurate results of the present thesis (see chapter 7) give hints to a minor role of electron-phonon scattering when calculating with a fixed band structure. It has to be tested whether the results change for a dynamical change of the band structure (see chapter 7) and whether combined single-electron spin-flip and atomic spin-flip scattering processes suggested by Schellekens and Koopmans [75] are realistic.

4.2.6 Superdiffusive spin transport

Only recently Battiato, Carva and Oppeneer suggested a demagnetization via superdiffusive spin transport into the non-insulating substrate [77]. They argue theoretically that excited electrons in the sp-bands have a high velocity (about 1 nm/fs) and that the excited electrons have different lifetimes dependent on their spins (according to a parallel or antiparallel alignment with the magnetization) which results in a high mobility of the majority carriers (high mean-free path) and a low mobility (low mean-free path) of the minority carriers. The gradient between the hot excitation in the ferromagnetic film (e.g., Ni) and the low excitation in the non-insulating substrate (e.g., Al) leads to a diffusion from the film toward the substrate. Because of the high velocity (1 nm/fs) the authors call it "superdiffusive". The majority carriers scatter much less than the minority carriers so that there is a depletion of majority carriers in the film whereas the minority carriers are trapped in the film. This builds a spin current but not a charge current. According to the authors this can lead to a demagnetization of about 50% within 200 fs without any spin-flip channel.

The same authors show in a further theoretical publication (which considers only superdiffusive spin transport but no other mechanisms for ultrafast demagnetization) the magnetic moment per atom as function of time and sample depth [80]. In addition they show the theoretical magneto-optical Kerr signal. The simulations are done for four different samples: 10 nm Ni on Al, 10 nm Ni on MgO, 10 nm Fe on Al, 10 nm Fe on MgO. The majority carriers can diffusive into the Al substrate, however this is not possible for the insulating MgO substrate. The calculated

magneto-optical Kerr signal for Ni on MgO and for Fe on MgO shows a decrease which is about 20 times smaller than for Ni on Al and Fe on Al. The simulations show an increase of magnetic moment per atom at the Ni/MgO-interface which is compensated by a decrease of magnetic moment per atom at the surface.

New experiments support the idea of superdiffusive spin transport [59, 81, 82, 83, 84]. It is successfully used to explain the experimental observations for conducting substrates. However, it is not yet clear how strong the influence of the superdiffusive spin transport is for an insulating substrate. Experiments with insulating substrates show an ultrafast demagnetization within about 100 fs, too [49, 52, 58, 60, 69], although superdiffusive spin transport is small for insulating substrates. For this reason not much attention was paid to the substrate before Battiato's publication [77]. Probably, the influence of the superdiffusive spin transport is rather low and spin-flip processes should be dominant in systems with insulating substrates. Superdiffusive spin-transport might enhance the demagnetization in systems with conducting substrates. This is in line with the latest publication by Schellekens et al. [85] and with the latest publication on Fe/X/Ni multilayers (X is an interlayer) [86] which supports the idea that both superdiffusive spin-transport and spin-flip processes contribute considerably to the demagnetization depending on the conductivity of the interlayer.

4.2.7 Domain structure

One could imagine that the domain structure changes during the demagnetization process. It is shown with time and spatially resolved soft x-ray measurements (spatial resolution: 100 nm) in ref. [84] that the magnetic structure for a Co/Pd multilayer film is not modified during the demagnetization process, i.e., no domain effects could be observed. Furthermore, arguments for a superdiffusive spin transport are given.

4.3 Angular momentum conservation

This section is based on ref. [87].

4.3.1 Conditions for angular momentum conservation

The demagnetization is directly linked to a loss of spin angular momentum (see eq. (4.1)). It is a fundamental law in physics that the total angular momentum is conserved in a rotationally invariant system. An important example is the Einstein-de Haas effect [88]: A paramagnetic cylinder is fixed to a thin thread. At some time the paramagnetic cylinder is magnetized by an external electromagnetic field and thereafter the cylinder starts to rotate. The rotation compensates the magnetization, fulfilling the total angular momentum conservation. The question arises whether the ultrafast demagnetization is something like an Einstein-de Haas effect [45]. The quenching of the magnetization could results in a small net rotation of the sample.

In literature the angular momentum conservation was usually discussed in the following way [45, 46, 58, 89, 90]: During the demagnetization experiment the magnetization, i.e., the spin angular momentum, is reduced and therefore the question arises where the spin angular momentum goes to. For simplicity we do not consider the substrate or capping layer as sink for angular momentum. Also we neglect that there might be a direct interaction between the electrons and the laser photons. Then, we are left with the following equation

$$\Delta\langle\widehat{\mathbf{J}}\rangle = \Delta\langle\widehat{\mathbf{L}}_e\rangle + \Delta\langle\widehat{\mathbf{S}}_e\rangle + \Delta\langle\widehat{\mathbf{L}}_l\rangle + \Delta\langle\widehat{\mathbf{L}}_{ph}\rangle = 0 \tag{4.5}$$

where Δ denotes the difference, $\langle\widehat{\mathbf{J}}\rangle$ is the expectation value of the total angular momentum operator, $\widehat{\mathbf{L}}_e$ and $\widehat{\mathbf{S}}_e$ are the orbital and spin angular momentum operators of the electrons, respectively, and $\widehat{\mathbf{L}}_l$ and $\widehat{\mathbf{L}}_{ph}$ denote the angular momentum operator of the lattice and the emitted photons. In principle, magnons can also change the spin angular momentum of the electrons $\langle\widehat{\mathbf{S}}_e\rangle$ but this conserves the total spin angular momentum and should not influence the demagnetization itself. An angular momentum flow from $\langle\widehat{\mathbf{S}}_e\rangle$ to $\langle\widehat{\mathbf{L}}_e\rangle$ seems to be unlikely since Stamm et al. [47] measured a decrease of both the spin angular momentum and the orbital angular momentum. An angular momentum flow from $\langle\widehat{\mathbf{S}}_e\rangle$ to $\langle\widehat{\mathbf{L}}_{ph}\rangle$ is also not reasonable since the emitted photons are linearly polarized. Looking at eq. (4.5) an angular momentum flow from $\langle\widehat{\mathbf{S}}_e\rangle$ to $\langle\widehat{\mathbf{L}}_l\rangle$ seems to be the most likely.

4.3.2 Doubts on the angular momentum conservation

One important precondition for the angular momentum conservation is the rotational invariance of the system. It is not fulfilled in the experiments because the sample is fixed on a holder which is fixed on a table. A possible rotation of the sample is therefore transferred to the holder. However, a net rotation is probably not possible within the short timescale of few hundred fs for the following reason: In order to build a net rotation the different phonon modes have to interact with each other (phonon-phonon interaction) via anharmonicities and finally collapse in a collective mode with phonon wavevector $\mathbf{q} = 0$ which carries the angular momentum. The lifetime of phonons in transition metals due to anharmonic phonon-phonon interaction was calculated in ref. [91]. It is about 10^{-10} s which is some magnitudes greater than the demagnetization timescale of about 100 fs. Therefore, the timescale of 100 fs is too short to build up a collective mode with phonon wavevector $\mathbf{q} = 0$ and hence, the system can be seen as rotationally invariant.

Furthermore, the electrons and phonons (which are in the THz frequency range) could reabsorb the emitted linearly polarized photons in the THz frequency range (see subsection 4.2.3). This would change the expectation value of the electron spin angular momentum operator $\langle \widehat{\mathbf{S}}_e \rangle$ and the phonon orbital angular momentum operator $\langle \widehat{\mathbf{L}}_l \rangle$ in eq. (4.5) because of two reasons: First, linearly polarized light can be decomposed in left- and right-circularly polarized light. In dichroic materials (e.g., Ni) left- and right-circularly polarized light is absorbed differently. Second, the emission of linearly polarized light is not spherically symmetric since the magnetization change is in-plane of a thin flat sample. Therefore some wavevector directions are preferred. As a result, the total situation for a thin flat sample is not rotationally invariant, and the precondition for angular momentum conservation is not fulfilled.

So far, the reabsorption of linearly polarized light has not been investigated quantitatively in any publication. Obviously it is assumed that the change of $\langle \widehat{\mathbf{S}}_e \rangle$ and $\langle \widehat{\mathbf{L}}_l \rangle$ due to reabsorption of linearly polarized light (with probably small magnitudes) is rather small and can be neglected within a good approximation.

In summary, eq. (4.5) should hold approximately if one can neglect the substrate, the capping layer and the irradiating laser photons.

5 Electron-phonon scattering, rate equations and relaxation time

It is the scope of this thesis to investigate whether the electron-phonon spin-flip scattering can in principle explain the ultrafast demagnetization. This is done by calculating the demagnetization rates and by calculating the Elliott-Yafet relaxation time which are then compared with the experimental values. The analytical equations are given in this chapter and are discussed very critically. The main source for this chapter is ref. [64].

5.1 Fermi's golden rule

An initial electronic state $\Psi^{s}_{j\mathbf{k}}$ with band index j, wavevector $\mathbf{k}$ and dominant spin-character s ($s = \uparrow, \downarrow$) can scatter at a phononic state with wavevector $\mathbf{q}$ and polarization λ. The final electronic state $\Psi^{s'}_{j'\mathbf{k}'}$ has the band index j', wavevector $\mathbf{k}'$ and dominant spin character s'. Thereby, quasi momentum conservation $\mathbf{k} + \mathbf{q} = \mathbf{k}' + \mathbf{G}$ ($\mathbf{G}$ is a reciprocal lattice vector) and energy conservation holds. The dominant spin-character can be conserved ($s = s'$) or changed ($s \neq s'$). In the following only spin-flip processes with $s \neq s'$ are considered because they are mainly responsible for the magnetization change. In principle also non-spin-flip processes can contribute to a magnetization change but it is shown in subsection 7.1.1 that this is only a minor effect in Ni and Fe (due to the very low spin-mixing for most of the states). The matrix element for such an electron-phonon spin-flip scattering is given by [12, 64]

$$M^{\lambda,B}_{j\mathbf{k}s,j'\mathbf{k}'s'} = \langle \Psi^{s'}_{j'\mathbf{k}'} | W'_{\lambda,B} | \Psi^{s}_{j\mathbf{k}} \rangle$$

with the electron-phonon scattering operator (here: only for paramagnets, extension to ferromagnets in section 6.1)

$$W'_{\lambda,B} = \sum_{n=1}^{\widetilde{N}} e^{i\mathbf{q}\mathbf{R}_n^0} \Bigg\{ \left(\mathbf{n}_{\mathbf{q}\lambda}^B \ \nabla_{n,B}\right) \cdot \Bigg[V(\mathbf{r};\{\mathbf{R}'_{n,B}\}) \begin{pmatrix} 1 & 0 \\ 0 & 1 \end{pmatrix} + \sum_i \frac{\hbar}{4m_e^2c^2} \left(\nabla_{\mathbf{r}} V(\mathbf{r};\{\mathbf{R}'_{n,B}\}) \times \widehat{\mathbf{p}}\right)_i \underline{\underline{\widehat{\sigma}}}_i \Bigg] \Bigg\} \Bigg|_{\mathbf{R}_{n,B}=\mathbf{R}^0_{n,B}} . \tag{5.1}$$

The detailed derivation can be found in appendix A of ref. [12].

$V(\mathbf{r};\{\mathbf{R}'_{n,B}\})$ denotes the lattice potential at position $\mathbf{r}$ which is dependent on all the positions of the lattice atoms $\{\mathbf{R}'_{n,B}\}$ with cell index n ($n = 1, ..., \widetilde{N}$; $\widetilde{N}$: number of elementary cells, in principle of an infinitely large solid but it is shown in section 6.2 that the problem reduces to one elementary cell) and basis index B ($B = 1, ..., \widetilde{B}$; $\widetilde{B}$: number of basis indices). The position of the lattice atom $\mathbf{R}_{n,B} = \mathbf{R}_n^0 + \mathbf{R}_B^0 + \delta\mathbf{R}_{n,B} = \mathbf{R}_{n,B}^0 + \delta\mathbf{R}_{n,B}$ is given by the equilibrium position of the elementary cell $\mathbf{R}_n^0$, the basis vector $\mathbf{R}_B^0$ and the displacement $\delta\mathbf{R}_{n,B}$. $\nabla_{n,B}$ is the gradient with respect to $\mathbf{R}_{n,B}$ and the prime in $\mathbf{R}'_{n,B}$ and $W'_{\lambda,B}$ indicates that the gradient $\nabla_{n,B}$ only applies to the lattice atom with indices n and B. $\mathbf{n}_{\mathbf{q}\lambda}^B$ denotes the phonon polarization vector, $\widehat{\mathbf{p}}$ the momentum operator and $\underline{\underline{\widehat{\sigma}}}_i$ the Pauli matrix.

The first summand of eq. (5.1) represents the distortion of the lattice potential and is called "Elliott term" because Elliott was the first who recognized that already the first summand does not vanish if the states are spin-mixed [63]

$$\left\langle \Psi^{s'}_{j'\mathbf{k}'} \middle| \sum_{n=1}^{\widetilde{N}} e^{i\mathbf{q}\mathbf{R}_n^0} \left(\mathbf{n}_{\mathbf{q}\lambda}^B \ \nabla_{n,B}\right) \cdot V(\mathbf{r};\{\mathbf{R}'_{n,B}\}) \begin{pmatrix} 1 & 0 \\ 0 & 1 \end{pmatrix} \middle| \Psi^{s}_{j\mathbf{k}} \right\rangle \neq 0. \tag{5.2}$$

The second summand represents the distortion of the spin-orbit coupling and is called "Yafet term" because Yafet was the first who recognized that the second term can be as large as the first term [64].

The transition rate (probability for a transition from state $\Psi^s_{j\mathbf{k}}$ to state

$\Psi^{s'}_{j'\mathbf{k}'}$ per unit time) is given by Fermi's golden rule [12, 64]

$$W^{\lambda}_{j\mathbf{k}s,j'\mathbf{k}'s'} = \frac{2\pi}{\hbar}\left|\sum_B \sqrt{\frac{1}{M_B}} M^{\lambda,B}_{j\mathbf{k}s,j'\mathbf{k}'s'}\right|^2 \frac{\hbar}{2N\ \omega_{\mathbf{q}\lambda}} \cdot$$
$$\cdot \left\{ b_{\mathbf{q}\lambda}\ \delta(\varepsilon^{s'}_{j'\mathbf{k}'} - (\varepsilon^{s}_{j\mathbf{k}} + \hbar\omega_{\mathbf{q}\lambda})) + \ (b_{-\mathbf{q}\lambda}+1)\ \delta(\varepsilon^{s'}_{j'\mathbf{k}'} - (\varepsilon^{s}_{j\mathbf{k}} - \hbar\omega_{-\mathbf{q}\lambda}))\right\}. \tag{5.3}$$

M_B is the atomic mass with basis index B, N denotes the number of atoms in the unit cell and $b_{\mathbf{q}\lambda} = [\exp(\hbar\omega_{\mathbf{q}\lambda}/kT_p) - 1]^{-1}$ is the phonon Bose distribution function with phonon temperature T_p. The first term in curly brackets represents an absorption of a phonon with wavevector $\mathbf{q}$ and polarization λ. Thereby quasi momentum conservation[4] $\mathbf{k} + \mathbf{q} = \mathbf{k}' + \mathbf{G}$ and energy conservation $\varepsilon^{s'}_{j'\mathbf{k}'} = \varepsilon^{s}_{j\mathbf{k}} + \hbar\omega_{\mathbf{q}\lambda}$ is demanded. The second term is the induced and spontaneous emission of a phonon with wavevector $-\mathbf{q}$ and polarization λ. Thereby quasi momentum conservation $\mathbf{k} = \mathbf{k}' + (-\mathbf{q}) + \mathbf{G}$ and energy conservation $\varepsilon^{s'}_{j'\mathbf{k}'} = \varepsilon^{s}_{j\mathbf{k}} - \hbar\omega_{-\mathbf{q}\lambda}$ is demanded. Since $\omega_{\mathbf{q}\lambda} = \omega_{-\mathbf{q}\lambda}$ always holds, also $b_{\mathbf{q}\lambda} = b_{-\mathbf{q}\lambda}$ holds.

5.2 Discussion of Fermi's golden rule

Fermi's golden rule is a time-dependent perturbation theory in first order. The higher orders can be neglected if the perturbation time is short and if the perturbation strength is weak. One does not have a more precise criterion at hand and has to accept this hand-waving statement. The first-order approximation makes Fermi's golden rule a Markov process, i.e., the scattering process does not depend on preceding scattering processes.

On the other hand the perturbation time must be long enough in order to replace the $\sin x/x$-function (appearing in the derivation of Fermi's golden rule) by a delta function. A criterion for this is

$$\frac{2\pi\hbar}{t} \ll \Delta\varepsilon. \tag{5.4}$$

[4]The origin of the quasi momentum conservation is the translational symmetry with respect to translation vectors (in contrast to the general translational symmetry). Due to Bloch's theorem a quasi momentum is only defined except for a reciprocal lattice vector. Therefore the quasi momentum is restricted to the first Brillouin zone.

$2\pi\hbar/t$ is the full width at half maximum of the $\sin x/x$-function which must be much less than the width of energy differences $\Delta\varepsilon$ between initial and final states. $\Delta\varepsilon$ is the maximum phonon energy (40 meV) in the case of electron-phonon scattering. Therefore, the perturbation time should be

$$t \gg \frac{2\pi\hbar}{40 \text{ meV}} \approx 100 \text{ fs}. \tag{5.5}$$

Together with the first criterion (short perturbation time) the perturbation time for electron-phonon scattering should be in the time range $1 \text{ s} \ggg t \gg 100$ fs. Since the phenomenon of ultrafast demagnetization is on the timescale of 100 fs, it is in principle not allowed to replace the $\sin x/x$-function by a delta-function.

In summary, it is not clear whether a perturbation theory in first order is valid and, furthermore, it is also not clear whether the replacement of the $\sin x/x$-function by a delta-function gives errors. It is therefore questionable whether Fermi's golden rule gives reliable results for such short timescales. However, Fermi's golden rule is used in the theory of conductivity with success. This is a hint that the approximations are nevertheless reasonable but it is only a hint. If one believes in the first-order approximation but not in the delta-function approximation, one could simply replace the delta-function in Fermi's golden rule by the $\sin x/x$-function.

Using a quantum kinetic theory (density-matrix theory) one could calculate the time-dependent quantum-mechanical expansion of the system without using Fermi's golden rule. Thereby, the processes are non-Markov, and energy is not conserved. The theory has been worked out in the master's thesis in ref. [92] (see also ref. [93]). After having implemented this theory, it is possible to compare the quantum kinetic results with the results of Fermi's golden rule. Something similar was published by Schilp et al. [94] who calculated the electron-phonon quantum kinetics for laser-pulse-excited semiconductors. They showed that the mean kinetic energy of electrons and holes is almost the same for a Boltzmann, a semi-classical and a quantum-kinetic calculation already after some fs. However, the electron energy distribution differs for the different models. This is a hint that mean quantities might give similar results for a quantum-kinetic calculation and a calculation with Fermi's golden rule. It is the hope that the results given in this thesis are approximately correct despite using Fermi's golden rule since all results are mean quantities.

5.3 Angular momentum conservation

We see in section 5.1 that energy conservation is explicitly fulfilled and quasi momentum conservation is implicitly demanded during single electron-phonon scattering processes when using Fermi's golden rule. Angular momentum conservation must also hold in isotropic systems (see section 4.3) but it does not appear explicitly in Fermi's golden rule. The question arises why it is not included.

If one solves the many-particle Schrödinger equation for M ions and N electrons (using suitable initial conditions which model the laser pulse irradiation), angular momentum conservation would definitely be fulfilled. Of course it is impossible to solve the many-particle Schrödinger equation. The Born-Oppenheimer approximation decouples the many-particle wavefunction of electrons and ions into a product of many-electron wavefunction and many-ion wavefunction. The complicated many-particle Schrödinger equation is reduced to a Schrödinger equation for the electrons and a Schrödinger equation for the ions. Then, the many-electron wavefunction is expressed via effective one-electron wavefunctions, and the many-ion wavefunction via independent phonon wavefunctions. The interaction between electrons and ions is calculated as perturbation of first order using Fermi's golden rule. The phononic states for the calculation of the electron-phonon scattering are usually linearly polarized. It can be shown [95] that linearly polarized phonon states are not sharp angular momentum states and that the expectation value of the angular momentum is zero. It is possible to construct circularly or elliptically polarized phonon states with non-zero angular momentum expectation value by combination of linearly polarized phonons [95] but these phonon states are not stationary phonon states. Moreover, also the electronic states are not sharp angular momentum states since the angular momentum of the electron does not correspond to a good quantum number. That's why angular momentum conservation does not make sense for a single scattering process. It is not clear if the single-electron and single-phonon description "loses" the total angular momentum conservation or if the total angular momentum conservation is fulfilled "somehow" when summing over all possible scattering processes. To the best of my knowledge this is unfortunately nowhere discussed in literature.

5.4 Long-wavelength limit and screening

It is interesting to look at the long-wavelength limit of the phonon, i.e., vanishing phonon wavevector $\mathbf{q} \to 0$. For small wavevectors the exponential in the phonon distribution function can be expanded

$$b_{\mathbf{q}\lambda} = \frac{1}{\exp(\hbar\omega_{\mathbf{q}\lambda})/kT_p - 1} \approx \frac{1}{1 + \hbar\omega_{\mathbf{q}\lambda}/kT_p - 1} = \frac{kT_p}{\hbar\omega_{\mathbf{q}\lambda}}. \tag{5.6}$$

For small wavevectors the acoustic phonon frequency behaves like $\omega_{\mathbf{q}\lambda} \propto |\mathbf{q}|$. Hence, in the long-wavelength limit also $b_{\mathbf{q}\lambda} \approx b_{\mathbf{q}\lambda} + 1$ holds and eq. (5.3) reads

$$\begin{aligned}\lim_{\mathbf{q}\to 0} W^{\lambda}_{j\mathbf{k}s,j'\mathbf{k}'s'} =& \frac{2\pi}{\hbar} \left| \sum_B \sqrt{\frac{1}{M_B}} \lim_{\mathbf{q}\to 0} M^{\lambda,B}_{j\mathbf{k}s,j'\mathbf{k}'s'} \right|^2 \frac{kT_p}{2N\ \omega^2_{\mathbf{q}\lambda}} \cdot \\ & \left\{ \delta(\varepsilon^{s'}_{j'\mathbf{k}'} - (\varepsilon^{s}_{j\mathbf{k}} + \hbar\omega_{\mathbf{q}\lambda})) + \delta(\varepsilon^{s'}_{j'\mathbf{k}'} - (\varepsilon^{s}_{j\mathbf{k}} - \hbar\omega_{-\mathbf{q}\lambda})) \right\}.\end{aligned} \tag{5.7}$$

To determine the long-wavelength limit of the transition rate it is necessary to determine the long-wavelength limit for the matrix element

$$M^{\lambda,B}_{j\mathbf{k}s,j'\mathbf{k}'s'} \approx M^{\lambda,B}_{j\mathbf{k}s,j'\mathbf{k}'s'}\Big|_{\mathbf{q}=0} + \nabla_{\mathbf{q}}\ M^{\lambda,B}_{j\mathbf{k}s,j'\mathbf{k}'s'}\Big|_{\mathbf{q}=0} \cdot \mathbf{q} + ... \tag{5.8}$$

Yafet showed for paramagnets using symmetry arguments [64] that the zeroth and first order vanish if $s \neq s'$ (spin-flip). For the non-spin-flip matrix element ($s = s'$) already the first order does not vanish [64]

$$\begin{aligned}&\lim_{\mathbf{q}\to 0} M^{\lambda,B}_{j\mathbf{k}s,j'\mathbf{k}'s'} \propto |\mathbf{q}| \quad \text{if } s = s' \\ &\lim_{\mathbf{q}\to 0} M^{\lambda,B}_{j\mathbf{k}s,j'\mathbf{k}'s'} \propto |\mathbf{q}|^2 \quad \text{if } s \neq s'.\end{aligned} \tag{5.9}$$

This dependence is important since it avoids a divergence in the transition rates in eq. (5.7). A divergence for small $\mathbf{q}$ would be very strange because $\mathbf{q} = 0$ corresponds to a rigid translation or rotation of the crystal (without lattice distortion) which results in a vanishing scattering operator (at least for acoustic phonons).

Grimaldi and Fulde showed for paramagnets and in a Hartree approximation [96] that the spin-flip matrix element is proportional to $|\mathbf{q}|^2$ only

if the electron-phonon interaction is screened by two interactions. It is already known from textbooks [19] that the first summand of eq. (5.1) (lattice distortion) is screened by Coulomb electron-electron repulsion. The second summand (distortion of the spin-orbit coupling) is screened by the spin-other-orbit interaction [96].

Rajagopal and Mochena published one year later [97] that one needs the spin-same-orbit and the spin-other-orbit interaction for the screening in magnetic systems[5]. Furthermore, he claimed that Grimaldi and Fulde do not mean the spin-other-orbit interaction but the spin-same-orbit interaction.

Now, I want to comment on the different methods for the calculations of the matrix element in eq. (5.1).

1. The electron-phonon matrix element is often calculated using a very simple model. Mueller and Rethfeld [98, 99] use a model matrix element from Ashcroft [19] which contains only the screened lattice distortion (using several approximations). The spin-orbit coupling distortion of the matrix element (Yafet part) is totally neglected.

2. Essert and Schneider [68, 73] calculate the electron-phonon matrix elements ab-initio (lattice distortion plus spin-orbit coupling distortion) within a rigid-ion approximation. The rigid-ion approximation avoids any screening of the lattice distortion or the spin-orbit coupling distortion because the potential is shifted rigidly without deformation (see subsection 6.1.1). This should give wrong transition rates for small $\mathbf{q}$.

3. Carva et al. [71, 72] calculate the electron-phonon matrix elements in a supercell calculation (lattice distortion plus spin-orbit coupling distortion). Definitely, the lattice distortion is screened correctly but the spin-orbit coupling cannot be screened correctly since the spin-other-orbit interaction and spin-same-orbit interaction is not taken into account. However, small $\mathbf{q}$ correspond to large supercells which are anyway not possible to calculate.

In this thesis the rigid-ion approximation is used (see subsection 6.1.1) which avoids (see point 2.) any screening of the electron-phonon scattering

[5] In principle, spin-same-orbit and spin-other-orbit interaction could give further contributions to the electron-phonon scattering operator in eq. (5.1). To the best of my knowledge this has never been discussed so far.

and one has to take care when calculating with small phonon wavevectors. We see in section 6.5 and 6.6 that the transition rates would diverge for small $\mathbf{q}$ within the rigid-ion approximation. This can happen if very fine k-point grids are used! Usually, the results are the better the finer the grid is. Here, it is not the case!

The method of choice to study screening effects are supercell calculations with spin-other-orbit and spin-same-orbit interaction, however, small phonon wavevectors (i.e., large supercells) make problems in supercell calculations.

5.5 Rate equations

In the following the expression "chemical potential" μ and "Fermi energy" ε_F are used synonymously since for free electrons the expansion [19]

$$\mu = \varepsilon_\mathrm{F}\left[1 - \frac{1}{3}\left(\frac{\pi kT}{2\varepsilon_\mathrm{F}}\right)^2\right] \tag{5.10}$$

holds. The correction is only 0.01% for room temperature.

5.5.1 Driving force

Elliott and Yafet considered the following situation [63, 64]: A paramagnet with an equilibrium Fermi energy ε_F^0 is in an external magnetic field B. Due to the field the density of states are shifted by $\pm\mu_\mathrm{B}B$:

$$Z_B^\uparrow(\varepsilon) = Z^\uparrow(\varepsilon - \mu_\mathrm{B}B) \tag{5.11}$$

$$Z_B^\downarrow(\varepsilon) = Z^\downarrow(\varepsilon + \mu_\mathrm{B}B) \tag{5.12}$$

where $Z_B^{\uparrow,\downarrow}$ is the density of states in the external field and $Z^{\uparrow,\downarrow}$ without external field. Now, a new equilibrium Fermi energy ε_F^B establishes. Then, the external magnetic field is suddenly turned off. The density of states without external magnetic field are not shifted anymore but the chemical potentials still differ

$$\varepsilon_\mathrm{F}^\uparrow = \varepsilon_\mathrm{F}^B - \mu_\mathrm{B}B \tag{5.13}$$

$$\varepsilon_\mathrm{F}^\downarrow = \varepsilon_\mathrm{F}^B + \mu_\mathrm{B}B. \tag{5.14}$$

The system relaxes back to the equilibrium Fermi energy $\varepsilon_{\mathrm{F}}^{0}$. This relaxation process is the Elliott-Yafet process. It is important to note that $\mu_{\mathrm{B}}B$ is a very small quantity for reasonable magnetic fields. Even for a very high field of $B = 10$ T the quantity is very small $\mu_{\mathrm{B}}B \approx 0.6$ meV. Therefore, the equilibrium with and without external field is approximately the same $\varepsilon_{\mathrm{F}}^{B} \approx \varepsilon_{\mathrm{F}}^{0}$. The driving force in the Elliott-Yafet process is the difference between up- and down-chemical potential. The electron and phonon temperature is assumed to be equal and constant all the time $T = T_e = T_p$ (e.g. room temperature). The electron system can be described by a Fermi-Dirac distribution at every time

$$f(\varepsilon_{j\mathbf{k}}^{\uparrow}, \varepsilon_{\mathrm{F}}^{\uparrow}(t)) = \frac{1}{\exp((\varepsilon_{j\mathbf{k}}^{\uparrow} - \varepsilon_{\mathrm{F}}^{\uparrow}(t))/kT) + 1} \tag{5.15}$$

$$f(\varepsilon_{j\mathbf{k}}^{\downarrow}, \varepsilon_{\mathrm{F}}^{\downarrow}(t)) = \frac{1}{\exp((\varepsilon_{j\mathbf{k}}^{\downarrow} - \varepsilon_{\mathrm{F}}^{\downarrow}(t))/kT) + 1} \tag{5.16}$$

and the phonon system is described by a Bose distribution $b_{\mathbf{q}\lambda} = [\exp(\hbar\omega_{\mathbf{q}\lambda}/kT) - 1]^{-1}$.

The process of ultrafast demagnetization is totally different. The laser pulse (excitation energy about 1.5 eV !) produces a highly non-equilibrium situation without Fermi-Dirac distribution (see fig. 4.1 (b)). After electron-electron scattering the system has thermalized with the Fermi-Dirac distribution (see fig. 4.1 (c))

$$f(\varepsilon_{j\mathbf{k}}^{\uparrow}, \varepsilon_{\mathrm{F}}^{\uparrow}(t), T_e(t)) = \frac{1}{\exp((\varepsilon_{j\mathbf{k}}^{\uparrow} - \varepsilon_{\mathrm{F}}^{\uparrow}(t))/kT_e(t)) + 1} \tag{5.17}$$

$$f(\varepsilon_{j\mathbf{k}}^{\downarrow}, \varepsilon_{\mathrm{F}}^{\downarrow}(t), T_e(t)) = \frac{1}{\exp((\varepsilon_{j\mathbf{k}}^{\downarrow} - \varepsilon_{\mathrm{F}}^{\downarrow}(t))/kT_e(t)) + 1}. \tag{5.18}$$

and the Bose distribution $b_{\mathbf{q}\lambda} = [\exp(\hbar\omega_{\mathbf{q}\lambda}/kT_p) - 1]^{-1}$. At this point the chemical potentials are different ($\varepsilon_{\mathrm{F}}^{\uparrow} \neq \varepsilon_{\mathrm{F}}^{\downarrow}$) and also the electron temperature T_e and phonon temperature T_p are different ($T_e \neq T_p$). In ref. [51] it is shown that the lattice heats up very slowly (within 2 ps) and therefore it is a good approximation to assume that the phonon temperature is time-independent $T_p(t) = 300$ K=constant. It is also demonstrated in ref. [73] that a time-dependent phonon temperature does not have a big influence on the demagnetization dynamics.

After electron-electron scattering the system relaxes to a point (minimum of the magnetic moment) where the chemical potentials still differ, $\varepsilon_{\mathrm{F}}^{\uparrow} \neq \varepsilon_{\mathrm{F}}^{\downarrow}$. Directly thereafter the remagnetization starts which is not a topic of this thesis. The driving force of the ultrafast demagnetization, i.e., before having reached the minimum, is the difference in the chemical potentials *and* the difference in the temperatures.

The Elliott-Yafet process describes a near-equilibrium system which relaxes to its equilibrium whereas the process of demagnetization is a relaxation to an "intermediate equilibrium". The assumption is that the latter process can be described by the Elliott-Yafet process even though these are two totally different processes. Especially the temperature is taken as constant in the Elliott-Yafet process which is not the case for the ultrafast demagnetization!

It should be noted that one could also introduce different electron temperatures $T_e^{\uparrow}$ and $T_e^{\downarrow}$ like in ref. [98]. This is not done in this work.

5.5.2 Magnetic moment

The spin magnetic moment is given by the expectation value of the spin operator $\widehat{S}_z$

$$\begin{aligned} m_{j\mathbf{k}}^{s} =& -\frac{g_e \mu_{\mathrm{B}}}{\hbar} \langle \widehat{S}_z \rangle_{j\mathbf{k}s} = -\frac{g_e \mu_{\mathrm{B}}}{\hbar} \frac{\hbar}{2} \langle \underline{\underline{\widehat{\sigma}}}_z \rangle_{j\mathbf{k}s} = -\mu_{\mathrm{B}} \, \langle \Psi_{j\mathbf{k}}^{s} | \begin{pmatrix} 1 & 0 \\ 0 & -1 \end{pmatrix} | \Psi_{j\mathbf{k}}^{s} \rangle \\ =& -\mu_{\mathrm{B}} \left(\int \mathrm{d}^3 r \, (a_{j\mathbf{k}}^{s})^* a_{j\mathbf{k}}^{s} - \int \mathrm{d}^3 r \, (b_{j\mathbf{k}}^{s})^* b_{j\mathbf{k}}^{s} \right) = -\mu_{\mathrm{B}} \, (p_{j\mathbf{k}}^{\uparrow} - p_{j\mathbf{k}}^{\downarrow}) \\ =& -\mu_{\mathrm{B}} \, (2p_{j\mathbf{k}}^{\uparrow} - 1). \end{aligned} \tag{5.19}$$

$g_e \approx 2$ is the g-factor and the expectation value of the orbital angular momentum is almost totally quenched in transition metals. For a transition from a state $\Psi_{j\mathbf{k}}^{s}$ to a state $\Psi_{j'\mathbf{k}'}^{s'}$ $(s \neq s')$ the magnetic moment change is

$$m_{j\mathbf{k}s,j'\mathbf{k}'s'} = -\mu_{\mathrm{B}} \, (2p_{j'\mathbf{k}'}^{\uparrow} - 1) + \mu_{\mathrm{B}} \, (2p_{j\mathbf{k}}^{\uparrow} - 1) = -2\mu_{\mathrm{B}} \, (p_{j'\mathbf{k}'}^{\uparrow} - p_{j\mathbf{k}}^{\uparrow}). \tag{5.20}$$

The magnetic moment change is between 0 (if $p_{j'\mathbf{k}'}^{\uparrow} = 0.5$ and $p_{j\mathbf{k}}^{\uparrow} = 0.5$) and $\pm 2\mu_{\mathrm{B}}$ (if $p_{j'\mathbf{k}'}^{\uparrow} = 0$ and $p_{j\mathbf{k}}^{\uparrow} = 1$, or vice versa). For most of the states the spin-mixing is not large (see subsection 7.1.1), say the magnetic

moment is $-m$ for dominant-up states and $+m$ for dominant-down states where $m \lessapprox \mu_{\mathrm{B}}$, which means that the magnetic moment change per atom is about $\pm 2m$ for most of the transitions (see subsection 7.1.1). The difference between dominant down and up electrons per atom

$$D(t) = N^{\downarrow}(t) - N^{\uparrow}(t) \text{ , in equilibrium: } D_0 = N_0^{\downarrow} - N_0^{\uparrow} \tag{5.21}$$

is related to the magnetic moment per atom

$$M(t) = mD(t) \text{ , in equilibrium: } M_0 = mD_0 \tag{5.22}$$

if one assumes that *all* states have the same magnetic moment $\pm m$. The number of states per atom can be calculated as follows

$$N^s(t) = \int_{-\infty}^{+\infty} \mathrm{d}\varepsilon \; f(\varepsilon, \varepsilon_{\mathrm{F}}^s(t)) \; Z^s(\varepsilon) \tag{5.23}$$

$$\text{in equilibrium: } N_0^s = \int_{-\infty}^{+\infty} \mathrm{d}\varepsilon \; f(\varepsilon, \varepsilon_{\mathrm{F}}^0) \; Z^s(\varepsilon). \tag{5.24}$$

The exact calculation of the magnetic moment is given by a weighted integral over all spin magnetic moments in the first Brillouin zone (BZ) with volume Ω_{BZ}

$$\begin{aligned} M = & -\frac{g_e \mu_{\mathrm{B}}}{\hbar \Omega_{BZ}} \sum_j \int_{BZ} \mathrm{d}^3k \; f(\varepsilon_{j\mathbf{k}}) \langle \widehat{S}_z \rangle \\ = & -\frac{\mu_{\mathrm{B}}}{\Omega_{BZ}} \sum_j \int_{BZ} \mathrm{d}^3k \; f(\varepsilon_{j\mathbf{k}}) (p_{j\mathbf{k}}^{\uparrow} - p_{j\mathbf{k}}^{\downarrow}). \end{aligned} \tag{5.25}$$

5.5.3 Demagnetization rates

The total transition rate from dominant s to dominant s' (number of transitions per unit time) due to electron-phonon scattering reads

$$\begin{aligned} W^{s,s'}(t) = & \frac{1}{\Omega_{BZ}^2} \sum_{j,j',\lambda} \int_{BZ} \mathrm{d}^3k \int_{BZ} \mathrm{d}^3k' \\ & f\left(\varepsilon_{j\mathbf{k}}^s, \varepsilon_{\mathrm{F}}^s(t), T_e(t)\right) \left[1 - f\left(\varepsilon_{j'\mathbf{k}'}^{s'}, \varepsilon_{\mathrm{F}}^{s'}(t), T_e(t)\right)\right] W_{j\mathbf{k}s,j'\mathbf{k}'s'}^{\lambda}. \end{aligned} \tag{5.26}$$

$f(\varepsilon^s_{j\mathbf{k}}, \varepsilon^s_{\mathrm{F}}(t), T_e(t))$ is the probability that the state $j\mathbf{k}s$ is occupied and $1 - f(\varepsilon^{s'}_{j'\mathbf{k}'}, \varepsilon^{s'}_{\mathrm{F}}(t), T_e(t))$ is the probability that the state $j'\mathbf{k}'s'$ is unoccupied. The change in the difference is given by

$$\frac{dD}{dt} = 2(W^{\uparrow,\downarrow}(t) - W^{\downarrow,\uparrow}(t)) \tag{5.27}$$

and the factor 2 arises because one spin-flip changes the difference D by a factor of 2. The rate of the magnetic moment change (proportional to the demagnetization rate) would be

$$\frac{dM}{dt} = m\frac{dD}{dt} \tag{5.28}$$

if every state had the same magnetic moment m. Since this is not the case for all states, the correct weights are introduced using eq. (5.20)

$$\begin{aligned}\frac{dM}{dt} =& \frac{1}{\Omega^2_{BZ}} \sum_{j,j',\lambda} \int_{BZ} \mathrm{d}^3k \int_{BZ} \mathrm{d}^3k' \; m_{j\mathbf{k}\uparrow, j'\mathbf{k}'\downarrow} \cdot \\ & \Big\{ f(\varepsilon^{\uparrow}_{j\mathbf{k}}, \varepsilon^{\uparrow}_{\mathrm{F}}(t), T_e(t)) \left[1 - f(\varepsilon^{\downarrow}_{j'\mathbf{k}'}, \varepsilon^{\downarrow}_{\mathrm{F}}(t), T_e(t))\right] W^{\lambda}_{j\mathbf{k}\uparrow, j'\mathbf{k}'\downarrow} \\ & - f(\varepsilon^{\downarrow}_{j'\mathbf{k}'}, \varepsilon^{\downarrow}_{\mathrm{F}}(t), T_e(t)) \left[1 - f(\varepsilon^{\uparrow}_{j\mathbf{k}}, \varepsilon^{\uparrow}_{\mathrm{F}}(t), T_e(t))\right] W^{\lambda}_{j'\mathbf{k}'\downarrow, j\mathbf{k}\uparrow} \Big\}. \end{aligned} \tag{5.29}$$

5.5.4 Equilibrium rate equations

I introduce a short notation for the Fermi-Dirac distribution in equilibrium

$$f_0(\varepsilon^s_{j\mathbf{k}}) \equiv f(\varepsilon^s_{j\mathbf{k}}, \varepsilon^0_{\mathrm{F}}, T_0). \tag{5.30}$$

where the electron temperature and phonon temperature are equal $T_e = T_p = T_0$. In equilibrium the rate of the magnetic moment change dM/dt has to be zero:

$$\begin{aligned}\frac{dM}{dt} =& \frac{1}{\Omega^2_{BZ}} \sum_{j,j',\lambda} \int_{BZ} \mathrm{d}^3k \int_{BZ} \mathrm{d}^3k' \; m_{j\mathbf{k}\uparrow, j'\mathbf{k}'\downarrow} \cdot \\ & \Big\{ f_0(\varepsilon^{\uparrow}_{j\mathbf{k}}) \left[1 - f_0(\varepsilon^{\downarrow}_{j'\mathbf{k}'})\right] W^{\lambda}_{j\mathbf{k}\uparrow, j'\mathbf{k}'\downarrow} - f_0(\varepsilon^{\downarrow}_{j'\mathbf{k}'}) \left[1 - f_0(\varepsilon^{\uparrow}_{j\mathbf{k}})\right] W^{\lambda}_{j'\mathbf{k}'\downarrow, j\mathbf{k}\uparrow} \Big\} \\ & = 0. \end{aligned} \tag{5.31}$$

The term in curly brackets reads

$$
\begin{aligned}
& f_0(\varepsilon^{\uparrow}_{j\mathbf{k}}) \left[1 - f_0(\varepsilon^{\downarrow}_{j'\mathbf{k}'})\right] \frac{\pi}{N\omega_{\mathbf{q}\lambda}} \left| \sum_B \sqrt{\frac{1}{M_B}} M^{\lambda,B}_{j\mathbf{k}\uparrow,j'\mathbf{k}'\downarrow} \right|^2 \cdot \\
& \left\{ b_{\mathbf{q}\lambda}\ \delta(\varepsilon^{\downarrow}_{j'\mathbf{k}'} - (\varepsilon^{\uparrow}_{j\mathbf{k}} + \hbar\omega_{\mathbf{q}\lambda})) + \ (b_{\mathbf{q}\lambda} + 1)\ \delta(\varepsilon^{\downarrow}_{j'\mathbf{k}'} - (\varepsilon^{\uparrow}_{j\mathbf{k}} - \hbar\omega_{\mathbf{q}\lambda})) \right\} \\
& - f_0(\varepsilon^{\downarrow}_{j'\mathbf{k}'}) \left[1 - f_0(\varepsilon^{\uparrow}_{j\mathbf{k}})\right] \frac{\pi}{N\omega_{\mathbf{q}\lambda}} \left| \sum_B \sqrt{\frac{1}{M_B}} M^{\lambda,B}_{j'\mathbf{k}'\downarrow,j\mathbf{k}\uparrow} \right|^2 \cdot \\
& \left\{ b_{\mathbf{q}\lambda}\ \delta(\varepsilon^{\uparrow}_{j\mathbf{k}} - (\varepsilon^{\downarrow}_{j'\mathbf{k}'} + \hbar\omega_{\mathbf{q}\lambda})) + \ (b_{\mathbf{q}\lambda} + 1)\ \delta(\varepsilon^{\uparrow}_{j\mathbf{k}} - (\varepsilon^{\downarrow}_{j'\mathbf{k}'} - \hbar\omega_{\mathbf{q}\lambda})) \right\} \\
= & \frac{\pi}{N\omega_{\mathbf{q}\lambda}} \left| \sum_B \sqrt{\frac{1}{M_B}} M^{\lambda,B}_{j'\mathbf{k}'\downarrow,j\mathbf{k}\uparrow} \right|^2 \cdot \\
& \Bigg\{ \Big[f_0(\varepsilon^{\uparrow}_{j\mathbf{k}})\ (1 - f_0(\varepsilon^{\downarrow}_{j'\mathbf{k}'}))\ b_{\mathbf{q}\lambda} - f_0(\varepsilon^{\downarrow}_{j'\mathbf{k}'})\ (1 - f_0(\varepsilon^{\uparrow}_{j\mathbf{k}}))\ (b_{\mathbf{q}\lambda} + 1) \Big] \cdot \\
& \quad \delta(\varepsilon^{\downarrow}_{j'\mathbf{k}'} - (\varepsilon^{\uparrow}_{j\mathbf{k}} + \hbar\omega_{\mathbf{q}\lambda})) \\
& + \Big[f_0(\varepsilon^{\uparrow}_{j\mathbf{k}})\ (1 - f_0(\varepsilon^{\downarrow}_{j'\mathbf{k}'}))\ (b_{\mathbf{q}\lambda} + 1) - f_0(\varepsilon^{\downarrow}_{j'\mathbf{k}'})\ (1 - f_0(\varepsilon^{\uparrow}_{j\mathbf{k}}))\ b_{\mathbf{q}\lambda} \Big] \cdot \\
& \quad \delta(\varepsilon^{\downarrow}_{j'\mathbf{k}'} - (\varepsilon^{\uparrow}_{j\mathbf{k}} - \hbar\omega_{\mathbf{q}\lambda})) \Bigg\}. \qquad (5.32)
\end{aligned}
$$

Thereby it is used that the scattering operator has to be Hermitian, therefore $M^{\lambda,B}_{j\mathbf{k}\uparrow,j'\mathbf{k}'\downarrow} = (M^{\lambda,B}_{j'\mathbf{k}'\downarrow,j\mathbf{k}\uparrow})^*$, and that the delta function is symmetric, therefore $\delta(\varepsilon^{\downarrow}_{j'\mathbf{k}'} - (\varepsilon^{\uparrow}_{j\mathbf{k}} \pm \hbar\omega_{\mathbf{q}\lambda})) = \delta(\varepsilon^{\uparrow}_{j\mathbf{k}} - (\varepsilon^{\downarrow}_{j'\mathbf{k}'} \mp \hbar\omega_{\mathbf{q}\lambda}))$. It is now straightforward to show that the terms in squared brackets are zero if energy conservation holds

$$
\begin{aligned}
& f_0(\varepsilon^{\uparrow}_{j\mathbf{k}})\ (1 - f_0(\varepsilon^{\downarrow}_{j'\mathbf{k}'}))\ b_{\mathbf{q}\lambda} - f_0(\varepsilon^{\downarrow}_{j'\mathbf{k}'})\ (1 - f_0(\varepsilon^{\uparrow}_{j\mathbf{k}}))\ (b_{\mathbf{q}\lambda} + 1) = 0 \\
& \text{if } \varepsilon^{\downarrow}_{j'\mathbf{k}'} = \varepsilon^{\uparrow}_{j\mathbf{k}} + \hbar\omega_{\mathbf{q}\lambda} \text{ and} \\
& f_0(\varepsilon^{\uparrow}_{j\mathbf{k}})\ (1 - f_0(\varepsilon^{\downarrow}_{j'\mathbf{k}'}))\ (b_{\mathbf{q}\lambda} + 1) - f_0(\varepsilon^{\downarrow}_{j'\mathbf{k}'})\ (1 - f_0(\varepsilon^{\uparrow}_{j\mathbf{k}}))\ b_{\mathbf{q}\lambda} = 0 \\
& \text{if } \varepsilon^{\downarrow}_{j'\mathbf{k}'} = \varepsilon^{\uparrow}_{j\mathbf{k}} - \hbar\omega_{\mathbf{q}\lambda}. \qquad (5.33)
\end{aligned}
$$

This means that $dM/dt = 0$ in equilibrium as long as the scattering operator is Hermitian and energy conservation holds.

5.6 Relaxation time

The equation for the relaxation time can be found in ref. [64] for paramagnets. It is extended to ferromagnets in this section which is already published in ref. [100].

It is shown in subsection 5.5.1 that the Fermi energies are only shifted slightly by $\pm\mu_\mathrm{B}B$ in the Elliott-Yafet theory. It is questionable whether this near-equilibrium excitation still holds for the the ultrafast demagnetization process directly after electron-electron scattering but it definitely holds for the Elliott-Yafet process. A Taylor expansion for small deviations from the equilibrium seems reasonable

$$\begin{aligned} f(\varepsilon^s_{j\mathbf{k}}, \varepsilon^s_\mathrm{F}(t)) &\approx f_0(\varepsilon^s_{j\mathbf{k}}) + \frac{1}{1!}\left.\frac{\partial}{\partial \varepsilon^s_\mathrm{F}(t)} f(\varepsilon^s_{j\mathbf{k}}, \varepsilon^s_\mathrm{F}(t))\right|_{\varepsilon^s_\mathrm{F}(t)=\varepsilon^0_\mathrm{F}} \cdot (\varepsilon^s_\mathrm{F}(t) - \varepsilon^0_\mathrm{F}) \\ &= f_0(\varepsilon^s_{j\mathbf{k}}) + \eta(\varepsilon^s_{j\mathbf{k}}) \cdot (\varepsilon^s_\mathrm{F}(t) - \varepsilon^0_\mathrm{F}) \end{aligned} \tag{5.34}$$

where

$$\eta(\varepsilon^s_{j\mathbf{k}}) = \left.\frac{\partial}{\partial \varepsilon^s_\mathrm{F}(t)} f(\varepsilon^s_{j\mathbf{k}}, \varepsilon^s_\mathrm{F}(t))\right|_{\varepsilon^s_\mathrm{F}(t)=\varepsilon^0_\mathrm{F}} = \frac{\partial}{\partial \varepsilon^0_\mathrm{F}} f_0(\varepsilon^s_{j\mathbf{k}}) \xrightarrow{T\to 0} \delta(\varepsilon^s_{j\mathbf{k}} - \varepsilon^0_\mathrm{F}). \tag{5.35}$$

With this near-equilibrium approximation and the assumption of an exponential demagnetization we will see that a constant spin-flip relaxation time T_1 can be defined with the ansatz

$$\frac{dD}{dt} = -\frac{D(t) - D_0}{T_1}. \tag{5.36}$$

If the spin-mixing is small for most of the states the difference D is related to the magnetic moment $M(t) = mD(t)$ and hence

$$\frac{dM}{dt} = -\frac{M(t) - M_0}{T_1}. \tag{5.37}$$

This implies an exponential magnetization dynamics

$$M(t) = \big[M(t=0) - M_0\big] \cdot \exp(-t/T_1) + M_0. \tag{5.38}$$

At time $t = T_1$ the magnetization is $M(T_1) = \big[M(t=0) - M_0\big] \cdot \exp(-1) + M_0$.

We want to find an analytical expression for T_1. This can be achieved by finding independently an expression for $D(t)-D_0$ and for dD/dt using the approximations given above. Yafet derived the equations for paramagnets [64]. Here, the equations for a ferromagnet are given (see also refs. [12, 100]):

1. The expression for $D(t) - D_0$ can be found quite easily:

   $$D(t) - D_0 = (N^{\downarrow}(t) - N_0^{\downarrow}) - (N^{\uparrow}(t) - N_0^{\uparrow})$$

   with number conservation $N^{\uparrow}(t) + N^{\downarrow}(t) = N_0^{\uparrow} + N_0^{\downarrow}$

   $$= 2(N^{\downarrow}(t) - N_0^{\downarrow}) \tag{5.39}$$

   and with eqs. (5.23), (5.24) and (5.34)

   $$\approx 2(\varepsilon_{\mathrm{F}}^{\downarrow}(t) - \varepsilon_{\mathrm{F}}^{0})\widetilde{Z}^{\downarrow}(\varepsilon_{\mathrm{F}}^{0}) \tag{5.40}$$

   where $\widetilde{Z}^{\downarrow}(\varepsilon_{\mathrm{F}}^{0}) = \int \mathrm{d}\varepsilon \; Z^{\downarrow}(\varepsilon)\eta(\varepsilon)$. We see that the time-dependent Fermi energy $\varepsilon_{\mathrm{F}}^{\downarrow}(t)$ enters the equation.

2. An expression for dD/dt is found with eqs. (5.26), (5.27) and using the Taylor expansion (5.34):

   $$\begin{aligned}\frac{dD}{dt} =& \frac{2}{\Omega_{BZ}^2} \sum_{j,j',\lambda} \int_{BZ} \mathrm{d}^3k \int_{BZ} \mathrm{d}^3k' \\ & \Big\{ \Big[f_0(\varepsilon_{j\mathbf{k}}^{\uparrow}) + \eta(\varepsilon_{j\mathbf{k}}^{\uparrow})(\varepsilon_{\mathrm{F}}^{\uparrow}(t) - \varepsilon_{\mathrm{F}}^{0}) \Big] \cdot \\ & \quad \Big[1 - f_0(\varepsilon_{j'\mathbf{k}'}^{\downarrow}) - \eta(\varepsilon_{j'\mathbf{k}'}^{\downarrow})(\varepsilon_{\mathrm{F}}^{\downarrow}(t) - \varepsilon_{\mathrm{F}}^{0}) \Big] W^{\lambda}_{j\mathbf{k}\uparrow,j'\mathbf{k}'\downarrow} \\ & - \Big[f_0(\varepsilon_{j'\mathbf{k}'}^{\downarrow}) + \eta(\varepsilon_{j'\mathbf{k}'}^{\downarrow})(\varepsilon_{\mathrm{F}}^{\downarrow}(t) - \varepsilon_{\mathrm{F}}^{0}) \Big] \cdot \\ & \quad \Big[1 - f_0(\varepsilon_{j\mathbf{k}}^{\uparrow}) - \eta(\varepsilon_{j\mathbf{k}}^{\uparrow})(\varepsilon_{\mathrm{F}}^{\uparrow}(t) - \varepsilon_{\mathrm{F}}^{0}) \Big] W^{\lambda}_{j'\mathbf{k}'\downarrow,j\mathbf{k}\uparrow} \Big\}. \end{aligned} \tag{5.41}$$

   When inserting the equilibrium condition, eq. (5.31), and neglecting the second order terms $(\varepsilon_{\mathrm{F}}^{s}(t) - \varepsilon_{\mathrm{F}}^{0})^2$ the equation reads

   $$\frac{dD}{dt} = \frac{2}{\Omega_{BZ}^2} \sum_{j,j',\lambda} \int_{BZ} \mathrm{d}^3k \int_{BZ} \mathrm{d}^3k'$$

$$\Big\{ W^{\lambda}_{j\mathbf{k}\uparrow,j'\mathbf{k}'\downarrow} \Big[-f_0(\varepsilon^{\uparrow}_{j\mathbf{k}})\ \eta(\varepsilon^{\downarrow}_{j'\mathbf{k}'})\ (\varepsilon^{\downarrow}_{\mathrm{F}}(t)-\varepsilon^{0}_{\mathrm{F}}) + (1-f_0(\varepsilon^{\downarrow}_{j'\mathbf{k}'}))\ \eta(\varepsilon^{\uparrow}_{j\mathbf{k}})\ (\varepsilon^{\uparrow}_{\mathrm{F}}(t)-\varepsilon^{0}_{\mathrm{F}}) \Big] + W^{\lambda}_{j'\mathbf{k}'\downarrow,j\mathbf{k}\uparrow} \Big[f_0(\varepsilon^{\downarrow}_{j'\mathbf{k}'})\ \eta(\varepsilon^{\uparrow}_{j\mathbf{k}})\ (\varepsilon^{\uparrow}_{\mathrm{F}}(t)-\varepsilon^{0}_{\mathrm{F}}) - (1-f_0(\varepsilon^{\uparrow}_{j\mathbf{k}}))\ \eta(\varepsilon^{\downarrow}_{j'\mathbf{k}'})\ (\varepsilon^{\downarrow}_{\mathrm{F}}(t)-\varepsilon^{0}_{\mathrm{F}}) \Big] \Big\}. \tag{5.42}$$

Again the number conservation can be used, $N^{\downarrow}(t)-N^{\downarrow}_0 = -(N^{\uparrow}(t)-N^{\uparrow}_0)$ or $(\varepsilon^{\downarrow}_{\mathrm{F}}(t)-\varepsilon^{0}_{\mathrm{F}})\widetilde{Z}^{\downarrow}(\varepsilon^{0}_{\mathrm{F}}) \approx -(\varepsilon^{\uparrow}_{\mathrm{F}}(t)-\varepsilon^{0}_{\mathrm{F}})\widetilde{Z}^{\uparrow}(\varepsilon^{0}_{\mathrm{F}})$:

$$\frac{dD}{dt} = \frac{2}{\Omega^2_{BZ}} \sum_{j,j',\lambda} \int_{BZ} \mathrm{d}^3k \int_{BZ} \mathrm{d}^3k' \ \Big(-(\varepsilon^{\downarrow}_{\mathrm{F}}(t)-\varepsilon^{0}_{\mathrm{F}}) \Big) \cdot \Big\{ W^{\lambda}_{j\mathbf{k}\uparrow,j'\mathbf{k}'\downarrow} \left[f_0(\varepsilon^{\uparrow}_{j\mathbf{k}})\ \eta(\varepsilon^{\downarrow}_{j'\mathbf{k}'}) \ + (1-f_0(\varepsilon^{\downarrow}_{j'\mathbf{k}'}))\ \eta(\varepsilon^{\uparrow}_{j\mathbf{k}})\ \frac{\widetilde{Z}^{\downarrow}(\varepsilon^{0}_{\mathrm{F}})}{\widetilde{Z}^{\uparrow}(\varepsilon^{0}_{\mathrm{F}})} \right] + W^{\lambda}_{j'\mathbf{k}'\downarrow,j\mathbf{k}\uparrow} \left[f_0(\varepsilon^{\downarrow}_{j'\mathbf{k}'})\ \eta(\varepsilon^{\uparrow}_{j\mathbf{k}})\ \frac{\widetilde{Z}^{\downarrow}(\varepsilon^{0}_{\mathrm{F}})}{\widetilde{Z}^{\uparrow}(\varepsilon^{0}_{\mathrm{F}})} + (1-f_0(\varepsilon^{\uparrow}_{j\mathbf{k}}))\ \eta(\varepsilon^{\downarrow}_{j'\mathbf{k}'}) \right] \Big\}. \tag{5.43}$$

Using the above expressions for $D(t)-D_0$ and dD/dt one finds an equation for $1/T_1$:

$$\frac{1}{T_1} = -\frac{dD/dt}{D(t)-D_0} = \frac{1}{\Omega^2_{BZ}} \sum_{j,j',\lambda} \int_{BZ} \mathrm{d}^3k \int_{BZ} \mathrm{d}^3k' \Big\{ W^{\lambda}_{j\mathbf{k}\uparrow,j'\mathbf{k}'\downarrow} \left[\frac{f_0(\varepsilon^{\uparrow}_{j\mathbf{k}})\ \eta(\varepsilon^{\downarrow}_{j'\mathbf{k}'})}{\widetilde{Z}^{\downarrow}(\varepsilon^{0}_{\mathrm{F}})} + \frac{(1-f_0(\varepsilon^{\downarrow}_{j'\mathbf{k}'}))\ \eta(\varepsilon^{\uparrow}_{j\mathbf{k}})}{\widetilde{Z}^{\uparrow}(\varepsilon^{0}_{\mathrm{F}})} \right] + W^{\lambda}_{j'\mathbf{k}'\downarrow,j\mathbf{k}\uparrow} \left[\frac{f_0(\varepsilon^{\downarrow}_{j'\mathbf{k}'})\ \eta(\varepsilon^{\uparrow}_{j\mathbf{k}})}{\widetilde{Z}^{\uparrow}(\varepsilon^{0}_{\mathrm{F}})} + \frac{(1-f_0(\varepsilon^{\uparrow}_{j\mathbf{k}}))\ \eta(\varepsilon^{\downarrow}_{j'\mathbf{k}'})}{\widetilde{Z}^{\downarrow}(\varepsilon^{0}_{\mathrm{F}})} \right] \Big\}. \tag{5.44}$$

Luckily, the time-dependent Fermi energy $(\varepsilon^{\downarrow}_{\mathrm{F}}(t)-\varepsilon^{0}_{\mathrm{F}})$ drops out! It would be very complicated to calculate the Fermi energy $\varepsilon^{\downarrow}_{\mathrm{F}}(t)$ as function of time

and furthermore it would not be possible to define a time-independent relaxation time T_1 if $(\varepsilon_{\mathrm{F}}^{\downarrow}(t) - \varepsilon_{\mathrm{F}}^{0})$ would not drop out.

To summarize one can define a time-independent spin-flip relaxation time for ferromagnets

$$\frac{1}{T_1} = -\frac{dM/dt}{M(t) - M_0} \tag{5.45}$$

if the following approximations hold:

1. The system is excited to a near-equilibrium situation.
2. The magnetization dynamics can be described by an exponential decay.
3. The spin-mixing is small for most of the states.

Let's make a short note on the demagnetization rate in the Elliott-Yafet process: Suppose that T_1 is known. Then, the demagnetization rate for $t = 0$ is given by (using eq. (5.40) and $\varepsilon_{\mathrm{F}}^{B} \approx \varepsilon_{\mathrm{F}}^{0}$, see subsection 5.5.1)

$$\begin{aligned}\left.\frac{dM}{dt}\right|_{t=0} &= -\frac{M(t=0) - M_0}{T_1} \approx -\frac{2m(\varepsilon_{\mathrm{F}}^{\downarrow}(t=0) - \varepsilon_{\mathrm{F}}^{0})\widetilde{Z}^{\downarrow}(\varepsilon_{\mathrm{F}}^{0})}{T_1} \\ &= -\frac{2m(\varepsilon_{\mathrm{F}}^{B} + \mu_{\mathrm{B}}B - \varepsilon_{\mathrm{F}}^{0})\widetilde{Z}^{\downarrow}(\varepsilon_{\mathrm{F}}^{0})}{T_1} \approx -\frac{2m\ \mu_{\mathrm{B}}B\ \widetilde{Z}^{\downarrow}(\varepsilon_{\mathrm{F}}^{0})}{T_1}.\end{aligned} \tag{5.46}$$

The demagnetization rate is proportional to the magnetic field B.

5.7 Comparison: experiment, demagnetization rate and relaxation time

The original Elliott-Yafet process describes a system in near-equilibrium which relaxes exponentially to the equilibrium when the magnetic field is switched off. The near-equilibrium assumption is certainly a good approximation because the quantity $\mu_{\mathrm{B}}B$ is very small. Nothing is said about the dependence of the Fermi energy as function of time $\varepsilon_{\mathrm{F}}^{s}(t)$ because it drops out in the expression for the relaxation time.

The ultrafast demagnetization directly after electron-electron scattering describes a thermalized electron system which relaxes to the "intermediate

equilibrium" before it remagnetizes. In the next chapters two quantities are calculated for this experiment:

1. the rate of the magnetic moment change dM/dt (proportional to the demagnetization rate) for special times: Using eq. (5.29) the rate of the magnetic moment change for a special time t_x can be calculated. Thereby, the Fermi energies $\varepsilon_{\mathrm{F}}^{\uparrow}(t_x), \varepsilon_{\mathrm{F}}^{\downarrow}(t_x)$ and the electron temperature $T_e(t_x)$ are required. It is explained later how to determine these quantities. It is important that the electron and phonon temperature differ $T_e(t_x) \neq T_p(t_x)$. I want to stress that eq. (5.29) is neither limited to near-equilibrium excitations nor to an exponential decay.

   In principle it is possible to calculate iteratively the rate of the magnetic moment change as function of time. The Fermi energies $\varepsilon_{\mathrm{F}}^{\uparrow}(t), \varepsilon_{\mathrm{F}}^{\downarrow}(t)$ and electron temperatures $T_e(t)$ have to be determined for every time step since the equilibration of Fermi energies and temperatures is not included in the rate equations!

2. the relaxation time T_1: First of all we have to assume that we can calculate the relaxation time with eq. (5.44) even though the process of ultrafast demagnetization is totally different from the original Elliott-Yafet process (see subsection 5.5.1). Furthermore, we are restricted to the three approximations given below eq. (5.44). Koopmans et al. argue in favor of a near-equilibrium (first approximation) since they show that the non-thermal electrons should not be important [18]. The experiments show an exponential decay (second approximation) but it could be that our model does not if one calculated the full time-dependent dynamics. The spin-mixing is usually small for almost all states (third approximation) [22] but it could well be that "hot spots" (i.e., k-points with large spin-mixing) are important as was argued in ref. [101].

To decide whether the electron-phonon scattering plays a crucial role in the demagnetization experiments the rate of the magnetic moment change dM/dt and the relaxation time T_1 must be compared with experimental values. The relaxation time alone only gives an information about the timescale without information about the demagnetization strength. Also the approximations necessary to derive the equation for T_1 are not on a firm footing (see above). The relaxation time is easy to compute since it

only depends on equilibrium quantities whereas the rate of the magnetic moment change also depends on non-equilibrium values ($\varepsilon_{\mathrm{F}}^{\uparrow}(t_x), \varepsilon_{\mathrm{F}}^{\downarrow}(t_x)$, $T_e(t_x)$)! However, the demagnetization rate is definitely the better quantity to compare with experimental values since the theoretical expression for it does not depend on approximations (see above).

5.8 Phase space estimation and maximum possible demagnetization

In the following two possibilities are shown to estimate the available phase space for scattering and to estimate the maximum possible demagnetization. The possibilities are discussed critically in section 7.4.

Possibility 1 considers a system which scatters toward non-equilibrium for the majority and minority Fermi distribution functions (*all* possible scattering processes which lead to a demagnetization are taken into account) whereas possibility 2 considers a system which scatters toward equilibrium for the majority Fermi distribution function but not for the minority Fermi distribution function. It turns out that the difference between possibility 1 and 2 is not large (see section 7.4).

The basic assumption for possibility 1 and possibility 2 is that the demagnetization starts directly after thermalization via electron-electron scattering which is quite fast, less than 100 fs [18], see also section 6.6. Therefore, the phase space is only estimated for thermalized electron distributions.

I want to make a remark on minority or majority holes which are discussed in the following. Both minority and majority holes are implicitly taken into account in all previous equations since the Brillouin zone integrals consider all occupied and unoccupied states!

Possibility 1

I want to motivate the phase space estimation with a discussion about the situation at zero temperature which is the simplest situation: At T=0 K the Fermi distribution function is a step function (see fig. 5.1 (a)). All states are occupied up to the Fermi energy. Electrons in an energy range between $\varepsilon - \varepsilon_{\mathrm{F}}^{0} = -\hbar\omega_{\mathbf{q}\lambda}^{\max}$ and $\varepsilon - \varepsilon_{\mathrm{F}}^{0} = 0$ could absorb phonons where $\hbar\omega_{\mathbf{q}\lambda}^{\max}$ is the maximum possible phonon energy (about 40 meV) and (in

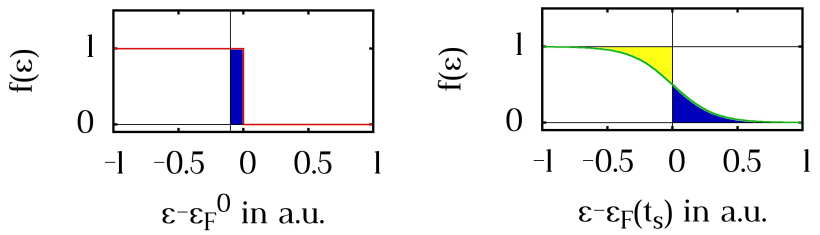

Figure 5.1: (a) Fermi distribution function for T=0 K. If the density of states was equal 1 for all energies, the blue area would give the number of electrons between $\varepsilon - \varepsilon_{\mathrm{F}}^{0} = -\hbar\omega_{\mathbf{q}\lambda}^{\max}$ and $\varepsilon - \varepsilon_{\mathrm{F}}^{0} = 0$. (b) Fermi distribution function for T=600 K. If the density of states was equal 1 for all energies, the blue area would give the number of electrons above the Fermi energy $\varepsilon_{\mathrm{F}}(t_s)$ and the yellow area would give the number of holes below the Fermi energy $\varepsilon_{\mathrm{F}}(t_s)$.

principle) could flip their spin (blue area in fig. 5.1 (a) if the density of states was equal 1 for all energies).

For higher electron temperatures $T_e(t_s)$ at time t_s (where electron-electron scattering is completed) with two different chemical potentials $\varepsilon_{\mathrm{F}}^{\uparrow}(t_s)$, $\varepsilon_{\mathrm{F}}^{\downarrow}(t_s)$ majority electrons above the Fermi energy $\varepsilon_{\mathrm{F}}^{\uparrow}(t_s)$ could absorb or emit phonons with spin-flip (blue area in fig. 5.1 (b) if the density of states was equal 1 for all energies) and minority holes below the Fermi energy $\varepsilon_{\mathrm{F}}^{\downarrow}(t_s)$ (yellow area in fig. 5.1 (b) if the density of states was equal 1 for all energies) could be filled by majority electrons via spin-flip scattering[6] in the energy range $\pm\hbar\omega_{\mathbf{q}\lambda}^{\max}$. Hence, the maximum possible demagnetization is achieved if all majority electrons above $\varepsilon_{\mathrm{F}}^{\uparrow}(t_s)$ make

[6]The minority holes are filled by minority electrons which were originally majority electrons but flipped their spin.

a spin-flip scattering[7,8] and all minority holes below $\varepsilon_{\mathrm{F}}^{\downarrow}(t_s)$ are filled by majority electrons (below $\varepsilon_{\mathrm{F}}^{\uparrow}(t_s)$) via spin-flip scattering while all minority electrons do not flip their spin. The number of majority electrons $\Delta N^{\uparrow}(t_s)$ above $\varepsilon_{\mathrm{F}}^{\uparrow}(t_s)$ and the number of majority holes $\Delta N^{h\uparrow}(t_s)$ below $\varepsilon_{\mathrm{F}}^{\uparrow}(t_s)$ is

$$\Delta N^{\uparrow}(t_s) = \int_{\varepsilon_{\mathrm{F}}^{\uparrow}(t_s)}^{+\infty} Z^{\uparrow}(\varepsilon) f^{\uparrow}(\varepsilon) \mathrm{d}\varepsilon \tag{5.47}$$

$$\Delta N^{h\uparrow}(t_s) = \int_{-\infty}^{\varepsilon_{\mathrm{F}}^{\uparrow}(t_s)} Z^{\uparrow}(\varepsilon) \left(1 - f^{\uparrow}(\varepsilon)\right) \mathrm{d}\varepsilon \tag{5.48}$$

where $f^{\uparrow}(\varepsilon) = f(\varepsilon, \varepsilon_{\mathrm{F}}^{\uparrow}(t_s), T_e(t_s))$.

Analogously, the number of minority electrons $\Delta N^{\downarrow}(t_s)$ above $\varepsilon_{\mathrm{F}}^{\downarrow}(t_s)$ and the number of minority holes $\Delta N^{h\downarrow}(t_s)$ below $\varepsilon_{\mathrm{F}}^{\downarrow}(t_s)$ is

$$\Delta N^{\downarrow}(t_s) = \int_{\varepsilon_{\mathrm{F}}^{\downarrow}(t_s)}^{+\infty} Z^{\downarrow}(\varepsilon) f^{\downarrow}(\varepsilon) \mathrm{d}\varepsilon \tag{5.49}$$

$$\Delta N^{h\downarrow}(t_s) = \int_{-\infty}^{\varepsilon_{\mathrm{F}}^{\downarrow}(t_s)} Z^{\downarrow}(\varepsilon) \left(1 - f^{\downarrow}(\varepsilon)\right) \mathrm{d}\varepsilon \tag{5.50}$$

where $f^{\downarrow}(\varepsilon) = f(\varepsilon, \varepsilon_{\mathrm{F}}^{\downarrow}(t_s), T_e(t_s))$.

The maximum possible decrease of the magnetic moment (proportional to the maximum possible demagnetization) is $\Delta M = 2\mu_{\mathrm{B}}(\Delta N^{\uparrow}(t_s) + \Delta N^{h\downarrow}(t_s))$ per atom[9].

Possibility 2

In equilibrium for $T_0 = 300$ K there are some electrons above the Fermi energy $\varepsilon_{\mathrm{F}}^{0}$ (see red curve of fig. 5.2). For the non-equilibrium situation

[7] It is implicitly assumed that majority electrons below the Fermi energy $\varepsilon_{\mathrm{F}}^{\uparrow}(t_s)$ do not absorb or emit phonons and flip their spins. This is a reasonable approximation since the energy range for absorption or emission below the Fermi energy $\varepsilon_{\mathrm{F}}^{\uparrow}(t_s)$ is only about $\hbar\omega_{\mathbf{q}\lambda}^{\max}$ which is quite small.

[8] It is assumed that majority electrons above the Fermi energy $\varepsilon_{\mathrm{F}}^{\uparrow}(t_s)$ scatter to minority electrons above $\varepsilon_{\mathrm{F}}^{\downarrow}(t_s)$, i.e., do not scatter into minority holes.

[9] It is neglected that majority electrons in an energy range of $\hbar\omega_{\mathbf{q}\lambda}^{\max}$ below the Fermi energy $\varepsilon_{\mathrm{F}}^{\uparrow}(t_s)$ also contribute to $\Delta N^{\uparrow}(t_s)$

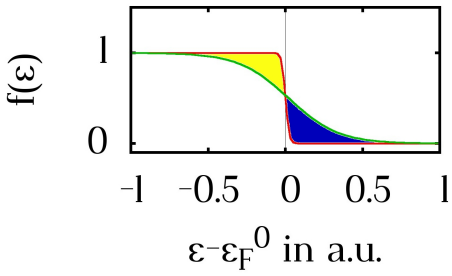

Figure 5.2: Fermi distribution function for 300 K (red curve) and 600 K with shifted Fermi energy (green curve). If the density of states was equal 1 for all energies, the blue area would give the number of *excited* electrons and the yellow area the number of *excited* holes.

at $t = t_s$ with two different chemical potentials $\varepsilon_{\mathrm{F}}^{\uparrow}(t_s)$, $\varepsilon_{\mathrm{F}}^{\downarrow}(t_s)$ and the electron temperature $T_e(t_s)$ even more electrons are excited (see green curve of fig. 5.2 with a shifted Fermi energy). The intersection points of the red and of the in principle two green curves (for majority and minority electrons) of fig. 5.2 is not exactly at $\varepsilon_{\mathrm{F}}^{0}$ (since the Fermi energies of the (in principle two) green curves are shifted) but at $\varepsilon_i^{\uparrow,\downarrow} = (kT_0\varepsilon_{\mathrm{F}}^{\uparrow,\downarrow}(t_s) - kT_e(t_s)\varepsilon_{\mathrm{F}}^{0})/(kT_0 - kT_e(t_s))$, obtained for $f_0(\varepsilon) = f^{\uparrow,\downarrow}(\varepsilon)$. The number of *excited*[10] majority electrons $\Delta N_{\mathrm{exc}}^{\uparrow}(t_s)$ and the number of *excited*[11] majority holes is

$$\Delta N_{\mathrm{exc}}^{\uparrow}(t_s) = \int_{\varepsilon_i^{\uparrow}}^{+\infty} \left[Z^{\uparrow}(\varepsilon)f^{\uparrow}(\varepsilon) - Z^{\uparrow}(\varepsilon)f_0(\varepsilon)\right] \mathrm{d}\varepsilon \tag{5.51}$$

$$\Delta N_{\mathrm{exc}}^{h\uparrow}(t_s) = \int_{-\infty}^{\varepsilon_i^{\uparrow}} \left[Z^{\uparrow}(\varepsilon)f_0(\varepsilon) - Z^{\uparrow}(\varepsilon)f^{\uparrow}(\varepsilon)\right] \mathrm{d}\varepsilon \tag{5.52}$$

with $f_0(\varepsilon) = f(\varepsilon, \varepsilon_{\mathrm{F}}^{0}, T_0)$ and $f^{\uparrow}(\varepsilon) = f(\varepsilon, \varepsilon_{\mathrm{F}}^{\uparrow}(t_s), T_e(t_s))$. If the density of states $Z^{\uparrow}(\varepsilon)$ was equal 1 for all energies, the blue area in fig. 5.2 would give the number of *excited* majority electrons and the yellow area the number of *excited* majority holes. Since number conservation is required the number

[10] excited with respect to the equilibrium situation
[11] excited with respect to the equilibrium situation

of *excited* majority electrons and the number of *excited* majority holes has to be the same, $\Delta N^{\uparrow}_{\mathrm{exc}}(t_s) = \Delta N^{h\uparrow}_{\mathrm{exc}}(t_s)$:

$$\int_{\varepsilon_i^{\uparrow}}^{+\infty} \left[Z^{\uparrow}(\varepsilon) f^{\uparrow}(\varepsilon) - Z^{\uparrow}(\varepsilon) f_0(\varepsilon)\right] \mathrm{d}\varepsilon = \int_{-\infty}^{\varepsilon_i^{\uparrow}} \left[Z^{\uparrow}(\varepsilon) f_0(\varepsilon) - Z^{\uparrow}(\varepsilon) f^{\uparrow}(\varepsilon)\right] \mathrm{d}\varepsilon \tag{5.53}$$

or equivalently

$$\int_{-\infty}^{+\infty} Z^{\uparrow}(\varepsilon) f^{\uparrow}(\varepsilon) \mathrm{d}\varepsilon = \int_{-\infty}^{+\infty} Z^{\uparrow}(\varepsilon) f_0(\varepsilon) \mathrm{d}\varepsilon. \tag{5.54}$$

We will see in eqs. (6.58), (6.59) and below that this condition is just the number conservation $N^{\uparrow}(t_s) = N_0^{\uparrow}$ for up-states which is required to determine the Fermi energy $\varepsilon_{\mathrm{F}}^{\uparrow}(t_s)$ at time t_s.

Analogously, the number of *excited* minority electrons $\Delta N^{\downarrow}_{\mathrm{exc}}(t_s)$ and the number of *excited* minority holes is

$$\Delta N^{\downarrow}_{\mathrm{exc}}(t_s) = \int_{\varepsilon_i^{\downarrow}}^{+\infty} \left[Z^{\downarrow}(\varepsilon) f^{\downarrow}(\varepsilon) - Z^{\downarrow}(\varepsilon) f_0(\varepsilon)\right] \mathrm{d}\varepsilon \tag{5.55}$$

$$\Delta N^{h\downarrow}_{\mathrm{exc}}(t_s) = \int_{-\infty}^{\varepsilon_i^{\downarrow}} \left[Z^{\downarrow}(\varepsilon) f_0(\varepsilon) - Z^{\downarrow}(\varepsilon) f^{\downarrow}(\varepsilon)\right] \mathrm{d}\varepsilon \tag{5.56}$$

where $f^{\downarrow}(\varepsilon) = f(\varepsilon, \varepsilon_{\mathrm{F}}^{\downarrow}(t_s), T_e(t_s))$ and $\Delta N^{\downarrow}_{\mathrm{exc}}(t_s) = \Delta N^{h\downarrow}_{\mathrm{exc}}(t_s)$.

The maximum possible demagnetization is achieved if all *excited* majority electrons $\Delta N^{\uparrow}_{\mathrm{exc}}(t_s)$ would flip their spin[12] and all *excited* minority holes $\Delta N^{h\downarrow}_{\mathrm{exc}}$ would be filled by majority electrons via spin-flip scattering[13] while all minority electrons would not flip their spin. Then the maximum possible decrease of the magnetic moment (proportional to the maximum possible demagnetization) is $\Delta M = 2\mu_{\mathrm{B}}(\Delta N^{\uparrow}_{\mathrm{exc}}(t_s) + \Delta N^{h\downarrow}_{\mathrm{exc}}(t_s))$ per atom.

[12] It is assumed that *excited* majority electrons do not scatter into *excited* minority holes.

[13] The minority holes are filled by minority electrons which were originally majority electrons but flipped their spin.

6 Implementation

This chapter is based on chapter 4 of ref. [12].

6.1 Electron-phonon scattering operator

6.1.1 Rigid-ion approximation

The electron-phonon scattering operator is given for a paramagnet in eq. (5.1)

$$W'_{\lambda,B} = \sum_{n=1}^{\widetilde{N}} e^{i\mathbf{q}\mathbf{R}^0_n} \Bigg\{ \left(\sum_j n^B_{\mathbf{q}\lambda;j} \, \frac{\partial}{\partial R_{n,B;j}} \right) \cdot \Bigg[V(\mathbf{r}; \{\mathbf{R}'_{n,B}\}) \begin{pmatrix} 1 & 0 \\ 0 & 1 \end{pmatrix} + \sum_i \frac{\hbar}{4m_e^2 c^2} \left(\nabla_{\mathbf{r}} V(\mathbf{r}; \{\mathbf{R}'_{n,B}\}) \times \widehat{\mathbf{p}} \right)_i \underline{\underline{\widehat{\sigma}}}_i \Bigg] \Bigg\} \Bigg|_{\mathbf{R}_{n,B} = \mathbf{R}^0_{n,B}} . \quad (6.1)$$

The equilibrium potential $V^0(\mathbf{r}; \{\mathbf{R}^0_{n,B}\})$ (where all lattice atoms are at their equilibrium positions $\mathbf{R}^0_{n,B}$) can be decomposed in atomic potentials $v^0_{n,B}$ which are centered around the equilibrium positions

$$V^0(\mathbf{r}; \{\mathbf{R}^0_{n,B}\}) = \sum_{n,B} v^0_{n,B}(\mathbf{r} - \mathbf{R}^0_{n,B}). \quad (6.2)$$

This is done in the atomic-sphere approximation by constructing overlapping atomic spheres so that the sum of the volumes of the spheres in the elementary cell is as large as the volume of the elementary cell. The atomic potentials are defined inside the sphere and are zero outside. In equilibrium the atomic potentials must be the same for every cell n, hence one could omit the index n.

The rigid-ion approximation or Nordheim approximation [102] says that one can still use the equilibrium atomic potentials $v^0_{n,B}$ in the non-equilibrium case (where the lattice atoms $\mathbf{R}_{n,B}$ are displaced from the

equilibrium position): The lattice atoms (ions) are shifted rigidly without changing the potential

$$V(\mathbf{r};\{\mathbf{R}_{n,B}\}) \approx \sum_{n,B} v^0_{n,B}(\mathbf{r}-\mathbf{R}_{n,B}). \tag{6.3}$$

To test whether this approximation is good one can calculate physical quantities with the rigid-ion approximation and compare it with experimental results or compare it with supercell calculations. Butler et al. used the rigid-ion approximation for the electron-phonon scattering operator to calculate quantities in superconductivity (e.g., the mass enhancement parameter) for transition metals and found a good agreement [103, 104, 105] which led to the conclusion that the rigid-ion approximation is valid in transition metals. This was justified by the localized d-orbitals and the high density of states which can screen very effectively. However, the rigid-ion approximation was also criticized in several publications [106, 107, 108]. It is argued in refs. [107, 108] that the rigid-ion approximation does not account correctly for screening and that matrix elements are too small for small phonon wavevectors $\mathbf{q}$. This fits to the argumentation in section 5.4, and one has to be careful for small $\mathbf{q}$. The best evidence that the rigid-ion approximation should be valid (at least in average) is the comparison of rigid-ion spin-flip Eliashberg functions with supercell calculations by Carva et al. [72]. The agreement is surprisingly good and gives a justification to use the rigid-ion approximation.

The electron-phonon scattering operator reads in rigid-ion approximation (eq. (6.3))

$$\begin{aligned} W'_{\lambda,B} &= \sum_{n,n',B'} e^{i\mathbf{q}\mathbf{R}^0_n} \Bigg\{ \Bigg(\sum_j n^B_{\mathbf{q}\lambda;j} \, \frac{\partial}{\partial R_{n,B;j}} \Bigg) \Bigg[v^0_{n',B'}(\mathbf{r}-\mathbf{R}_{n',B'}) \, \underline{\underline{1}} \\ &\quad + \sum_i \frac{\hbar}{4m_e^2c^2} \Big(\nabla_{\mathbf{r}} v^0_{n',B'}(\mathbf{r}-\mathbf{R}_{n',B'}) \times \widehat{\mathbf{p}} \Big)_i \, \underline{\underline{\widehat{\sigma}}}_i \Bigg] \Bigg\} \Bigg|_{\mathbf{R}_{n,B}=\mathbf{R}^0_{n,B}} \\ &= \sum_{n,n',B',j} e^{i\mathbf{q}\mathbf{R}^0_n} \Bigg\{ -\delta_{n,n'}\delta_{B,B'} \, n^B_{\mathbf{q}\lambda;j} \, \Bigg[\frac{\partial}{\partial r_j} v^0_{n,B}(\mathbf{r}-\mathbf{R}_{n,B}) \, \underline{\underline{1}} \end{aligned}$$

$$+\sum_i \frac{\hbar}{4m_e^2c^2}\left(\nabla_{\mathbf{r}}\left(\frac{\partial}{\partial r_j}v^0_{n,B}(\mathbf{r}-\mathbf{R}_{n,B})\right)\times\widehat{\mathbf{p}}\right)_i \underline{\underline{\widehat{\sigma}}}_i\Bigg]\Bigg\}\Bigg|_{\mathbf{R}_{n,B}=\mathbf{R}^0_{n,B}}. \tag{6.4}$$

It is used that

$$\frac{\partial}{\partial R_{n,B;j}}\, v^0_{n,B}(\mathbf{r}-\mathbf{R}_{n,B}) = -\frac{\partial}{\partial r_j}\, v^0_{n,B}(\mathbf{r}-\mathbf{R}_{n,B}). \tag{6.5}$$

Now, the equilibrium positions can be inserted $\mathbf{R}_{n,B}=\mathbf{R}^0_{n,B}$

$$W'_{\lambda,B} = \sum_n -e^{i\mathbf{q}\mathbf{R}^0_n}\, \mathbf{n}^B_{\mathbf{q}\lambda}\nabla_{\mathbf{r}}\Bigg\{v^0_{n,B}(\mathbf{r}-\mathbf{R}^0_{n,B})\,\underline{\underline{1}} + \sum_i \frac{\hbar}{4m_e^2c^2}\left(\nabla_{\mathbf{r}}v^0_{n,B}(\mathbf{r}-\mathbf{R}^0_{n,B})\times\widehat{\mathbf{p}}\right)_i \underline{\underline{\widehat{\sigma}}}_i\Bigg\} \tag{6.6}$$

and more convenient coordinates are introduced

$$\mathbf{r}^0_{n,B} = \mathbf{r}-\mathbf{R}^0_{n,B} \quad \text{and} \quad \nabla_{\mathbf{r}^0_{n,B}} = \nabla_{\mathbf{r}}. \tag{6.7}$$

Therefore also the momentum operator $\widehat{\mathbf{p}} = -i\hbar\nabla_{\mathbf{r}} = -i\hbar\nabla_{\mathbf{r}^0_{n,B}}$ is the same in the new coordinates. In the atomic sphere approximation the potential only depends on the distance $|\mathbf{r}^0_{n,B}| = r^0_{n,B}$ from the center $\mathbf{R}^0_{n,B}$ (no dependence on ϑ and ϕ). It is convenient to use spherical coordinates where

$$\mathbf{e}_r = \begin{pmatrix}\sin\vartheta\cos\phi\\ \sin\vartheta\sin\phi\\ \cos\vartheta\end{pmatrix}, \quad \mathbf{e}_\vartheta = \begin{pmatrix}\cos\vartheta\cos\phi\\ \cos\vartheta\sin\phi\\ -\sin\vartheta\end{pmatrix}, \quad \mathbf{e}_\phi = \begin{pmatrix}-\sin\phi\\ \cos\phi\\ 0\end{pmatrix}, \tag{6.8}$$

$$\mathbf{r} = |\mathbf{r}|\cdot\begin{pmatrix}\sin\vartheta\cos\phi\\ \sin\vartheta\sin\phi\\ \cos\vartheta\end{pmatrix} = |\mathbf{r}|\cdot\mathbf{e}_r, \tag{6.9}$$

$$\frac{\partial\mathbf{e}_r}{\partial\vartheta} = \mathbf{e}_\vartheta, \quad \frac{\partial\mathbf{e}_r}{\partial\phi} = \sin\vartheta\cdot\mathbf{e}_\phi, \tag{6.10}$$

$$\nabla_{\mathbf{r}} = \mathbf{e}_r\frac{\partial}{\partial r} + \mathbf{e}_\vartheta\frac{1}{r}\frac{\partial}{\partial\vartheta} + \mathbf{e}_\phi\frac{1}{r\sin\vartheta}\frac{\partial}{\partial\phi}. \tag{6.11}$$

Eq. (6.6) then reads

$$
\begin{aligned}
W'_{\lambda,B} = &\sum_n -e^{i\mathbf{q}\mathbf{R}^0_n}\ \mathbf{n}^B_{\mathbf{q}\lambda}\nabla_{\mathbf{r}^0_{n,B}}\Bigg\{ v^0_{n,B}(r^0_{n,B})\ \underline{\underline{1}} \\
&+ \sum_i \frac{\hbar}{4m_e^2c^2}\left(\mathbf{e}_{r^0_{n,B}}\frac{\partial v^0_{n,B}(r^0_{n,B})}{\partial r^0_{n,B}} \times \widehat{\mathbf{p}}\right)_i \underline{\underline{\widehat{\sigma}}}_i \Bigg\} \\
= &\sum_n -e^{i\mathbf{q}\mathbf{R}^0_n}\ \mathbf{n}^B_{\mathbf{q}\lambda}\nabla_{\mathbf{r}^0_{n,B}}\Bigg\{ v^0_{n,B}(r^0_{n,B})\ \underline{\underline{1}} \\
&+ \sum_i \frac{\hbar}{4m_e^2c^2}\left(\frac{\partial v^0_{n,B}(r^0_{n,B})}{\partial r^0_{n,B}}\frac{\mathbf{r}^0_{n,B}}{r^0_{n,B}} \times \widehat{\mathbf{p}}\right)_i \underline{\underline{\widehat{\sigma}}}_i \Bigg\} \\
= &\sum_n -e^{i\mathbf{q}\mathbf{R}^0_n}\ \mathbf{n}^B_{\mathbf{q}\lambda}\nabla_{\mathbf{r}^0_{n,B}}\Bigg\{ v^0_{n,B}(r^0_{n,B})\ \underline{\underline{1}} \\
&+ \sum_i \frac{\hbar}{4m_e^2c^2r^0_{n,B}}\frac{\partial v^0_{n,B}(r^0_{n,B})}{\partial r^0_{n,B}}(\widehat{\mathbf{L}}^0_{n,B})_i\ \underline{\underline{\widehat{\sigma}}}_i \Bigg\}
\end{aligned}
\tag{6.12}
$$

where $\widehat{\mathbf{L}}^0_{n,B} = \mathbf{r}^0_{n,B} \times \widehat{\mathbf{p}}$ is the angular momentum operator. The electron-phonon scattering operator only depends on the equilibrium positions of the lattice atoms $\mathbf{R}^0_{n,B}$ and is expressed in local coordinates $\mathbf{r}^0_{n,B}$ with respect to the equilibrium positions. In the following the index "0" is omitted and it is clear that the positions are in equilibrium.

6.1.2 Hermitian form

It is demonstrated in the following that the scattering operator in eq. (6.12) is Hermitian. With the abbreviation

$$
v_{\text{eff}} \equiv v_{n,B}(r_{n,B})\ \underline{\underline{1}} + \sum_i \underbrace{\frac{\hbar}{4m_e^2c^2r_{n,B}}\frac{\partial v_{n,B}(r_{n,B})}{\partial r_{n,B}}}_{\Xi(r_{n,B})}(\widehat{\mathbf{L}}_{n,B})_i\ \underline{\underline{\widehat{\sigma}}}_i \tag{6.13}
$$

the scattering operator reads

$$
W'_{\lambda,B} = \sum_n -e^{i\mathbf{q}\mathbf{R}_n}\ \mathbf{n}^B_{\mathbf{q}\lambda}\nabla_{\mathbf{r}_{n,B}} v_{\text{eff}}. \tag{6.14}
$$

It is possible to express the scattering operator as commutator [64] ($\widehat{H}_{\text{eff}}$: effective Hamiltonian, ψ: wavefunction):

$$\begin{aligned}[\widehat{\mathbf{p}},\ \widehat{H}_{\text{eff}}]\ \psi &= [\widehat{\mathbf{p}},\ \frac{\widehat{\mathbf{p}}^2}{2m_e} + v_{\text{eff}}]\ \psi \\ &= \widehat{\mathbf{p}}\frac{\widehat{\mathbf{p}}^2}{2m_e}\ \psi + \widehat{\mathbf{p}}\ (v_{\text{eff}}\ \psi) - \frac{\widehat{\mathbf{p}}^2}{2m_e}\widehat{\mathbf{p}}\ \psi - v_{\text{eff}}\ (\widehat{\mathbf{p}}\ \psi) \\ &= \widehat{\mathbf{p}}\ (v_{\text{eff}}\ \psi) - v_{\text{eff}}\ (\widehat{\mathbf{p}}\ \psi) = (\widehat{\mathbf{p}}\ v_{\text{eff}})\ \psi = (-i\hbar\nabla v_{\text{eff}})\ \psi \end{aligned} \quad (6.15)$$

and hence

$$W'_{\lambda,B} = \sum_n -e^{i\mathbf{q}\mathbf{R}_n}\ \mathbf{n}^B_{\mathbf{q}\lambda}\ \frac{i}{\hbar}[\widehat{\mathbf{p}},\ \widehat{H}_{\text{eff}}]. \quad (6.16)$$

It is easy to show that the commutator is Hermitian

$$\begin{aligned}\left(\frac{i}{\hbar}[\widehat{\mathbf{p}},\ \widehat{H}_{\text{eff}}]\right)^\dagger &= -\frac{i}{\hbar}\left(\widehat{\mathbf{p}}\ \widehat{H}_{\text{eff}} - \widehat{H}_{\text{eff}}\ \widehat{\mathbf{p}}\right)^\dagger = -\frac{i}{\hbar}\left(\widehat{H}^\dagger_{\text{eff}}\ \widehat{\mathbf{p}}^\dagger - \widehat{\mathbf{p}}^\dagger \widehat{H}^\dagger_{\text{eff}}\right) \\ &= -\frac{i}{\hbar}\left(\widehat{H}_{\text{eff}}\ \widehat{\mathbf{p}} - \widehat{\mathbf{p}}\ \widehat{H}_{\text{eff}}\right) = \frac{i}{\hbar}[\widehat{\mathbf{p}},\ \widehat{H}_{\text{eff}}]. \end{aligned} \quad (6.17)$$

Thereby it is used that $\widehat{\mathbf{p}}^\dagger = \widehat{\mathbf{p}}$ and $\widehat{H}^\dagger_{\text{eff}} = \widehat{H}_{\text{eff}}$ are Hermitian[14]. The scattering operator is Hermitian

$$\begin{aligned}{W'_{\lambda,B}}^\dagger &= \sum_n -e^{-i\mathbf{q}\mathbf{R}_n}\ \mathbf{n}^B_{\mathbf{q}\lambda}\ \left(\frac{i}{\hbar}[\widehat{\mathbf{p}},\ \widehat{H}_{\text{eff}}]\right)^\dagger \\ &= \sum_n -e^{i\mathbf{q}\mathbf{R}_n}\ \mathbf{n}^B_{\mathbf{q}\lambda}\ \frac{i}{\hbar}[\widehat{\mathbf{p}},\ \widehat{H}_{\text{eff}}] = W'_{\lambda,B} \end{aligned} \quad (6.18)$$

because of the sum over n. A Hermitian form of the scattering operator is very important to fulfill the equilibrium rate equations, see subsection 5.5.4.

[14] $\widehat{H}_{\text{eff}} = \frac{\widehat{\mathbf{p}}^2}{2m_e} + v_{\text{eff}}$ is Hermitian since $\left[\Xi(r_{n,B})\ (\widehat{\mathbf{L}}_{n,B})_i\ \underline{\widehat{\sigma}}_i\right]^\dagger = \underline{\widehat{\sigma}}^\dagger_i\ (\widehat{\mathbf{L}}_{n,B})^\dagger_i\ \Xi(r_{n,B})^\dagger = \underline{\widehat{\sigma}}_i\ (\widehat{\mathbf{L}}_{n,B})_i\ \Xi(r_{n,B}) = \Xi(r_{n,B})\ (\widehat{\mathbf{L}}_{n,B})_i\ \underline{\widehat{\sigma}}_i$.

6.1.3 Electron-phonon scattering operator in the LMTO-ASA method

So far the electron-phonon scattering operator has been constructed for a paramagnet because it has been assumed that the potential matrix $V(\mathbf{r};\{\mathbf{R}'_{n,B}\})$ has only a diagonal part. The goal is to construct the scattering operator for a ferromagnet and to implement it in the LMTO-ASA code. The potential is given in the relativistic Dirac equation (2.27)

$$
\begin{aligned}
&V_{\text{eff}}(r_{n,B})\underline{\underline{1}} + \mu_{\text{B}}\beta \begin{pmatrix} \underline{\underline{\sigma_z}} & 0 \\ 0 & \underline{\underline{\sigma_z}} \end{pmatrix} B_{\text{eff,z}}(r_{n,B}) \\
&= \begin{pmatrix} v^{\uparrow}_{n,B}(r_{n,B}) & 0 & 0 & 0 \\ 0 & v^{\downarrow}_{n,B}(r_{n,B}) & 0 & 0 \\ 0 & 0 & v^{\downarrow}_{n,B}(r_{n,B}) & 0 \\ 0 & 0 & 0 & v^{\uparrow}_{n,B}(r_{n,B}) \end{pmatrix}
\end{aligned}
\tag{6.19}
$$

with $v^{\uparrow}_{n,B}(r_{n,B}) = V_{\text{eff}} + \mu_{\text{B}}B_{\text{eff,z}}$ and $v^{\downarrow}_{n,B}(r_{n,B}) = V_{\text{eff}} - \mu_{\text{B}}B_{\text{eff,z}}$. In the scalar-relativistic case the spin-orbit coupling is not included and has to be added to the potential given in eq. (6.19), see eq. (2.32). The spin-orbit coupling only applies to the large component of the four-vector. The spin-orbit matrix in the Hermitian form (see text below eq. (2.32)) reads

$$
\begin{aligned}
&\sum_i \frac{\hbar}{4M^2_{\mathbf{R}l\alpha,\mathbf{R}'l'\alpha'}(r_{n,B})c^2 r_{n,B}} \frac{\partial v^{\alpha,\alpha'}_{n,B}}{\partial r_{n,B}} \begin{pmatrix} (\widehat{\mathbf{L}}_{n,B})_i \underline{\underline{\widehat{\sigma}}}_i & & 0 & 0 \\ & & 0 & 0 \\ 0 & 0 & 0 & 0 \\ 0 & 0 & 0 & 0 \end{pmatrix} \\
&= \sum_i \frac{\hbar}{4M^2_{\mathbf{R}l\alpha,\mathbf{R}'l'\alpha'}(r_{n,B})c^2} \frac{\partial v^{\alpha,\alpha'}_{n,B}}{\partial r_{n,B}} \begin{pmatrix} (\mathbf{e}_{r_{n,B}} \times \widehat{\mathbf{p}})_i \underline{\underline{\widehat{\sigma}}}_i & & 0 & 0 \\ & & 0 & 0 \\ 0 & 0 & 0 & 0 \\ 0 & 0 & 0 & 0 \end{pmatrix} \\
&\equiv \sum_i \xi(r_{n,B}) \begin{pmatrix} (\mathbf{e}_{r_{n,B}} \times \widehat{\mathbf{p}})_i \underline{\underline{\widehat{\sigma}}}_i & & 0 & 0 \\ & & 0 & 0 \\ 0 & 0 & 0 & 0 \\ 0 & 0 & 0 & 0 \end{pmatrix}
\end{aligned}
\tag{6.20}
$$

with $\xi(r_{n,B}) = \frac{\hbar}{4M^2_{\mathbf{R}l\alpha,\mathbf{R}'l'\alpha'}(r_{n,B})c^2} \frac{\partial v^{\alpha,\alpha'}_{n,B}}{\partial r_{n,B}}$. The scattering operator can now be constructed very similarly to the paramagnetic case. The only

difference is that the mass $M_{\mathbf{R}l\alpha,\mathbf{R}'l'\alpha'}(r_{n,B}) = m_e + \frac{1}{2c^2}(\varepsilon_{\mathbf{R}l\alpha,\mathbf{R}'l'\alpha'} - v^{\alpha,\alpha'}_{n,B}(r_{n,B}))$ is now a function of $r_{n,B}$. According to eq. (6.6), the electron-phonon scattering operator reads using eqs. (6.8)-(6.11) (note that the gradient does not apply to the momentum operator $\widehat{\mathbf{p}}$ as in the paramagnetic case)

$$
\begin{aligned}
W'_{\lambda,B} = \sum_n -e^{i\mathbf{q}\mathbf{R}_n} \left(\mathbf{n}^B_{\mathbf{q}\lambda} \nabla_{r_{n,B}} \right) \Bigg\{ & \begin{pmatrix} v^{\uparrow}_{n,B} & 0 & 0 & 0 \\ 0 & v^{\downarrow}_{n,B} & 0 & 0 \\ 0 & 0 & v^{\downarrow}_{n,B} & 0 \\ 0 & 0 & 0 & v^{\uparrow}_{n,B} \end{pmatrix} \\
& + \sum_i \xi(r_{n,B}) \begin{pmatrix} \left(\mathbf{e}_{r_{n,B}} \times \widehat{\mathbf{p}}\right)_i \widehat{\underline{\underline{\sigma}}}_i & & 0 & 0 \\ & & 0 & 0 \\ 0 & & 0 & 0 \\ 0 & & 0 & 0 \end{pmatrix} \Bigg\} \\
= \sum_n -e^{i\mathbf{q}\mathbf{R}_n} \, \mathbf{n}^B_{\mathbf{q}\lambda} \Bigg\{ & \mathbf{e}_{r_{n,B}} \begin{pmatrix} \frac{\partial v^{\uparrow}_{n,B}}{\partial r_{n,B}} & 0 & 0 & 0 \\ 0 & \frac{\partial v^{\downarrow}_{n,B}}{\partial r_{n,B}} & 0 & 0 \\ 0 & 0 & \frac{\partial v^{\downarrow}_{n,B}}{\partial r_{n,B}} & 0 \\ 0 & 0 & 0 & \frac{\partial v^{\uparrow}_{n,B}}{\partial r_{n,B}} \end{pmatrix} \\
& + \mathbf{e}_{r_{n,B}} \frac{\partial \xi(r_{n,B})}{\partial r_{n,B}} \sum_i \begin{pmatrix} \left(\mathbf{e}_{r_{n,B}} \times \widehat{\mathbf{p}}\right)_i \widehat{\underline{\underline{\sigma}}}_i & & 0 & 0 \\ & & 0 & 0 \\ 0 & & 0 & 0 \\ 0 & & 0 & 0 \end{pmatrix} \\
& + \mathbf{e}_{\vartheta_{n,B}} \frac{\xi(r_{n,B})}{r_{n,B}} \sum_i \begin{pmatrix} \left(\frac{\partial \mathbf{e}_{r_{n,B}}}{\partial \vartheta_{n,B}} \times \widehat{\mathbf{p}}\right)_i \widehat{\underline{\underline{\sigma}}}_i & & 0 & 0 \\ & & 0 & 0 \\ 0 & & 0 & 0 \\ 0 & & 0 & 0 \end{pmatrix} \\
& + \mathbf{e}_{\phi_{n,B}} \frac{\xi(r_{n,B})}{r_{n,B}\sin(\vartheta_{n,B})} \sum_i \begin{pmatrix} \left(\frac{\partial \mathbf{e}_{r_{n,B}}}{\partial \phi_{n,B}} \times \widehat{\mathbf{p}}\right)_i \widehat{\underline{\underline{\sigma}}}_i & & 0 & 0 \\ & & 0 & 0 \\ 0 & & 0 & 0 \\ 0 & & 0 & 0 \end{pmatrix} \Bigg\}
\end{aligned}
$$

$$
\begin{aligned}
&= \sum_n -e^{i\mathbf{q}\mathbf{R}_n}\ \mathbf{n}^B_{\mathbf{q}\lambda} \left\{ \mathbf{e}_{r_{n,B}} \begin{pmatrix} \frac{\partial v^{\uparrow}_{n,B}}{\partial r_{n,B}} & 0 & 0 & 0 \\ 0 & \frac{\partial v^{\downarrow}_{n,B}}{\partial r_{n,B}} & 0 & 0 \\ 0 & 0 & \frac{\partial v^{\downarrow}_{n,B}}{\partial r_{n,B}} & 0 \\ 0 & 0 & 0 & \frac{\partial v^{\uparrow}_{n,B}}{\partial r_{n,B}} \end{pmatrix} \right. \\
&+ \mathbf{e}_{r_{n,B}} \frac{1}{r_{n,B}} \frac{\partial \xi(r_{n,B})}{\partial r_{n,B}} \sum_i \begin{pmatrix} (\widehat{\mathbf{L}}^0_{n,B})_i\ \widehat{\underline{\underline{\sigma}}}_i & & 0 & 0 \\ & & 0 & 0 \\ 0 & 0 & 0 & 0 \\ 0 & 0 & 0 & 0 \end{pmatrix} \\
&+ \mathbf{e}_{\vartheta_{n,B}} \frac{\xi(r_{n,B})}{r_{n,B}} \sum_i \begin{pmatrix} \left(\mathbf{e}_{\vartheta_{n,B}} \times \widehat{\mathbf{p}}\right)_i \widehat{\underline{\underline{\sigma}}}_i & & 0 & 0 \\ & & 0 & 0 \\ 0 & 0 & 0 & 0 \\ 0 & 0 & 0 & 0 \end{pmatrix} \\
&+ \mathbf{e}_{\phi_{n,B}} \frac{\xi(r_{n,B})}{r_{n,B}} \sum_i \left. \begin{pmatrix} \left(\mathbf{e}_{\phi_{n,B}} \times \widehat{\mathbf{p}}\right)_i \widehat{\underline{\underline{\sigma}}}_i & & 0 & 0 \\ & & 0 & 0 \\ 0 & 0 & 0 & 0 \\ 0 & 0 & 0 & 0 \end{pmatrix} \right\}
\end{aligned}
\tag{6.21}
$$

with

$$
\frac{\partial \xi}{\partial r_{n,B}} = \frac{\partial}{\partial r_{n,B}} \left(\frac{\hbar \frac{\partial v^{\alpha,\alpha'}_{n,B}}{\partial r_{n,B}}}{4M^2_{\mathbf{R}l\alpha,\mathbf{R}'l'\alpha'}c^2} \right) = \frac{\hbar \frac{\partial^2 v^{\alpha,\alpha'}_{n,B}}{\partial r^2_{n,B}}}{4M^2_{\mathbf{R}l\alpha,\mathbf{R}'l'\alpha'}c^2} + \frac{\hbar \left(\frac{\partial v^{\alpha,\alpha'}_{n,B}}{\partial r_{n,B}} \right)^2}{4M^3_{\mathbf{R}l\alpha,\mathbf{R}'l'\alpha'}c^4}. \tag{6.22}
$$

In eq. (6.22) it is neglected that the energies $\varepsilon_{\mathbf{R}l\alpha,\mathbf{R}'l'\alpha'}$ occurring in the generalized mass $M_{\mathbf{R}l\alpha,\mathbf{R}'l'\alpha'}$ also change under a displacement of the atoms. The energy dependence of the mass $M_{\mathbf{R}l\alpha}$ has already been neglected in $\dot{\Phi}_{\mathbf{R}lm\alpha}$ (see text below eq. (2.30)). A short notation of the scattering operator is introduced

$$
W'_{\lambda,B} = \sum_n -e^{i\mathbf{q}\mathbf{R}_n}\ \widetilde{W}'_{n,\lambda,B} \tag{6.23}
$$

where

$$\begin{aligned}\widetilde{W}'_{n,\lambda,B} =& \mathbf{n}^B_{\mathbf{q}\lambda} \left\{ \mathbf{e}_{r_{n,B}} \begin{pmatrix} \frac{\partial v^{\uparrow}_{n,B}}{\partial r_{n,B}} & 0 & 0 & 0 \\ 0 & \frac{\partial v^{\downarrow}_{n,B}}{\partial r_{n,B}} & 0 & 0 \\ 0 & 0 & \frac{\partial v^{\downarrow}_{n,B}}{\partial r_{n,B}} & 0 \\ 0 & 0 & 0 & \frac{\partial v^{\uparrow}_{n,B}}{\partial r_{n,B}} \end{pmatrix} \right. \\ &+ \mathbf{e}_{r_{n,B}} \frac{1}{r_{n,B}} \frac{\partial \xi(r_{n,B})}{\partial r_{n,B}} \sum_i \begin{pmatrix} (\widehat{\mathbf{L}}^0_{n,B})_i \, \widehat{\underline{\underline{\sigma}}}_i & & 0 & 0 \\ & & 0 & 0 \\ 0 & 0 & 0 & 0 \\ 0 & 0 & 0 & 0 \end{pmatrix} \\ &+ \mathbf{e}_{\vartheta_{n,B}} \frac{\xi(r_{n,B})}{r_{n,B}} \sum_i \begin{pmatrix} \left(\mathbf{e}_{\vartheta_{n,B}} \times \widehat{\mathbf{p}}\right)_i \widehat{\underline{\underline{\sigma}}}_i & & 0 & 0 \\ & & 0 & 0 \\ 0 & 0 & 0 & 0 \\ 0 & 0 & 0 & 0 \end{pmatrix} \\ &+ \left. \mathbf{e}_{\phi_{n,B}} \frac{\xi(r_{n,B})}{r_{n,B}} \sum_i \begin{pmatrix} \left(\mathbf{e}_{\phi_{n,B}} \times \widehat{\mathbf{p}}\right)_i \widehat{\underline{\underline{\sigma}}}_i & & 0 & 0 \\ & & 0 & 0 \\ 0 & 0 & 0 & 0 \\ 0 & 0 & 0 & 0 \end{pmatrix} \right\}. \end{aligned} \tag{6.24}$$

6.2 Matrix element

Using the expansion of crystal wavefunctions into atomic wavefunctions and their energy derivatives, eq. (2.25), the matrix element for a spin-flip from a state $\Psi^s_{j\mathbf{k}}$ to a state $\Psi^{s'}_{j'\mathbf{k}'}$ reads

$$\begin{aligned} M^{\lambda,B}_{j\mathbf{k}s,j'\mathbf{k}'s'} =& \langle \Psi^{s'}_{j'\mathbf{k}'} | W'_{\lambda,B} | \Psi^s_{j\mathbf{k}} \rangle \\ =& \frac{1}{\widetilde{N}} \sum_{\substack{\mathbf{T} \\ \mathbf{T}'}} e^{i(\mathbf{k}\mathbf{T} - \mathbf{k}'\mathbf{T}')} \sum_{\substack{\mathbf{R}lm\alpha \\ \mathbf{R}'l'm'\alpha'}} \\ & \left\{ \left(c^{j'\mathbf{k}'s'}_{\mathbf{R}'l'm'\alpha'} \right)^* c^{j\mathbf{k}s}_{\mathbf{R}lm\alpha} \langle \Phi_{(\mathbf{R}'+\mathbf{T}')l'm'\alpha'} | W'_{\lambda,B} | \Phi_{(\mathbf{R}+\mathbf{T})lm\alpha} \rangle \right. \\ & + \left(c^{j'\mathbf{k}'s'}_{\mathbf{R}'l'm'\alpha'} \right)^* d^{j\mathbf{k}s}_{\mathbf{R}lm\alpha} \langle \Phi_{(\mathbf{R}'+\mathbf{T}')l'm'\alpha'} | W'_{\lambda,B} | \dot{\Phi}_{(\mathbf{R}+\mathbf{T})lm\alpha} \rangle \\ & + \left. \left(d^{j'\mathbf{k}'s'}_{\mathbf{R}'l'm'\alpha'} \right)^* c^{j\mathbf{k}s}_{\mathbf{R}lm\alpha} \langle \dot{\Phi}_{(\mathbf{R}'+\mathbf{T}')l'm'\alpha'} | W'_{\lambda,B} | \Phi_{(\mathbf{R}+\mathbf{T})lm\alpha} \rangle \right. \end{aligned}$$

$$
\begin{aligned}
&+\left(d^{j'\mathbf{k}'s'}_{\mathbf{R}'l'm'\alpha'}\right)^* d^{j\mathbf{k}s}_{\mathbf{R}lm\alpha}\langle\dot{\Phi}_{(\mathbf{R}'+\mathbf{T}')l'm'\alpha'}|W'_{\lambda,B}|\dot{\Phi}_{(\mathbf{R}+\mathbf{T})lm\alpha}\rangle\Big\}\\
=&\frac{1}{\widetilde{N}}\sum_{\substack{\mathbf{T}\\\mathbf{T}'}}\sum_{\substack{\mathbf{R}lm\alpha\\\mathbf{R}'l'm'\alpha'}}\sum_{n}-e^{i\mathbf{q}\mathbf{R}_n}\;e^{i(\mathbf{k}\mathbf{T}-\mathbf{k}'\mathbf{T}')}\,\cdot\\
&\Big\{\left(c^{j'\mathbf{k}'s'}_{\mathbf{R}'l'm'\alpha'}\right)^* c^{j\mathbf{k}s}_{\mathbf{R}lm\alpha}\langle\Phi_{(\mathbf{R}'+\mathbf{T}')l'm'\alpha'}|\widetilde{W}'_{n,\lambda,B}|\Phi_{(\mathbf{R}+\mathbf{T})lm\alpha}\rangle\\
&\qquad+\dots\Big\}.
\end{aligned}
\tag{6.25}
$$

The atomic functions Φ, $\dot{\Phi}$ and the potential $v^{\alpha}_{n,B}(r_{n,B})$ are only defined in the corresponding atomic sphere and are zero outside. All matrix elements are zero unless $\mathbf{R}'+\mathbf{T}'=\mathbf{R}+\mathbf{T}$ and $\mathbf{R}+\mathbf{T}=\mathbf{R}^0_B+\mathbf{R}^0_n$. This is true if $\mathbf{R}'=\mathbf{R}$, $\mathbf{T}'=\mathbf{T}$, $\mathbf{R}=\mathbf{R}^0_B$ and $\mathbf{T}=\mathbf{R}^0_n$:

$$
\begin{aligned}
M^{\lambda,B}_{j\mathbf{k}s,j'\mathbf{k}'s'}=&\frac{1}{\widetilde{N}}\sum_{\mathbf{T}}\sum_{\substack{\mathbf{R}lm\alpha\\l'm'\alpha'}}-e^{i\mathbf{q}\mathbf{T}}\;e^{i(\mathbf{k}-\mathbf{k}')\mathbf{T}}\delta_{\mathbf{R}^0_B\mathbf{R}}\,\cdot\\
&\Big\{\left(c^{j'\mathbf{k}'s'}_{\mathbf{R}l'm'\alpha'}\right)^* c^{j\mathbf{k}s}_{\mathbf{R}lm\alpha}\langle\Phi_{(\mathbf{R}+\mathbf{T})l'm'\alpha'}|\widetilde{W}'_{\lambda,\mathbf{R}+\mathbf{T}}|\Phi_{(\mathbf{R}+\mathbf{T})lm\alpha}\rangle\\
&\qquad+\dots\Big\}\\
=&\frac{1}{\widetilde{N}}\sum_{\mathbf{T}}\sum_{\substack{\mathbf{R}lm\alpha\\l'm'\alpha'}}-e^{i\mathbf{q}\mathbf{T}}\;e^{i(\mathbf{k}-\mathbf{k}')\mathbf{T}}\delta_{\mathbf{R}^0_B\mathbf{R}}\,\cdot\\
&\Big\{\left(c^{j'\mathbf{k}'s'}_{\mathbf{R}l'm'\alpha'}\right)^* c^{j\mathbf{k}s}_{\mathbf{R}lm\alpha}\langle\Phi_{\mathbf{R}l'm'\alpha'}|\widetilde{W}'_{\lambda,\mathbf{R}}|\Phi_{\mathbf{R}lm\alpha}\rangle+\dots\Big\}\\
=&\delta_{\mathbf{G},\mathbf{k}-\mathbf{k}'+\mathbf{q}}\sum_{\substack{\mathbf{R}lm\alpha\\l'm'\alpha'}}-\delta_{\mathbf{R}^0_B\mathbf{R}}\,\cdot\\
&\Big\{\left(c^{j'\mathbf{k}'s'}_{\mathbf{R}l'm'\alpha'}\right)^* c^{j\mathbf{k}s}_{\mathbf{R}lm\alpha}\langle\Phi_{\mathbf{R}l'm'\alpha'}|\widetilde{W}'_{\lambda,\mathbf{R}}|\Phi_{\mathbf{R}lm\alpha}\rangle+\dots\Big\}
\end{aligned}
\tag{6.26}
$$

where it is used that the matrix element is the same for every $\mathbf{T}$ and that the identity holds[15,16] $\sum_{\mathbf{T}} e^{i(\mathbf{k}-\mathbf{k}'+\mathbf{q})\mathbf{T}} = \widetilde{N}\delta_{\mathbf{G},\mathbf{k}-\mathbf{k}'+\mathbf{q}}$. We see that the quasi momentum conservation is fulfilled $\mathbf{k}+\mathbf{q} = \mathbf{k}'+\mathbf{G}$.

It is now useful to separate the scattering operator $\widetilde{W}'_{\lambda,\mathbf{R}}$ into a spin-diagonal (sd) Elliott and a non-spin-diagonal Yafet part (nsd)

$$\widetilde{W}'_{\lambda,\mathbf{R}} = \widetilde{W'}^{sd}_{\lambda,\mathbf{R}} + \widetilde{W'}^{nsd}_{\lambda,\mathbf{R}}. \tag{6.27}$$

6.2.1 Spin-diagonal part (Elliott part)

Here, only the result of the implementation of the spin-diagonal matrix element (Elliott part) in the LMTO-ASA code is given. The full calculation and the explanation of the notation can be found in appendix A or in ref. [12].

The spin-diagonal matrix element (Elliott part) $\langle \Phi_{\mathbf{R}l'm'\alpha'} | \widetilde{W'}^{sd}_{\lambda,\mathbf{R}} | \Phi_{\mathbf{R}lm\alpha} \rangle$ of the spin-diagonal part of the operator given in eq. (6.24) reads

$$\mathbf{n}^{\mathbf{R}}_{\mathbf{q}\lambda} \left\langle \Phi_{\mathbf{R}l'm'\alpha'} \right| \mathbf{e}_{r_{\mathbf{R}}} \begin{pmatrix} \frac{\partial v^{\uparrow}_{\mathbf{R}}}{\partial r_{\mathbf{R}}} & 0 & 0 & 0 \\ 0 & \frac{\partial v^{\downarrow}_{\mathbf{R}}}{\partial r_{\mathbf{R}}} & 0 & 0 \\ 0 & 0 & \frac{\partial v^{\downarrow}_{\mathbf{R}}}{\partial r_{\mathbf{R}}} & 0 \\ 0 & 0 & 0 & \frac{\partial v^{\uparrow}_{\mathbf{R}}}{\partial r_{\mathbf{R}}} \end{pmatrix} \left| \Phi_{\mathbf{R}lm\alpha} \right\rangle$$

$$= \mathbf{n}^{\mathbf{R}}_{\mathbf{q}\lambda} \cdot \Bigg\{$$

$$\left\langle \phi_{\mathbf{R}l'\alpha'} \left| \frac{\partial v^{\alpha}_{\mathbf{R}}}{\partial r_{\mathbf{R}}} \right| \phi_{\mathbf{R}l\alpha} \right\rangle \widetilde{\mathbf{G}}^{lm}_{l'm'} \delta_{\alpha\alpha'} + \left\langle \gamma_{\mathbf{R}l'\alpha'} \left| \frac{\partial v^{\alpha}_{\mathbf{R}}}{\partial r_{\mathbf{R}}} \right| \gamma_{\mathbf{R}l\alpha} \right\rangle \widetilde{\mathbf{G}}^{lm}_{l'm'} \delta_{\alpha\alpha'}$$

[15] $\mathbf{T} = n_1\mathbf{a}_1 + n_2\mathbf{a}_2 + n_3\mathbf{a}_3$ can be written as multiples of primitive translation vectors (n_1, n_2, n_3: integers) and $\mathbf{k}-\mathbf{k}'+\mathbf{q} = \nu_1\mathbf{b}_1 + \nu_2\mathbf{b}_2 + \nu_3\mathbf{b}_3$ can be written as multiples of reciprocal lattice vectors (ν_1, ν_2, ν_3: integers). Using $\mathbf{a}_i\mathbf{b}_j = 2\pi\delta_{ij}$, the identity reads $\sum_{\mathbf{T}} e^{i(\mathbf{k}-\mathbf{k}'+\mathbf{q})\mathbf{T}} = \sum_{n_1,n_2,n_3} e^{2\pi i(n_1\nu_1+n_2\nu_2+n_3\nu_3)}$ which is always zero unless $\nu_1 = \nu_2 = \nu_3 = 0$.

[16] At this point the calculation for an infinitely large solid reduces to a calculation for an elementary unit cell. The infinitely large solid is necessary in order to obtain the quasi momentum conservation for all $\mathbf{q}$ (especially very small ones).

$$
- \left\langle \frac{\phi_{\mathbf{R}l'\alpha'}}{2M_{\mathbf{R}l'\alpha'}cr_{\mathbf{R}}} \left| \frac{\partial v^{\alpha}_{\mathbf{R}}}{\partial r_{\mathbf{R}}} \right| \gamma_{\mathbf{R}l\alpha} \right\rangle \sum_{\substack{m_0=-l \\ m_1=-l'}}^{\substack{m_1=l' \\ m_0=l}} K^{*}_{l'm'm_1} K_{lmm_0} \hbar \cdot
$$

$$
\cdot \left[\delta_{-\alpha\alpha'} S^{-\alpha}_{l'm_1} \mathbf{C}^{lm_0}_{l'(m_1-\alpha)} + \delta_{\alpha\alpha'} \alpha m_1 \mathbf{C}^{lm_0}_{l'm_1} \right]
$$

$$
- \sum_{\substack{m_0=-l \\ m_1=-l'}}^{\substack{m_1=l' \\ m_0=l}} K^{*}_{l'm'm_1} K_{lmm_0} \hbar \Big[\left\langle \gamma | \partial v^{-\alpha} | \phi \right\rangle \delta_{-\alpha\alpha'} S^{+\alpha}_{lm_0} \mathbf{C}^{l(m_0+\alpha)}_{l'm_1}
$$

$$
+ \left\langle \gamma | \partial v^{\alpha} | \phi \right\rangle \delta_{\alpha\alpha'} \alpha m_0 \mathbf{C}^{lm_0}_{l'm_1} \Big]
$$

$$
+ \delta_{\alpha\alpha'} \sum_{\substack{m_0=-l \\ m_1=-l'}}^{\substack{m_1=l' \\ m_0=l}} K^{*}_{l'm'm_1} K_{lmm_0} \hbar^2 \cdot
$$

$$
\Big\{ \left\langle \phi | \partial v^{-\alpha} | \phi \right\rangle \cdot S^{+\alpha}_{l'm_1} S^{+\alpha}_{lm_0} \mathbf{C}^{l(m_0+\alpha)}_{l'(m_1+\alpha)} + \left\langle \phi | \partial v^{\alpha} | \phi \right\rangle m_1 m_0 \mathbf{C}^{lm_0}_{l'm_1} \Big\}
$$

$$
+ \delta_{-\alpha\alpha'} \sum_{\substack{m_0=-l \\ m_1=-l'}}^{\substack{m_1=l' \\ m_0=l}} K^{*}_{l'm'm_1} K_{lmm_0} \hbar^2 \alpha \cdot
$$

$$
\Big\{ - \left\langle \phi | \partial v^{-\alpha} | \phi \right\rangle \cdot m_1 S^{+\alpha}_{lm_0} \mathbf{C}^{l(m_0+\alpha)}_{l'm_1} + \left\langle \phi | \partial v^{\alpha} | \phi \right\rangle S^{-\alpha}_{l'm_1} m_0 \mathbf{C}^{lm_0}_{l'(m_1-\alpha)} \Big\}
$$

$$
+ \left\langle \gamma | \Delta | \gamma \right\rangle \sum_{LM} \quad \Big\{ \delta_{-\alpha\alpha'} \sqrt{\frac{4\pi}{15}} \widetilde{G}_{l'm',LM,lm} \big[\widetilde{\mathbf{G}}^{21}_{LM} + i\alpha \widetilde{\mathbf{G}}^{2-1}_{LM} \big]
$$

$$
+ \delta_{\alpha\alpha'} \frac{1}{3} \alpha \big[\widetilde{\mathbf{G}}^{20}_{LM} \sqrt{\frac{16\pi}{5}} \widetilde{G}_{l'm',LM,lm} + \widetilde{\mathbf{G}}^{lm}_{l'm'} \big] \Big\}
$$

$$
- \left\langle \phi | \Delta | \gamma \right\rangle \sum_{m_0,m_1,LM} K^{*}_{l'm'm_1} K_{lmm_0} \hbar \cdot
$$

$$\Big\{\delta_{\alpha\alpha'}\Big[\sqrt{\frac{4\pi}{15}}S^{+\alpha}_{l'm_1}C_{l'(m_1+\alpha),LM,lm_0}\Big(\widetilde{\mathbf{G}}^{21}_{LM}+i\alpha\widetilde{\mathbf{G}}^{2-1}_{LM}\Big)$$
$$+\frac{1}{3}m_1\Big(\sqrt{\frac{16\pi}{5}}\widetilde{\mathbf{G}}^{20}_{LM}C_{l'm_1,LM,lm_0}+\mathbf{C}^{lm_0}_{l'm_1}\Big)\Big]$$
$$+\delta_{-\alpha\alpha'}\Big[\sqrt{\frac{4\pi}{15}}m_1C_{l'm_1,LM,lm_0}\Big(-\alpha\widetilde{\mathbf{G}}^{21}_{LM}-i\widetilde{\mathbf{G}}^{2-1}_{LM}\Big)$$
$$+\alpha\frac{1}{3}S^{-\alpha}_{l'm_1}\Big(\sqrt{\frac{16\pi}{5}}\widetilde{\mathbf{G}}^{20}_{LM}C_{l'(m_1-\alpha),LM,lm_0}+\mathbf{C}^{lm_0}_{l'(m_1-\alpha)}\Big)\Big]\Big\}$$

$$-\langle\gamma|\Delta|\phi\rangle\sum_{m_0,m_1,LM}K^*_{l'm'm_1}K_{lmm_0}\hbar\cdot$$
$$\Big\{\delta_{\alpha\alpha'}\Big[\sqrt{\frac{4\pi}{15}}S^{+\alpha}_{lm_0}C_{l'm_1,LM,l(m_0+\alpha)}\Big(\widetilde{\mathbf{G}}^{21}_{LM}-i\alpha\widetilde{\mathbf{G}}^{2-1}_{LM}\Big)$$
$$+\frac{1}{3}m_0\Big(\sqrt{\frac{16\pi}{5}}\widetilde{\mathbf{G}}^{20}_{LM}C_{l'm_1,LM,lm_0}+\mathbf{C}^{lm_0}_{l'm_1}\Big)\Big]$$
$$+\delta_{-\alpha\alpha'}\Big[\sqrt{\frac{4\pi}{15}}m_0C_{l'm_1,LM,lm_0}\Big(\alpha\widetilde{\mathbf{G}}^{21}_{LM}+i\widetilde{\mathbf{G}}^{2-1}_{LM}\Big)$$
$$-\alpha\frac{1}{3}S^{+\alpha}_{lm_0}\Big(\sqrt{\frac{16\pi}{5}}\widetilde{\mathbf{G}}^{20}_{LM}C_{l'm_1,LM,l(m_0+\alpha)}+\mathbf{C}^{l(m_0+\alpha)}_{l'm_1}\Big)\Big]\Big\}$$

$$+\langle\phi|\Delta|\phi\rangle\sum_{m_0,m_1,LM}K^*_{l'm'm_1}K_{lmm_0}\hbar^2\cdot$$
$$\Big\{\delta_{-\alpha\alpha'}\cdot\Big[S^{-\alpha}_{l'm_1}S^{+\alpha}_{lm_0}\sqrt{\frac{4\pi}{15}}\,C_{l'(m_1-\alpha),LM,l(m_0+\alpha)}\Big(\widetilde{\mathbf{G}}^{21}_{LM}-i\alpha\widetilde{\mathbf{G}}^{2-1}_{LM}\Big)$$
$$+S^{-\alpha}_{l'm_1}m_0\frac{1}{3}\Big(\sqrt{\frac{16\pi}{5}}\,\widetilde{\mathbf{G}}^{20}_{LM}C_{l'(m_1-\alpha),LM,lm_0}+\mathbf{C}^{lm_0}_{l'(m_1-\alpha)}\Big)$$
$$-m_1m_0\sqrt{\frac{4\pi}{15}}\,C_{l'm_1,LM,lm_0}\Big(\widetilde{\mathbf{G}}^{21}_{LM}+i\alpha\widetilde{\mathbf{G}}^{2-1}_{LM}\Big)$$
$$+m_1S^{+\alpha}_{lm_0}\frac{1}{3}\Big(\sqrt{\frac{16\pi}{5}}\,\widetilde{\mathbf{G}}^{20}_{LM}C_{l'm_1,LM,l(m_0+\alpha)}+\mathbf{C}^{l(m_0+\alpha)}_{l'm_1}\Big)\Big]$$
$$+\delta_{\alpha\alpha'}\cdot\Big[S^{+\alpha}_{l'm_1}m_0\sqrt{\frac{4\pi}{15}}\,C_{l'(m_1+\alpha),LM,lm_0}\Big(\alpha\widetilde{\mathbf{G}}^{21}_{LM}+i\widetilde{\mathbf{G}}^{2-1}_{LM}\Big)$$

$$
\begin{aligned}
&- \frac{\alpha}{3} S^{+\alpha}_{l'm_1} S^{+\alpha}_{lm_0} \Big(\sqrt{\frac{16\pi}{5}}\ \widetilde{\mathbf{G}}^{20}_{LM} C_{l'(m_1+\alpha),LM,l(m_0+\alpha)} + \mathbf{C}^{l(m_0+\alpha)}_{l'(m_1+\alpha)} \Big) \\
&+ m_1 S^{+\alpha}_{lm_0} \sqrt{\frac{4\pi}{15}}\ C_{l'm_1,LM,l(m_0+\alpha)} \Big(\alpha \widetilde{\mathbf{G}}^{21}_{LM} - i \widetilde{\mathbf{G}}^{2-1}_{LM} \Big) \\
&+ \frac{\alpha}{3} m_1 m_0 \Big(\sqrt{\frac{16\pi}{5}}\ \widetilde{\mathbf{G}}^{20}_{LM} C_{l'm_1,LM,lm_0} + \mathbf{C}^{lm_0}_{l'm_1} \Big) \Big] \Big\} \\
\Big\}. \qquad (6.28)
\end{aligned}
$$

Thus, a lot of implementation has to be done for the spin-diagonal part. The other matrix elements with the energy derivative of the atomic functions $\dot{\Phi}_{\mathbf{R}lm\alpha}$ can be obtained analogously just by replacing $\phi_{\mathbf{R}l\alpha} \to \dot{\phi}_{\mathbf{R}l\alpha}$ and $\gamma_{\mathbf{R}l\alpha} \to \dot{\gamma}_{\mathbf{R}l\alpha}$. All radial matrix elements have to be calculated numerically. The angular and spin parts are calculated analytically.

6.2.2 Non-spin-diagonal part (Yafet part)

Here, only the result of the implementation of the non-spin-diagonal matrix element (Yafet part) in the LMTO-ASA code is given. The full calculation and the explanation of the notation can be found in appendix B. Using eq. (2.29) the non-spin-diagonal matrix element (Yafet part) $\langle \Phi_{\mathbf{R}l'm'\alpha'} | \widetilde{W'}^{nsd}_{\lambda,\mathbf{R}} | \Phi_{\mathbf{R}lm\alpha} \rangle$ of the non-spin-diagonal part of the operator given in eq. (6.24) reads

$$
\begin{aligned}
\mathbf{n}^{\mathbf{R}}_{\mathbf{q}\lambda} \Bigg\langle \Phi_{\mathbf{R}l'm'\alpha'} \Bigg| & \mathbf{e}_{r_{\mathbf{R}}} \frac{1}{r_{\mathbf{R}}} \frac{\partial \xi(r_{\mathbf{R}})}{\partial r_{\mathbf{R}}} \sum_i \begin{pmatrix} (\widehat{\mathbf{L}}_{\mathbf{R}})_i \, \widehat{\sigma}_i & & 0 & 0 \\ & & 0 & 0 \\ 0 & 0 & 0 & 0 \\ 0 & 0 & 0 & 0 \end{pmatrix} \\
& + \mathbf{e}_{\vartheta_{\mathbf{R}}} \frac{\xi(r_{\mathbf{R}})}{r_{\mathbf{R}}} \sum_i \begin{pmatrix} (\mathbf{e}_{\vartheta_{\mathbf{R}}} \times \widehat{\mathbf{p}})_i \, \widehat{\sigma}_i & & 0 & 0 \\ & & 0 & 0 \\ 0 & 0 & 0 & 0 \\ 0 & 0 & 0 & 0 \end{pmatrix} \\
& + \mathbf{e}_{\phi_{\mathbf{R}}} \frac{\xi(r_{\mathbf{R}})}{r_{\mathbf{R}}} \sum_i \begin{pmatrix} (\mathbf{e}_{\phi_{\mathbf{R}}} \times \widehat{\mathbf{p}})_i \, \widehat{\sigma}_i & & 0 & 0 \\ & & 0 & 0 \\ 0 & 0 & 0 & 0 \\ 0 & 0 & 0 & 0 \end{pmatrix} \Bigg| \Phi_{\mathbf{R}lm\alpha} \Bigg\rangle
\end{aligned}
$$

$$= \mathbf{n}_{\mathbf{q}\lambda} \Bigg\{ \left\langle \phi_{\mathbf{R}l'\alpha'} \left| \frac{1}{r_{\mathbf{R}}} \frac{\partial \xi(r_{\mathbf{R}})}{\partial r_{\mathbf{R}}} \right| \phi_{\mathbf{R}l\alpha} \right\rangle \sum_{\substack{m_0=-l \\ m_1=-l'}}^{\substack{m_1=l' \\ m_0=l}} K^*_{l'm'm_1} K_{lmm_0} \hbar \cdot$$

$$\left[\delta_{-\alpha\alpha'} S^{+\alpha}_{lm_0} \mathbf{C}^{l(m_0+\alpha)}_{l'm_1} + \delta_{\alpha\alpha'} \alpha m_0 \mathbf{C}^{lm_0}_{l'm_1} \right]$$

$$- i\hbar \left\langle \phi_{\mathbf{R}l'\alpha'} \left| \frac{\xi(r_{\mathbf{R}})}{r_{\mathbf{R}}} \frac{\partial}{\partial r_{\mathbf{R}}} \right| \phi_{\mathbf{R}l\alpha} \right\rangle \cdot \sqrt{\frac{4\pi}{3}} \cdot$$

$$\Bigg[\begin{pmatrix} 0 \\ \widetilde{G}_{l'm',10,lm} \\ -\widetilde{G}_{l'm',1-1,lm} \end{pmatrix} \delta_{-\alpha\alpha'} + \begin{pmatrix} -\widetilde{G}_{l'm',10,lm} \\ 0 \\ \widetilde{G}_{l'm',11,lm} \end{pmatrix} i\alpha\delta_{-\alpha\alpha'}$$

$$+ \begin{pmatrix} \widetilde{G}_{l'm',1-1,lm} \\ -\widetilde{G}_{l'm',11,lm} \\ 0 \end{pmatrix} \alpha\delta_{\alpha\alpha'} \Bigg]$$

$$- \left\langle \phi_{\mathbf{R}l'\alpha'} \left| \frac{\xi(r_{\mathbf{R}})}{r^2_{\mathbf{R}}} \right| \phi_{\mathbf{R}l\alpha} \right\rangle \cdot \Big\{ \langle Z_{l'm'} | \sin\vartheta_{\mathbf{R}} \cos\phi_{\mathbf{R}} \ \widehat{\mathbf{L}}_{\mathbf{R}} | Z_{lm} \rangle \ \delta_{-\alpha\alpha'}$$

$$+ \langle Z_{l'm'} | \sin\vartheta_{\mathbf{R}} \sin\phi_{\mathbf{R}} \ \widehat{\mathbf{L}}_{\mathbf{R}} | Z_{lm} \rangle \ i\alpha\delta_{-\alpha\alpha'}$$

$$+ \langle Z_{l'm'} | \cos\vartheta_{\mathbf{R}} \ \widehat{\mathbf{L}}_{\mathbf{R}} | Z_{lm} \rangle \ \alpha\delta_{\alpha\alpha'} \Big\} \Bigg\}. \tag{6.29}$$

All radial integrals are calculated numerically. The angular and spin parts are calculated analytically. Again, the other matrix elements with the energy derivative of the atomic functions $\dot{\Phi}_{\mathbf{R}lm\alpha}$ can be obtained analogously just by replacing $\phi_{\mathbf{R}l\alpha} \to \dot{\phi}_{\mathbf{R}l\alpha}$.

6.3 Transition rates

The transition rate is given by Fermi's golden rule (eq. (5.3))

$$W^{\lambda}_{j\mathbf{k}s,j'\mathbf{k}'s'} = \frac{2\pi}{\hbar} \left| \sum_B \sqrt{\frac{1}{M_B}} M^{\lambda,B}_{j\mathbf{k}s,j'\mathbf{k}'s'} \right|^2 \frac{\hbar}{2N \ \omega_{\mathbf{q}\lambda}} \cdot$$

$$\cdot \left\{ b_{\mathbf{q}\lambda} \ \delta(\varepsilon^{s'}_{j'\mathbf{k}'} - (\varepsilon^{s}_{j\mathbf{k}} + \hbar\omega_{\mathbf{q}\lambda})) + \ (b_{-\mathbf{q}\lambda} + 1) \ \delta(\varepsilon^{s'}_{j'\mathbf{k}'} - (\varepsilon^{s}_{j\mathbf{k}} - \hbar\omega_{-\mathbf{q}\lambda})) \right\} \tag{6.30}$$

with the matrix element (eq. (6.26))

$$M^{\lambda,B}_{j\mathbf{k}s,j'\mathbf{k}'s'} = \delta_{\mathbf{k}+\mathbf{q},\mathbf{k}'+\mathbf{G}} \sum_{\substack{\mathbf{R}lm\alpha \\ l'm'\alpha'}} -\delta_{\mathbf{R}^0_B\mathbf{R}} \cdot \left\{ \left(c^{j'\mathbf{k}'s'}_{\mathbf{R}l'm'\alpha'} \right)^* c^{j\mathbf{k}s}_{\mathbf{R}lm\alpha} \langle \Phi_{\mathbf{R}l'm'\alpha'} | \widetilde{W}'_{\lambda,\mathbf{R}} | \Phi_{\mathbf{R}lm\alpha} \rangle + \dots \right\}. \quad (6.31)$$

Combining the last two equations gives

$$W^{\lambda}_{j\mathbf{k}s,j'\mathbf{k}'s'} = \frac{\pi}{N\omega_{\mathbf{q}\lambda}} \, \delta_{\mathbf{k}+\mathbf{q},\mathbf{k}'+\mathbf{G}} \left| \sum_{\substack{\mathbf{R}lm\alpha \\ l'm'\alpha'}} \sqrt{\frac{1}{M_{\mathbf{R}}}} \, m^{\lambda,\mathbf{R}}_{j\mathbf{k}s,j'\mathbf{k}'s'} \right|^2 \cdot \left\{ b_{\mathbf{q}\lambda} \, \delta(\varepsilon^{s'}_{j'\mathbf{k}'} - (\varepsilon^{s}_{j\mathbf{k}} + \hbar\omega_{\mathbf{q}\lambda})) + \, (b_{-\mathbf{q}\lambda} + 1) \, \delta(\varepsilon^{s'}_{j'\mathbf{k}'} - (\varepsilon^{s}_{j\mathbf{k}} - \hbar\omega_{-\mathbf{q}\lambda})) \right\} \quad (6.32)$$

where

$$m^{\lambda,\mathbf{R}}_{j\mathbf{k}s,j'\mathbf{k}'s'} = \left(c^{j'\mathbf{k}'s'}_{\mathbf{R}l'm'\alpha'} \right)^* c^{j\mathbf{k}s}_{\mathbf{R}lm\alpha} \langle \Phi_{\mathbf{R}l'm'\alpha'} | \widetilde{W}'_{\lambda,\mathbf{R}} | \Phi_{\mathbf{R}lm\alpha} \rangle + \dots \quad (6.33)$$

Looking at eq. (6.29) we see that the non-spin-diagonal matrix element can be written as a scalar product

$$\langle \Phi_{\mathbf{R}l'm'\alpha'} | \widetilde{W}'^{nsd}_{\lambda,\mathbf{R}} | \Phi_{\mathbf{R}lm\alpha} \rangle = \mathbf{n}^{\mathbf{R}}_{\mathbf{q}\lambda} \cdot (\mathbf{m}^{\mathbf{R}l'm'\alpha'}_{\mathbf{R}lm\alpha})^{nsd} \quad (6.34)$$

where

$$(\mathbf{m}^{\mathbf{R}l'm'\alpha'}_{\mathbf{R}lm\alpha})^{nsd} = \left\langle \phi_{\mathbf{R}l'\alpha'} \left| \frac{1}{r_{\mathbf{R}}} \frac{\partial \xi(r_{\mathbf{R}})}{\partial r_{\mathbf{R}}} \right| \phi_{\mathbf{R}l\alpha} \right\rangle \sum_{\substack{m_0=-l \\ m_1=-l'}}^{\substack{m_1=l' \\ m_0=l}} K^*_{l'm'm_1} K_{lmm_0} \hbar \cdot \left[\delta_{-\alpha\alpha'} S^{+\alpha}_{lm_0} \mathbf{C}^{l(m_0+\alpha)}_{l'm_1} + \delta_{\alpha\alpha'} \alpha m_0 \mathbf{C}^{lm_0}_{l'm_1} \right] - i\hbar \left\langle \phi_{\mathbf{R}l'\alpha'} \left| \frac{\xi(r_{\mathbf{R}})}{r_{\mathbf{R}}} \frac{\partial}{\partial r_{\mathbf{R}}} \right| \phi_{\mathbf{R}l\alpha} \right\rangle \cdot \sqrt{\frac{4\pi}{3}} \cdot \left[\begin{pmatrix} 0 \\ \widetilde{G}_{l'm',10,lm} \\ -\widetilde{G}_{l'm',1-1,lm} \end{pmatrix} \delta_{-\alpha\alpha'} + \begin{pmatrix} -\widetilde{G}_{l'm',10,lm} \\ 0 \\ \widetilde{G}_{l'm',11,lm} \end{pmatrix} i\alpha\delta_{-\alpha\alpha'} \right.$$

$$+\begin{pmatrix} \widetilde{G}_{l'm',1-1,lm} \\ -\widetilde{G}_{l'm',11,lm} \\ 0 \end{pmatrix} \alpha\delta_{\alpha\alpha'}\Bigg]$$

$$-\left\langle \phi_{\mathbf{R}l'\alpha'} \left| \frac{\xi(r_{\mathbf{R}})}{r_{\mathbf{R}}^2} \right| \phi_{\mathbf{R}l\alpha} \right\rangle \cdot \Big\{ \langle Z_{l'm'}|\sin\vartheta_{\mathbf{R}}\cos\phi_{\mathbf{R}}\ \widehat{\mathbf{L}}_{\mathbf{R}}|Z_{lm}\rangle\ \delta_{-\alpha\alpha'}$$
$$+ \langle Z_{l'm'}|\sin\vartheta_{\mathbf{R}}\sin\phi_{\mathbf{R}}\ \widehat{\mathbf{L}}_{\mathbf{R}}|Z_{lm}\rangle\ i\alpha\delta_{-\alpha\alpha'}$$
$$+ \langle Z_{l'm'}|\cos\vartheta_{\mathbf{R}}\ \widehat{\mathbf{L}}_{\mathbf{R}}|Z_{lm}\rangle\ \alpha\delta_{\alpha\alpha'}\Big\}. \quad (6.35)$$

The same can be done for the spin-diagonal case, eq. (6.28), and therefore one can rewrite the matrix elements of the total scattering operator

$$\langle \Phi_{\mathbf{R}l'm'\alpha'}|\widetilde{W'}_{\lambda,\mathbf{R}}|\Phi_{\mathbf{R}lm\alpha}\rangle = \mathbf{n}_{\mathbf{q}\lambda}^{\mathbf{R}}\ \cdot \mathbf{m}_{\mathbf{R}lm\alpha}^{\mathbf{R}l'm'\alpha'}. \quad (6.36)$$

For a monatomic crystal (Ni and Fe are monatomic) the transition rate simplifies

$$W_{j\mathbf{k}s,j'\mathbf{k}'s'}^{\lambda}$$
$$= \frac{\pi}{NM\omega_{\mathbf{q}\lambda}}\ \delta_{\mathbf{k}+\mathbf{q},\mathbf{k}'+\mathbf{G}} \left| \overbrace{\mathbf{n}_{\mathbf{q}\lambda}\ \cdot \sum_{\substack{lm\alpha \\ l'm'\alpha'}} \left[\left(c_{l'm'\alpha'}^{j'\mathbf{k}'s'} \right)^* c_{lm\alpha}^{j\mathbf{k}s} \mathbf{m}_{lm\alpha}^{l'm'\alpha'} + \ldots \right]}^{M_{j\mathbf{k}s,j'\mathbf{k}'s'}^{\lambda}} \right|^2 \cdot$$
$$\cdot \Big\{ b_{\mathbf{q}\lambda}\ \delta(\varepsilon_{j'\mathbf{k}'}^{s'} - (\varepsilon_{j\mathbf{k}}^{s} + \hbar\omega_{\mathbf{q}\lambda})) + \ (b_{-\mathbf{q}\lambda}+1)\ \delta(\varepsilon_{j'\mathbf{k}'}^{s'} - (\varepsilon_{j\mathbf{k}}^{s} - \hbar\omega_{-\mathbf{q}\lambda}))\Big\}. \quad (6.37)$$

The big advantage of this notation is that the $\mathbf{m}_{lm\alpha}^{l'm'\alpha'}$ do not depend on $(j,\mathbf{k},s)$, $(j',\mathbf{k}',s')$ and $(\mathbf{q},\lambda)$. The $\mathbf{m}_{lm\alpha}^{l'm'\alpha'}$ can be calculated independently from the scattering process. They are stored in a file for all combinations of (l,m,α) and (l',m',α') where $(\alpha=1,-1)$, $(\alpha'=1,-1)$, $(l=0,1,2)$, $(l'=0,1,2)$, $(m=-l,...,+l)$ and $(m'=-l',...,+l')$.

6.4 Brillouin zone integration and smearing of the delta function

Here, it is demonstrated how the Brillouin zone integration and the smearing of the delta function is made:

If we only consider the absorption of phonons (without emission) the total transition rate in eq. (5.26) reads

$$W^{s,s'}(t) = \frac{1}{\Omega_{BZ}^2} \sum_{j,j',\lambda} \int_{BZ} \mathrm{d}^3k \int_{BZ} \mathrm{d}^3k' \; f_t(\varepsilon^s_{j\mathbf{k}}) \left[1 - f_t(\varepsilon^{s'}_{j'\mathbf{k}'})\right] \frac{\pi \; b_{\mathbf{q}\lambda}}{NM\omega_{\mathbf{q}\lambda}} \cdot \left|M^{\lambda}_{j\mathbf{k}s,j'\mathbf{k}'s'}\right|^2 \cdot \delta(\varepsilon^{s'}_{j'\mathbf{k}'} - (\varepsilon^s_{j\mathbf{k}} + \hbar\omega_{\mathbf{q}\lambda})). \tag{6.38}$$

$f_t(\varepsilon^s_{j\mathbf{k}})$ is an abbreviation for $f(\varepsilon^s_{j\mathbf{k}}, \varepsilon^s_{\mathrm{F}}(t), T_e(t))$, and it is demanded that $\mathbf{k} + \mathbf{q} = \mathbf{k}' + \mathbf{G}$. For a calculation on a discrete grid of k-points we have to choose $\mathbf{k}$ and $\mathbf{k}'$ on the grid because otherwise we cannot calculate the matrix element according to eq. (6.37). For a combination of $\mathbf{k}$ and $\mathbf{k}'$ we can calculate $\mathbf{q} = \mathbf{k}' - \mathbf{k}$ (or $\mathbf{q} = \mathbf{k}' - \mathbf{k} + \mathbf{G}$ if $\mathbf{q}$ is not in the first Brillouin zone; note: this is not necessary for $\omega_{\mathbf{q}\lambda}$ and $\mathbf{n}_{\mathbf{q}\lambda}$ which are already lattice-periodic functions). For this $\mathbf{q}$ the three phonon frequencies $\omega_{\mathbf{q}\lambda}$ and polarization vectors $\mathbf{n}_{\mathbf{q}\lambda}$ are calculated with the force-constant model (see chapter 3). Using this procedure the energy conservation $\varepsilon^{s'}_{j'\mathbf{k}'} = \varepsilon^s_{j\mathbf{k}} + \hbar\omega_{\mathbf{q}\lambda}$ is in general not fulfilled, only maybe by chance. This is a serious problem because for coarse grids the energy conservation is for no combination of $\mathbf{k}$ and $\mathbf{k}'$ fulfilled and the total transition rates are zero. One would have to calculate with an infinitely dense k-grid to fulfill the energy conservation. The easiest solution to this problem is to smear the delta function which gives a large contribution if the energy conservation is almost fulfilled and a very small contribution if the energy conservation is very badly fulfilled. To do this we have to replace the delta function by its identity, and here the Gaussian identity is chosen

$$\int \mathrm{d}k \; f(k)\delta(k) = \lim_{\sigma\to 0} \int \mathrm{d}k \; f(k) \frac{1}{\sqrt{\pi\sigma^2}} \exp\left(-\frac{k^2}{\sigma^2}\right) \approx \int \mathrm{d}k \; f(k)\delta_\sigma(k) \tag{6.39}$$

where the smeared delta function is defined by

$$\delta_\sigma(k) \equiv \frac{1}{\sqrt{\pi\sigma^2}} \exp\left(-\frac{k^2}{\sigma^2}\right). \tag{6.40}$$

$f(k)$ is some function that depends on a variable k and the approximation is only good for small smearing parameters σ. Eq. (6.38) has a more complicated form: The integration is with respect to $\mathbf{k}$ and the delta

function is with respect to the energy ε that depends on $\mathbf{k}$. To the best of my knowledge it is not discussed in literature if the following equation holds in general

$$\int \mathrm{d}k\ f(k)\delta(\varepsilon) \overset{???}{=} \lim_{\sigma\to 0}\int \mathrm{d}k\ f(k)\frac{1}{\sqrt{\pi\sigma^2}}\exp\left(-\frac{\varepsilon^2}{\sigma^2}\right) \approx \int \mathrm{d}k\ f(k)\delta_\sigma(\varepsilon). \tag{6.41}$$

The question marks are only concerning the identity but not concerning the smearing! I will show that under certain circumstances eq. (6.41) really holds. To do this, I avoid for the moment the problem by changing the integration variable from k to ε. Using

$$\mathrm{d}^3k = \frac{1}{|\nabla_{\mathbf{k}}\varepsilon^s_{j\mathbf{k}}|}\ \mathrm{d}\varepsilon^s_{j\mathbf{k}}\ \mathrm{d}S \tag{6.42}$$

eq. (6.38) reads (S is the surface of constant energy $\varepsilon^s_{j\mathbf{k}}$)

$$\begin{aligned}
W^{s,s'}(t) = {} & \frac{1}{\Omega^2_{BZ}}\sum_{j,j',\lambda}\int_S \mathrm{d}S\int_{S'}\mathrm{d}S'\int_{\varepsilon^s_{j\mathbf{k}}}\mathrm{d}\varepsilon^s_{j\mathbf{k}}\int_{\varepsilon^{s'}_{j'\mathbf{k}'}}\mathrm{d}\varepsilon^{s'}_{j'\mathbf{k}'}\cdot \\
& \frac{\pi\ b_{\mathbf{q}\lambda}}{NM\omega_{\mathbf{q}\lambda}}\cdot\left|M^\lambda_{j\mathbf{k}s,j'\mathbf{k}'s'}\right|^2\cdot\frac{f_t(\varepsilon^s_{j\mathbf{k}})\left[1-f_t(\varepsilon^{s'}_{j'\mathbf{k}'})\right]}{|\nabla_{\mathbf{k}}\varepsilon^s_{j\mathbf{k}}||\nabla_{\mathbf{k}'}\varepsilon^{s'}_{j'\mathbf{k}'}|}\ \delta(\varepsilon^{s'}_{j'\mathbf{k}'}-(\varepsilon^s_{j\mathbf{k}}+\hbar\omega_{\mathbf{q}\lambda})) \\
\approx {} & \frac{1}{\Omega^2_{BZ}}\sum_{j,j',\lambda}\int_S \mathrm{d}S\int_{S'}\mathrm{d}S'\frac{\pi\ b_{\mathbf{q}\lambda}}{NM\omega_{\mathbf{q}\lambda}}\cdot\left|M^\lambda_{j\mathbf{k}s,j'\mathbf{k}'s'}\right|^2\int_{\varepsilon^s_{j\mathbf{k}}}\mathrm{d}\varepsilon^s_{j\mathbf{k}}\int_{\varepsilon^{s'}_{j'\mathbf{k}'}}\mathrm{d}\varepsilon^{s'}_{j'\mathbf{k}'}\cdot \\
& \frac{f_t(\varepsilon^s_{j\mathbf{k}})\left[1-f_t(\varepsilon^{s'}_{j'\mathbf{k}'})\right]}{|\nabla_{\mathbf{k}}\varepsilon^s_{j\mathbf{k}}||\nabla_{\mathbf{k}'}\varepsilon^{s'}_{j'\mathbf{k}'}|}\ \delta(\varepsilon^{s'}_{j'\mathbf{k}'}-(\varepsilon^s_{j\mathbf{k}}+\hbar\omega_{\mathbf{q}\lambda})).
\end{aligned} \tag{6.43}$$

The last transformation is approximately true if the quantity $b_{\mathbf{q}\lambda}\left|M^\lambda_{j\mathbf{k}s,j'\mathbf{k}'s'}\right|^2/\omega_{\mathbf{q}\lambda}$ is only weakly energy dependent (these are the circumstances mentioned above). In fact only processes near the Fermi energy are relevant for the total transition rates (which is shown in section 6.6) so that the latter quantity can be assumed as weakly energy dependent for relevant scattering processes around the Fermi energy. Now, we see that the integrands for the integrals with respect to $\varepsilon^s_{j\mathbf{k}}$ and $\varepsilon^{s'}_{j'\mathbf{k}'}$ only depend on the energy and we are certainly allowed to replace the delta

function by its identity. Then, we use a smeared delta function and reverse the change of the integration variable. The expression for the total transition rate on a discrete k-grid reads (here: only absorption)

$$W^{s,s'}(t) = \sum_{j,j',\lambda} \sum_{\mathbf{k},\mathbf{k}'} \frac{\Omega_{\mathbf{k}}\Omega_{\mathbf{k}'}}{\Omega_{BZ}^2} \; f_t(\varepsilon^s_{j\mathbf{k}}) \left[1 - f_t(\varepsilon^{s'}_{j'\mathbf{k}'})\right] \frac{\pi \; b_{\mathbf{q}\lambda}}{NM\omega_{\mathbf{q}\lambda}} \cdot \left|M^{\lambda}_{j\mathbf{k}s,j'\mathbf{k}'s'}\right|^2 \cdot \delta_\sigma(\varepsilon^{s'}_{j'\mathbf{k}'} - (\varepsilon^s_{j\mathbf{k}} + \hbar\omega_{\mathbf{q}\lambda})) \tag{6.44}$$

where the integrals with respect to $\mathbf{k}$ and $\mathbf{k}'$ are replaced by sums ($\Omega_{\mathbf{k}}/\Omega_{BZ}$ is the weight of the k-point in the Brillouin zone). For an equidistant k-point net we have $\Omega_{\mathbf{k}}/\Omega_{BZ} = 1/N_{\mathbf{k}}$ where $N_{\mathbf{k}}$ is the total number of k-points.

Finally, I make some important comments:

1. The calculations have to be performed for different smearing parameters σ and different k-point grids. Of course, the k-point grid should be dense enough so that a phonon absorption or emission (with phonon energies up to 3 mRy) is enough to change the energy of an initial state by electron-phonon scattering. The smearing parameter is related to the energy variation between neighboring k-points. For denser k-point grids the smearing parameter should be smaller. In ref. [9] it is shown that $\sigma \cdot N_1 = const$ (where N_1 is the number of k-points in one direction) is a good relation to test the convergence for different smearing parameters and k-point grids. We will see in chapter 7 that the results do not depend so much on the smearing parameter.

2. A big advantage of the smearing used in eq. (6.44) is that the phonon energy $\hbar\omega_{\mathbf{q}\lambda}$ in the delta function is taken explicitly into account. It is often neglected in other publications on electron-phonon scattering because $\hbar\omega_{\mathbf{q}\lambda}$ is much smaller than typical electron energies, see, e.g., refs. [71, 72].

3. In principle, it is also possible to use the tetrahedron method as an alternative to the smearing method. The tetrahedron method is described in the PhD theses of Meyer [11] and Grotheer [9]. It is definitely more complicated and not used in this thesis.

4. One could also smear the Fermi-Dirac functions $f_t(\varepsilon^s_{j\mathbf{k}})$ and $f_t(\varepsilon^{s'}_{j'\mathbf{k}'})$ in order to improve the convergence [9]. In this thesis the Fermi-Dirac functions are not smeared because the k-point grids are so dense that an improvement of the convergence is not necessary. Please note that the smearing of the delta function is really indispensable to obtain total transition rates unequal zero and that the smearing of the Fermi-Dirac functions is not necessary at all if dense k-point grids are used.

6.5 Relaxation time

The relaxation time for a discrete k-point grid reads (compare with eq. (5.44))

$$\frac{1}{T_1} = \sum_{j,j',\lambda} \sum_{\mathbf{k},\mathbf{k}'} \frac{\Omega_{\mathbf{k}}\Omega_{\mathbf{k}'}}{\Omega^2_{BZ}} \cdot \Bigg\{ W^{\lambda}_{j\mathbf{k}\uparrow,j'\mathbf{k}'\downarrow} \left[\frac{f_0(\varepsilon^{\uparrow}_{j\mathbf{k}})\ \eta(\varepsilon^{\downarrow}_{j'\mathbf{k}'})}{\widetilde{Z}^{\downarrow}(\varepsilon^0_{\mathrm{F}})} + \frac{(1-f_0(\varepsilon^{\downarrow}_{j'\mathbf{k}'}))\ \eta(\varepsilon^{\uparrow}_{j\mathbf{k}})}{\widetilde{Z}^{\uparrow}(\varepsilon^0_{\mathrm{F}})} \right] + W^{\lambda}_{j'\mathbf{k}'\downarrow,j\mathbf{k}\uparrow} \left[\frac{f_0(\varepsilon^{\downarrow}_{j'\mathbf{k}'})\ \eta(\varepsilon^{\uparrow}_{j\mathbf{k}})}{\widetilde{Z}^{\uparrow}(\varepsilon^0_{\mathrm{F}})} + \frac{(1-f_0(\varepsilon^{\uparrow}_{j\mathbf{k}}))\ \eta(\varepsilon^{\downarrow}_{j'\mathbf{k}'})}{\widetilde{Z}^{\downarrow}(\varepsilon^0_{\mathrm{F}})} \right] \Bigg\}, \tag{6.45}$$

and the transition rate $W^{\lambda}_{j\mathbf{k}s,j'\mathbf{k}'s'}$ reads (compare with eq. (6.37))

$$W^{\lambda}_{j\mathbf{k}s,j'\mathbf{k}'s'} = \frac{\pi}{NM\omega_{\mathbf{q}\lambda}} \left| \mathbf{n}_{\mathbf{q}\lambda} \cdot \sum_{\substack{lm\alpha \\ l'm'\alpha'}} \left[\left(c^{j'\mathbf{k}'s'}_{l'm'\alpha'} \right)^* c^{j\mathbf{k}s}_{lm\alpha} \mathbf{m}^{l'm'\alpha'}_{lm\alpha} + \dots \right] \right|^2 \cdot \cdot \left\{ b_{\mathbf{q}\lambda}\ \delta_\sigma(\varepsilon^{s'}_{j'\mathbf{k}'} - (\varepsilon^s_{j\mathbf{k}} + \hbar\omega_{\mathbf{q}\lambda})) + \ (b_{\mathbf{q}\lambda}+1)\ \delta_\sigma(\varepsilon^{s'}_{j'\mathbf{k}'} - (\varepsilon^s_{j\mathbf{k}} - \hbar\omega_{\mathbf{q}\lambda})) \right\}. \tag{6.46}$$

Thereby quasi momentum conservation is demanded.

Temperature

In Yafet's theory only one temperature enters the equation for the relaxation time (in the Fermi-Dirac function $f_0(\varepsilon^s_{j\mathbf{k}})$, in its derivative $\eta(\varepsilon^s_{j\mathbf{k}})$

and in the Bose function $b_{\mathbf{q}\lambda}$), namely the electron and lattice temperature for which the experiment is performed. Here, I choose room temperature $T = 300$ K since most experiments are performed at room temperature. The band structure calculations with the LMTO-ASA code are made for $T = 0$ K and it is assumed that the band structure does not change a lot for room temperature (which is normally a good approximation). Especially the exchange splitting is approximately the same for room temperature. I.e., the matrix elements $|M^{\lambda}_{j\mathbf{k}s,j'\mathbf{k}'s'}|^2$, the energies $\varepsilon^s_{j\mathbf{k}}$, the density of states $Z^s(\varepsilon)$ and the phonon polarization vectors $\mathbf{n}_{\mathbf{q}\lambda}$ and frequencies $\omega_{\mathbf{q}\lambda}$ are calculated for $T = 0$ K and it is assumed that this gives approximately the same results for $T = 300$ K.

Numerical aspects

Some numerical aspects have to be respected:

1. The derivative of the Fermi-Dirac function is defined in eq. (5.35)

$$\eta(\varepsilon^s_{j\mathbf{k}}) = \frac{\partial}{\partial\varepsilon^0_{\mathrm{F}}} f_0(\varepsilon^s_{j\mathbf{k}}) = \frac{1}{kT}\ \exp\left(\frac{\varepsilon^s_{j\mathbf{k}} - \varepsilon^0_{\mathrm{F}}}{kT}\right)\ \cdot f_0^2(\varepsilon^s_{j\mathbf{k}}). \tag{6.47}$$

   This form is not suitable for a numerical calculation because the exponential $\exp((\varepsilon^s_{j\mathbf{k}} - \varepsilon^0_{\mathrm{F}})/kT)$ can be very large. Using simple algebra one can see that the following forms are equivalent

$$\eta(\varepsilon^s_{j\mathbf{k}}) = \frac{1}{kT}\ f_0(\varepsilon^s_{j\mathbf{k}})(1 - f_0(\varepsilon^s_{j\mathbf{k}})) = \frac{1}{4kT}\ \cosh^{-2}\left(\frac{\varepsilon^s_{j\mathbf{k}} - \varepsilon^0_{\mathrm{F}}}{2kT}\right) \tag{6.48}$$

   which are more suitable for a numerical calculation.

2. The density of states $Z^s(\varepsilon)$ is calculated with the LMTO-ASA code as explained in subsection 2.2.4. The delta function is smeared by a smearing parameter and hence, the density of states depends also on the chosen smearing parameter. However, in eq. (6.45) only the quantity $\widetilde{Z}^s(\varepsilon^0_{\mathrm{F}})$ defined below eq. (5.40) enters which is almost the density of states at the Fermi energy because $\eta(\varepsilon)$ is approximately given by $\delta(\varepsilon - \varepsilon^0_{\mathrm{F}})$. This quantity does not depend much on the chosen smearing parameter for $Z^s(\varepsilon)$.

Summation of k-points

1. The summation runs over all dominant-up and all dominant-down states. A state is dominant-up if the probability for spin-up is larger than the probability for spin-down $p^{\uparrow}_{j\mathbf{k}} > p^{\downarrow}_{j\mathbf{k}}$ or $p^{\uparrow}_{j\mathbf{k}} > 0.5$. However, in order to define the relaxation time T_1 Yafet assumes that every state has the same magnetic moment $\pm m$ and that every scattering process changes the magnetic moment by $\pm 2m$. According to eq. (5.19) this is approximately fulfilled for a stricter definition, say, e.g., only states with $p^{\uparrow,\downarrow}_{j\mathbf{k}} > 0.9$ are taken into account and states with $0 < p^{\uparrow,\downarrow}_{j\mathbf{k}} \leq 0.9$ do not contribute. The results are tested for different definitions in subsection 7.1.2.

2. It is excluded in the summations of eq. (6.45) that the initial and final wavevector are equal, $\mathbf{k} = \mathbf{k}'$, which means that the phonon wavevector $\mathbf{k}' - \mathbf{k} = \mathbf{q} = 0$ and the phonon frequency $\omega_{\mathbf{q}\lambda}$ is zero for the acoustic case. A phonon with $\mathbf{q} = 0$ is a translation or rigid rotation of the lattice and should not give a contribution to the relaxation time $1/T_1$ since there is no distortion of the lattice.

3. Because of the missing screening effects[17] (see section 5.4) eq. (6.45) even diverges for small phonon frequencies[18] although the transition rate should go to zero if the phonon wavevector goes to zero (see 2.). Therefore small phonon frequencies and hence small phonon wavevectors also have to be excluded which means that the k-point grid should not be too fine. The fundamental law in numerics, "the finer the grid the more reliable the results", may not be fulfilled if the grid is too fine!

4. Let N_1 be the number of k-points in one direction. Then the total number of k-points is N_1^3. The total number of considered bands is 18 in Ni and Fe (one atom in the unit cell) since there are s-, p- and d-orbitals ($l = 0, 1, 2$ and $m_l = -l, ..., +l$) and in addition

[17] Screening of the electron-phonon scattering is per definition excluded if the rigid-ion approximation is used.

[18] The matrix element depends on $\mathbf{q}$ only via the polarization vector $\mathbf{n}_{\mathbf{q}\lambda}$ and indirectly via the expansion coefficients $c^{j\mathbf{k}s}_{lm\alpha}$, $c^{j'\mathbf{k}'s'}_{l'm'\alpha'}$ and $d^{j\mathbf{k}s}_{lm\alpha}$, $d^{j'\mathbf{k}'s'}_{l'm'\alpha'}$. However, the polarization vector $\mathbf{n}_{\mathbf{q}\lambda}$ is definitely not zero for $\mathbf{q} = 0$ and does not go to zero for $\mathbf{q} \to 0$. The same holds for the expansion coefficients.

two spin orientations. Then, the total number of states is $18 \cdot N_1^3$. Let us assume for simplicity that there are as many dominant-up as dominant-down states, i.e., $9 \cdot N_1^3$ dominant-up states and $9 \cdot N_1^3$ dominant-down states. For a scattering process one can combine each dominant-up state with a dominant-down state, i.e., there are in principle $(9 \cdot N_1^3)^2 = 81 \cdot N_1^6$ scattering processes possible. The computational time goes like N_1^6.

Selection of k-points

For dense grids it is very time-consuming to sum over all possible $(j, \mathbf{k}, s)$ and $(j', \mathbf{k}', s')$. Therefore a preselection of relevant k-points and relevant scattering processes is necessary. The functions $\eta(\varepsilon^{\uparrow}_{j\mathbf{k}})$, $\eta(\varepsilon^{\downarrow}_{j'\mathbf{k}'})$ and $\delta_\sigma(\varepsilon^{s'}_{j'\mathbf{k}'} - (\varepsilon^{s}_{j\mathbf{k}} \pm \hbar\omega_{\mathbf{q}\lambda}))$ are suitable for a preselection, i.e., we have to decide which $\eta(\varepsilon^{\uparrow}_{j\mathbf{k}})$, $\eta(\varepsilon^{\downarrow}_{j'\mathbf{k}'})$ and $\delta_\sigma(\varepsilon^{s'}_{j'\mathbf{k}'} - (\varepsilon^{s}_{j\mathbf{k}} \pm \hbar\omega_{\mathbf{q}\lambda}))$ are necessary to be calculated in eq. (6.45). Let us first examine the two functions:

- For zero temperature the function

$$\eta(\varepsilon) = \frac{1}{kT}\, f_0(\varepsilon)(1 - f_0(\varepsilon)) = \frac{1}{4kT}\, \cosh^{-2}\left(\frac{\varepsilon - \varepsilon_{\mathrm{F}}^0}{2kT}\right) \tag{6.49}$$

  is a delta function centered at the Fermi energy $\varepsilon_{\mathrm{F}}^0$, and for higher temperatures it is a broadened delta function. This means that the function $\eta(\varepsilon)$ is certainly very small if the energy ε is far away from the Fermi energy $\varepsilon_{\mathrm{F}}^0$. We can define a threshold value ζ_1 which $\eta(\varepsilon)$ should not fall below in order to consider $\eta(\varepsilon)$ as relevant for the calculation: $\eta(\varepsilon) > \zeta_1$. This means that the following condition for the energy has to be fulfilled

$$|\varepsilon - \varepsilon_{\mathrm{F}}^0| < 2kT\ \mathrm{arccosh}((4kT\zeta_1)^{-\frac{1}{2}}) \equiv \Delta\varepsilon_\eta. \tag{6.50}$$

  For room temperature the energy kT is 1.9 mRy. Let the threshold value be very small, say $\zeta_1 = 10^{-15}$ Ry^{-1}. Then the energy distance from the Fermi energy should be less than 77.5 mRy, $|\varepsilon - \varepsilon_{\mathrm{F}}^0| <$ 77.5 mRy.

- δ_σ is a smeared delta function

$$\delta_\sigma(\varepsilon^{s'}_{j'\mathbf{k}'} - (\varepsilon^{s}_{j\mathbf{k}} \pm \hbar\omega_{\mathbf{q}\lambda})) = \frac{1}{\sqrt{\pi\sigma^2}} \exp\left(-\frac{(\varepsilon^{s'}_{j'\mathbf{k}'} - (\varepsilon^{s}_{j\mathbf{k}} \pm \hbar\omega_{\mathbf{q}\lambda}))^2}{\sigma^2}\right). \tag{6.51}$$

The phonon energy $\hbar\omega_{\mathbf{q}\lambda}$ is between 0 and 3 mRy, i.e., much smaller than an electron energy. Hence, if the energies $\varepsilon^{s}_{j\mathbf{k}}$ and $\varepsilon^{s'}_{j'\mathbf{k}'}$ are very much different (this cannot be "compensated" by the phonon energy), the delta function is certainly very small. Again, one can define a threshold value ζ_1 which δ_σ should not fall below in order to consider δ_σ as relevant for the calculation: $\delta_\sigma > \zeta_1$. This means for the energies

$$|\varepsilon^{s'}_{j'\mathbf{k}'} - \varepsilon^{s}_{j\mathbf{k}}| < \sqrt{-\sigma^2 \ \ln(\zeta_1\sqrt{\pi\sigma^2})} \pm \hbar\omega_{\mathbf{q}\lambda} \equiv \Delta\varepsilon_\delta. \tag{6.52}$$

σ has to be varied for convergence tests. We will see in chapter 7 that $\sigma = 3$ mRy is a reasonable value and that the results do not depend so much on the smearing parameter. The phonon energy $\hbar\omega_{\mathbf{q}\lambda}$ is between 0 and 3 mRy. Let the threshold value be very small, say again $\zeta_1 = 10^{-15}$ Ry^{-1}. Then, the energy difference should be less than 21.9 mRy (at most for $+\hbar\omega_{\mathbf{q}\lambda} = 3$ mRy): $|\varepsilon^{s'}_{j'\mathbf{k}'} - \varepsilon^{s}_{j\mathbf{k}}| <$ 21.9 mRy.

After the discussion of the two functions we realize that if either $\eta(\varepsilon)$ or $\delta_\sigma(\varepsilon^{s'}_{j'\mathbf{k}'} - (\varepsilon^{s}_{j\mathbf{k}} \pm \hbar\omega_{\mathbf{q}\lambda}))$ falls below the threshold value ζ_1, the contribution to $1/T_1$ for this scattering process is definitely negligible because of the following reasons[19]: The Fermi-Dirac functions $f_0(\varepsilon)$ are between 0 and 1, the integrated densities of states $\widetilde{Z}^s(\varepsilon^0_{\mathrm{F}})$ are constants and the matrix element $|M^{\lambda}_{j\mathbf{k}s,j'\mathbf{k}'s'}|^2$ does not become very large (which has been tested). Furthermore, we do not allow very small phonon frequencies $\omega_{\mathbf{q}\lambda}$ which avoids a divergence in the transition rate $W^{\lambda}_{j\mathbf{k}s,j'\mathbf{k}'s'}$ (because of the missing screening). Finally, $\eta(\varepsilon)$ is limited to a maximum of $(4kT)^{-1}$ =131.6 mRy due to $T = 300$ K and δ_σ is limited to a maximum of $(\pi\sigma^2)^{-1/2}$ which is 188 mRy for $\sigma \approx 3$ mRy.

[19] We have to guarantee that the smallness of either $\eta(\varepsilon)$ or $\delta_\sigma(\varepsilon^{s'}_{j'\mathbf{k}'} - (\varepsilon^{s}_{j\mathbf{k}} \pm \hbar\omega_{\mathbf{q}\lambda}))$ is not compensated accidentally by very large values of other quantities (appearing in eq. (6.45)) for considered values of $\varepsilon^{s}_{j\mathbf{k}}$ and $\varepsilon^{s'}_{j'\mathbf{k}'}$.

Because of the last considerations the smallness of either $\eta(\varepsilon)$ or $\delta_\sigma(\varepsilon^{s'}_{j'\mathbf{k}'} - (\varepsilon^{s}_{j\mathbf{k}} \pm \hbar\omega_{\mathbf{q}\lambda}))$ is not compensated accidentally by other quantities (appearing in eq. (6.45)).

Obviously, we can take δ_σ in order to decide if the scattering process from $(j, \mathbf{k}, s)$ to $(j', \mathbf{k}', s')$ or vice versa makes a relevant contribution to $1/T_1$ or not. The criterion is $|\varepsilon^{s'}_{j'\mathbf{k}'} - \varepsilon^{s}_{j\mathbf{k}}| < \Delta\varepsilon_\delta$ (in the example above: 21.9 mRy) to be a relevant scattering process (selection with respect to the distance between $\varepsilon^{s}_{j\mathbf{k}}$ and $\varepsilon^{s'}_{j'\mathbf{k}'}$).

Obviously, $\eta(\varepsilon^{s}_{j\mathbf{k}})$ is suitable to decide whether a state $(j, \mathbf{k}, s)$ is relevant for the calculation of $1/T_1$ or not (selection with respect to the distance from the Fermi energy ε^0_F). We would like to throw away from the very beginning all states with $|\varepsilon - \varepsilon^0_\mathrm{F}| > \Delta\varepsilon_\eta$ irrespective of the scattering process but with this criterion this is not possible since we have to distinguish the following cases for the contribution to $1/T_1$:

1. We can certainly neglect processes in which $|\varepsilon^{s}_{j\mathbf{k}} - \varepsilon^0_\mathrm{F}| > \Delta\varepsilon_\eta$ and $|\varepsilon^{s'}_{j'\mathbf{k}'} - \varepsilon^0_\mathrm{F}| > \Delta\varepsilon_\eta$ (see fig. 6.1 (a) 1.).

2. A process must be taken into account when $|\varepsilon^{s}_{j\mathbf{k}} - \varepsilon^0_\mathrm{F}| < \Delta\varepsilon_\eta$ and $|\varepsilon^{s'}_{j'\mathbf{k}'} - \varepsilon^0_\mathrm{F}| < \Delta\varepsilon_\eta$ (see fig. 6.1 (a) 2.).

3. If $|\varepsilon^{s}_{j\mathbf{k}} - \varepsilon^0_\mathrm{F}| < \Delta\varepsilon_\eta$ and $|\varepsilon^{s'}_{j'\mathbf{k}'} - \varepsilon^0_\mathrm{F}| > \Delta\varepsilon_\eta$ (or vice versa), the process also has to be taken into account (see fig. 6.1 (a) 3.), because then one of the terms in the squared brackets of eq. (6.45), respectively, cannot be neglected. Obviously, a process for which only one of the two energy differences to ε^0_F is greater than $\Delta\varepsilon_\eta$ cannot be neglected.

Because of the third case it is not possible to throw away from the very beginning all states with energies $|\varepsilon - \varepsilon^0_\mathrm{F}| > \Delta\varepsilon_\eta$ irrespective of the scattering process. However, we can definitely throw away all states with energies $|\varepsilon - \varepsilon^0_\mathrm{F}| > \Delta\varepsilon_\eta + \Delta\varepsilon_\delta$ because of the following argument: The first and second case with extended limit $\Delta\varepsilon_\eta + \Delta\varepsilon_\delta$ are still valid because with the new limit we even take more processes into account. In the third case $|\varepsilon^{s}_{j\mathbf{k}} - \varepsilon^0_\mathrm{F}| < \Delta\varepsilon_\eta + \Delta\varepsilon_\delta$ and $|\varepsilon^{s'}_{j'\mathbf{k}'} - \varepsilon^0_\mathrm{F}| > \Delta\varepsilon_\eta + \Delta\varepsilon_\delta$ (or vice versa), I distinguish two cases:

1. If $|\varepsilon^{s}_{j\mathbf{k}} - \varepsilon^0_\mathrm{F}| < \Delta\varepsilon_\eta$, then $\eta(\varepsilon^{s}_{j\mathbf{k}}) > \zeta_1$ and therefore a process in which such an $\varepsilon^{s}_{j\mathbf{k}}$ is involved cannot be neglected (see fig. 6.1 (b) 1.). But then the energies are too far away from each other because

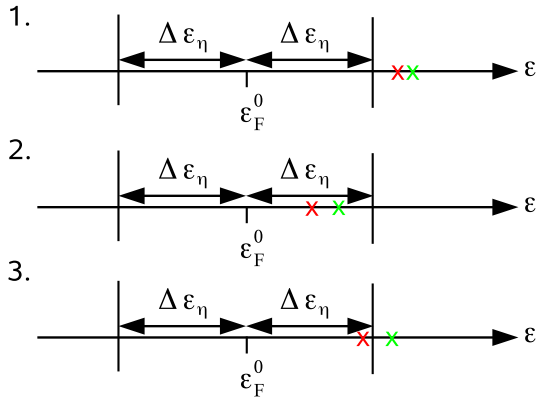

(a) 1.) Both energies are outside the relevant energy range: $|\varepsilon^s_{j\mathbf{k}} - \varepsilon^0_{\mathrm{F}}| > \Delta\varepsilon_\eta$ and $|\varepsilon^{s'}_{j'\mathbf{k}'} - \varepsilon^0_{\mathrm{F}}| > \Delta\varepsilon_\eta$. 2.) Both energies are inside the relevant energy range: $|\varepsilon^s_{j\mathbf{k}} - \varepsilon^0_{\mathrm{F}}| < \Delta\varepsilon_\eta$ and $|\varepsilon^{s'}_{j'\mathbf{k}'} - \varepsilon^0_{\mathrm{F}}| < \Delta\varepsilon_\eta$. 3.) One energy is inside and one energy is outside the relevant energy range: $|\varepsilon^s_{j\mathbf{k}} - \varepsilon^0_{\mathrm{F}}| < \Delta\varepsilon_\eta$ and $|\varepsilon^{s'}_{j'\mathbf{k}'} - \varepsilon^0_{\mathrm{F}}| > \Delta\varepsilon_\eta$.

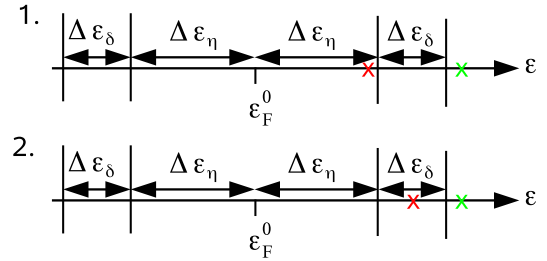

(b) One energy is inside and one energy is outside the extended energy range: $|\varepsilon^s_{j\mathbf{k}} - \varepsilon^0_{\mathrm{F}}| < \Delta\varepsilon_\eta + \Delta\varepsilon_\delta$ and $|\varepsilon^{s'}_{j'\mathbf{k}'} - \varepsilon^0_{\mathrm{F}}| > \Delta\varepsilon_\eta + \Delta\varepsilon_\delta$.
1.) $|\varepsilon^s_{j\mathbf{k}} - \varepsilon^0_{\mathrm{F}}| < \Delta\varepsilon_\eta$. 2.) $|\varepsilon^s_{j\mathbf{k}} - \varepsilon^0_{\mathrm{F}}| > \Delta\varepsilon_\eta$.

Figure 6.1: $\varepsilon^s_{j\mathbf{k}}$ is marked as a red cross and $\varepsilon^{s'}_{j'\mathbf{k}'}$ is marked as a green cross.

$|\varepsilon^{s'}_{j'\mathbf{k}'} - \varepsilon^0_{\mathrm{F}}| > \Delta\varepsilon_\eta + \Delta\varepsilon_\delta$ is demanded and hence $|\varepsilon^{s'}_{j'\mathbf{k}'} - \varepsilon^s_{j\mathbf{k}}| > \Delta\varepsilon_\delta$ which means $\delta_\sigma < \zeta_1$. Then it does not matter how large $\eta(\varepsilon^s_{j\mathbf{k}})$ is.

2. If $|\varepsilon^s_{j\mathbf{k}} - \varepsilon^0_{\mathrm{F}}| > \Delta\varepsilon_\eta$, then $\eta(\varepsilon^s_{j\mathbf{k}}) < \zeta_1$ (see fig. 6.1 (b) 2.). Then it does not matter how large δ_σ is, and the process can be thrown away.

To make a long story short, one can throw away all states which are too far away from the Fermi energy $|\varepsilon - \varepsilon^0_{\mathrm{F}}| > \Delta\varepsilon_\eta + \Delta\varepsilon_\delta$ and in addition one can throw away all scattering processes for which the energies are too distant from each other $|\varepsilon^{s'}_{j'\mathbf{k}'} - \varepsilon^s_{j\mathbf{k}}| < \Delta\varepsilon_\delta$. The two criteria depend on the threshold value ζ_1 and it has to be tested if ζ_1 is chosen too large.

Parallelization

Obviously, eq. (6.45) is associative with respect to $(j, \mathbf{k})$ and $(j', \mathbf{k}')$, i.e., the summation order does not play a role. This means that it makes sense to split the outer loop, say the loop over $(j, \mathbf{k})$, in N parts and distribute them to N jobs. The result for T_1 is just the sum over the results of the N jobs. Clearly, this reduces the calculational time by a factor of N.

Crystal symmetry

In principle the crystal symmetry could be used: The matrix elements $M^\lambda_{j\mathbf{k}s,j'\mathbf{k}'s'}$ are invariant under crystal symmetry operations on the states $(j\mathbf{k}s)$ and $(j'\mathbf{k}'s')$ since the crystal wavefunctions $\Psi^s_{j\mathbf{k}}$, $\Psi^{s'}_{j'\mathbf{k}'}$ and the phonon frequencies $\omega_{\mathbf{q}\lambda}$ and polarization vectors $\mathbf{n}_{\mathbf{q}\lambda}$ are invariant under crystal symmetry operations. This has not been done until now since the calculations have always been fast enough (about few days).

6.6 Demagnetization rates

The rate of the magnetic moment change (proportional to the demagnetization rate) for a discrete k-point grid reads (compare with eq. (5.29))

$$\frac{dM}{dt} = \sum_{j,j',\lambda} \sum_{\mathbf{k},\mathbf{k}'} \frac{\Omega_{\mathbf{k}}\Omega_{\mathbf{k}'}}{\Omega^2_{BZ}} \; m_{j\mathbf{k}\uparrow,j'\mathbf{k}'\downarrow} \cdot$$

$$\Big\{ f(\varepsilon^{\uparrow}_{j\mathbf{k}}, \varepsilon^{\uparrow}_{\mathrm{F}}(t), T_e(t)) \left[1 - f(\varepsilon^{\downarrow}_{j'\mathbf{k}'}, \varepsilon^{\downarrow}_{\mathrm{F}}(t), T_e(t))\right] W^{\lambda}_{j\mathbf{k}\uparrow, j'\mathbf{k}'\downarrow}$$
$$- f(\varepsilon^{\downarrow}_{j'\mathbf{k}'}, \varepsilon^{\downarrow}_{\mathrm{F}}(t), T_e(t)) \left[1 - f(\varepsilon^{\uparrow}_{j\mathbf{k}}, \varepsilon^{\uparrow}_{\mathrm{F}}(t), T_e(t))\right] W^{\lambda}_{j'\mathbf{k}'\downarrow, j\mathbf{k}\uparrow} \Big\}, \quad (6.53)$$

where the transition rates $W^{\lambda}_{j\mathbf{k}s, j'\mathbf{k}'s'}$ are again given by eq. (6.46).

Temperature

Here, we have two temperatures: one for the electrons $T_e(t)$ which enters the Fermi-Dirac function and one for the phonons $T_p = 300$ K$= const.$ which enters the Bose function. The electron temperature is a function of time (due to the laser heating and equilibration) whereas the phonon temperature is assumed to be constant since the phonon heating is quite slow, on a ps timescale [51]. In simulations it was also shown that the phonon heating does not change the demagnetization behavior a lot [73]. Note that in the Elliott-Yafet theory for the relaxation time T_1 (see section 6.5) it is not respected that the electron temperature changes and equilibrates (due to scattering).

The electron temperature has to be taken from experimental fits to the three-temperature model or can be considered as parameter. Atxitia et al. [79] show the electron temperature as function of time for different laser fluences. The maximum electron temperature T_e^{max} is 350 K for the lowest fluence ($F = 10$ mJ/cm^2) and 630 K for the highest fluence ($F = 50$ mJ/cm^2). One can also find electron temperatures as function of time in refs. [1, 18, 60] with T_e^{max} equals 700 K ($F = 7$ mJ/cm^2), 500 K (no fluence specified but certainly low) and 1000 K (no fluence specified but certainly high), respectively. We see that the electron temperature does not only depend on the fluence but also on the model and other parameters. However, one can conclude that T_e^{max} is between 350 K and 1000 K for reasonable fluences which do not destroy the sample. Note that the electron temperatures can be higher than the Curie temperature which is 627 K for Ni. Because of the non-equilibrium situation where Bloch's $T^{3/2}$-law is not valid it does not necessarily lead to a complete demagnetization.

I want to emphasize again that the band structure is calculated for 0 K, and it is assumed that it does not change much for higher temperatures (e.g., room temperature). I.e., the matrix elements $|M^{\lambda}_{j\mathbf{k}s, j'\mathbf{k}'s'}|^2$, the

energies $\varepsilon^s_{j\mathbf{k}}$ and the phonon polarization vectors $\mathbf{n}_{\mathbf{q}\lambda}$ and frequencies $\omega_{\mathbf{q}\lambda}$ are calculated for $T = 0$ K and it is assumed that this gives approximately the same results for higher temperatures[20].

Determination of the chemical potentials

We assume that directly after the laser pulse irradiation there are many electron-electron scattering processes which generate for the electrons an electron temperature T_e. Electron-electron scattering alone cannot lead to a demagnetization since there is no "sink" for angular momentum (apart from the orbital moment but an increase in the orbital moment has never been observed experimentally, see subsection 4.2.4). According to ref. [18] the main part of the demagnetization sets in after the thermalization among the electrons via electron-electron scattering in a time less than 100 fs [18, 49] for a demagnetization time up to 500 fs. Let us denote the time at which the electron-electron thermalization is completed by t_s. At this time the magnetic moment is still the equilibrium magnetic moment M_0 and directly thereafter the demagnetization sets in. I model the effect of the laser pulse by two different chemical potentials $\varepsilon^{\uparrow}_{\mathrm{F}}$, $\varepsilon^{\downarrow}_{\mathrm{F}}$ for the dominant-up and dominant-down states (as in the Elliott-Yafet model).

In equilibrium the temperatures are equal $T_e = T_p = T_0 = 300$ K, and also the chemical potentials are equal $\varepsilon^{\uparrow}_{\mathrm{F}} = \varepsilon^{\downarrow}_{\mathrm{F}} = \varepsilon^{0}_{\mathrm{F}}$. The number of dominant-up states $N^{\uparrow}_0$ and the number of dominant-down states $N^{\downarrow}_0$ enter the two equilibrium conditions

$$N_0 = N^{\uparrow}_0 + N^{\downarrow}_0 \tag{6.54}$$

$$M_0 = \mu_{\mathrm{B}} \, (N^{\uparrow}_0 - N^{\downarrow}_0) \tag{6.55}$$

where N_0 is the total number of electrons. Here, it is assumed that every state has a magnetic moment of μ_{B} per atom which is true for most of the states (see subsection 7.1.1 and ref. [22]). The exact magnetic moment can be calculated with eq. (5.25), however, the deviation from eq. (6.55) is only small.

[20] Rates unequal zero are only due to the difference between the Fermi distribution function $f(\varepsilon^s_{j\mathbf{k}}, \varepsilon^s_{\mathrm{F}}(t), T_e(t))$ and the Fermi distribution function in equilibrium $f(\varepsilon^s_{j\mathbf{k}}, \varepsilon^0_{\mathrm{F}}, T_0)$.

The conservation of the total number of electrons[21], $N_0 = const.$, holds for every time t and especially for the time $t = t_s$. For $t = t_s$ the magnetic moment is still M_0, i.e.,

$$N_0 = N^{\uparrow}(t_s) + N^{\downarrow}(t_s) \tag{6.56}$$

$$M_0 = \mu_{\mathrm{B}}\ (N^{\uparrow}(t_s) - N^{\downarrow}(t_s)). \tag{6.57}$$

Adding and subtracting the equations (6.56), (6.57) and in addition doing the same for equations (6.54), (6.55) gives

$$N_0 + \frac{M_0}{\mu_{\mathrm{B}}} = 2N^{\uparrow}(t_s) = 2N_0^{\uparrow} \tag{6.58}$$

$$N_0 - \frac{M_0}{\mu_{\mathrm{B}}} = 2N^{\downarrow}(t_s) = 2N_0^{\downarrow} \tag{6.59}$$

i.e., $N_0^{\uparrow} = N^{\uparrow}(t_s)$ and $N_0^{\downarrow} = N^{\downarrow}(t_s)$, or equivalently using eq. (5.23)

$$N_0^{\uparrow} - \int_{-\infty}^{+\infty} \mathrm{d}\varepsilon\ \frac{Z^{\uparrow}(\varepsilon)}{\exp((\varepsilon - \varepsilon_{\mathrm{F}}^{\uparrow}(t_s))/kT_e(t_s)) + 1} = 0 \tag{6.60}$$

$$N_0^{\downarrow} - \int_{-\infty}^{+\infty} \mathrm{d}\varepsilon\ \frac{Z^{\downarrow}(\varepsilon)}{\exp((\varepsilon - \varepsilon_{\mathrm{F}}^{\downarrow}(t_s))/kT_e(t_s)) + 1} = 0. \tag{6.61}$$

The chemical potentials $\varepsilon_{\mathrm{F}}^{\uparrow}(t_s)$, $\varepsilon_{\mathrm{F}}^{\downarrow}(t_s)$ can now easily be found with a root finding algorithm. We can consider the electron temperature $T_e(t_s)$ as a parameter and insert several values or take it directly from a publication (t_s is the time where the demagnetization starts). As discussed above the electron temperature is between 350 K and 1000 K depending on the fluence, on the model and on the parameters. Eqs. (6.60) and (6.61) say that the number of dominant-up and dominant-down electrons does not change, $N^{\uparrow}(t_s) = N_0^{\uparrow}$ and $N^{\downarrow}(t_s) = N_0^{\downarrow}$, but the distribution changes! This is in accordance with the picture that the electrons are excited by the laser pulse without spin-flip and then undergo electron-electron scattering without spin-flip until $t = t_s$.

We see that the conservation of the total number of electrons N_0 always holds but to determine the chemical potentials $\varepsilon_{\mathrm{F}}^{\uparrow}(t)$, $\varepsilon_{\mathrm{F}}^{\downarrow}(t)$ we need in addition the magnetic moment which we only know for the time t_s.

[21] Superdiffusive processes are neglected.

Suppose we calculated $dM/dt(t_s)$. Then, one could calculate the magnetization behavior iteratively for very small time steps Δt:

$$M(t_s + \Delta t) = M_0 + \frac{dM}{dt}(t_s) \cdot \Delta t. \tag{6.62}$$

Together with the number conservation and the experimental value for the electron temperature $T_e(t_s + \Delta t)$ the chemical potentials can again be determined $\varepsilon_{\mathrm{F}}^{\uparrow}(t_s + \Delta t)$, $\varepsilon_{\mathrm{F}}^{\downarrow}(t_s + \Delta t)$. With the chemical potentials at hand the rate of the magnetic moment change $dM/dt(t_s + \Delta t)$ can be calculated. Then one can continue with the next time step and so on. This procedure can be continued for the whole time range. I make two important remarks for this procedure:

- Note that the time-dependent electron temperature enters in eq. (6.53). T_e has to be taken from the three-temperature model for every time step.
- It must be considered that the band structure changes when the magnetic moment changes! In principle, a new band structure calculation for every time step is necessary.

Alternatively, it is possible to take both the magnetic moment $M(t)$ and the electron temperature $T_e(t)$ from experiment for an arbitrary time t and calculate the rate of the magnetic moment change $dM/dt(t)$. Note again that the band structure changes since the magnetic moment changes! However, this rate contains implicitly a lot of experimental information and it might well be that this rate is very different from the rate determined iteratively for the same time t. Therefore it is not a good idea to take both the magnetic moment $M(t)$ and the electron temperature $T_e(t)$ from experiment.

Equilibrium rate equations

If the scattering operator is Hermitian and the energy conservation holds, the rate of the magnetic moment change vanishes in equilibrium (see subsection 5.5.4). The scattering operator is indeed Hermitian (see subsection 6.1.2) but because of smearing the energy conservation is not fulfilled exactly. Therefore one cannot expect that the rate vanishes exactly in equilibrium, however, we will see in section 7.2 that the equilibrium rates are almost zero for most of the smearing parameters.

Summation of k-points

1. The summation runs over all dominant up ($p^{\uparrow}_{j\mathbf{k}} > 0.5$) and all dominant down states ($p^{\downarrow}_{j\mathbf{k}} > 0.5$). The factor $m_{j\mathbf{k}\uparrow,j'\mathbf{k}'\downarrow} = -2\mu_{\mathrm{B}}$ ($p^{\uparrow}_{j'\mathbf{k}'} - p^{\uparrow}_{j\mathbf{k}}$) keeps track of the changed magnetic moment.
2. $\mathbf{k} = \mathbf{k}'$, i.e., $\mathbf{q} = 0$, is excluded for the same reason as in section 6.5.
3. Small phonon wavevectors $\mathbf{q}$ and hence small phonon frequencies $\omega_{\mathbf{q},\lambda}$ are also excluded for the same reason as in section 6.5.
4. The computational time also goes like N_1^6 where N_1 is the number of k-points in one direction (see section 6.5).

Selection of k-points

The argumentation is very similar to the argumentation in section 6.5. Here, the function $f_t(\varepsilon^{\uparrow}_{j\mathbf{k}}) \cdot (1 - f_t(\varepsilon^{\downarrow}_{j'\mathbf{k}'}))$ and the delta function δ_σ is used for a selection of k-points. We now demand that the former function is larger than some threshold value ζ_2 ($\zeta_2 \ll 1$) in order to consider a scattering process as relevant: $f_t(\varepsilon^{\uparrow}_{j\mathbf{k}}) \cdot (1 - f_t(\varepsilon^{\downarrow}_{j'\mathbf{k}'})) > \zeta_2$. This cannot be fulfilled if either $f_t(\varepsilon^{\uparrow}_{j\mathbf{k}}) < \zeta_2$ or $(1 - f_t(\varepsilon^{\downarrow}_{j'\mathbf{k}'})) < \zeta_2$. Hence, we demand in the following $f_t(\varepsilon^{\uparrow}_{j\mathbf{k}}) > \zeta_2$ and in addition $(1 - f_t(\varepsilon^{\downarrow}_{j'\mathbf{k}'})) > \zeta_2$. This also includes irrelevant scattering processes[22], $f_t(\varepsilon^{\uparrow}_{j\mathbf{k}}) \cdot (1 - f_t(\varepsilon^{\downarrow}_{j'\mathbf{k}'})) < \zeta_2$, which does not matter (more scattering processes than necessary are taken into account). Let us discuss the two conditions separately:

- It is claimed: $f_t(\varepsilon^{\uparrow}_{j\mathbf{k}}) > \zeta_2$. For the energy $\varepsilon^{\uparrow}_{j\mathbf{k}}$ the condition

$$\varepsilon^{\uparrow}_{j\mathbf{k}} - \varepsilon^{\uparrow}_{\mathrm{F}} < kT_e(t)\ \ln(\zeta_2^{-1} - 1) \approx -kT_e(t)\ \ln\zeta_2 \equiv \Delta\varepsilon_f \tag{6.63}$$

  must hold. Let us take $\zeta_2 = 10^{-15}$ and a reasonable electron temperature $T_e = 500$ K ($kT_e = 3.2$ mRy). Then the energy condition reads $\varepsilon^{\uparrow}_{j\mathbf{k}} - \varepsilon^{\uparrow}_{\mathrm{F}} < 110.5$ mRy.

- It is claimed: $(1 - f_t(\varepsilon^{\downarrow}_{j'\mathbf{k}'})) > \zeta_2$. This means for the energy $\varepsilon^{\downarrow}_{j'\mathbf{k}'}$

$$\varepsilon^{\downarrow}_{j'\mathbf{k}'} - \varepsilon^{\downarrow}_{\mathrm{F}} > -kT_e(t)\ \ln(\zeta_2^{-1} - 1) \approx kT_e(t)\ \ln\zeta_2 = -\Delta\varepsilon_f. \tag{6.64}$$

[22] For example: $\zeta_2 = 10^{-15}$, $f_t(\varepsilon^{\uparrow}_{j\mathbf{k}}) = 10^{-10}$, $(1 - f_t(\varepsilon^{\downarrow}_{j'\mathbf{k}'})) = 10^{-10}$.

Together, both conditions (eq. (6.63) and eq. (6.64)) are only fulfilled in an energy range where $\varepsilon^{\uparrow}_{j\mathbf{k}} < \Delta\varepsilon_f + \varepsilon^{\uparrow}_{\mathrm{F}}$ and in addition $\varepsilon^{\downarrow}_{j'\mathbf{k}'} > \varepsilon^{\downarrow}_{\mathrm{F}} - \Delta\varepsilon_f$. In the following the energy range $\varepsilon^{\downarrow}_{\mathrm{F}} - \Delta\varepsilon_f < \varepsilon < \Delta\varepsilon_f + \varepsilon^{\uparrow}_{\mathrm{F}}$ is called "relevant" energy range.

Let us consider the scattering process where both functions $f_t(\varepsilon^{\uparrow}_{j\mathbf{k}}) \cdot (1 - f_t(\varepsilon^{\downarrow}_{j'\mathbf{k}'}))$ and $f_t(\varepsilon^{\downarrow}_{j'\mathbf{k}'}) \cdot (1 - f_t(\varepsilon^{\uparrow}_{j\mathbf{k}}))$ enter (see eq. (6.53)). The energies $\varepsilon^{\uparrow}_{j\mathbf{k}}$ and $\varepsilon^{\downarrow}_{j'\mathbf{k}'}$ for the scattering process can be categorized like this:

1. Both energies are inside the relevant energy range (see fig. 6.2 (a) 1.): $\varepsilon^{\downarrow}_{\mathrm{F}} - \Delta\varepsilon_f < \varepsilon^{s}_{j\mathbf{k}} < \varepsilon^{\uparrow}_{\mathrm{F}} + \Delta\varepsilon_f$ and $\varepsilon^{\downarrow}_{\mathrm{F}} - \Delta\varepsilon_f < \varepsilon^{s'}_{j'\mathbf{k}'} < \varepsilon^{\uparrow}_{\mathrm{F}} + \Delta\varepsilon_f$. According to eqs. (6.63) and (6.64) this means
   - $f_t(\varepsilon^{\uparrow}_{j\mathbf{k}}) > \zeta_2$ or equivalently $(1 - f_t(\varepsilon^{\uparrow}_{j\mathbf{k}})) < 1 - \zeta_2 \approx 1$
   - $(1 - f_t(\varepsilon^{\downarrow}_{j'\mathbf{k}'})) > \zeta_2$ or equivalently $f_t(\varepsilon^{\downarrow}_{j'\mathbf{k}'}) < 1 - \zeta_2 \approx 1$.

   Therefore $f_t(\varepsilon^{\uparrow}_{j\mathbf{k}}) \cdot (1 - f_t(\varepsilon^{\downarrow}_{j'\mathbf{k}'}))$ and also $f_t(\varepsilon^{\downarrow}_{j'\mathbf{k}'}) \cdot (1 - f_t(\varepsilon^{\uparrow}_{j\mathbf{k}}))$ can be larger than ζ_2 (but of course can also be less than ζ_2). So, this scattering process is definitely relevant.

2. Both energies are outside the relevant energy range. Here we have to distinguish two cases (see fig. 6.2 (a) 2.):

   top: Both energies are on the same side of the energy scale, e.g., $\varepsilon^{\uparrow}_{j\mathbf{k}} > \varepsilon^{\uparrow}_{\mathrm{F}} + \Delta\varepsilon_f$ and $\varepsilon^{\downarrow}_{j'\mathbf{k}'} > \varepsilon^{\uparrow}_{\mathrm{F}} + \Delta\varepsilon_f$. According to eqs. (6.63) and (6.64) this means
   - $f_t(\varepsilon^{\uparrow}_{j\mathbf{k}}) < \zeta_2$ or equivalently $(1 - f_t(\varepsilon^{\uparrow}_{j\mathbf{k}})) > 1 - \zeta_2 \approx 1$
   - $(1 - f_t(\varepsilon^{\downarrow}_{j'\mathbf{k}'})) > \zeta_2$ or equivalently $f_t(\varepsilon^{\downarrow}_{j'\mathbf{k}'}) < 1 - \zeta_2 \approx 1$.

   Therefore $f_t(\varepsilon^{\uparrow}_{j\mathbf{k}}) \cdot (1 - f_t(\varepsilon^{\downarrow}_{j'\mathbf{k}'})) < \zeta_2$ but $f_t(\varepsilon^{\downarrow}_{j'\mathbf{k}'}) \cdot (1 - f_t(\varepsilon^{\uparrow}_{j\mathbf{k}}))$ can be greater than ζ_2. However, according to eq. (6.63)[23] $f_t(\varepsilon^{\downarrow}_{j'\mathbf{k}'}) > \zeta_2$ only if $\varepsilon^{\downarrow}_{j'\mathbf{k}'} < \varepsilon^{\downarrow}_{\mathrm{F}} + \Delta\varepsilon_f$ (blue dashed line in fig. 6.2 (a) 2.). This is not the case, since the down Fermi energy is normally less than the up Fermi energy $\varepsilon^{\downarrow}_{\mathrm{F}} < \varepsilon^{\uparrow}_{\mathrm{F}}$, and hence $f_t(\varepsilon^{\downarrow}_{j'\mathbf{k}'}) < \zeta_2$ and also $f_t(\varepsilon^{\downarrow}_{j'\mathbf{k}'}) \cdot (1 - f_t(\varepsilon^{\uparrow}_{j\mathbf{k}})) < \zeta_2$ normally holds. This scattering process is therefore negligible.

   bottom: The energies are on different sides of the energy scale, e.g., $\varepsilon^{\uparrow}_{j\mathbf{k}} < \varepsilon^{\downarrow}_{\mathrm{F}} - \Delta\varepsilon_f$ and $\varepsilon^{\downarrow}_{j'\mathbf{k}'} > \varepsilon^{\uparrow}_{\mathrm{F}} + \Delta\varepsilon_f$. Then, the energies have a

[23] The argument $\varepsilon^{\uparrow}_{j\mathbf{k}}$ is replaced by the argument $\varepsilon^{\downarrow}_{j'\mathbf{k}'}$ in eq. (6.63).

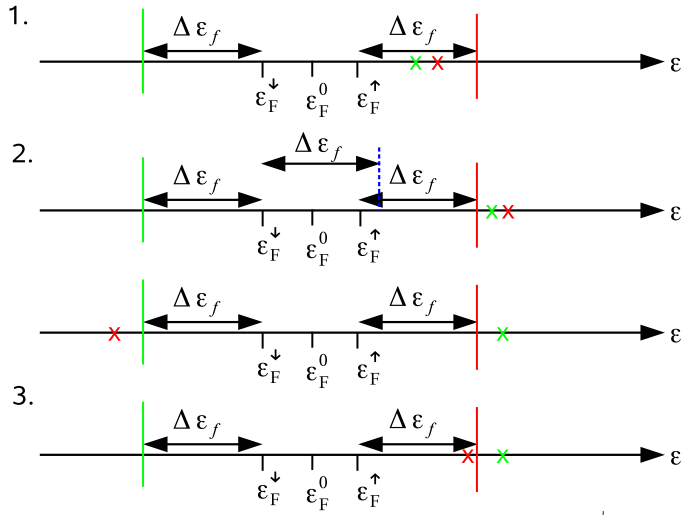

(a) 1.) Both energies are inside the relevant energy range: $\varepsilon_{\mathrm{F}}^{\downarrow} - \Delta\varepsilon_f < \varepsilon_{j\mathbf{k}}^{s} < \varepsilon_{\mathrm{F}}^{\uparrow} + \Delta\varepsilon_f$ and $\varepsilon_{\mathrm{F}}^{\downarrow} - \Delta\varepsilon_f < \varepsilon_{j'\mathbf{k}'}^{s'} < \varepsilon_{\mathrm{F}}^{\uparrow} + \Delta\varepsilon_f$. 2.) Both energies are outside the relevant energy range: $\varepsilon_{j\mathbf{k}}^{s} > \varepsilon_{\mathrm{F}}^{\uparrow} + \Delta\varepsilon_f$ or $\varepsilon_{j\mathbf{k}}^{s} < \varepsilon_{\mathrm{F}}^{\downarrow} - \Delta\varepsilon_f$ and $\varepsilon_{j'\mathbf{k}'}^{s'} > \varepsilon_{\mathrm{F}}^{\uparrow} + \Delta\varepsilon_f$ or $\varepsilon_{j'\mathbf{k}'}^{s'} < \varepsilon_{\mathrm{F}}^{\downarrow} - \Delta\varepsilon_f$. 3.) One energy is inside and one energy is outside the relevant energy range.

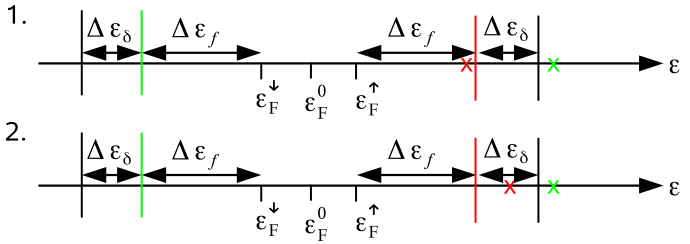

(b) One energy is inside and one energy is outside the extended energy range.
1.) $\varepsilon_{j\mathbf{k}}^{s} < \varepsilon_{\mathrm{F}}^{\uparrow} + \Delta\varepsilon_f$. 2.) $\varepsilon_{j\mathbf{k}}^{s} > \varepsilon_{\mathrm{F}}^{\uparrow} + \Delta\varepsilon_f$.

Figure 6.2: $\varepsilon_{j\mathbf{k}}^{s}$ is marked as a red cross and $\varepsilon_{j'\mathbf{k}'}^{s'}$ is marked as a green cross.

distance of at least $|\varepsilon^{\uparrow}_{j\mathbf{k}} - \varepsilon^{\downarrow}_{j'\mathbf{k}'}| > 2\Delta\varepsilon_f + \varepsilon^{\uparrow}_{\mathrm{F}} - \varepsilon^{\downarrow}_{\mathrm{F}}$. For reasonable threshold values ζ_2 and reasonable electron temperatures T_e this distance is already so large that $|\varepsilon^{\uparrow}_{j\mathbf{k}} - \varepsilon^{\downarrow}_{j'\mathbf{k}'}| > \Delta\varepsilon_\delta$ and hence the delta function δ_σ falls below the threshold value ζ_1: $\delta_\sigma < \zeta_1$. Then, this scattering process is certainly irrelevant.

3. One energy is inside the relevant energy range, and the other energy is outside, e.g., $\varepsilon^{\downarrow}_{\mathrm{F}} - \Delta\varepsilon_f < \varepsilon^{\uparrow}_{j\mathbf{k}} < \Delta\varepsilon_f + \varepsilon^{\uparrow}_{\mathrm{F}}$ and $\varepsilon^{\downarrow}_{j'\mathbf{k}'} > \varepsilon^{\uparrow}_{\mathrm{F}} + \Delta\varepsilon_f$. According to eqs. (6.63) and (6.64) this means

   - $f_t(\varepsilon^{\uparrow}_{j\mathbf{k}}) > \zeta_2$ or equivalently $(1 - f_t(\varepsilon^{\uparrow}_{j\mathbf{k}})) < 1 - \zeta_2 \approx 1$
   - $(1 - f_t(\varepsilon^{\downarrow}_{j'\mathbf{k}'})) > \zeta_2$ or equivalently $f_t(\varepsilon^{\downarrow}_{j'\mathbf{k}'}) < 1 - \zeta_2 \approx 1$.

   Therefore $f_t(\varepsilon^{\uparrow}_{j\mathbf{k}}) \cdot (1 - f_t(\varepsilon^{\downarrow}_{j'\mathbf{k}'}))$ and $f_t(\varepsilon^{\downarrow}_{j'\mathbf{k}'}) \cdot (1 - f_t(\varepsilon^{\uparrow}_{j\mathbf{k}}))$ could be greater or less than ζ_2 and therefore, this scattering process could be relevant.

As in section 6.5 we would like to select k-points from the very beginning irrespective of the scattering process but the third case makes problems. Again the same trick as in section 6.5 is used: The relevant energy range is extended by $\Delta\varepsilon_\delta$: $\varepsilon^{\downarrow}_{\mathrm{F}} - \Delta\varepsilon_f - \Delta\varepsilon_\delta < \varepsilon < \varepsilon^{\uparrow}_{\mathrm{F}} + \Delta\varepsilon_f + \Delta\varepsilon_\delta$. The first and second case with extended limits are still valid (even more k-points are taken into account). The third case with extended limit has to be reconsidered. It reads: One energy is inside the extended energy range, e.g., $\varepsilon^{\downarrow}_{\mathrm{F}} - \Delta\varepsilon_f - \Delta\varepsilon_\delta < \varepsilon^{\uparrow}_{j\mathbf{k}} < \varepsilon^{\uparrow}_{\mathrm{F}} + \Delta\varepsilon_f + \Delta\varepsilon_\delta$, and the other energy is outside the extended energy range, e.g., $\varepsilon^{\downarrow}_{j'\mathbf{k}'} > \varepsilon^{\uparrow}_{\mathrm{F}} + \Delta\varepsilon_f + \Delta\varepsilon_\delta$. I distinguish two cases:

1. Assume that $\varepsilon^{\uparrow}_{j\mathbf{k}} < \Delta\varepsilon_f + \varepsilon^{\uparrow}_{\mathrm{F}}$ (see fig. 6.2 (b) 1.). The energy difference is at least $\Delta\varepsilon_\delta$ which means that the delta function δ_σ falls below the threshold value ζ_1. Then, this scattering process is irrelevant.

2. Assume that $\varepsilon^{\uparrow}_{j\mathbf{k}} > \Delta\varepsilon_f + \varepsilon^{\uparrow}_{\mathrm{F}}$ (see fig. 6.2 (b) 2.). This is exactly the same situation as discussed in top of fig. 6.2 (a) 2. Again, this scattering process is negligible.

To summarize, only states in the energy range $\varepsilon^{\downarrow}_{\mathrm{F}} - \Delta\varepsilon_f - \Delta\varepsilon_\delta < \varepsilon < \varepsilon^{\uparrow}_{\mathrm{F}} + \Delta\varepsilon_f + \Delta\varepsilon_\delta$ are taken into account and in addition only scattering processes for which the energy difference is not too large $|\varepsilon^{s'}_{j'\mathbf{k}'} - \varepsilon^{s}_{j\mathbf{k}}| < \Delta\varepsilon_\delta$

are considered. The two conditions depend on the threshold values ζ_1 and ζ_2 and the results are tested for different threshold values.

Rounding errors

It can be shown [109] that subtraction of two quantities which are almost equal leads to large rounding errors. Therefore the rate of the magnetic moment change is split into a rate from dominant-up to dominant-down and vice versa:

$$\frac{dM^{\uparrow,\downarrow}}{dt} = \sum_{j,j',\lambda} \sum_{\mathbf{k},\mathbf{k}'} \frac{\Omega_{\mathbf{k}}\Omega_{\mathbf{k}'}}{\Omega_{BZ}^2} \quad m_{j\mathbf{k}\uparrow,j'\mathbf{k}'\downarrow} \cdot \\ f(\varepsilon^{\uparrow}_{j\mathbf{k}}, \varepsilon^{\uparrow}_{\mathrm{F}}(t), T_e(t)) \left[1 - f(\varepsilon^{\downarrow}_{j'\mathbf{k}'}, \varepsilon^{\downarrow}_{\mathrm{F}}(t), T_e(t))\right] W^{\lambda}_{j\mathbf{k}\uparrow,j'\mathbf{k}'\downarrow} \tag{6.65}$$

$$\frac{dM^{\downarrow,\uparrow}}{dt} = \sum_{j,j',\lambda} \sum_{\mathbf{k},\mathbf{k}'} \frac{\Omega_{\mathbf{k}}\Omega_{\mathbf{k}'}}{\Omega_{BZ}^2} \quad m_{j\mathbf{k}\uparrow,j'\mathbf{k}'\downarrow} \cdot \\ f(\varepsilon^{\downarrow}_{j'\mathbf{k}'}, \varepsilon^{\downarrow}_{\mathrm{F}}(t), T_e(t)) \left[1 - f(\varepsilon^{\uparrow}_{j\mathbf{k}}, \varepsilon^{\uparrow}_{\mathrm{F}}(t), T_e(t))\right] W^{\lambda}_{j'\mathbf{k}'\downarrow,j\mathbf{k}\uparrow}. \tag{6.66}$$

The total rate is

$$\frac{dM}{dt} = \frac{dM^{\uparrow,\downarrow}}{dt} - \frac{dM^{\downarrow,\uparrow}}{dt}. \tag{6.67}$$

Parallelization and crystal symmetry

Obviously, eq. (6.53) is associative with respect to $(j, \mathbf{k})$ and $(j', \mathbf{k}')$, i.e., the summation order does not play a role. A parallelization is made as described in section 6.5. Again the crystal symmetry is not used since the calculations have always been fast enough.

7 Numerical results and discussion

The results of this chapter are published in ref. [110].

7.1 Relaxation time

7.1.1 Spin-mixing and magnetic moment change

In order to define the relaxation time T_1 it is assumed in eq. (5.37) that the spin-mixing is small (or at least constant) for most of the states so that the magnetic moment $M(t)$ is directly proportional to the difference $D(t)$: $M(t) = mD(t)$. Hence, the change of the magnetic moment is $\pm 2m$ for a spin-flip. This precondition is investigated in the following.

Fig. 7.1 shows the number of states within 50 mRy around the Fermi energy (k-point grid: 50×50×50) vs. the up-probability $p^{\uparrow}_{j\mathbf{k}}$. We see that most of the states have an up-probability which is either less than 0.1 or greater than 0.9. Only few states have an up-probability in between. One can also see that Ni has more dominant-down states than dominant-up states in an energy range of 50 mRy around the Fermi energy (top of fig. 7.1) whereas Fe has more dominant-up states than dominant-down states in the same energy range (bottom of fig. 7.1). This is not surprising since the spin-down density of states at the Fermi energy is high for Ni but low for Fe (see figs. 2.6, 2.7).

Fig. 7.2 shows the number of transitions within 50 mRy around the Fermi energy (k-point grid: 50×50×50) vs. the magnetic moment change for transitions from one state to another in units of $2\mu_{\mathrm{B}}$.

The magnetic moment change of all possible non-spin-flip transitions is shown in the top of fig. 7.2 for Ni. Most non-spin-flip transitions make a magnetic moment change of about zero but few also make a magnetic moment change up to $\pm 0.5 \cdot 2\mu_{\mathrm{B}}$ per atom. This is neglected in the calcu-

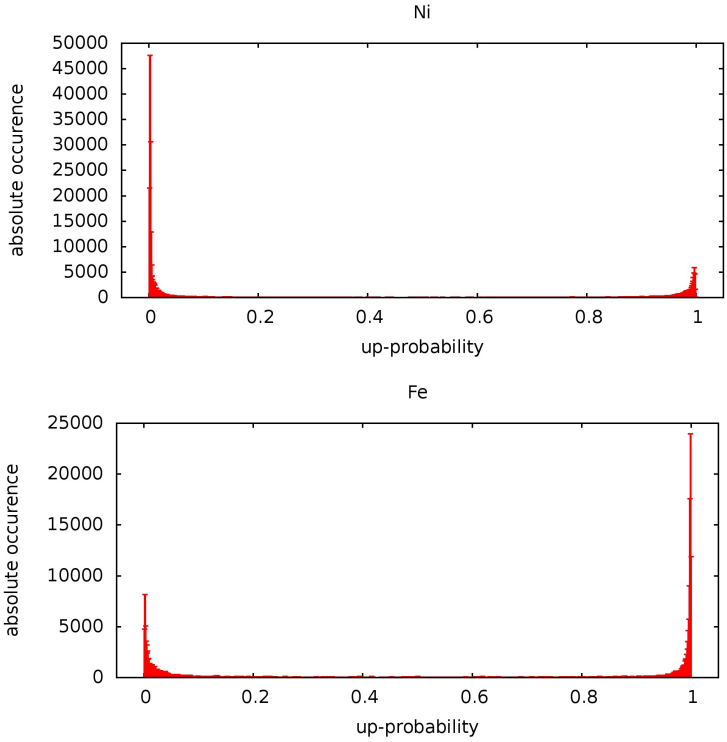

Figure 7.1: Number of states within 50 mRy around the Fermi energy (k-point grid: 50×50×50) vs. up-probability $p^{\uparrow}_{j\mathbf{k}}$. Top: Ni (279248 states within 50 mRy around the Fermi energy). Bottom: Fe (204162 states within 50 mRy around the Fermi energy).

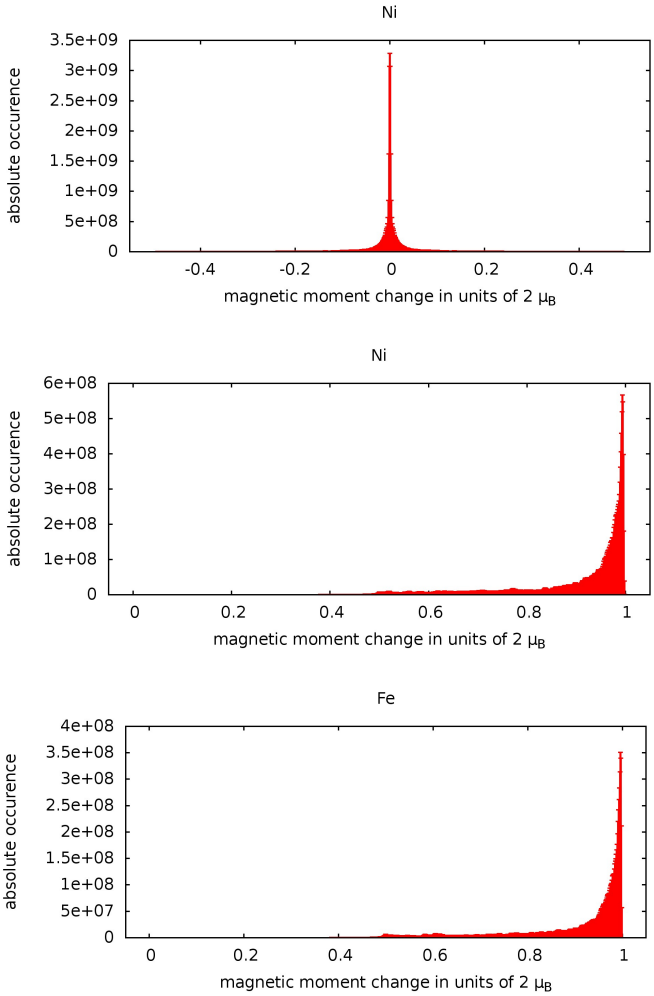

Figure 7.2: Number of transitions within 50 mRy around the Fermi energy (k-point grid: 50×50×50) vs. magnetic moment change in units of $2\mu_B$. Top: all possible non-spin-flip transitions for Ni (279248 states within 50 mRy around the Fermi energy). Middle: all possible spin-flip transitions from dominant-down to dominant-up for Ni . Bottom: all possible spin-flip transitions from dominant-down to dominant-up for Fe (204162 states within 50 mRy around the Fermi energy).

lation for both the relaxation time T_1 and the demagnetization rate dM/dt in the following since only spin-flip transitions are taken into account.

The magnetic moment change of all possible spin-flip transitions from dominant-down to dominant-up is shown in the middle and bottom of fig. 7.2. Most spin-flips make a magnetic moment change larger than $0.9 \cdot 2\mu_B$ for both Ni (middle of fig. 7.2) and Fe (bottom of fig. 7.2). However, the number of spin-flips which makes a change less than $0.9 \cdot 2\mu_B$ is not negligible.

One has two possibilities:

1. One could take all states which have an up-probability $p^{\uparrow}_{j\mathbf{k}} > 0.5$ as dominant-up and all states which have an up-probability $p^{\uparrow}_{j\mathbf{k}} < 0.5$ as dominant-down. Then, all states and all possible spin-flips are taken into account but the precondition that all states have a small or at least constant spin-mixing is not fulfilled and therefore, the equation for the relaxation time T_1 can in principle not be used.

2. One could exclude states so that the precondition is approximately fulfilled. E.g., one could take all states with an up-probability $p^{\uparrow}_{j\mathbf{k}} > 0.8$ as dominant-up and all states with an up-probability $p^{\uparrow}_{j\mathbf{k}} < 0.2$ as dominant-down, i.e., the spin-mixing $|b_{j\mathbf{k}}|^2 = \min(p^{\uparrow}_{j\mathbf{k}}, p^{\downarrow}_{j\mathbf{k}})$ is less than 0.2: $|b_{j\mathbf{k}}|^2 < 0.2$. However, one excludes with this definition many possible spin-flips which could contribute to the relaxation time.

The only remedy is to test the results for the relaxation time for different definitions of dominant-up and dominant-down states. This is presented in the next subsection.

7.1.2 Convergence

The relaxation time T_1 for Ni and Fe is calculated according to eqs. (6.45) and (6.46). Different smearing parameters σ as well as different k-grids are used so that $\sigma \cdot N_1 = const.$ where N_1 is the number of k-points in one direction (see remarks in section 6.4). $N_1 = 10, 20, 30, 40, 50$ is chosen for Ni and for Fe. The smearing parameter is $\sigma = 3$mRy independent from N_1 and $\sigma = 20\text{mRy}/N_1$, $40\text{mRy}/N_1$, $80\text{mRy}/N_1$, $160\text{mRy}/N_1$,

320mRy/N_1 dependent on N_1. Five different definitions of the dominant-up and dominant-down states are tested: $|b_{j\mathbf{k}}|^2 < 0.5$, $|b_{j\mathbf{k}}|^2 < 0.35$, $|b_{j\mathbf{k}}|^2 < 0.2$, $|b_{j\mathbf{k}}|^2 < 0.05$, $|b_{j\mathbf{k}}|^2 < 0.005$. The results for Ni and Fe are shown in figs. 7.3 up to 7.7.

We see that the results vary for different smearing parameters σ and coarse k-point grids ($N_1 = 10$ and $N_1 = 20$) whereas the convergence of the relaxation time is pretty good for denser k-point grids (already for $N_1 = 30$). Because of the very good convergence it can be excluded that missing screening effects (see section 5.4) influenced the results, i.e., the grid density up to $N_1 = 50$ does not lead to very small phonon frequencies which falsify the result. The smallest phonon frequency that occurred for $N_1 = 50$ is 0.297 THz for Ni and 0.278 THz for Fe.

Furthermore, the definition of dominant-up and dominant-down states does not change the results a lot. Even for the extreme definition of $|b_{j\mathbf{k}}|^2 < 0.005$ the results have the same order of magnitude for dense k-point grids. The reason is that most of the states have an almost pure spin-character, i.e., $|b_{j\mathbf{k}}|^2$ is about zero.

Comparing figs. 7.3 up to 7.7 I find that the relaxation time T_1 is about 16 fs for Ni and about 22 fs for Fe. For dense k-point grids the results do neither depend much on the smearing parameter σ nor on the definition of dominant-up and dominant-down states except for the extreme definition of $|b_{j\mathbf{k}}|^2 < 0.005$.

With the relaxation time T_1 at hand it is possible to determine the material-dependent parameter p in the Elliott-Yafet relation, see eq. (4.2),

$$p = \frac{\tau}{b^2\, T_1} \tag{7.1}$$

where b^2 is 0.024 for Fe and 0.025 for Ni [22, 23]. τ is the non-spin-flip Drude relaxation time which is about 2.4 fs for Fe [19]. This gives a material-dependent parameter $p \approx 4.5$ for Fe which is perfectly in the range $1 < p < 10$ found by Beuneu and Monod [65] showing the validity of the present results. The non-spin-flip Drude relaxation time for Ni can be calculated with the equations given in ref. [19] and it turns out that it is almost the same as for Fe. Since τ, T_1 and b^2 for Ni is very similar to the values for Fe, the material-dependent parameter p for Ni is also about 4.5.

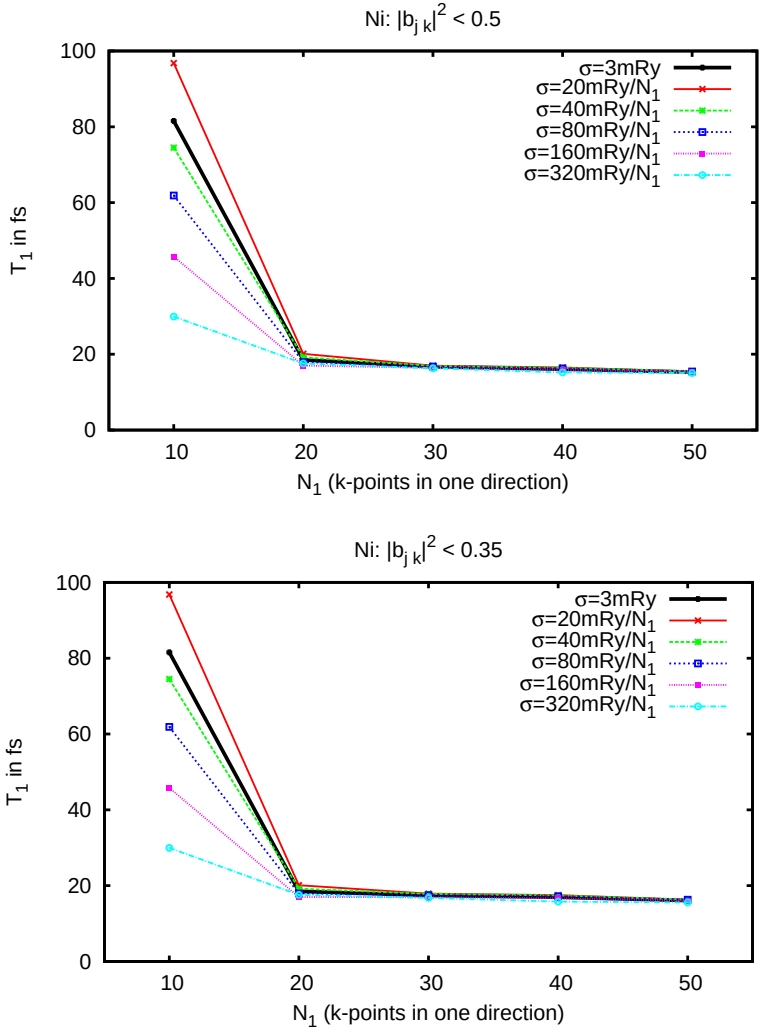

Figure 7.3: Relaxation time T_1 vs. number of k-points in one direction N_1 for different smearing parameters σ. Top: Ni $|b_{j\mathbf{k}}|^2 < 0.5$. Bottom: Ni $|b_{j\mathbf{k}}|^2 < 0.35$.

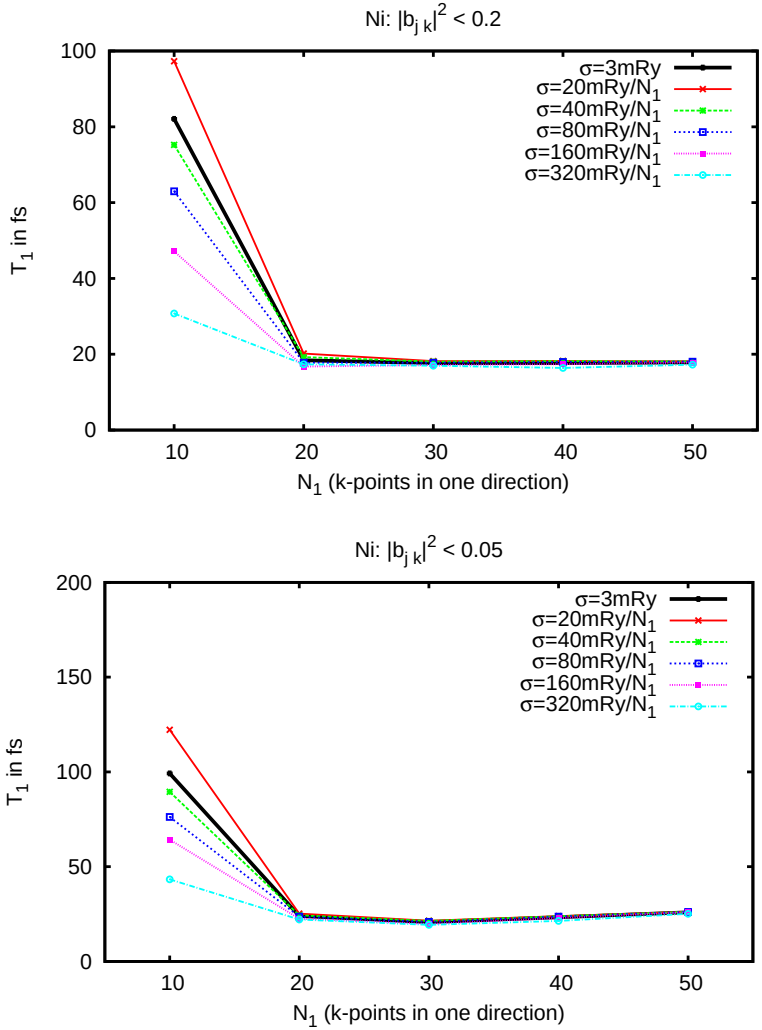

Figure 7.4: Relaxation time T_1 vs. number of k-points in one direction N_1 for different smearing parameters σ. Top: Ni $|b_{j\mathbf{k}}|^2 < 0.2$. Bottom: Ni $|b_{j\mathbf{k}}|^2 < 0.05$.

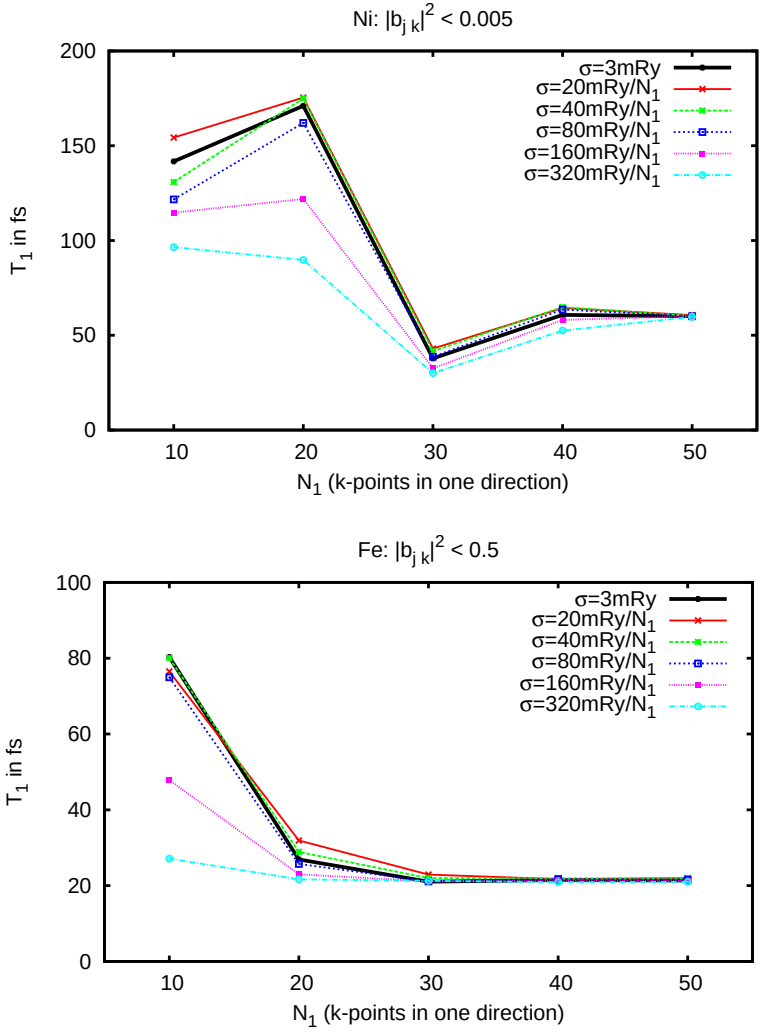

Figure 7.5: Relaxation time T_1 vs. number of k-points in one direction N_1 for different smearing parameters σ. Top: Ni $|b_{j\mathbf{k}}|^2 < 0.005$. Bottom: Fe $|b_{j\mathbf{k}}|^2 < 0.5$.

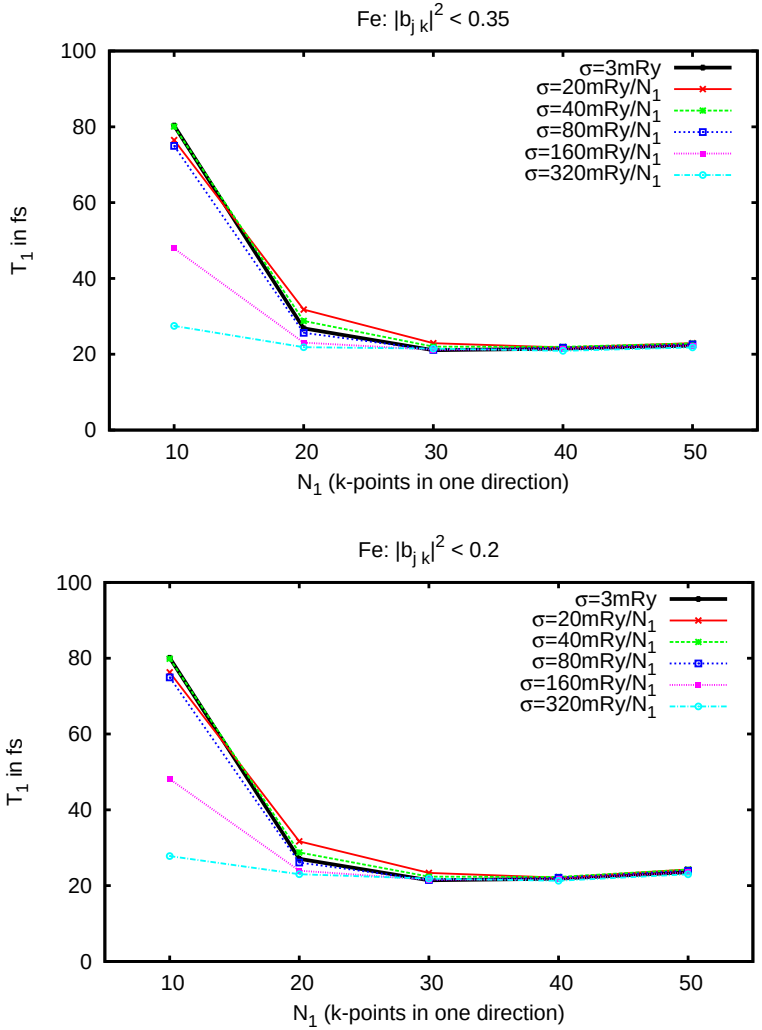

Figure 7.6: Relaxation time T_1 vs. number of k-points in one direction N_1 for different smearing parameters σ. Top: Fe $|b_{j\mathbf{k}}|^2 < 0.35$. Bottom: Fe $|b_{j\mathbf{k}}|^2 < 0.2$.

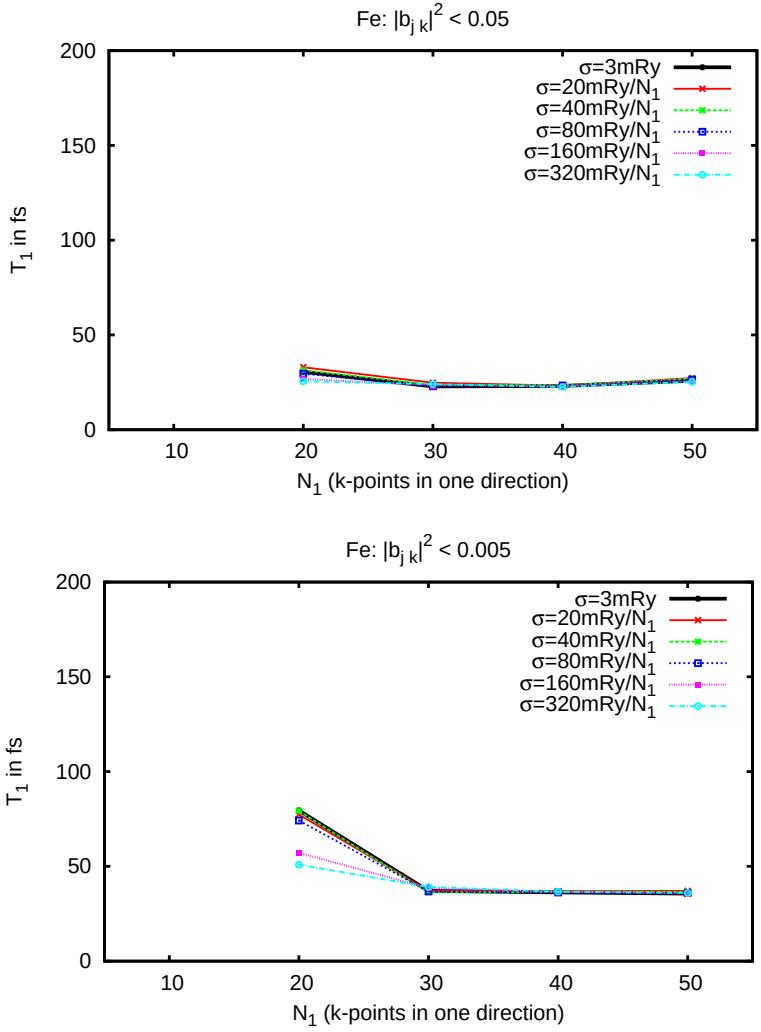

Figure 7.7: Relaxation time T_1 vs. number of k-points in one direction N_1 for different smearing parameters σ. Top: Fe $|b_{j\mathbf{k}}|^2 < 0.05$. Bottom: Fe $|b_{j\mathbf{k}}|^2 < 0.005$. The values for $N_1 = 10$ are not shown since they are very large.

	T_1^{E}	T_1^{Y}	T_1
Ni	55.5 fs	64.9 fs	15.6 fs
Fe	76.9 fs	94.3 fs	21.7 fs

Table 7.1: Relaxation time split into the Elliott part T_1^{E} and the Yafet part T_1^{Y} in comparison with the total relaxation time T_1 for $N_1 = 50$ and $|b_{j\mathbf{k}}|^2 < 0.5$.

7.1.3 Elliott part and Yafet part

Yafet pointed out [64] that the distortion of the spin-orbit coupling is important and has to be taken into account. In order to see how large the contribution of this part is, the calculation of the relaxation time T_1 is split into an Elliott part (only spin-diagonal matrix element, see eq. (6.28)) which represents the lattice distortion and a Yafet part (only non-spin-diagonal matrix element, see eq. (6.29)) which represents the distortion of the spin-orbit coupling.

The results are shown in table 7.1. For Ni ($N_1 = 50$) and $|b_{j\mathbf{k}}|^2 < 0.5$ (all possible spin-flip transitions) the Elliott part is $T_1^{\mathrm{E}} = 55.5$ fs and the Yafet part is $T_1^{\mathrm{Y}} = 64.9$ fs. For Fe ($N_1 = 50$) and $|b_{j\mathbf{k}}|^2 < 0.5$ (all possible spin-flip transitions) the Elliott part is $T_1^{\mathrm{E}} = 76.9$ fs and the Yafet part is $T_1^{\mathrm{Y}} = 94.3$ fs. Hence, the contribution of the Yafet part to the relaxation time T_1 is as large as the Elliott part and indeed not negligible! Also other authors come to the conclusion that the Elliott part and the Yafet part give similar contributions, see refs. [111, 112, 113], demonstrating the correctness of the present numerical calculations.

7.2 Demagnetization rates

7.2.1 Convergence for thermalized electron distributions

The rates of the magnetic moment change dM/dt (proportional to the demagnetization rates) are calculated according to eq. (6.53). Here, the factor $m_{j\mathbf{k}\uparrow,j'\mathbf{k}'\downarrow}$ accounts for the magnetic moment change per spin-flip and it is not necessary to distinguish between different definitions for dominant-up and dominant-down states. As in the last section different smearing parameters σ as well as different k-grids are used so that

		300K	500K	700K	1000K	1500K	2000K
Ni	$\varepsilon_{\mathrm{F}}^{\uparrow}(t_s) - \varepsilon_{\mathrm{F}}^{0}$	—	+1.3	+2.8	+9.3	+39.8	+88.8
	$\varepsilon_{\mathrm{F}}^{\downarrow}(t_s) - \varepsilon_{\mathrm{F}}^{0}$	—	-4.5	-9.0	-14.4	-18.0	-14.6
	$dM/dt(t_s)$	0.0	0.01	0.02	0.05	0.12	0.22
Fe	$\varepsilon_{\mathrm{F}}^{\uparrow}(t_s) - \varepsilon_{\mathrm{F}}^{0}$	—	+2.2	+6.4	+16.4	+43.5	+82.6
	$\varepsilon_{\mathrm{F}}^{\downarrow}(t_s) - \varepsilon_{\mathrm{F}}^{0}$	—	+2.4	+5.9	+14.3	+35.9	+60.6
	$dM/dt(t_s)$	0.0	0.0	0.0	0.0	0.02	0.05

Table 7.2: Shift of the chemical potentials $\varepsilon_{\mathrm{F}}^{\uparrow}(t_s) - \varepsilon_{\mathrm{F}}^{0}$, $\varepsilon_{\mathrm{F}}^{\downarrow}(t_s) - \varepsilon_{\mathrm{F}}^{0}$ in meV and rate of the magnetic moment change $dM/dt(t_s)$ in units of μ_{B} per 100 fs per atom.

$\sigma \cdot N_1 = const.$ $N_1 = 10$, 20, 30, 40, 50 is chosen for Ni and for Fe. The smearing parameter is σ = 3mRy, 20mRy/N_1, 40mRy/N_1, 80mRy/N_1, 160mRy/N_1, 320mRy/N_1. The rates of the magnetic moment change are calculated for time t_s for different electron temperatures T_e, and the shifted chemical potentials $\varepsilon_{\mathrm{F}}^{\uparrow}(t_s)$ and $\varepsilon_{\mathrm{F}}^{\downarrow}(t_s)$ are determined as described in section 6.6. T_e = 300 K, 500 K, 700 K, 1000 K, 1500 K and 2000 K is chosen. An electron temperature up to 1000 K is reasonable (see section 6.6) whereas 1500 K and 2000 K is very hot and probably not reasonable. Figs. 7.8 up to 7.13 show the corresponding convergence tests for Ni and Fe.

The rate for T_e = 300 K has to vanish since this is the equilibrium case where electron and phonon temperature are equal $T_e = T_p = 300$ K. The equilibrium rate vanishes indeed for dense k-point grids and small deviations are due to the fact that the energy conservation is not exactly fulfilled because of the smearing of the delta function. For coarse k-point grids (especially $N_1 = 10$) one cannot expect that the equilibrium rates are zero.

We see that the results for different smearing parameters σ converge very well already for $N_1 = 30$ in Ni and Fe. Therefore, it can be excluded that missing screening effects (see section 5.4) influenced the results, i.e., the grid density up to $N_1 = 50$ does not lead to very small phonon frequencies which falsify the results. Table 7.2 summarizes the results for all electron temperatures and also gives the shifts of the chemical potentials. If $dM/dt(t_s)$ is positive, more states flip from dominant-up (majority)

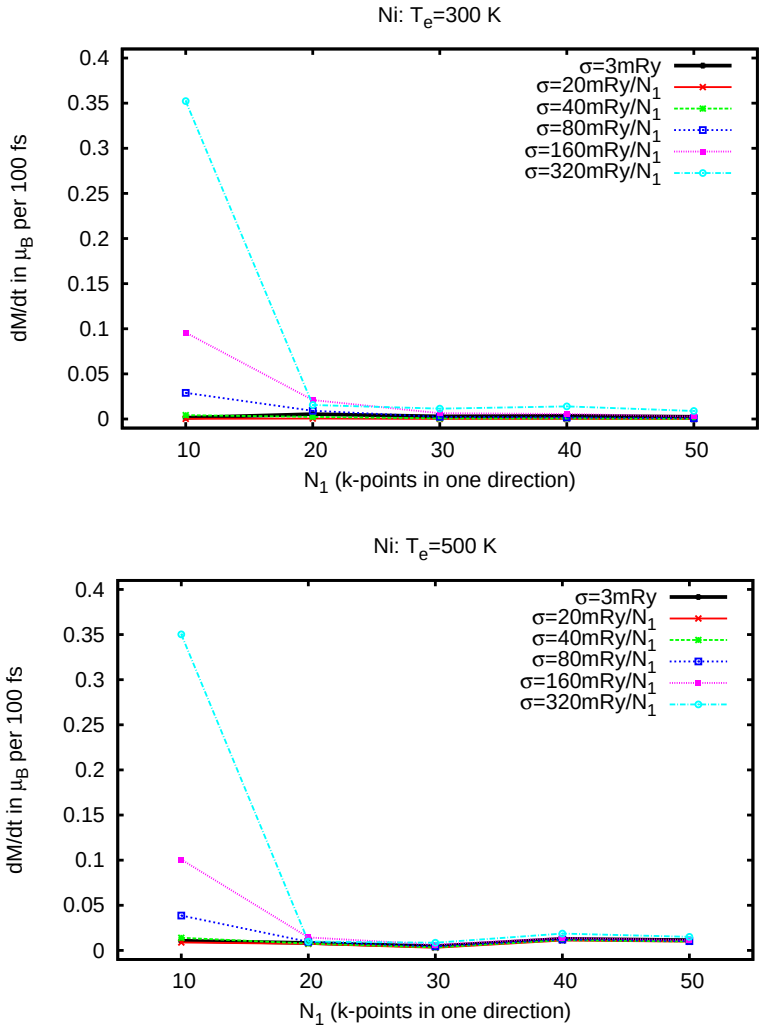

Figure 7.8: Rate of the magnetic moment change per atom $dM/dt(t_s)$ vs. number of k-points in one direction N_1 for different smearing parameters σ. Top: Ni $T_e = 300$ K. Bottom: Ni $T_e = 500$ K.

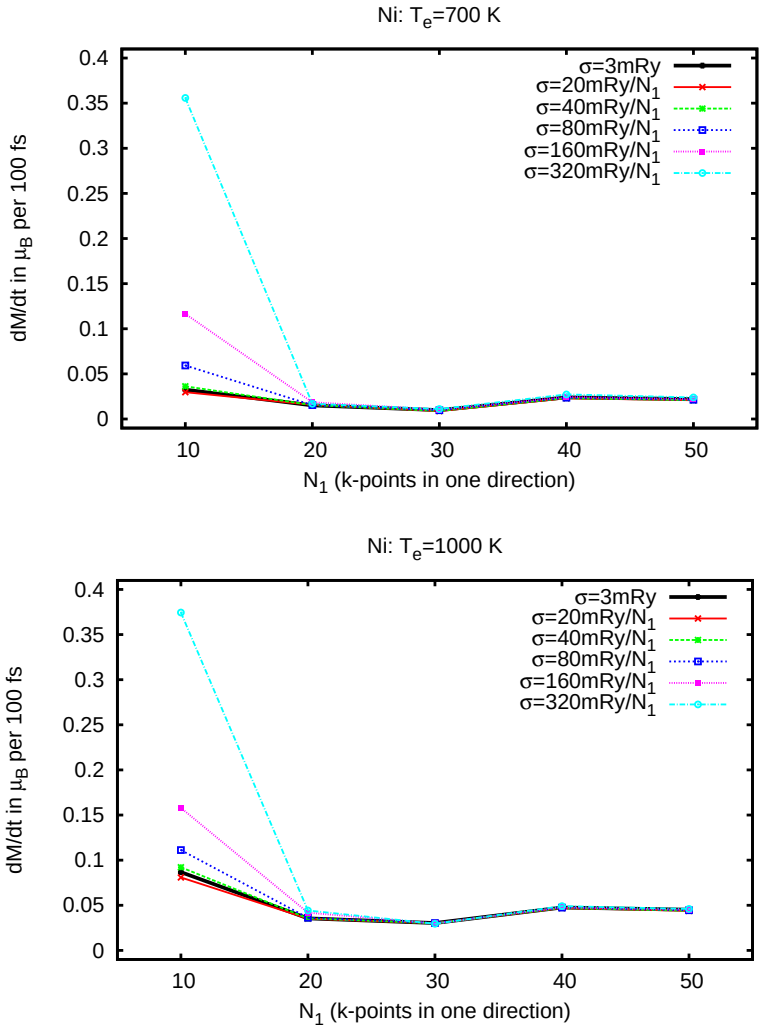

Figure 7.9: Rate of the magnetic moment change per atom $dM/dt(t_s)$ vs. number of k-points in one direction N_1 for different smearing parameters σ. Top: Ni $T_e = 700$ K. Bottom: Ni $T_e = 1000$ K.

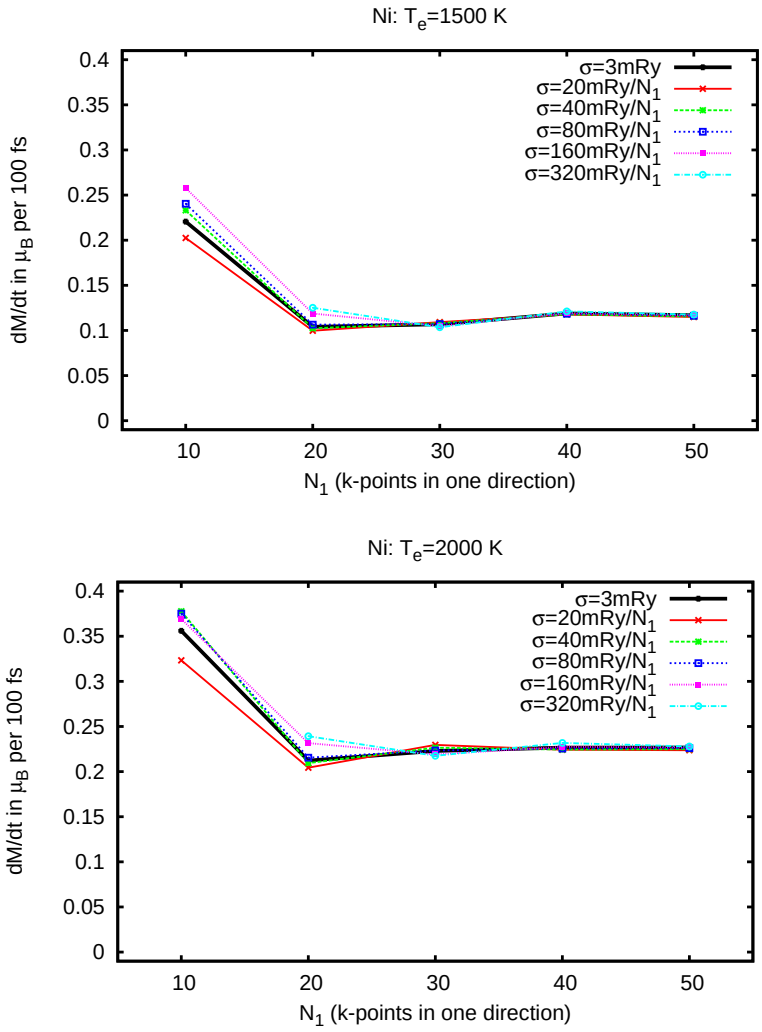

Figure 7.10: Rate of the magnetic moment change per atom $dM/dt(t_s)$ vs. number of k-points in one direction N_1 for different smearing parameters σ. Top: Ni $T_e = 1500$ K. Bottom: Ni $T_e = 2000$ K. For $N_1 = 10$ the value for $\sigma = 320$ mRy/N_1 is omitted since it is too large.

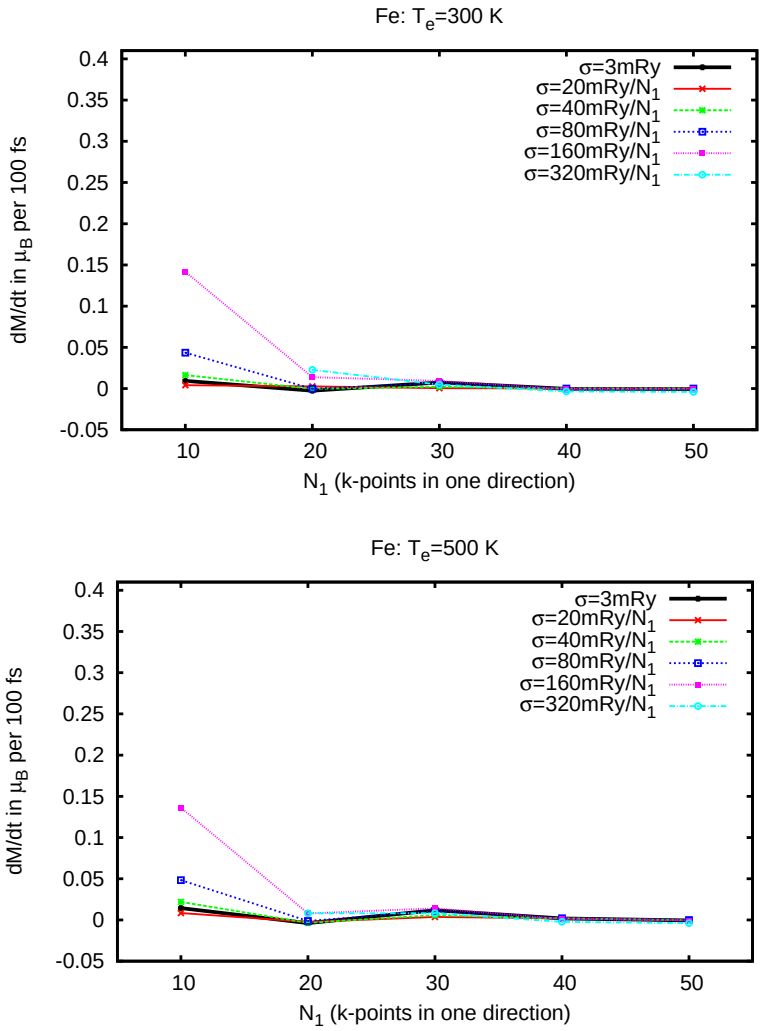

Figure 7.11: Rate of the magnetic moment change per atom $dM/dt(t_s)$ vs. number of k-points in one direction N_1 for different smearing parameters σ. Top: Fe $T_e = 300$ K. Bottom: Fe $T_e = 500$ K. For $N_1 = 10$ the value for $\sigma = 320$ mRy/N_1 is omitted since it is too large.

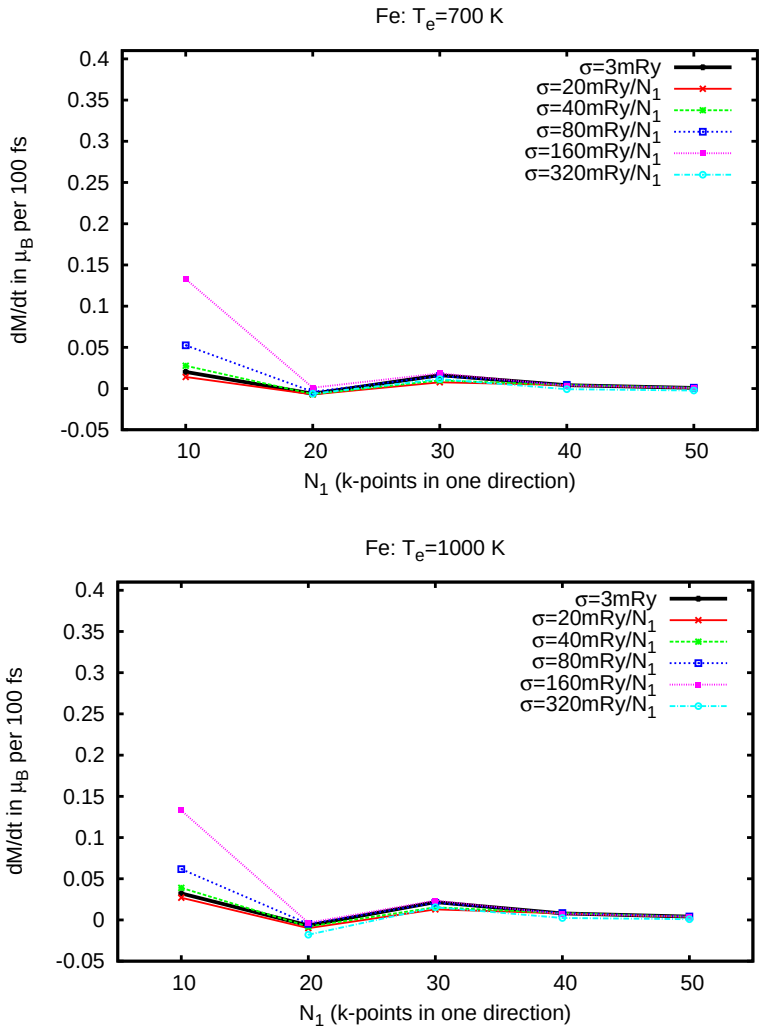

Figure 7.12: Rate of the magnetic moment change per atom $dM/dt(t_s)$ vs. number of k-points in one direction N_1 for different smearing parameters σ. Top: Fe $T_e = 700$ K. Bottom: Fe $T_e = 1000$ K. For $N_1 = 10$ the value for $\sigma = 320$ mRy/N_1 is omitted since it is too large.

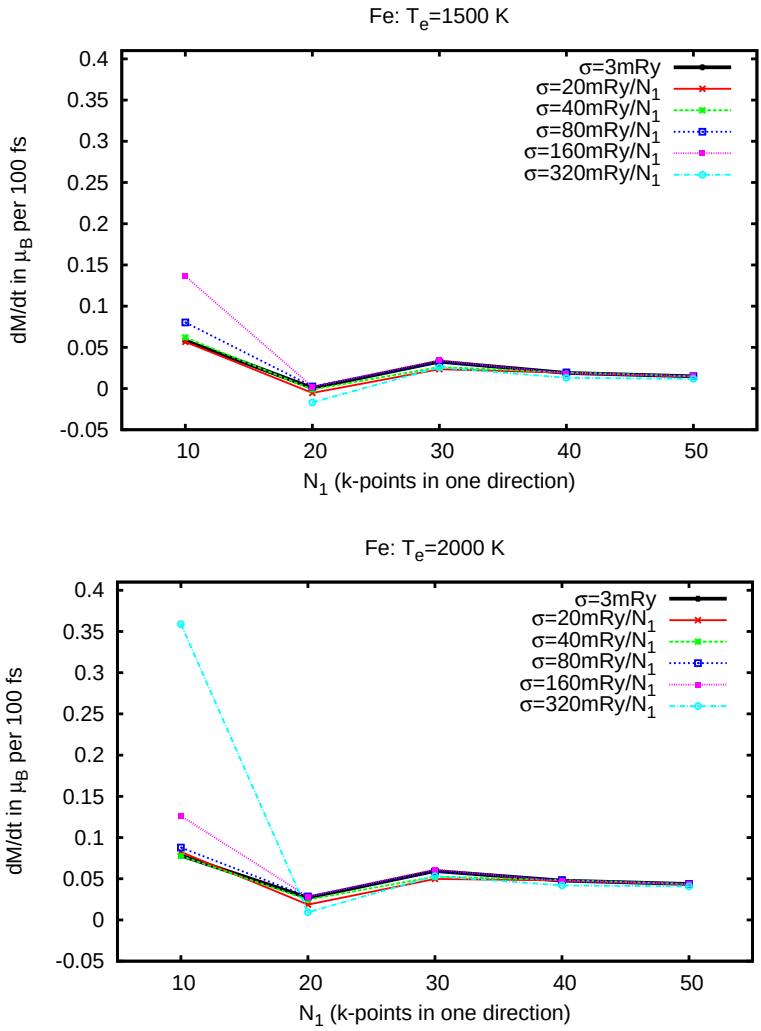

Figure 7.13: Rate of the magnetic moment change per atom $dM/dt(t_s)$ vs. number of k-points in one direction N_1 for different smearing parameters σ. Top: Fe $T_e = 1500$ K. For $N_1 = 10$ the value for $\sigma = 320$ mRy/N_1 is omitted since it is too large. Bottom: Fe $T_e = 2000$ K.

to dominant-down (minority) than vice versa (see eq. (6.53)), hence, the modulus of the magnetic moment per atom has to decrease. Vice versa, if $dM/dt(t_s)$ is negative, the modulus of the magnetic moment per atom has to increase. An increase is in principle not prohibited[24] by eq. (6.53) but the numerical results give only positive values of $dM/dt(t_s)$.

Ni has a ground-state magnetic moment of 0.64 μ_B per atom. For T_e = 500 K, 700 K and 1000 K $dM/dt(t_s)$ is almost zero. $dM/dt(t_s)$ for an electron temperature of T_e = 1500 K is about 0.12 μ_B per 100 fs per atom, which seems to be still too small to explain the experimental rate up to $dM^{exp}/dt(t_s) \approx 0.3$ μ_B per 100 fs per atom in Ni [18]. For T_e = 2000 K the calculated rate is about 0.22 μ_B per 100 fs per atom which could in principle explain the experimental value, however, electron temperatures greater than 1000 K are rather unreasonable and to the best of my knowledge have never been reported before.

Fe has a ground-state magnetic moment of 2.2 μ_B per atom. $dM/dt(t_s)$ is almost zero even for very high electron temperatures. The rate of the magnetic moment change is only 0.05 μ_B per 100 fs per atom for T_e = 2000 K. This is much smaller than the experimental value up to $dM^{exp}/dt(t_s) \approx 1.0$ μ_B per 100 fs per atom [69] and can definitely not explain the experiments.

7.2.2 Elliott part and Yafet part

The rate of the magnetic moment change is split into the Elliott part (only spin-diagonal matrix element, see eq. (6.28)) and the Yafet part (only non-spin-diagonal matrix element, see eq. (6.29)). Table 7.3 shows the results for T_e = 300 K, 500 K, 700 K, 1000 K, 1500 K and 2000 K (N_1 = 50). Both Elliott part and Yafet part are Hermitian. This can be easily seen in subsection 6.1.2. Therefore, the Elliott part $dM^E/dt(t_s)$ and the Yafet part $dM^Y/dt(t_s)$ at 300 K must vanish (since this is the equilibrium). Again one can see that Elliott part and Yafet part make similar contributions to the total rate of the magnetic moment change $dM/dt(t_s)$ in accordance with refs. [111, 112, 113].

[24] The only restriction is that on a long timescale the system has to relax to the equilibrium.

		300K	500K	700K	1000K	1500K	2000K
Ni	$dM^{\mathrm{E}}/dt(t_s)$	0.0	0.003	0.006	0.012	0.030	0.060
	$dM^{\mathrm{Y}}/dt(t_s)$	0.0	0.002	0.005	0.010	0.028	0.055
	$dM/dt(t_s)$	0.0	0.011	0.020	0.044	0.116	0.220
Fe	$dM^{\mathrm{E}}/dt(t_s)$	0.0	0.0	0.0	0.001	0.004	0.012
	$dM^{\mathrm{Y}}/dt(t_s)$	0.0	0.0	0.0	0.001	0.004	0.010
	$dM/dt(t_s)$	0.0	0.0	0.0	0.004	0.015	0.044

Table 7.3: Rate of the magnetic moment change $dM/dt(t_s)$ in units of μ_{B} per 100 fs per atom split into the Elliott part $dM^{\mathrm{E}}/dt(t_s)$ and the Yafet part $dM^{\mathrm{Y}}/dt(t_s)$.

7.3 Reduced magnetization

It was claimed [68, 75] that a calculation in a rigid-band structure would never reproduce the experimental demagnetization rates and it was suggested [68] that a dynamical change of the exchange splitting could give realistic rates. Therefore, the rate of magnetic moment change is also calculated for band structures with reduced magnetic moment obtained from a self-consistent calculation with Lagrangian fields (only for a 40×40×40 k-point grid where the convergence is already very good). For Ni a reduced magnetic moment of 0.5 μ_{B}, 0.4 μ_{B} and 0.3 μ_{B} per atom is chosen (ground state: 0.64 μ_{B}) and for Fe a reduced magnetic moment of 1.6 μ_{B} and 1.1 μ_{B} per atom is chosen (ground state: 2.2 μ_{B}). Note that this is a longitudinal reduction (length reduction) and not a transverse reduction caused by disorder of the atomic moments (magnons) (see ref. [75]).

7.3.1 Density of states

Fig. 7.14 shows the spin-up and spin-down density of states $Z^{\uparrow,\downarrow}(\varepsilon)$ in Ni, Fe and fcc Co for the ground-state atomic magnetic moment (Ni: 0.64 μ_{B}, Fe: 2.2 μ_{B}, fcc Co: 1.6 μ_{B}) and for reduced atomic magnetic moments (Ni: 0.5 μ_{B} and 0.3 μ_{B}, Fe: 1.6 μ_{B} and 1.1 μ_{B}, fcc Co: 1.1 μ_{B} and 0.8 μ_{B}). For the sake of completeness the density of states for fcc Co is already shown here but it is only needed for section 7.4. One can see clearly that the exchange splitting is reduced for a band structure with reduced atomic magnetic moments in all materials.

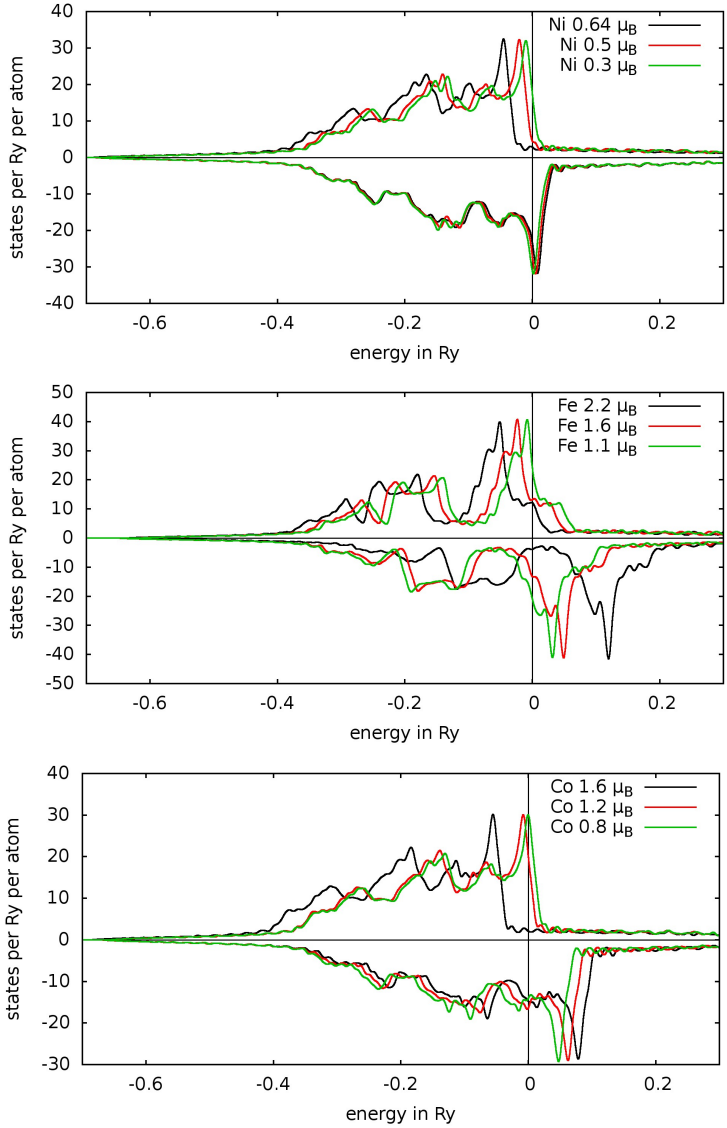

Figure 7.14: Density of states $Z^{\uparrow,\downarrow}(\varepsilon)$ according to eq. (2.48) calculated with the LMTO-ASA code. The Fermi energy is set to zero. Positive values denote spin-up, negative values denote spin-down. Top: Ni. Middle: Fe. Bottom: fcc Co.

	Ni				Fe			
	$0.64\mu_B$	$0.5\mu_B$	$0.3\mu_B$	$0.2\mu_B$	$2.2\mu_B$	$1.6\mu_B$	$1.1\mu_B$	$0.6\mu_B$
b^2	0.026	0.039	0.019	0.013	0.026	0.038	0.055	0.068

Table 7.4: Spin-mixing factor b^2 for a smearing of 25 meV around the Fermi energy ($N_1 = 50$).

	Ni				Fe		
	$0.64\mu_B$	$0.5\mu_B$	$0.4\mu_B$	$0.3\mu_B$	$2.2\mu_B$	$1.6\mu_B$	$1.1\mu_B$
T_1	16.1 fs	43.5 fs	90.9 fs	86.2 fs	21.7 fs	57.5 fs	89.3 fs

Table 7.5: Relaxation time T_1 for the band structure with ground-state atomic magnetic moment and for band structures with reduced atomic magnetic moments ($|b_{j\mathbf{k}}|^2 < 0.5$ and $N_1 = 40$).

7.3.2 Spin-mixing factor

The spin-mixing factor b^2 defined in eq. (2.46) changes for a band structure with reduced magnetic moment. Table 7.4 summarizes the results for different reduced magnetic moments for a smearing of 25 meV around the Fermi energy (50×50×50 k-point grid). For Fe the spin-mixing for a band structure with reduced magnetic moment is stronger than the spin-mixing for the band structure with ground-state magnetic moment, however this is not true for Ni.

7.3.3 Relaxation time

The relaxation times for the band structure with ground-state atomic magnetic moment and for band structures with reduced atomic magnetic moments are given in table 7.5 for a definition of the dominant-up and dominant-down states with $|b_{j\mathbf{k}}|^2 < 0.5$ on a 40×40×40 k-point grid. Obviously, the relaxation times for the reduced atomic magnetic moments are greater than for the ground-state atomic magnetic moment. It is about 90 fs for a 50%-reduction of the atomic magnetic moment in Ni and in Fe.

Ni		300K	400K	500K	600K	700K	1000K
$0.5\mu_B$	$\varepsilon_F^{\uparrow}(t_*) - \varepsilon_F^0$	—	+7.0	+15.6	+25.5	+36.5	+73.1
	$\varepsilon_F^{\downarrow}(t_*) - \varepsilon_F^0$	—	-1.9	-3.7	-5.5	-7.0	-10.1
	$dM/dt(t_*)$	0.0	0.012	0.031	0.052	0.074	0.152
$0.4\mu_B$	$\varepsilon_F^{\uparrow}(t_*) - \varepsilon_F^0$	—	+6.7	+14.6	+23.5	+33.2	+65.4
	$\varepsilon_F^{\downarrow}(t_*) - \varepsilon_F^0$	—	-1.2	-2.4	-3.4	-4.1	-4.6
	$dM/dt(t_*)$	0.0	0.012	0.026	0.043	0.063	0.130
$0.3\mu_B$	$\varepsilon_F^{\uparrow}(t_*) - \varepsilon_F^0$	—	+5.2	+11.5	+18.5	+26.2	+52.2
	$\varepsilon_F^{\downarrow}(t_*) - \varepsilon_F^0$	—	-0.5	-0.8	-0.9	-0.7	+1.5
	$dM/dt(t_*)$	0.0	0.009	0.019	0.031	0.043	0.086
Fe							
$1.6\mu_B$	$\varepsilon_F^{\uparrow}(t_*) - \varepsilon_F^0$	—	+0.7	+2.0	+4.1	+6.8	+18.1
	$\varepsilon_F^{\downarrow}(t_*) - \varepsilon_F^0$	—	-1.8	-4.3	-7.5	-11.3	-26.5
	$dM/dt(t_*)$	0.0	0.004	0.010	0.018	0.027	0.066
$1.1\mu_B$	$\varepsilon_F^{\uparrow}(t_*) - \varepsilon_F^0$	—	+4.0	+8.4	+13.1	+18.0	+33.1
	$\varepsilon_F^{\downarrow}(t_*) - \varepsilon_F^0$	—	-2.2	-4.9	-7.8	-11.0	-22.6
	$dM/dt(t_*)$	0.0	0.010	0.022	0.034	0.047	0.088

Table 7.6: Shift of the chemical potentials $\varepsilon_F^{\uparrow}(t_*) - \varepsilon_F^0$, $\varepsilon_F^{\downarrow}(t_*) - \varepsilon_F^0$ in meV and rate of the magnetic moment change $dM/dt(t_*)$ in units of μ_B per 100 fs per atom. t_* is the time at which the magnetic moment per atom is reduced to the value used for the calculation.

7.3.4 Demagnetization rates

The rate of the magnetic moment change for the electron temperatures $T_e = 300$ K, 400 K, 500 K, 600 K, 700 K, 1000 K and for reduced atomic magnetic moments in Ni and Fe are summarized in table 7.6. Here, it does not make sense to calculate for higher electron temperatures because the electron temperature is certainly quite low when the atomic magnetic moment has already reduced by 75% up to 50% (see refs. [1, 18, 79] for reasonable electron temperatures). $T_e = 700$ K and $T_e = 1000$ K are probably already much too high, but nevertheless shown in table 7.6.

Table 7.2 (rates for ground-state atomic magnetic moments) shows that the rate of the magnetic moment change does not vary a lot for $T_e = 300$ K,

500 K, 700 K and 1000 K. We see in table 7.6 (rates for reduced atomic magnetic moments) that the rates vary much more for the same electron temperatures. However, the rates $dM/dt(t_*)$ for Fe are small with respect to the atomic magnetic moment and are much smaller than experimental values for $dM/dt(t_*)$ where t_* is the time at which the magnetic moment per atom is reduced to the value used for the calculation ($1.6\mu_B$ and $1.1\mu_B$ for Fe). The rates $dM/dt(t_*)$ for Ni are greater with respect to the atomic magnetic moment but still smaller than experimental values for $dM/dt(t_*)$ for electron temperatures up to 700 K. $dM/dt(t_*)$ is similar to experimental values for $T_e = 1000$ K which is unreasonably high.

7.4 Phase space estimation and maximum possible demagnetization

Finally, the available phase space is estimated. The calculation of the phase space of majority/minority electrons and majority/minority holes is explained in section 5.8. Table 7.7, 7.8 and 7.9 give an overview over the phase space in Ni, Fe and fcc Co[25] with the ground-state atomic magnetic moment (Ni: 0.64 μ_B, Fe: 2.2 μ_B, fcc Co: 1.6 μ_B) and reduced magnetic moments (Ni: 0.5 μ_B and 0.3 μ_B, Fe: 1.6 μ_B and 1.1 μ_B, fcc Co: 1.2 μ_B and 0.8 μ_B) using possibility 1 of section 5.8. Table 7.10 uses possibility 2 of section 5.8 for the estimation of the available phase space.

For Ni the number of minority electrons $\Delta N^{\downarrow}$ and minority holes $\Delta N^{h\downarrow}$ is much greater than the number of majority electrons $\Delta N^{\uparrow}$ and majority holes $\Delta N^{h\uparrow}$. This is also true for the reduced magnetic moments and is due to the density of states (see fig. 7.14). For Fe it is the other way round. For fcc Co the number of minority electrons $\Delta N^{\downarrow}$ and minority holes $\Delta N^{h\downarrow}$ is only for the ground state much greater than the number of majority electrons $\Delta N^{\uparrow}$ and majority holes $\Delta N^{h\uparrow}$.

The maximum possible decrease of the magnetic moment $\Delta M = 2\mu_B \cdot (\Delta N^{\uparrow} + \Delta N^{h\downarrow})$ can be quite large for Ni with ground-state magnetic moment of $0.64\mu_B$, up to $\Delta M = 2\mu_B \cdot 0.178 = 0.356\mu_B$ for $T_e = 2000$ K, but several points have to be considered:

[25] Co is also an interesting material for ultrafast demagnetization [18]. The lattice structure of Co is hcp, however, in the ultrafast demagnetization experiments Co on MgO is used [18] where the Co film has an fcc structure.

Ni		500K	700K	1000K	1500K	2000K
$0.64\mu_B$	$\Delta N^{\uparrow}$	0.005	0.007	0.010	0.015	0.020
	$\Delta N^{h\uparrow}$	0.006	0.008	0.013	0.023	0.035
	$\Delta N^{\downarrow}$	0.059	0.083	0.114	0.158	0.188
	$\Delta N^{h\downarrow}$	0.046	0.061	0.084	0.119	0.158
	$\Delta N^{\uparrow} + \Delta N^{h\downarrow}$	**0.051**	**0.068**	**0.094**	**0.134**	**0.178**
	$\Delta N^{\downarrow} + \Delta N^{h\uparrow}$	0.065	0.091	0.126	0.180	0.223
$0.5\mu_B$	$\Delta N^{\uparrow}$	0.008	0.010	0.012	0.016	0.022
	$\Delta N^{h\uparrow}$	0.015	0.023	0.036	0.054	0.071
	$\Delta N^{\downarrow}$	0.065	0.089	0.118	0.154	0.177
	$\Delta N^{h\downarrow}$	0.051	0.066	0.091	0.130	0.170
	$\Delta N^{\uparrow} + \Delta N^{h\downarrow}$	**0.059**	**0.076**	**0.103**	**0.146**	**0.192**
	$\Delta N^{\downarrow} + \Delta N^{h\uparrow}$	0.080	0.113	0.153	0.208	0.248
$0.3\mu_B$	$\Delta N^{\uparrow}$	0.024	0.028	0.026	0.025	0.026
	$\Delta N^{h\uparrow}$	0.050	0.067	0.093	0.124	0.147
	$\Delta N^{\downarrow}$	0.064	0.084	0.105	0.127	0.136
	$\Delta N^{h\downarrow}$	0.060	0.079	0.108	0.154	0.199
	$\Delta N^{\uparrow} + \Delta N^{h\downarrow}$	**0.083**	**0.107**	**0.134**	**0.179**	**0.225**
	$\Delta N^{\downarrow} + \Delta N^{h\uparrow}$	0.114	0.151	0.198	0.251	0.283

Table 7.7: Phase space estimation according to possibility 1 in section 5.8 for Ni (atomic magnetic moment: 0.64 μ_B, 0.5 μ_B, 0.3 μ_B) for different electron temperatures T_e. Important for the maximum possible demagnetization is the quantity $\Delta N^{\uparrow} + \Delta N^{h\downarrow}$, hence, the numbers are printed in bold.

Fe		500K	700K	1000K	1500K	2000K
$2.2\mu_B$	$\Delta N^{\uparrow}$	0.022	0.028	0.034	0.038	0.037
	$\Delta N^{h\uparrow}$	0.026	0.037	0.053	0.080	0.108
	$\Delta N^{\downarrow}$	0.007	0.010	0.014	0.022	0.032
	$\Delta N^{h\downarrow}$	0.009	0.012	0.019	0.031	0.047
	$\Delta N^{\uparrow} + \Delta N^{h\downarrow}$	**0.031**	**0.040**	**0.052**	**0.070**	**0.084**
	$\Delta N^{\downarrow} + \Delta N^{h\uparrow}$	0.034	0.047	0.067	0.102	0.140
$1.6\mu_B$	$\Delta N^{\uparrow}$	0.029	0.040	0.055	0.077	0.094
	$\Delta N^{h\uparrow}$	0.030	0.045	0.070	0.117	0.165
	$\Delta N^{\downarrow}$	0.029	0.041	0.062	0.095	0.127
	$\Delta N^{h\downarrow}$	0.022	0.028	0.033	0.042	0.047
	$\Delta N^{\uparrow} + \Delta N^{h\downarrow}$	**0.051**	**0.068**	**0.088**	**0.118**	**0.141**
	$\Delta N^{\downarrow} + \Delta N^{h\uparrow}$	0.059	0.086	0.133	0.212	0.292
$1.1\mu_B$	$\Delta N^{\uparrow}$	0.035	0.046	0.062	0.085	0.105
	$\Delta N^{h\uparrow}$	0.058	0.083	0.119	0.175	0.227
	$\Delta N^{\downarrow}$	0.049	0.068	0.101	0.151	0.199
	$\Delta N^{h\downarrow}$	0.036	0.049	0.063	0.081	0.093
	$\Delta N^{\uparrow} + \Delta N^{h\downarrow}$	**0.071**	**0.095**	**0.124**	**0.166**	**0.198**
	$\Delta N^{\downarrow} + \Delta N^{h\uparrow}$	0.107	0.152	0.220	0.327	0.426

Table 7.8: Phase space estimation according to possibility 1 in section 5.8 for Fe (atomic magnetic moment: 2.2 μ_B, 1.6 μ_B, 1.1 μ_B) for different electron temperatures T_e. Important for the maximum possible demagnetization is the quantity $\Delta N^{\uparrow} + \Delta N^{h\downarrow}$, hence, the numbers are printed in bold.

Co		500K	700K	1000K	1500K	2000K
$1.6\mu_B$	$\Delta N^{\uparrow}$	0.004	0.006	0.009	0.014	0.019
	$\Delta N^{h\uparrow}$	0.005	0.007	0.011	0.018	0.028
	$\Delta N^{\downarrow}$	0.033	0.046	0.067	0.099	0.131
	$\Delta N^{h\downarrow}$	0.031	0.042	0.058	0.083	0.108
	$\Delta N^{\uparrow} + \Delta N^{h\downarrow}$	**0.036**	**0.049**	**0.067**	**0.097**	**0.126**
	$\Delta N^{\downarrow} + \Delta N^{h\uparrow}$	0.038	0.054	0.077	0.117	0.159
$1.2\mu_B$	$\Delta N^{\uparrow}$	0.031	0.036	0.036	0.032	0.027
	$\Delta N^{h\uparrow}$	0.053	0.073	0.101	0.138	0.166
	$\Delta N^{\downarrow}$	0.034	0.045	0.064	0.095	0.128
	$\Delta N^{h\downarrow}$	0.035	0.049	0.068	0.099	0.128
	$\Delta N^{\uparrow} + \Delta N^{h\downarrow}$	**0.066**	**0.085**	**0.104**	**0.131**	**0.156**
	$\Delta N^{\downarrow} + \Delta N^{h\uparrow}$	0.087	0.118	0.166	0.234	0.294
$0.8\mu_B$	$\Delta N^{\uparrow}$	0.060	0.073	0.094	0.104	0.106
	$\Delta N^{h\uparrow}$	0.058	0.081	0.107	0.157	0.201
	$\Delta N^{\downarrow}$	0.028	0.041	0.060	0.092	0.128
	$\Delta N^{h\downarrow}$	0.033	0.046	0.065	0.100	0.132
	$\Delta N^{\uparrow} + \Delta N^{h\downarrow}$	**0.093**	**0.118**	**0.159**	**0.203**	**0.238**
	$\Delta N^{\downarrow} + \Delta N^{h\uparrow}$	0.086	0.122	0.167	0.249	0.329

Table 7.9: Phase space estimation according to possibility 1 in section 5.8 for fcc Co (atomic magnetic moment: 1.6 μ_B, 1.2 μ_B, 0.8 μ_B) for different electron temperatures T_e. Important for the maximum possible demagnetization is the quantity $\Delta N^{\uparrow} + \Delta N^{h\downarrow}$, hence, the numbers are printed in bold.

Ni		500K	700K	1000K	1500K	2000K
$0.64\mu_B$	$\Delta N_{exc}^{\uparrow}$	0.002	0.004	0.008	0.016	0.026
	$\Delta N_{exc}^{\downarrow}$	0.021	0.041	0.068	0.108	0.142
	$\Delta N_{exc}^{\uparrow} + \Delta N_{exc}^{h\downarrow}$	**0.023**	**0.045**	**0.076**	**0.124**	**0.168**
$0.5\mu_B$	$\Delta N_{exc}^{\uparrow}$	0.006	0.011	0.020	0.035	0.049
	$\Delta N_{exc}^{\downarrow}$	0.022	0.042	0.069	0.106	0.138
	$\Delta N_{exc}^{\uparrow} + \Delta N_{exc}^{h\downarrow}$	**0.028**	**0.053**	**0.089**	**0.141**	**0.187**
$0.3\mu_B$	$\Delta N_{exc}^{\uparrow}$	0.014	0.027	0.043	0.064	0.081
	$\Delta N_{exc}^{\downarrow}$	0.023	0.042	0.067	0.102	0.130
	$\Delta N_{exc}^{\uparrow} + \Delta N_{exc}^{h\downarrow}$	**0.037**	**0.069**	**0.110**	**0.166**	**0.221**
Fe						
$2.2\mu_B$	$\Delta N_{exc}^{\uparrow}$	0.009	0.018	0.029	0.046	0.063
	$\Delta N_{exc}^{\downarrow}$	0.003	0.006	0.012	0.022	0.035
	$\Delta N_{exc}^{\uparrow} + \Delta N_{exc}^{h\downarrow}$	**0.012**	**0.024**	**0.041**	**0.068**	**0.098**
$1.6\mu_B$	$\Delta N_{exc}^{\uparrow}$	0.012	0.025	0.046	0.082	0.116
	$\Delta N_{exc}^{\downarrow}$	0.010	0.019	0.033	0.057	0.079
	$\Delta N_{exc}^{\uparrow} + \Delta N_{exc}^{h\downarrow}$	**0.022**	**0.044**	**0.079**	**0.139**	**0.195**
$1.1\mu_B$	$\Delta N_{exc}^{\uparrow}$	0.019	0.039	0.066	0.109	0.148
	$\Delta N_{exc}^{\downarrow}$	0.017	0.034	0.058	0.095	0.128
	$\Delta N_{exc}^{\uparrow} + \Delta N_{exc}^{h\downarrow}$	**0.036**	**0.073**	**0.124**	**0.204**	**0.276**
Co						
$1.6\mu_B$	$\Delta N_{exc}^{\uparrow}$	0.002	0.004	0.007	0.013	0.021
	$\Delta N_{exc}^{\downarrow}$	0.013	0.025	0.043	0.072	0.101
	$\Delta N_{exc}^{\uparrow} + \Delta N_{exc}^{h\downarrow}$	**0.015**	**0.029**	**0.050**	**0.085**	**0.122**
$1.2\mu_B$	$\Delta N_{exc}^{\uparrow}$	0.016	0.030	0.047	0.069	0.087
	$\Delta N_{exc}^{\downarrow}$	0.013	0.026	0.045	0.076	0.107
	$\Delta N_{exc}^{\uparrow} + \Delta N_{exc}^{h\downarrow}$	**0.029**	**0.056**	**0.092**	**0.145**	**0.194**
$0.8\mu_B$	$\Delta N_{exc}^{\uparrow}$	0.021	0.040	0.063	0.094	0.119
	$\Delta N_{exc}^{\downarrow}$	0.012	0.025	0.044	0.078	0.112
	$\Delta N_{exc}^{\uparrow} + \Delta N_{exc}^{h\downarrow}$	**0.033**	**0.065**	**0.107**	**0.172**	**0.231**

Table 7.10: Phase space estimation according to possibility 2 in section 5.8 for Ni (atomic magnetic moments: 0.64 μ_B, 0.5 μ_B, 0.3 μ_B), Fe (atomic magnetic moments: 2.2 μ_B, 1.6 μ_B, 1.1 μ_B) and fcc Co (atomic magnetic moments: 1.6 μ_B, 1.2 μ_B, 0.8 μ_B) for different electron temperatures T_e. Important for the maximum possible demagnetization is the quantity $\Delta N_{exc}^{\uparrow} + \Delta N_{exc}^{h\downarrow}$, hence, the numbers are printed in bold.

1. It is questionable whether such high electron temperatures are realistic. As explained earlier, electron temperatures up to at most 1000 K are realistic.

2. The electrons only flip their spins with a spin-flip probability a_{sf} which is between 0.03 and 0.45 for Ni [18, 23]. For $a_{sf} = 0.1$ the maximum possible decrease of the ground-state magnetic moment ($0.64\mu_B$) at $T_e = 2000$ K is only $\Delta M = 0.0356\mu_B$ which is very small.

   In fig. 2e of ref. [75] the maximum quenching for $a_{sf} = 0.5$ and for a large laser fluence is 20% (decrease of the magnetic moment: $20\% \cdot 0.64\ \mu_B = 0.128\ \mu_B$) which agrees quite well with the phase space estimation in table 7.7 at $T_e = 1500$ K ($\Delta M = 2\mu_B \cdot 0.134 = 0.268\ \mu_B$) and a spin-flip probability $a_{sf} = 0.5$.

3. The phase space for an increase of the magnetic moment $2\mu_B(\Delta N^{\downarrow} + \Delta N^{h\uparrow})$ is even greater than for a decrease of the magnetic moment. If a spin-flip from dominant-up to dominant-down was as probable as a spin-flip from dominant-down to dominant-up, the magnetic moment would rather increase than decrease.

One can clearly see in table 7.7, 7.8 and 7.9 that the phase space becomes larger for a band structure with reduced magnetic moment, both for Ni, Fe and Co. Note that one has to consider the relative enlargement (ΔM/magnetic moment), not the absolute enlargement of the phase space (ΔM)! This supports the suggestion of Essert and Schneider [68] that a dynamical exchange splitting enhances the demagnetization, however, the objections 1. to 3. still hold and electron temperatures up to 2000 K are not realistic for reduced magnetic moments since the electron temperature has already cooled down at this stage. A realistic electron temperature is at most 700 K which gives $\Delta M = 2\mu_B \cdot 0.076 = 0.152\mu_B$ for a reduced magnetic moment of $0.5\mu_B$ in Ni. Even without multiplying with the spin-flip probability this is too small to explain a demagnetization of 50% or more. Furthermore, it is not clear whether a reduced magnetic moment of 0.5 μ_B or 0.3 μ_B is ever reachable if one starts with the ground-state magnetic moment and calculates the full time-resolved dynamics.

For Fe the same arguments as for Ni hold, but the relative decrease of magnetic moment (ΔM/magnetic moment) is much smaller. Even for reduced magnetic moments and high electron temperatures ΔM is

much too small to explain an experimental decrease of 50% (except for $T_e = 2000$ K)!

For fcc Co the relative decrease of magnetic moment (ΔM/magnetic moment) is small for the ground-state magnetic moment and only large for very high (unreasonable) electron temperatures and reduced magnetic moments. I conclude that the phase space is also too small to explain the experimental decrease except for $T_e = 1500$ K and $T_e = 2000$ K in combination with a reduced magnetic moment.

The phase space given in table 7.7, 7.8 and 7.9 (possibility 1) is in the same order of magnitude as the phase space given in table 7.10 (possibility 2). For possibility 2 the phase space for an increase of the magnetic moment $\Delta N^{\downarrow}_{\mathrm{exc}} + \Delta N^{h\uparrow}_{\mathrm{exc}}$ is the same as for a decrease $\Delta N^{\uparrow}_{\mathrm{exc}} + \Delta N^{h\downarrow}_{\mathrm{exc}}$, because $\Delta N^{\uparrow}_{\mathrm{exc}} = \Delta N^{h\uparrow}_{\mathrm{exc}}$ and $\Delta N^{\downarrow}_{\mathrm{exc}} = \Delta N^{h\downarrow}_{\mathrm{exc}}$ due to number conservation.

To be honest, the phase space estimation given here only considers the phase space at time t_s or t_* (t_* is the time at which the magnetic moment per atom is reduced to the value used for the calculation), respectively, but makes a statement on the maximum possible decrease of the magnetic moment for the whole time range. In reality the phase space changes all the time by non-spin-flip and spin-flip scattering processes, and therefore it is very hard to make an absolute quantitative statement on the maximum possible decrease of magnetic moment. ΔM is in principle only reasonable for a system which scatters at any time toward equilibrium for the majority-electron distribution and in addition toward a non-equilibrium distribution for the minority-electron distribution.

7.5 Discussion of the results

The results for the relaxation time T_1 are about 16 fs for Ni and 22 fs for Fe. The relaxation times seem to be in the right order of magnitude compared with experimental values of about 100 fs but several assumptions have to be used in order to define T_1 which are perhaps not fulfilled (see section 5.6) and T_1 does not give any information about the strength of the demagnetization.

I want to stress that the relaxation time for Ni and Fe is much smaller than a typical phonon period which is in the ps-range (since the phonon frequencies are in the THz-range, see chapter 3). This is not a contradiction since it was already shown in quantum-kinetic calculations [94] that

the dynamics of electron-phonon scattering processes can be in the fs-range even though the phonon dynamics is in the ps-range. Furthermore, ref. [66] also comes to the conclusion (using a model calculation) that it is possible to obtain a demagnetization time which is smaller than the electron-phonon thermalization time and that this is not a contradiction.

After having calculated the relaxation time T_1, the material-dependent parameter p appearing in the Elliott-Yafet relation is estimated. For Fe a material-dependent parameter $p \approx 4.5$ is estimated which perfectly fits to the estimation $1 < p < 10$ of Beuneu and Monod [65]. Together with the spin-mixing factor $b^2 = 0.024$ this gives a spin-flip probability of $a_{sf} = pb^2 \approx 0.11$ for Fe.

Since the relaxation time T_1 does not give any information about the strength of the demagnetization, the rate of the magnetic moment change $dM/dt(t_s)$ at time t_s is also calculated which does not require the above mentioned assumptions (in order to define T_1). For electron temperatures up to 1000 K in Ni and up to 2000 K in Fe $dM/dt(t_s)$ is almost zero. Only for a very high electron temperature of 2000 K the rate $dM/dt(t_s)$ for Ni is similar to the experimental value which is up to $dM^{\mathrm{exp}}/dt(t_s) \approx 0.3\ \mu_{\mathrm{B}}$ per 100 fs per atom [18]. However, such high electron temperatures are rather unrealistic and have never been reported in other publications.

The calculations for the relaxation time and the rates are split in the Elliott part and the Yafet part. It could be shown that they make similar contributions to the relaxation time and to the rates which is in good agreement with other publications [111, 112, 113].

For a band structure with reduced magnetic moment (reduced exchange splitting) the absolute and relative change of the magnetic moment (relative with respect to the atomic magnetic moment) is indeed greater for Ni and for Fe, however, it is still too small to explain experimental rates (except for $T_e = 1000$ K in Ni which is unreasonably high) and the question arises whether one would ever reach the reduced magnetic moment (used for the calculation) if one calculated the full time-resolved dynamics. It would be interesting to calculate the full time-resolved dynamics which was done in ref. [68] for a fixed ground-state band structure only (no reduced exchange splitting), though, it seems to be a useless endeavor since the rate of the magnetic moment change at t_s is already very small for reasonable electron temperatures and one would expect that it does not become much greater for further time steps!

Essert and Schneider [68] and Carva et al. [71, 72] also calculated the ex-

citation of electrons by the laser pulse via perturbation theory with dipole matrix elements and considered the change of this electron distribution by electron-phonon scatterings, neglecting electron-electron scattering and electron thermalization by this scattering completely. In principle, one can do this but one has to be aware of the fact that electron-electron scattering is definitely very dominant and leads to a fast thermalization [18]. I model the situation after thermalization by calculating the thermalized up- and down-electron distributions at time t_s or t_*, respectively (see section 6.6). Thereby, the up- and down-chemical potentials and the electron temperature are needed (the electron temperature can also be seen as parameter).

It was mentioned in ref. [75] that for a rigid-band calculation the rate of the magnetic moment change can either be positive or negative depending on the Fermi energy and the exchange parameter. I want to note that there is no law that prohibits a temporary increase of the magnetic moment. The system only has to relax to equilibrium in the end (on a longer timescale). However, in the present thesis only positive rates are obtained which means a decrease of the modulus of the magnetic moment.

The convergence tests of the present work up to $N_1 = 50$ showed that the results are not falsified by the fact that screening effects are not taken into account (see section 5.4). Nevertheless, more research is necessary to understand for which conditions screening effects are important.

The phase space estimation revealed that the maximum possible decrease of the magnetic moment ΔM is too small for Fe and fcc Co to explain experimental values, even for a band structure with reduced magnetic moment and high electron temperatures (except for $T_e = 1500$ K and $T_e = 2000$ K in combination with a reduced magnetic moment).

The maximum possible decrease of the magnetic moment ΔM is probably also too small for Ni with ground-state magnetic moment if one considers that spin-flip scattering only occurs with a probability of a_{sf} which is between 0.03 and 0.45 [18] and if one considers that only electron temperatures up to 1000 K are reasonable. For band structures with reduced magnetic moment the relative maximum possible decrease of the magnetic moment is greater but also quite small for realistic electron temperatures (up to 700 K) and spin-flip probabilities about $a_{sf} = 0.1$.

The phase space estimation is not restricted to electron-phonon scatter-

ing. It holds in principle for every scattering process[26,27]. I stress that the phase space estimation is only true for time t_s or t_*, respectively, where the system has already thermalized. In reality the phase space changes for each time step by non-spin-flip and spin-flip scattering processes, and in principle it is very difficult to give an absolute quantitative statement on the maximum possible decrease of the magnetic moment ΔM for the whole time range. ΔM should be interpreted as the maximum possible decrease of the magnetic moment for a system which always scatters toward equilibrium for the majority-electron distribution only. This implies a non-equilibrium for the minority-electron distribution.

Next, I want to comment on the objections given in ref. [75] regarding the fact that a realistic treatment of the demagnetization should include the thermal disorder of the orientations of the atomic moments. Indeed, the calculations in the present work only respect a longitudinal increase or decrease of the magnetic moment. A transversal increase or decrease via disorder of the magnetic moments by magnons is per definition not taken into account. Therefore, within a rigid-band model one could never determine a correct Curie temperature or a correct Bloch's $T^{3/2}$-law. The transversal dynamics might be slower than the longitudinal dynamics, but calculations with the Landau-Lifshitz-Bloch equation [79] suggest that the transversal dynamics is fast enough on a fs-timescale. The calculations in the present work support the notion that electron-phonon scattering processes alone cannot reproduce the experimental demagnetization (except for very high electron temperatures). One could include magnons, e.g., via combined electron-phonon and electron-magnon spin-flip scattering processes (see subsection 4.2.5). This could enhance the demagnetization process.

To conclude, it was not possible to explain the experimental demagnetization rates by electron-phonon spin-flip scattering processes, neither for a ground-state band structure nor for a band structure with reduced magnetic moment (except for very high unrealistic electron temperatures). I suggest several possibilities for further research projects which are defi-

[26] It also does not matter that maybe contributions from the spin-same- or spin-other-orbit interaction are missing (see section 5.4).

[27] However, the implicit assumption that majority electrons below the Fermi energy do not flip their spins (see section 5.8) could be violated for other scattering processes, e.g., electron-magnon scattering since magnons have an energy up to 30 mRy whereas phonons have an energy up to 3 mRy.

nitely necessary: First, it has to be tested whether the combined electron-spin-flip and atomic spin-flip scattering processes suggested by Schellekens and Koopmans [75] are a possible scenario (see subsection 4.2.5). Second, it has to be studied whether electron-magnon spin-flip scattering processes with subsequent orbital quenching (faster than the time resolution of ref. [47]) suggested in ref. [69] could be the reason for ultrafast demagnetization (see subsection 4.2.5). Third, quantum-kinetic calculations (without using Fermi's golden rule) are desirable to test whether the results for the demagnetization of the system obtained by Fermi's golden rule are still valid on a fs-timescale (see subsection 5.2).

8 Summary

8.1 English summary

This work deals with ultrafast demagnetization within few hundred femtoseconds after laser pulse irradiation in nickel, iron and face-centered cubic (fcc) cobalt. It is examined with ab-initio density-functional theory and physical modeling whether the electron-phonon spin-flip scattering can be considered as underlying mechanism for ultrafast demagnetization.

It is already known since 1996 that the in-plane magnetization of a thin ferromagnetic nickel film can reduce considerably within few hundred femtoseconds after irradiation with a strong linearly-polarized laser pulse. The strength of the demagnetization depends on several parameters, especially on the fluence of the laser pulse. Until now plenty of experimental and theoretical investigations for nickel and other ferromagnetic materials have been made but the underlying mechanisms for ultrafast demagnetization are still mainly unknown. There are a lot of possible explanations in the literature. The most important ones are summarized and discussed critically in this thesis. Among those are mainly two categories: different spin-flip mechanisms and superdiffusive spin transport.

The topic of this work is the investigation of the electron-phonon spin-flip scattering and its relevance for ultrafast demagnetization. The electronic and phononic states are calculated by ab-initio density-functional theory, i.e., the electronic and phononic properties are calculated without parameters ("ab initio") for a temperature of 0 K. It is assumed that the single electron states and the phonon states do not change a lot for room temperature which is usually a good approximation. The electronic states are calculated with the linear-muffin-tin-orbital method in local-spin-density approximation (LSDA) and atomic-sphere approximation (ASA) whereas the phononic states are calculated with the pseudopotential method and the generalized gradient approximation (GGA).

The frequencies and polarization vectors of the phonons (quantized lat-

tice vibrations) are calculated with a force-constant model that uses the ab initio calculated force constants. The determined frequencies and polarization vectors are compared with frequencies and polarization vectors obtained from fitted force constants (fitted to experimental phonon frequencies or to experimental phonon density of states). It is revealed for nickel, iron and aluminum that the frequencies and polarization vectors agree very well for most regions in the phonon Brillouin zone and that there are only few regions with small deviations. Thereby a scientific uncertainty could be removed:

The fitting procedure is not unique for the following reasons. First, the fitted force constants are normally only fitted to experimental frequencies in high-symmetry directions of the phonon Brillouin zone. Second, even if one made a fit to frequencies in all directions, a unitary transformation would alter the force constants and polarization vectors while leaving the frequencies unchanged. Therefore, it was unclear how reliable the frequencies and especially polarization vectors are for the whole Brillouin zone. The above-mentioned comparison of results obtained from ab-initio force constants with results obtained from fitted force constants demonstrated that frequencies and polarization vectors obtained from fitted force constants are reliable in the whole phonon Brillouin zone. Hence, in order to get reliable frequencies and polarization vectors it suffices to use the fitted force constants. Tedious ab-initio calculations are not necessary. This holds at least for nickel, iron and aluminum and probably for all three-dimensional metals.

The electron-phonon scattering operator is represented with the rigid-ion approximation (Nordheim approximation). This is critically discussed, and in this context problems with the screening of the electron-phonon scattering are pointed out. Furthermore, it is demonstrated how to implement the electron-phonon scattering matrix elements including spin-orbit coupling in the existing ab-initio density-functional-theory program (linear-muffin-tin-orbital method with LSDA and ASA).

The transition rates are calculated with Fermi's golden rule and Boltzmann rate equations. It is investigated if the preconditions for the use of Fermi's golden rule are fulfilled and it is remarked that in principle quantum-kinetic calculations are necessary. The angular momentum conservation during a single scattering process and during the total scattering processes is discussed.

Finally, it is shown how to model and calculate the relaxation time

and the demagnetization rate (after laser pulse irradiation and subsequent thermalization) with the electron-phonon spin-flip transition rates at hand. The relaxation time is about 22 femtoseconds in iron and 16 femtoseconds in nickel which is smaller than the experimentally observed relaxation time (few hundred femtoseconds). This shows that the electron-phonon spin-flip scattering is in principle fast enough for a dynamics on the 100 fs timescale but the relaxation time alone does not give any information about the strength of demagnetization. This information is given by the demagnetization rate. However, both for nickel and for iron the calculated demagnetization rate of the present work is too small for realistic electron temperatures to explain the experimental demagnetization rates. Calculations with reduced atomic magnetic moment and hence reduced exchange splitting also could not explain the experimental demagnetization values. The calculated rates are similar to experimental rates only for very high, probably unreasonable electron temperatures.

Additionally, the available phase space for (in principle) any spin-flip scattering involving small energies (such as phonon energies) is estimated in a band structure with ground-state atomic magnetic moment and in band structures with reduced atomic magnetic moment. This phase space is linked to the maximum possible demagnetization. For iron and fcc cobalt the phase space is definitely too small to explain a demagnetization of 50% or even more (except for very high electron temperatures of 1500 K or 2000 K). For nickel the phase space is not necessarily too small (depending on the electron temperature and on the reduction of the atomic magnetic moment). But in combination with a reasonable spin-flip probability a demagnetization of 50% and more seems to be very unrealistic also for Ni.

In conclusion, it seems to be rather unlikely that the electron-phonon spin-flip scattering in a rigid-band model alone can be the explanation for a experimentally observed ultrafast demagnetization of 50% or even more. Calculations using band structures with reduced atomic magnetic moment (reduced exchange splitting) could also not explain the experimental phenomenon. However, it is discussed in the present work that electron-phonon spin-flip scattering is indispensable for the removal of spin angular momentum. Maybe combined scattering processes, e.g., combined electron-phonon and electron-magnon spin-flip scattering processes including a longitudinal and transverse reduction of the magnetization, could be relevant which requires further scientific research.

8.2 Deutsche Zusammenfassung

Diese Arbeit beschäftigt sich mit der ultraschnellen Entmagnetisierung innerhalb weniger hundert Femtosekunden nach Laserpulsbestrahlung in Nickel, Eisen und kubisch-flächenzentriertem (fcc) Kobalt. Es wird mit Hilfe der ab-initio Dichtefunktionaltheorie und physikalischer Modellierung untersucht, ob die Elektron-Phonon-Spin-Flip-Streuung als zu Grunde liegender Mechanismus für die ultraschnelle Entmagnetisierung in Frage kommt.

Schon seit 1996 ist bekannt, dass die planare Magnetisierung eines dünnen, ferromagnetischen Nickel-Films innerhalb weniger hundert Femtosekunden nach Bestrahlung mit einem starken linear-polarisierten Laserpuls deutlich reduziert wird. Die Stärke der Entmagnetisierung hängt von mehreren Parametern, insbesondere von der Fluenz des Laserpulses ab. Bis heute sind viele weitere experimentelle und theoretische Untersuchungen für Nickel und andere ferromagnetische Materialien durchgeführt worden, aber die zu Grunde liegenden Mechanismen für die ultraschnelle Entmagnetisierung sind immer noch weitgehend unbekannt. In der Literatur gibt es eine Vielzahl von möglichen Erklärungen. Die wichtigsten Erklärungsversuche werden unter anderem in dieser Arbeit zusammengefasst und kritisch diskutiert. Dazu zählen vor allem zwei Hauptkategorien: verschiedene Spin-Flip-Mechanismen und superdiffusiver Spintransport.

Das Thema dieser Arbeit ist die Untersuchung der Elektron-Phonon-Spin-Flip-Streuung und deren Relevanz für die ultraschnelle Entmagnetisierung. Die elektronischen und phononischen Zustände werden mit Hilfe der ab-initio Dichtefunktionaltheorie berechnet. Damit können praktisch parameterfrei ("ab initio") die elektronischen und phononischen Eigenschaften für eine Temperatur von 0 K berechnet werden. Es wird angenommen, dass sich die Einzel-Elektronenzustände und die Phononenzustände für Zimmertemperatur nicht ändern, was normalerweise eine gute Näherung ist. Die elektronischen Zustände werden mit der Linear-Muffin-Tin-Orbital-Methode in lokaler Spindichtenäherung (LSDA) und Atomkugelnäherung (ASA) berechnet, während die phononischen Zustände mit der Pseudopotentialmethode in verallgemeinerter Gradientennäherung (GGA) berechnet werden.

Die Frequenzen und Polarisationsvektoren der Phononen (quantisierte Gitterschwingungen) werden mit einem Kraftkonstantenmodell, das die ab initio berechneten Kraftkonstanten verwendet, berechnet. Die so be-

stimmten Frequenzen und Polarisationsvektoren werden mit Frequenzen und Polarisationsvektoren verglichen, die mit gefitteten Kraftkonstanten (gefittet an experimentelle Phononfrequenzen oder Phononzustandsdichten) bestimmt wurden. Für Nickel, Eisen und Aluminium wird festgestellt, dass die Frequenzen und Polarisationsvektoren für die meisten Bereiche in der Phonon-Brillouin-Zone sehr gut übereinstimmen und dass es nur wenige Bereiche mit kleinen Abweichungen gibt. Damit konnte eine wissenschaftliche Unklarheit beseitigt werden:

Die Fit-Prozedur ist aus folgenden Gründen nicht eindeutig: Erstens, die gefitteten Kraftkonstanten werden normalerweise nur an experimentelle Frequenzen für Hochsymmetrierichtungen der Phonon-Brillouin-Zone angepasst. Zweitens, selbst wenn man einen Fit an Frequenzen in alle Richtungen machen würde, würde eine unitäre Transformation die Kraftkonstanten und Polarisationsvektoren ändern, während die Frequenzen unverändert blieben. Daher war unklar, wie verlässlich die bestimmten Frequenzen und vor allem Polarisationsvektoren für die gesamte Phonon-Brillouin-Zone sind. Der oben genannte Vergleich zwischen Ergebnissen, die durch gefittete Kraftkonstanten erhalten wurden, und Ergebnissen, die durch ab-initio-Kraftkonstanten erhalten wurden, hat gezeigt, dass Frequenzen und Polarisationsvektoren, die mit gefitteten Kraftkonstanten bestimmt werden, in der gesamten Phonon-Brillouin-Zone sehr verlässlich sind. Um verlässliche Frequenzen und Polarisationsvektoren zu bekommen, genügt es daher, die gefitteten Kraftkonstanten zu verwenden. Aufwändige ab-initio Rechnungen sind also nicht notwendig. Dies gilt zumindest für Nickel, Eisen und Aluminium und damit vermutlich für alle dreidimensionalen Metalle.

Die Elektron-Phonon-Streuung wird mit Hilfe der Nordheim-Näherung ("Rigid-Ion-Näherung") berechnet. Diese wird kritisch diskutiert, und es wird in diesem Kontext auf Probleme mit der Abschirmung der Elektron-Phonon-Streuung hingewiesen. Es wird außerdem dargestellt, wie die Elektron-Phonon-Streumatrixelemente mit Spin-Bahn-Kopplung in das bestehende ab-initio Dichtefunktionaltheorie-Programm (Linear-Muffin-Tin-Orbital-Methode mit LSDA und ASA) implementiert wurden.

Die Übergangsraten werden mit Fermis Goldener Regel und mit Boltzmannschen Ratengleichungen berechnet. Die Gültigkeit der Verwendung Fermis Goldener Regel wird ausführlich untersucht, und es wird festgestellt, dass im Prinzip quantenkinetische Rechnungen erforderlich sind. Die Drehimpulserhaltung während des Einzelstreuprozesses und während

der gesamten Streuprozesse wird diskutiert.

Schließlich wird gezeigt, wie die Relaxationszeit und die Entmagnetisierungsrate (nach Laserbestrahlung und anschließender Thermalisierung) mit den Elektron-Phonon-Spin-Flip-Übergangsraten modelliert und berechnet werden können. Die Relaxationszeit wird zu 22 Femtosekunden in Eisen und zu 16 Femtosekunden in Nickel bestimmt, was kleiner ist als die experimentell beobachtete Relaxationszeit (wenige hundert Femtosekunden). Dies zeigt, dass die Elektron-Phonon-Spin-Flip-Streuung im Prinzip schnell genug für eine 100 fs-Zeitskala ist, aber die Relaxationszeit alleine gibt noch keine Information über die Stärke der Entmagnetisierung. Diese Information steckt in der Entmagnetisierungsrate. Die in dieser Arbeit berechnete Entmagnetisierungsrate für realistische Elektronentemperaturen ist aber sowohl für Eisen als auch für Nickel zu klein, um die experimentelle Entmagnetisierungsrate zu erklären. Rechnungen mit reduzierter Magnetisierung und damit veränderter Austauschaufspaltung konnten ebenfalls nicht die experimentellen Werte der Entmagnetisierung erklären. Nur für sehr hohe, wahrscheinlich unrealistische Elektronentemperaturen waren die berechneten Entmagnetisierungsraten und die experimentellen Entmagnetisierungsraten ähnlich.

Zusätzlich wird noch der zur Verfügung stehende Phasenraum für eine (im Prinzip) beliebige Spin-Flip-Streuung, die mit kleinen Energien (wie Phononenergien) einhergeht, in einer Bandstruktur mit magnetischem Moment des Grundzustands und in Bandstrukturen mit reduziertem magnetischen Moment abgeschätzt. Dieser Phasenraum ist mit der maximal möglichen Entmagnetisierung verknüpft. Für Eisen und fcc Kobalt ist der Phasenraum definitiv zu klein, um eine Entmagnetisierung von 50% oder mehr erklären zu können (außer für sehr hohe Elektronentemperaturen von 1500 K oder 2000 K). Für Nickel ist der Phasenraum (abhängig von der Elektronentemperatur und der Reduktion des atomaren magnetischen Moments) nicht unbedingt zu klein, zusammen mit einer vernünftigen Spin-Flip-Wahrscheinlichkeit erscheint eine Reduktion der Magnetisierung von 50% und mehr allerdings äußerst unrealistisch.

Zusammenfassend lässt sich sagen, dass es damit eher unwahrscheinlich ist, dass die Elektron-Phonon-Spin-Flip-Streuung in einem festen Bandstruktur-Modell allein als Erklärung für die experimentell beobachtete, ultraschnelle Entmagnetisierung von mehr als 50% in Frage kommt. Ebenso konnten diese in einer Bandstruktur mit reduziertem magnetischen Moment (reduzierter Austauschaufspaltung) nicht erklärt werden. In die-

ser Arbeit wird allerdings auch diskutiert, dass die Elektron-Phonon-Spin-Flip-Streuung unabdingbar für die Abfuhr des Spindrehimpulses ist. Eventuell könnten kombinierte Streuprozesse, z.B. kombinierte Elektron-Phonon- und Elektron-Magnon-Spin-Flip-Streuprozesse inklusive einer longitudinalen und transversalen Reduktion des magnetischen Moments relevant sein, die weiterer wissenschaftlicher Forschung bedürfen.

A Spin-diagonal matrix element (Elliott part)

The following calculation for the spin-diagonal matrix element (Elliott part) of subsection 6.2.1 is mostly taken from ref. [12].

The spin-diagonal matrix element $\langle \Phi_{\mathbf{R}l'm'\alpha'} | \widetilde{W'}^{sd}_{\lambda,\mathbf{R}} | \Phi_{\mathbf{R}lm\alpha} \rangle$ reads using eq. (2.29)

$$
\begin{aligned}
&\left\langle \Phi_{\mathbf{R}l'm'\alpha'} \middle| \left(\mathbf{n}^{\mathbf{R}}_{\mathbf{q}\lambda}\ \mathbf{e}_{r_{\mathbf{R}}} \right) \begin{pmatrix} \frac{\partial v^{\uparrow}_{\mathbf{R}}}{\partial r_{\mathbf{R}}} & 0 & 0 & 0 \\ 0 & \frac{\partial v^{\downarrow}_{\mathbf{R}}}{\partial r_{\mathbf{R}}} & 0 & 0 \\ 0 & 0 & \frac{\partial v^{\downarrow}_{\mathbf{R}}}{\partial r_{\mathbf{R}}} & 0 \\ 0 & 0 & 0 & \frac{\partial v^{\uparrow}_{\mathbf{R}}}{\partial r_{\mathbf{R}}} \end{pmatrix} \middle| \Phi_{\mathbf{R}lm\alpha} \right\rangle \\
&= \left\langle \begin{matrix} \phi_{\mathbf{R}l'\alpha'} Z_{l'm'} \chi_{\alpha'} \\ i\widehat{\underline{\underline{\sigma}}}_{r_{\mathbf{R}}} \left(-\gamma_{\mathbf{R}l'\alpha'} + \frac{\phi_{\mathbf{R}l'\alpha'} \sum_i \widehat{\underline{\underline{\sigma}}}_i \widehat{L}_i}{2M_{\mathbf{R}l'\alpha'} c r_{\mathbf{R}}} \right) Z_{l'm'} \chi_{\alpha'} \end{matrix} \middle| \left(\mathbf{n}^{\mathbf{R}}_{\mathbf{q}\lambda}\ \mathbf{e}_{r_{\mathbf{R}}} \right) \cdot \right. \\
&\left. \begin{pmatrix} \frac{\partial v^{\uparrow}_{\mathbf{R}}}{\partial r_{\mathbf{R}}} & 0 & 0 & 0 \\ 0 & \frac{\partial v^{\downarrow}_{\mathbf{R}}}{\partial r_{\mathbf{R}}} & 0 & 0 \\ 0 & 0 & \frac{\partial v^{\downarrow}_{\mathbf{R}}}{\partial r_{\mathbf{R}}} & 0 \\ 0 & 0 & 0 & \frac{\partial v^{\uparrow}_{\mathbf{R}}}{\partial r_{\mathbf{R}}} \end{pmatrix} \middle| \begin{matrix} \phi_{\mathbf{R}l\alpha} Z_{lm} \chi_{\alpha} \\ i\widehat{\underline{\underline{\sigma}}}_{r_{\mathbf{R}}} \left(-\gamma_{\mathbf{R}l\alpha} + \frac{\phi_{\mathbf{R}l\alpha} \sum_j \widehat{\underline{\underline{\sigma}}}_j \widehat{L}_j}{2M_{\mathbf{R}l\alpha} c r_{\mathbf{R}}} \right) Z_{lm} \chi_{\alpha} \end{matrix} \right\rangle \\
&= \left\langle \phi_{\mathbf{R}l'\alpha'} Z_{l'm'} \chi_{\alpha'} \middle| \left(\mathbf{n}^{\mathbf{R}}_{\mathbf{q}\lambda}\ \mathbf{e}_{r_{\mathbf{R}}} \right) \begin{pmatrix} \frac{\partial v^{\uparrow}_{\mathbf{R}}}{\partial r_{\mathbf{R}}} & 0 \\ 0 & \frac{\partial v^{\downarrow}_{\mathbf{R}}}{\partial r_{\mathbf{R}}} \end{pmatrix} \middle| \phi_{\mathbf{R}l\alpha} Z_{lm} \chi_{\alpha} \right\rangle \\
&\quad + \left\langle i\widehat{\underline{\underline{\sigma}}}_{r_{\mathbf{R}}} \left(-\gamma_{\mathbf{R}l'\alpha'} + \frac{\phi_{\mathbf{R}l'\alpha'} \sum_i \widehat{\underline{\underline{\sigma}}}_i \widehat{L}_i}{2M_{\mathbf{R}l'\alpha'} c r_{\mathbf{R}}} \right) Z_{l'm'} \chi_{\alpha'} \middle| \left(\mathbf{n}^{\mathbf{R}}_{\mathbf{q}\lambda}\ \mathbf{e}_{r_{\mathbf{R}}} \right) \cdot \right.
\end{aligned}
$$

$$
\begin{aligned}
&\left(\begin{array}{cc} \frac{\partial v^{\downarrow}_{\mathbf{R}}}{\partial r_{\mathbf{R}}} & 0 \\ 0 & \frac{\partial v^{\uparrow}_{\mathbf{R}}}{\partial r_{\mathbf{R}}} \end{array} \right) \left| i\widehat{\underline{\sigma}}_{r_{\mathbf{R}}} \left(-\gamma_{\mathbf{R}l\alpha} + \frac{\phi_{\mathbf{R}l\alpha} \sum_j \widehat{\underline{\sigma}}_j \widehat{L}_j}{2M_{\mathbf{R}l\alpha} c r_{\mathbf{R}}} \right) Z_{lm}\chi_\alpha \right\rangle \\
= &\left\langle \phi_{\mathbf{R}l'\alpha'} \left| \frac{\partial v^{\alpha}_{\mathbf{R}}}{\partial r_{\mathbf{R}}} \right| \phi_{\mathbf{R}l\alpha} \right\rangle \left\langle Z_{l'm'} | \mathbf{n}^{\mathbf{R}}_{\mathbf{q}\lambda}\ \mathbf{e}_{r_{\mathbf{R}}} | Z_{lm} \right\rangle \delta_{\alpha\alpha'} \\
&+ \left\langle -\gamma_{\mathbf{R}l'\alpha'} Z_{l'm'}\chi_{\alpha'} + \frac{\phi_{\mathbf{R}l'\alpha'} \sum_i \widehat{\underline{\sigma}}_i \widehat{L}_i}{2M_{\mathbf{R}l'\alpha'} c r_{\mathbf{R}}} Z_{l'm'}\chi_{\alpha'} \right| (\mathbf{n}^{\mathbf{R}}_{\mathbf{q}\lambda}\ \mathbf{e}_{r_{\mathbf{R}}}) \cdot \\
&\widehat{\underline{\sigma}}^{\dagger}_{r_{\mathbf{R}}} \left(\begin{array}{cc} \frac{\partial v^{\downarrow}_{\mathbf{R}}}{\partial r_{\mathbf{R}}} & 0 \\ 0 & \frac{\partial v^{\uparrow}_{\mathbf{R}}}{\partial r_{\mathbf{R}}} \end{array} \right) \widehat{\underline{\sigma}}_{r_{\mathbf{R}}} \Big| - \gamma_{\mathbf{R}l\alpha} Z_{lm}\chi_\alpha + \frac{\phi_{\mathbf{R}l\alpha} \sum_j \widehat{\underline{\sigma}}_j \widehat{L}_j}{2M_{\mathbf{R}l\alpha} c r_{\mathbf{R}}} Z_{lm}\chi_\alpha \Big\rangle
\end{aligned}
\tag{A.1}
$$

where

$$
v^{\alpha}_{\mathbf{R}} = \left\{ \begin{array}{ll} v^{\uparrow}_{\mathbf{R}} & \text{if } \alpha = \uparrow \\ v^{\downarrow}_{\mathbf{R}} & \text{if } \alpha = \downarrow \end{array} \right. . \tag{A.2}
$$

With the relation

$$
\begin{aligned}
&\left(\begin{array}{cc} \frac{\partial v^{\downarrow}_{\mathbf{R}}}{\partial r_{\mathbf{R}}} & 0 \\ 0 & \frac{\partial v^{\uparrow}_{\mathbf{R}}}{\partial r_{\mathbf{R}}} \end{array} \right) \widehat{\underline{\sigma}}_{r_{\mathbf{R}}} \\
= &\left(\begin{array}{cc} \frac{\partial v^{\downarrow}_{\mathbf{R}}}{\partial r_{\mathbf{R}}} & 0 \\ 0 & \frac{\partial v^{\uparrow}_{\mathbf{R}}}{\partial r_{\mathbf{R}}} \end{array} \right) \widehat{x}\widehat{\underline{\sigma}}_x + \left(\begin{array}{cc} \frac{\partial v^{\downarrow}_{\mathbf{R}}}{\partial r_{\mathbf{R}}} & 0 \\ 0 & \frac{\partial v^{\uparrow}_{\mathbf{R}}}{\partial r_{\mathbf{R}}} \end{array} \right) \widehat{y}\widehat{\underline{\sigma}}_y + \left(\begin{array}{cc} \frac{\partial v^{\downarrow}_{\mathbf{R}}}{\partial r_{\mathbf{R}}} & 0 \\ 0 & \frac{\partial v^{\uparrow}_{\mathbf{R}}}{\partial r_{\mathbf{R}}} \end{array} \right) \widehat{z}\widehat{\underline{\sigma}}_z \\
= &\widehat{x}\widehat{\underline{\sigma}}_x \left(\begin{array}{cc} \frac{\partial v^{\uparrow}_{\mathbf{R}}}{\partial r_{\mathbf{R}}} & 0 \\ 0 & \frac{\partial v^{\downarrow}_{\mathbf{R}}}{\partial r_{\mathbf{R}}} \end{array} \right) + \widehat{y}\widehat{\underline{\sigma}}_y \left(\begin{array}{cc} \frac{\partial v^{\uparrow}_{\mathbf{R}}}{\partial r_{\mathbf{R}}} & 0 \\ 0 & \frac{\partial v^{\downarrow}_{\mathbf{R}}}{\partial r_{\mathbf{R}}} \end{array} \right) + \Bigg[\widehat{z}\widehat{\underline{\sigma}}_z \left(\begin{array}{cc} \frac{\partial v^{\uparrow}_{\mathbf{R}}}{\partial r_{\mathbf{R}}} & 0 \\ 0 & \frac{\partial v^{\downarrow}_{\mathbf{R}}}{\partial r_{\mathbf{R}}} \end{array} \right) \\
&- \widehat{z}\widehat{\underline{\sigma}}_z \left(\begin{array}{cc} \frac{\partial v^{\uparrow}_{\mathbf{R}}}{\partial r_{\mathbf{R}}} & 0 \\ 0 & \frac{\partial v^{\downarrow}_{\mathbf{R}}}{\partial r_{\mathbf{R}}} \end{array} \right) \Bigg] + \widehat{z}\widehat{\underline{\sigma}}_z \left(\begin{array}{cc} \frac{\partial v^{\downarrow}_{\mathbf{R}}}{\partial r_{\mathbf{R}}} & 0 \\ 0 & \frac{\partial v^{\uparrow}_{\mathbf{R}}}{\partial r_{\mathbf{R}}} \end{array} \right) \\
= &\widehat{\underline{\sigma}}_{r_{\mathbf{R}}} \left(\begin{array}{cc} \frac{\partial v^{\uparrow}_{\mathbf{R}}}{\partial r_{\mathbf{R}}} & 0 \\ 0 & \frac{\partial v^{\downarrow}_{\mathbf{R}}}{\partial r_{\mathbf{R}}} \end{array} \right) + \widehat{z} \left(\frac{\partial v^{\downarrow}_{\mathbf{R}}}{\partial r_{\mathbf{R}}} - \frac{\partial v^{\uparrow}_{\mathbf{R}}}{\partial r_{\mathbf{R}}} \right) \underline{\underline{1}}
\end{aligned}
\tag{A.3}
$$

where $\widehat{x} = x/r_{\mathbf{R}}$, $\widehat{y} = y/r_{\mathbf{R}}$, $\widehat{z} = z/r_{\mathbf{R}}$ has been used, eq. (A.1) reads with $\underline{\widehat{\sigma}}^{\dagger}_{r_{\mathbf{R}}} = \underline{\widehat{\sigma}}_{r_{\mathbf{R}}}$, $\underline{\widehat{\sigma}}_{r_{\mathbf{R}}}\underline{\widehat{\sigma}}_{r_{\mathbf{R}}} = \underline{1}$:

$$\begin{aligned}
&\left\langle \phi_{\mathbf{R}l'\alpha'} \left| \frac{\partial v^{\alpha}_{\mathbf{R}}}{\partial r_{\mathbf{R}}} \right| \phi_{\mathbf{R}l\alpha} \right\rangle \, \left\langle Z_{l'm'} | \mathbf{n}^{\mathbf{R}}_{\mathbf{q}\lambda} \, \mathbf{e}_{r_{\mathbf{R}}} | Z_{lm} \right\rangle \delta_{\alpha\alpha'} \\
&+ \left\langle -\gamma_{\mathbf{R}l'\alpha'} Z_{l'm'}\chi_{\alpha'} + \frac{\phi_{\mathbf{R}l'\alpha'} \sum_i \widehat{\underline{\sigma}}_i \widehat{L}_i}{2M_{\mathbf{R}l'\alpha'} c r_{\mathbf{R}}} Z_{l'm'}\chi_{\alpha'} \right| (\mathbf{n}^{\mathbf{R}}_{\mathbf{q}\lambda} \, \mathbf{e}_{r_{\mathbf{R}}}) \cdot \\
&\left(\begin{array}{cc} \frac{\partial v^{\uparrow}_{\mathbf{R}}}{\partial r_{\mathbf{R}}} & 0 \\ 0 & \frac{\partial v^{\downarrow}_{\mathbf{R}}}{\partial r_{\mathbf{R}}} \end{array} \right) \left| - \gamma_{\mathbf{R}l\alpha} Z_{lm}\chi_{\alpha} + \frac{\phi_{\mathbf{R}l\alpha} \sum_j \widehat{\underline{\sigma}}_j \widehat{L}_j}{2M_{\mathbf{R}l\alpha} c r_{\mathbf{R}}} Z_{lm}\chi_{\alpha} \right\rangle \\
&+ \left\langle -\gamma_{\mathbf{R}l'\alpha'} Z_{l'm'}\chi_{\alpha'} + \frac{\phi_{\mathbf{R}l'\alpha'} \sum_i \widehat{\underline{\sigma}}_i \widehat{L}_i}{2M_{\mathbf{R}l'\alpha'} c r_{\mathbf{R}}} Z_{l'm'}\chi_{\alpha'} \right| (\mathbf{n}^{\mathbf{R}}_{\mathbf{q}\lambda} \, \mathbf{e}_{r_{\mathbf{R}}}) (\widehat{x}\widehat{z}\widehat{\underline{\sigma}}_x + \widehat{y}\widehat{z}\widehat{\underline{\sigma}}_y \\
&\qquad + \widehat{z}^2 \widehat{\underline{\sigma}}_z) \left(\frac{\partial v^{\downarrow}_{\mathbf{R}}}{\partial r_{\mathbf{R}}} - \frac{\partial v^{\uparrow}_{\mathbf{R}}}{\partial r_{\mathbf{R}}} \right) \left| - \gamma_{\mathbf{R}l\alpha} Z_{lm}\chi_{\alpha} + \frac{\phi_{\mathbf{R}l\alpha} \sum_j \widehat{\underline{\sigma}}_j \widehat{L}_j}{2M_{\mathbf{R}l\alpha} c r_{\mathbf{R}}} Z_{lm}\chi_{\alpha} \right\rangle .
\end{aligned} \tag{A.4}$$

The three summands of eq. (A.4) are considered separately now.

First summand of eq. (A.4)

The radial integral of the first summand of eq. (A.4) can be calculated numerically. Now we have a look at the angular part of the matrix element:

We can use that the following relation holds [11]

$$\mathbf{e}_{r_{\mathbf{R}}} = \begin{pmatrix} \sin\vartheta\cos\phi \\ \sin\vartheta\sin\phi \\ \cos\vartheta \end{pmatrix} = \sqrt{\frac{4\pi}{3}} \begin{pmatrix} Z_{11} \\ Z_{1-1} \\ Z_{10} \end{pmatrix} \tag{A.5}$$

where Z_{lm} are the cubic harmonics. With the cubic Gaunt coefficients

$$\widetilde{G}_{l''m'',l'm',lm} \equiv \langle Z_{l''m''} | Z_{l'm'} | Z_{lm} \rangle \tag{A.6}$$

(an arbitrary permutation of the three cubic harmonics does not change anything) the angular part reads

$$\langle Z_{l'm'} | \mathbf{n}^{\mathbf{R}}_{\mathbf{q}\lambda} \, \mathbf{e}_{r_{\mathbf{R}}} | Z_{lm} \rangle = \mathbf{n}^{\mathbf{R}}_{\mathbf{q}\lambda} \, \sqrt{\frac{4\pi}{3}} \cdot \begin{pmatrix} \widetilde{G}_{l'm',11,lm} \\ \widetilde{G}_{l'm',1-1,lm} \\ \widetilde{G}_{l'm',10,lm} \end{pmatrix} = \mathbf{n}^{\mathbf{R}}_{\mathbf{q}\lambda} \, \widetilde{\mathbf{G}}^{lm}_{l'm'} \tag{A.7}$$

where

$$\widetilde{\mathbf{G}}^{lm}_{l'm'} \equiv \sqrt{\frac{4\pi}{3}} \begin{pmatrix} \widetilde{G}_{l'm',11,lm} \\ \widetilde{G}_{l'm',1-1,lm} \\ \widetilde{G}_{l'm',10,lm} \end{pmatrix}. \tag{A.8}$$

Together, the first summand of eq. (A.4) reads:

$$\left\langle \phi_{\mathbf{R}l'\alpha'} \left| \frac{\partial v^{\alpha}_{\mathbf{R}}}{\partial r_{\mathbf{R}}} \right| \phi_{\mathbf{R}l\alpha} \right\rangle \; \mathbf{n}^{\mathbf{R}}_{\mathbf{q}\lambda} \; \widetilde{\mathbf{G}}^{lm}_{l'm'} \delta_{\alpha\alpha'}. \tag{A.9}$$

The orbital angular momentum quantum number l is in the range $l = 0, 1, 2$ for iron, cobalt and nickel and the magnetic quantum number is in the range $m = -l, \ldots, l$. Hence, not too many cubic Gaunt coefficients will be needed for the calculation.

Second summand of eq. (A.4)

The second summand of eq. (A.4) can be written as

$$\begin{aligned}
&\left\langle -\gamma_{\mathbf{R}l'\alpha'} Z_{l'm'\chi\alpha'} \left| (\mathbf{n}^{\mathbf{R}}_{\mathbf{q}\lambda} \; \mathbf{e}_{r_{\mathbf{R}}}) \frac{\partial v^{\alpha}_{\mathbf{R}}}{\partial r_{\mathbf{R}}} \right| - \gamma_{\mathbf{R}l\alpha} Z_{lm\chi\alpha} \right\rangle \\
&+ \sum_{i_1} \left\langle \frac{\phi_{\mathbf{R}l'\alpha'} \; \widehat{\underline{\sigma}}_{i_1} \widehat{L}_{i_1}}{2M_{\mathbf{R}l'\alpha'} c r_{\mathbf{R}}} Z_{l'm'\chi\alpha'} \left| (\mathbf{n}^{\mathbf{R}}_{\mathbf{q}\lambda} \; \mathbf{e}_{r_{\mathbf{R}}}) \frac{\partial v^{\alpha}_{\mathbf{R}}}{\partial r_{\mathbf{R}}} \right| - \gamma_{\mathbf{R}l\alpha} Z_{lm\chi\alpha} \right\rangle \\
&+ \sum_{i_2} \left\langle -\gamma_{\mathbf{R}l'\alpha'} Z_{l'm'\chi\alpha'} \left| (\mathbf{n}^{\mathbf{R}}_{\mathbf{q}\lambda} \; \mathbf{e}_{r_{\mathbf{R}}}) \frac{\partial v^{\alpha,i_2}_{\mathbf{R}}}{\partial r_{\mathbf{R}}} \right| \frac{\phi_{\mathbf{R}l\alpha}}{2M_{\mathbf{R}l\alpha} c r_{\mathbf{R}}} \widehat{\underline{\sigma}}_{i_2} \widehat{L}_{i_2} Z_{lm\chi\alpha} \right\rangle \\
&+ \sum_{i_3, i_4} \left\langle \frac{\phi_{\mathbf{R}l'\alpha'} \widehat{\underline{\sigma}}_{i_3} \widehat{L}_{i_3}}{2M_{\mathbf{R}l'\alpha'} c r_{\mathbf{R}}} Z_{l'm'\chi\alpha'} \left| (\mathbf{n}^{\mathbf{R}}_{\mathbf{q}\lambda} \; \mathbf{e}_{r_{\mathbf{R}}}) \frac{\partial v^{\alpha,i_4}_{\mathbf{R}}}{\partial r_{\mathbf{R}}} \right| \frac{\phi_{\mathbf{R}l\alpha} \widehat{\underline{\sigma}}_{i_4} \widehat{L}_{i_4}}{2M_{\mathbf{R}l\alpha} c r_{\mathbf{R}}} Z_{lm\chi\alpha} \right\rangle
\end{aligned} \tag{A.10}$$

where

$$v^{\alpha,i}_{\mathbf{R}} = \begin{cases} v^{\uparrow}_{\mathbf{R}} & \text{if } \alpha = \downarrow \text{ and i=1 or i=2; if } \alpha = \uparrow \text{ and i=3} \\ v^{\downarrow}_{\mathbf{R}} & \text{if } \alpha = \uparrow \text{ and i=1 or i=2; if } \alpha = \downarrow \text{ and i=3} \end{cases} \tag{A.11}$$

for which the relation holds

$$v_{\mathbf{R}}^{\alpha,1} = v_{\mathbf{R}}^{\alpha,2} = v_{\mathbf{R}}^{-\alpha} \quad \text{and} \quad v_{\mathbf{R}}^{\alpha,3} = v_{\mathbf{R}}^{\alpha}. \tag{A.12}$$

Eq. (A.10) can be rewritten with the relation $\underline{\widehat{\sigma}}_i^{\dagger} = \underline{\widehat{\sigma}}_i$

$$\begin{aligned}
&\left\langle \gamma_{\mathbf{R}l'\alpha'} \middle| \frac{\partial v_{\mathbf{R}}^{\alpha}}{\partial r_{\mathbf{R}}} \middle| \gamma_{\mathbf{R}l\alpha} \right\rangle \left\langle Z_{l'm'} \middle| \mathbf{n}_{\mathbf{q}\lambda}^{\mathbf{R}}\ \mathbf{e}_{r_{\mathbf{R}}} \middle| Z_{lm} \right\rangle \delta_{\alpha\alpha'} \\
&- \left\langle \frac{\phi_{\mathbf{R}l'\alpha'}}{2M_{\mathbf{R}l'\alpha'} c r_{\mathbf{R}}} \middle| \frac{\partial v_{\mathbf{R}}^{\alpha}}{\partial r_{\mathbf{R}}} \middle| \gamma_{\mathbf{R}l\alpha} \right\rangle \sum_{i_1} \left\langle \widehat{L}_{i_1} Z_{l'm'} \middle| \mathbf{n}_{\mathbf{q}\lambda}^{\mathbf{R}}\ \mathbf{e}_{r_{\mathbf{R}}} \middle| Z_{lm} \right\rangle \left\langle \chi_{\alpha'} | \underline{\widehat{\sigma}}_{i_1} | \chi_{\alpha} \right\rangle \\
&- \sum_{i_2} \left\langle \gamma_{\mathbf{R}l'\alpha'} \middle| \frac{\partial v_{\mathbf{R}}^{\alpha,i_2}}{\partial r_{\mathbf{R}}} \middle| \frac{\phi_{\mathbf{R}l\alpha}}{2M_{\mathbf{R}l\alpha} c r_{\mathbf{R}}} \right\rangle \left\langle Z_{l'm'} \middle| \mathbf{n}_{\mathbf{q}\lambda}^{\mathbf{R}}\ \mathbf{e}_{r_{\mathbf{R}}} \middle| \widehat{L}_{i_2} Z_{lm} \right\rangle \left\langle \chi_{\alpha'} | \underline{\widehat{\sigma}}_{i_2} | \chi_{\alpha} \right\rangle \\
&+ \sum_{i_3,i_4} \left\langle \frac{\phi_{\mathbf{R}l'\alpha'}}{2M_{\mathbf{R}l'\alpha'} c r_{\mathbf{R}}} \middle| \frac{\partial v_{\mathbf{R}}^{\alpha,i_4}}{\partial r_{\mathbf{R}}} \middle| \frac{\phi_{\mathbf{R}l\alpha}}{2M_{\mathbf{R}l\alpha} c r_{\mathbf{R}}} \right\rangle \left\langle \widehat{L}_{i_3} Z_{l'm'} \middle| \mathbf{n}_{\mathbf{q}\lambda}^{\mathbf{R}}\ \mathbf{e}_{r_{\mathbf{R}}} \middle| \widehat{L}_{i_4} Z_{lm} \right\rangle \cdot \\
&\left\langle \chi_{\alpha'} | \underline{\widehat{\sigma}}_{i_3} \underline{\widehat{\sigma}}_{i_4} | \chi_{\alpha} \right\rangle .
\end{aligned} \tag{A.13}$$

All radial parts can be calculated numerically. Again it is useful to split the equation in the different parts.

1. The first line of eq. (A.13) can be implemented analogously to the first summand of eq. (A.4):

$$\left\langle \gamma_{\mathbf{R}l'\alpha'} \middle| \frac{\partial v_{\mathbf{R}}^{\alpha}}{\partial r_{\mathbf{R}}} \middle| \gamma_{\mathbf{R}l\alpha} \right\rangle \mathbf{n}_{\mathbf{q}\lambda}^{\mathbf{R}}\ \widetilde{\mathbf{G}}_{l'm'}^{lm} \delta_{\alpha\alpha'} \tag{A.14}$$

2. For the angular and spin part of the second line of eq. (A.13) we need the lowering and raising operator

$$\begin{aligned}
&\widehat{L}^{\pm} \equiv \widehat{L}_x \pm i\widehat{L}_y \\
\text{or} \quad &\widehat{L}^{\pm\alpha} \equiv \widehat{L}_x \pm i\alpha\widehat{L}_y
\end{aligned} \tag{A.15}$$

and the relations

$$\langle \chi_{\alpha'} | \underline{\widehat{\sigma}}_x | \chi_{\alpha} \rangle = \delta_{-\alpha\alpha'},\ \langle \chi_{\alpha'} | \underline{\widehat{\sigma}}_y | \chi_{\alpha} \rangle = i\alpha\delta_{-\alpha\alpha'},\ \langle \chi_{\alpha'} | \underline{\widehat{\sigma}}_z | \chi_{\alpha} \rangle = \alpha\delta_{\alpha\alpha'}. \tag{A.16}$$

We can use the expansion of the cubic harmonics in the spherical harmonics

$$Z_{lm} = \sum_{m_0=-l}^{l} K_{lmm_0} Y_{lm_0} \tag{A.17}$$

in order to apply the operators

$$\widehat{L}^{\pm} Y_{lm} = \hbar\sqrt{(l \mp m)(l \pm m + 1)}\; Y_{l(m\pm1)} = \hbar S^{\pm}_{lm} Y_{l(m\pm1)} \tag{A.18}$$

$$\widehat{L}^{\pm\alpha} Y_{lm} = \hbar\sqrt{(l \mp \alpha m)(l \pm \alpha m + 1)}\; Y_{l(m\pm\alpha)} = \hbar S^{\pm\alpha}_{lm} Y_{l(m\pm\alpha)} \tag{A.19}$$

$$\text{with } S^{\pm}_{lm} \equiv \sqrt{(l \mp m)(l \pm m + 1)},\; S^{\pm\alpha}_{lm} \equiv \sqrt{(l \mp \alpha m)(l \pm \alpha m + 1)} \tag{A.20}$$

$$\text{and} \quad \widehat{L}_z Y_{lm} = \hbar m\; Y_{lm}. \tag{A.21}$$

The conjugate-complex operators read

$$\left(\widehat{L}^{\pm}\right)^* = \widehat{L}^*_x \mp i\widehat{L}^*_y \qquad \text{or} \qquad \left(\widehat{L}^{\pm\alpha}\right)^* = \widehat{L}^*_x \mp i\alpha\widehat{L}^*_y. \tag{A.22}$$

Thus, the angular and spin part reads

$$\begin{aligned}
&\delta_{-\alpha\alpha'} \left\langle \widehat{L}^{-\alpha} Z_{l'm'} \middle| (\mathbf{n}^{\mathbf{R}}_{\mathbf{q}\lambda}\ \mathbf{e}_{r_{\mathbf{R}}}) \middle| Z_{lm} \right\rangle + \alpha\delta_{\alpha\alpha'} \left\langle \widehat{L}_z Z_{l'm'} \middle| (\mathbf{n}^{\mathbf{R}}_{\mathbf{q}\lambda}\ \mathbf{e}_{r_{\mathbf{R}}}) \middle| Z_{lm} \right\rangle \\
&= \sum_{\substack{m_0=-l \\ m_1=-l'}}^{\substack{m_1=l' \\ m_0=l}} K^*_{l'm'm_1} K_{lmm_0} \Big[\delta_{-\alpha\alpha'} \hbar S^{-\alpha}_{l'm_1} \left\langle Y_{l'(m_1-\alpha)} \middle| (\mathbf{n}^{\mathbf{R}}_{\mathbf{q}\lambda}\ \mathbf{e}_{r_{\mathbf{R}}}) \middle| Y_{lm_0} \right\rangle \\
&\qquad\qquad + \delta_{\alpha\alpha'} \alpha\hbar m_1 \left\langle Y_{l'm_1} \middle| (\mathbf{n}^{\mathbf{R}}_{\mathbf{q}\lambda}\ \mathbf{e}_{r_{\mathbf{R}}}) \middle| Y_{lm_0} \right\rangle \Big] \\
&= \mathbf{n}^{\mathbf{R}}_{\mathbf{q}\lambda} \sum_{\substack{m_0=-l \\ m_1=-l'}}^{\substack{m_1=l' \\ m_0=l}} K^*_{l'm'm_1} K_{lmm_0} \Big[\delta_{-\alpha\alpha'} \hbar S^{-\alpha}_{l'm_1} \mathbf{C}^{lm_0}_{l'(m_1-\alpha)} \\
&\qquad\qquad + \delta_{\alpha\alpha'} \hbar\alpha m_1 \mathbf{C}^{lm_0}_{l'm_1} \Big]
\end{aligned} \tag{A.23}$$

where eq. (A.5), the coefficients

$$C_{l''m'',l'm',lm} \equiv \langle Y_{l''m''} | Z_{l'm'} | Y_{lm} \rangle \tag{A.24}$$

and the vector

$$\mathbf{C}^{lm}_{l'm'} \equiv \sqrt{\frac{4\pi}{3}} \begin{pmatrix} C_{l'm',11,lm} \\ C_{l'm',1-1,lm} \\ C_{l'm',10,lm} \end{pmatrix} \tag{A.25}$$

have been used. Together the second line of eq. (A.13) reads

$$-\left\langle \frac{\phi_{\mathbf{R}l'\alpha'}}{2M_{\mathbf{R}l'\alpha'}cr_{\mathbf{R}}} \middle| \frac{\partial v^{\alpha}_{\mathbf{R}}}{\partial r_{\mathbf{R}}} \middle| \gamma_{\mathbf{R}l\alpha} \right\rangle \mathbf{n}^{\mathbf{R}}_{\mathbf{q}\lambda} \sum_{\substack{m_0=-l \\ m_1=-l'}}^{\substack{m_1=l' \\ m_0=l}} K^{*}_{l'm'm_1} K_{lmm_0} \cdot$$

$$\cdot \left[\delta_{-\alpha\alpha'} \hbar S^{-\alpha}_{l'm_1} \mathbf{C}^{lm_0}_{l'(m_1-\alpha)} + \delta_{\alpha\alpha'} \alpha \hbar m_1 \mathbf{C}^{lm_0}_{l'm_1} \right]. \tag{A.26}$$

3. The third line can be evaluated analogously with eq. (A.12) and the abbreviation

$$\left\langle \gamma_{\mathbf{R}l'\alpha'} \middle| \frac{\partial v^{\alpha,i_2}_{\mathbf{R}}}{\partial r_{\mathbf{R}}} \middle| \frac{\phi_{\mathbf{R}l\alpha}}{2M_{\mathbf{R}l\alpha}cr_{\mathbf{R}}} \right\rangle \equiv \left\langle \gamma | \partial v^{\alpha,i_2} | \phi \right\rangle : \tag{A.27}$$

$$\begin{aligned} &- \mathbf{n}^{\mathbf{R}}_{\mathbf{q}\lambda} \sum_{\substack{m_0=-l \\ m_1=-l'}}^{\substack{m_1=l' \\ m_0=l}} K^{*}_{l'm'm_1} K_{lmm_0} \Big[\left\langle \gamma | \partial v^{\alpha,1} | \phi \right\rangle \delta_{-\alpha\alpha'} \hbar S^{+\alpha}_{lm_0} \mathbf{C}^{l(m_0+\alpha)}_{l'm_1} \\ &\qquad + \left\langle \gamma | \partial v^{\alpha,3} | \phi \right\rangle \delta_{\alpha\alpha'} \alpha \hbar m_0 \mathbf{C}^{lm_0}_{l'm_1} \Big] \\ = &- \mathbf{n}^{\mathbf{R}}_{\mathbf{q}\lambda} \sum_{\substack{m_0=-l \\ m_1=-l'}}^{\substack{m_1=l' \\ m_0=l}} K^{*}_{l'm'm_1} K_{lmm_0} \Big[\left\langle \gamma | \partial v^{-\alpha} | \phi \right\rangle \delta_{-\alpha\alpha'} \hbar S^{+\alpha}_{lm_0} \mathbf{C}^{l(m_0+\alpha)}_{l'm_1} \\ &\qquad + \left\langle \gamma | \partial v^{\alpha} | \phi \right\rangle \delta_{\alpha\alpha'} \alpha \hbar m_0 \mathbf{C}^{lm_0}_{l'm_1} \Big]. \end{aligned} \tag{A.28}$$

4. For the fourth line eq. (A.16) is used as well as the relation

$$\underline{\underline{\widehat{\sigma}}}_i \underline{\underline{\widehat{\sigma}}}_j = \delta_{ij} \underline{\underline{1}} + i \sum_k \varepsilon_{ijk} \underline{\underline{\widehat{\sigma}}}_k. \tag{A.29}$$

Thus, the fourth line reads with the abbreviation

$$\left\langle \frac{\phi_{\mathbf{R}l'\alpha'}}{2M_{\mathbf{R}l'\alpha'}cr_{\mathbf{R}}} \middle| \frac{\partial v_{\mathbf{R}}^{\alpha,i_4}}{\partial r_{\mathbf{R}}} \middle| \frac{\phi_{\mathbf{R}l\alpha}}{2M_{\mathbf{R}l\alpha}cr_{\mathbf{R}}} \right\rangle \equiv \langle \phi | \partial v^{\alpha,i_4} | \phi \rangle : \tag{A.30}$$

$$\begin{aligned}
&\langle \phi | \partial v^{\alpha,1} | \phi \rangle \, \mathbf{n}_{\mathbf{q}\lambda}^{\mathbf{R}} \cdot \\
&\Big\{ \Big\langle Z_{l'm'} \big| \widehat{L}_x^* \mathbf{e}_{r_{\mathbf{R}}} \widehat{L}_x \delta_{\alpha\alpha'} + \widehat{L}_y^* \mathbf{e}_{r_{\mathbf{R}}} \widehat{L}_x (-i\alpha) \delta_{\alpha\alpha'} + \widehat{L}_z^* \mathbf{e}_{r_{\mathbf{R}}} \widehat{L}_x (-\alpha) \delta_{-\alpha\alpha'} \\
&+ \widehat{L}_x^* \mathbf{e}_{r_{\mathbf{R}}} \widehat{L}_y i\alpha \delta_{\alpha\alpha'} + \widehat{L}_y^* \mathbf{e}_{r_{\mathbf{R}}} \widehat{L}_y \delta_{\alpha\alpha'} + \widehat{L}_z^* \mathbf{e}_{r_{\mathbf{R}}} \widehat{L}_y (-i) \delta_{-\alpha\alpha'} \big| Z_{lm} \Big\rangle \Big\} \\
&+ \langle \phi | \partial v^{\alpha,3} | \phi \rangle \, \mathbf{n}_{\mathbf{q}\lambda}^{\mathbf{R}} \cdot \\
&\Big\{ \Big\langle Z_{l'm'} \big| \widehat{L}_x^* \mathbf{e}_{r_{\mathbf{R}}} \widehat{L}_z \alpha \delta_{-\alpha\alpha'} + \widehat{L}_y^* \mathbf{e}_{r_{\mathbf{R}}} \widehat{L}_z i \delta_{-\alpha\alpha'} + \widehat{L}_z^* \mathbf{e}_{r_{\mathbf{R}}} \widehat{L}_z \delta_{\alpha\alpha'} \big| Z_{lm} \Big\rangle \Big\} \\
&= \delta_{\alpha\alpha'} \mathbf{n}_{\mathbf{q}\lambda}^{\mathbf{R}} \cdot \Big\{ \langle \phi | \partial v^{\alpha,1} | \phi \rangle \cdot \\
&\Big[\Big\langle Z_{l'm'} \big| \widehat{L}_x^* \mathbf{e}_{r_{\mathbf{R}}} \widehat{L}_x + i\alpha \widehat{L}_x^* \mathbf{e}_{r_{\mathbf{R}}} \widehat{L}_y - i\alpha (\widehat{L}_y^* \mathbf{e}_{r_{\mathbf{R}}} \widehat{L}_x + i\alpha \widehat{L}_y^* \mathbf{e}_{r_{\mathbf{R}}} \widehat{L}_y) \big| Z_{lm} \Big\rangle \Big] \\
&+ \langle \phi | \partial v^{\alpha,3} | \phi \rangle \Big\langle Z_{l'm'} \big| \widehat{L}_z^* \mathbf{e}_{r_{\mathbf{R}}} \widehat{L}_z \big| Z_{lm} \Big\rangle \Big\} \\
&+ \delta_{-\alpha\alpha'} \mathbf{n}_{\mathbf{q}\lambda}^{\mathbf{R}} \Big\{ \langle \phi | \partial v^{\alpha,1} | \phi \rangle \cdot \\
&\Big[\Big\langle Z_{l'm'} \big| - \alpha (\widehat{L}_z^* \mathbf{e}_{r_{\mathbf{R}}} \widehat{L}_x + i\alpha \widehat{L}_z^* \mathbf{e}_{r_{\mathbf{R}}} \widehat{L}_y) \big| Z_{lm} \Big\rangle \Big] \\
&+ \langle \phi | \partial v^{\alpha,3} | \phi \rangle \Big\langle Z_{l'm'} \big| \alpha (\widehat{L}_x^* \mathbf{e}_{r_{\mathbf{R}}} \widehat{L}_z + i\alpha \widehat{L}_y^* \mathbf{e}_{r_{\mathbf{R}}} \widehat{L}_z) \big| Z_{lm} \Big\rangle \Big\} \\
&= \delta_{\alpha\alpha'} \mathbf{n}_{\mathbf{q}\lambda}^{\mathbf{R}} \Big\{ \langle \phi | \partial v^{\alpha,1} | \phi \rangle \Big\langle \widehat{L}^{\alpha} Z_{l'm'} \big| \mathbf{e}_{r_{\mathbf{R}}} \big| \widehat{L}^{\alpha} Z_{lm} \Big\rangle \\
&\qquad + \langle \phi | \partial v^{\alpha,3} | \phi \rangle \Big\langle \widehat{L}_z Z_{l'm'} \big| \mathbf{e}_{r_{\mathbf{R}}} \big| \widehat{L}_z Z_{lm} \Big\rangle \Big\} \\
&\quad + \delta_{-\alpha\alpha'} \mathbf{n}_{\mathbf{q}\lambda}^{\mathbf{R}} \Big\{ \langle \phi | \partial v^{\alpha,1} | \phi \rangle (-\alpha) \Big\langle \widehat{L}_z Z_{l'm'} \big| \mathbf{e}_{r_{\mathbf{R}}} \big| \widehat{L}^{\alpha} Z_{lm} \Big\rangle \\
&\qquad + \langle \phi | \partial v^{\alpha,3} | \phi \rangle \, \alpha \Big\langle \widehat{L}^{-\alpha} Z_{l'm'} \big| \mathbf{e}_{r_{\mathbf{R}}} \big| \widehat{L}_z Z_{lm} \Big\rangle \Big\}
\end{aligned}$$

$$
\begin{aligned}
&= \delta_{\alpha\alpha'}\mathbf{n}^{\mathbf{R}}_{\mathbf{q}\lambda} \sum_{\substack{m_0=-l \\ m_1=-l'}}^{\substack{m_1=l' \\ m_0=l}} K^*_{l'm'm_1}K_{lmm_0}\cdot \\
&\Big\{ \left\langle\phi|\partial v^{\alpha,1}|\phi\right\rangle \cdot \hbar^2 S^{+\alpha}_{l'm_1} S^{+\alpha}_{lm_0} \left\langle Y_{l'(m_1+\alpha)}\middle|\mathbf{e}_{r_{\mathbf{R}}}\middle|Y_{l(m_0+\alpha)}\right\rangle \\
&\qquad + \left\langle\phi|\partial v^{\alpha,3}|\phi\right\rangle \hbar^2 m_1 m_0 \left\langle Y_{l'm_1}\middle|\mathbf{e}_{r_{\mathbf{R}}}\middle|Y_{lm_0}\right\rangle \Big\} \\
&+ \delta_{-\alpha\alpha'}\mathbf{n}^{\mathbf{R}}_{\mathbf{q}\lambda} \sum_{\substack{m_0=-l \\ m_1=-l'}}^{\substack{m_1=l' \\ m_0=l}} K^*_{l'm'm_1}K_{lmm_0}\cdot \\
&\Big\{ \left\langle\phi|\partial v^{\alpha,1}|\phi\right\rangle \cdot (-\alpha)\hbar^2 m_1 S^{+\alpha}_{lm_0} \left\langle Y_{l'm_1}\middle|\mathbf{e}_{r_{\mathbf{R}}}\middle|Y_{l(m_0+\alpha)}\right\rangle \\
&\qquad + \left\langle\phi|\partial v^{\alpha,3}|\phi\right\rangle \alpha\hbar^2 S^{-\alpha}_{l'm_1} m_0 \left\langle Y_{l'(m_1-\alpha)}\middle|\mathbf{e}_{r_{\mathbf{R}}}\middle|Y_{lm_0}\right\rangle \Big\} \\
&= \delta_{\alpha\alpha'}\mathbf{n}^{\mathbf{R}}_{\mathbf{q}\lambda} \sum_{\substack{m_0=-l \\ m_1=-l'}}^{\substack{m_1=l' \\ m_0=l}} K^*_{l'm'm_1}K_{lmm_0}\hbar^2\cdot \\
&\Big\{ \left\langle\phi|\partial v^{-\alpha}|\phi\right\rangle \cdot S^{+\alpha}_{l'm_1} S^{+\alpha}_{lm_0} \mathbf{C}^{l(m_0+\alpha)}_{l'(m_1+\alpha)} + \langle\phi|\partial v^{\alpha}|\phi\rangle\, m_1 m_0 \mathbf{C}^{lm_0}_{l'm_1} \Big\} \\
&+ \delta_{-\alpha\alpha'}\mathbf{n}^{\mathbf{R}}_{\mathbf{q}\lambda} \sum_{\substack{m_0=-l \\ m_1=-l'}}^{\substack{m_1=l' \\ m_0=l}} K^*_{l'm'm_1}K_{lmm_0}\hbar^2\alpha\cdot \\
&\Big\{ -\left\langle\phi|\partial v^{-\alpha}|\phi\right\rangle \cdot m_1 S^{+\alpha}_{lm_0} \mathbf{C}^{l(m_0+\alpha)}_{l'm_1} + \langle\phi|\partial v^{\alpha}|\phi\rangle\, S^{-\alpha}_{l'm_1} m_0 \mathbf{C}^{lm_0}_{l'(m_1-\alpha)} \Big\}.
\end{aligned}
\tag{A.31}
$$

Third summand of eq. (A.4)

The third summand of eq. (A.4) can be written as

$$
\left\langle \gamma_{\mathbf{R}l'\alpha'} Z_{l'm'}\chi_{\alpha'} \middle| \Xi \middle| \gamma_{\mathbf{R}l\alpha} Z_{lm}\chi_{\alpha} \right\rangle
$$

$$
\begin{aligned}
&- \sum_{i_1} \left\langle \frac{\phi_{\mathbf{R}l'\alpha'}}{2M_{\mathbf{R}l'\alpha'}cr_{\mathbf{R}}} \underline{\widehat{\sigma}}_{i_1} \widehat{L}_{i_1} Z_{l'm'}\chi_{\alpha'} \middle| \Xi \middle| \gamma_{\mathbf{R}l\alpha} Z_{lm}\chi_{\alpha} \right\rangle \\
&- \sum_{i_2} \left\langle \gamma_{\mathbf{R}l'\alpha'} Z_{l'm'}\chi_{\alpha'} \middle| \Xi \middle| \frac{\phi_{\mathbf{R}l\alpha}}{2M_{\mathbf{R}l\alpha}cr_{\mathbf{R}}} \underline{\widehat{\sigma}}_{i_2} \widehat{L}_{i_2} Z_{lm}\chi_{\alpha} \right\rangle \\
&+ \sum_{i_3,i_4} \left\langle \frac{\phi_{\mathbf{R}l'\alpha'}}{2M_{\mathbf{R}l'\alpha'}cr_{\mathbf{R}}} \underline{\widehat{\sigma}}_{i_3} \widehat{L}_{i_3} Z_{l'm'}\chi_{\alpha'} \middle| \Xi \middle| \frac{\phi_{\mathbf{R}l\alpha}}{2M_{\mathbf{R}l\alpha}cr_{\mathbf{R}}} \underline{\widehat{\sigma}}_{i_4} \widehat{L}_{i_4} Z_{lm}\chi_{\alpha} \right\rangle
\end{aligned}
\tag{A.32}
$$

with

$$
\begin{aligned}
\Xi &\equiv (\mathbf{n}^{\mathbf{R}}_{\mathbf{q}\lambda}\ \mathbf{e}_{r_{\mathbf{R}}})(\widehat{x}\widehat{z}\underline{\widehat{\sigma}}_x + \widehat{y}\widehat{z}\underline{\widehat{\sigma}}_y + \widehat{z}^2\underline{\widehat{\sigma}}_z) \left(\frac{\partial v^{\downarrow}_{\mathbf{R}}}{\partial r_{\mathbf{R}}} - \frac{\partial v^{\uparrow}_{\mathbf{R}}}{\partial r_{\mathbf{R}}} \right) \\
&= (\mathbf{n}^{\mathbf{R}}_{\mathbf{q}\lambda}\ \mathbf{e}_{r_{\mathbf{R}}}) \left(\sqrt{\frac{4\pi}{15}} Z_{21} \underline{\widehat{\sigma}}_x + \sqrt{\frac{4\pi}{15}} Z_{2-1} \underline{\widehat{\sigma}}_y + \left(\sqrt{\frac{16\pi}{45}} Z_{20} + \frac{1}{3} \right) \underline{\widehat{\sigma}}_z \right) \cdot \Delta \\
&= \mathbf{n}^{\mathbf{R}}_{\mathbf{q}\lambda} \cdot \Delta \cdot \\
&\quad \left[\sqrt{\frac{4\pi}{15}} \left(\mathbf{e}_{r_{\mathbf{R}}} Z_{21} \underline{\widehat{\sigma}}_x + \mathbf{e}_{r_{\mathbf{R}}} Z_{2-1} \underline{\widehat{\sigma}}_y \right) + \frac{1}{3} \left(\sqrt{\frac{16\pi}{5}} \mathbf{e}_{r_{\mathbf{R}}} Z_{20} + \mathbf{e}_{r_{\mathbf{R}}} \right) \underline{\widehat{\sigma}}_z \right] \\
&\text{where} \quad \Delta \equiv \frac{\partial v^{\downarrow}_{\mathbf{R}}}{\partial r_{\mathbf{R}}} - \frac{\partial v^{\uparrow}_{\mathbf{R}}}{\partial r_{\mathbf{R}}}.
\end{aligned}
\tag{A.33}
$$

Again it is useful to split the equation in the different parts.

1. The first line of eq. (A.32) reads with the relation of eq. (A.16) and the short notation of eq. (A.27)

$$
\begin{aligned}
&\langle\gamma|\Delta|\gamma\rangle\, \mathbf{n}^{\mathbf{R}}_{\mathbf{q}\lambda} \cdot \\
&\Big\{ \delta_{-\alpha\alpha'} \sqrt{\frac{4\pi}{15}} \big[\langle Z_{l'm'} | \mathbf{e}_{r_{\mathbf{R}}} Z_{21} | Z_{lm} \rangle + i\alpha \langle Z_{l'm'} | \mathbf{e}_{r_{\mathbf{R}}} Z_{2-1} | Z_{lm} \rangle \big] \\
&\qquad + \delta_{\alpha\alpha'} \frac{1}{3} \alpha \big[\sqrt{\frac{16\pi}{5}} \langle Z_{l'm'} | \mathbf{e}_{r_{\mathbf{R}}} Z_{20} | Z_{lm} \rangle + \langle Z_{l'm'} | \mathbf{e}_{r_{\mathbf{R}}} | Z_{lm} \rangle \big] \Big\} \\
&= \langle\gamma|\Delta|\gamma\rangle\, \mathbf{n}^{\mathbf{R}}_{\mathbf{q}\lambda} \sum_{LM} \\
&\Big\{ \delta_{-\alpha\alpha'} \sqrt{\frac{4\pi}{15}} \big[\widetilde{\mathbf{G}}^{21}_{LM} \langle Z_{l'm'} | Z_{LM} | Z_{lm} \rangle + i\alpha \widetilde{\mathbf{G}}^{2-1}_{LM} \langle Z_{l'm'} | Z_{LM} | Z_{lm} \rangle \big]
\end{aligned}
$$

$$
\begin{aligned}
&+ \delta_{\alpha\alpha'} \frac{1}{3}\alpha \big[\widetilde{\mathbf{G}}^{20}_{LM} \sqrt{\frac{16\pi}{5}} \left\langle Z_{l'm'} \middle| Z_{LM} \middle| Z_{lm} \right\rangle + \widetilde{\mathbf{G}}^{lm}_{l'm'}\big] \Big\} \\
&= \left\langle \gamma \middle| \Delta \middle| \gamma \right\rangle \mathbf{n}^{\mathbf{R}}_{\mathbf{q}\lambda} \sum_{LM} \\
&\quad \Big\{ \delta_{-\alpha\alpha'} \sqrt{\frac{4\pi}{15}} \widetilde{G}_{l'm',LM,lm} \big[\widetilde{\mathbf{G}}^{21}_{LM} + i\alpha \widetilde{\mathbf{G}}^{2-1}_{LM}\big] \\
&\quad + \delta_{\alpha\alpha'} \frac{1}{3}\alpha \big[\widetilde{\mathbf{G}}^{20}_{LM} \sqrt{\frac{16\pi}{5}} \widetilde{G}_{l'm',LM,lm} + \widetilde{\mathbf{G}}^{lm}_{l'm'}\big] \Big\}
\end{aligned} \tag{A.34}
$$

where [11]

$$
\begin{aligned}
\mathbf{e}_{r_\mathbf{R}} Z_{lm} &= \sqrt{\frac{4\pi}{3}} \begin{pmatrix} Z_{11} \\ Z_{1-1} \\ Z_{10} \end{pmatrix} Z_{lm} \\
&= \sum_{LM} \sqrt{\frac{4\pi}{3}} \begin{pmatrix} \widetilde{G}_{11,lm,LM} \\ \widetilde{G}_{1-1,lm,LM} \\ \widetilde{G}_{10,lm,LM} \end{pmatrix} Z_{LM} = \sum_{LM} \widetilde{\mathbf{G}}^{lm}_{LM} Z_{LM}.
\end{aligned} \tag{A.35}
$$

Only the following coefficients

$$
\begin{aligned}
&\widetilde{G}_{11,lm,(l+1)(m+1)},\ \widetilde{G}_{11,lm,(l+1)(m-1)},\ \widetilde{G}_{11,lm,(l-1)(m+1)}, \\
&\widetilde{G}_{11,lm,(l-1)(m-1)},\ \widetilde{G}_{1-1,lm,(l+1)(m+1)},\ \widetilde{G}_{1-1,lm,(l+1)(m-1)}, \\
&\widetilde{G}_{1-1,lm,(l-1)(m+1)},\ \widetilde{G}_{1-1,lm,(l-1)(m-1)},\ \widetilde{G}_{10,lm,(l+1)m},\ \widetilde{G}_{10,lm,(l-1)m}
\end{aligned} \tag{A.36}
$$

are not zero [11]. Hence, a calculation is feasible.

2. The second line of eq. (A.32) reads (again with the short notation of eq. (A.27) and the relations (A.29), (A.16))

$$
\begin{aligned}
&- \left\langle \phi \middle| \Delta \middle| \gamma \right\rangle \mathbf{n}^{\mathbf{R}}_{\mathbf{q}\lambda} \big\{ \langle Z_{l'm'} | \widehat{L}^*_x \mathbf{e}_{r_\mathbf{R}} (\widehat{x}\widehat{z}\delta_{\alpha\alpha'} + \widehat{y}\widehat{z} i\alpha \delta_{\alpha\alpha'} + \widehat{z}^2 \alpha \delta_{-\alpha\alpha'}) \\
&\qquad + \widehat{L}^*_y \mathbf{e}_{r_\mathbf{R}} (\widehat{x}\widehat{z}(-i\alpha)\delta_{\alpha\alpha'} + \widehat{y}\widehat{z}\delta_{\alpha\alpha'} + \widehat{z}^2 i\delta_{-\alpha\alpha'}) \\
&\qquad + \widehat{L}^*_z \mathbf{e}_{r_\mathbf{R}} (\widehat{x}\widehat{z}(-\alpha)\delta_{-\alpha\alpha'} + \widehat{y}\widehat{z}(-i)\delta_{-\alpha\alpha'} + \widehat{z}^2 \delta_{\alpha\alpha'}) | Z_{lm} \rangle \big\} \\
&= - \left\langle \phi \middle| \Delta \middle| \gamma \right\rangle \mathbf{n}^{\mathbf{R}}_{\mathbf{q}\lambda} \ \cdot
\end{aligned}
$$

$$
\begin{aligned}
&\Big\{\delta_{\alpha\alpha'}\Big\langle Z_{l'm'}\Big|\Big(\widehat{L}^{\alpha}\Big)^{*}\mathbf{e}_{r_{\mathbf{R}}}\widehat{x}\widehat{z}+i\alpha\Big(\widehat{L}^{\alpha}\Big)^{*}\mathbf{e}_{r_{\mathbf{R}}}\widehat{y}\widehat{z}+\widehat{L}_z^{*}\mathbf{e}_{r_{\mathbf{R}}}\widehat{z}^2\Big|Z_{lm}\Big\rangle\\
&\quad+\delta_{-\alpha\alpha'}\Big\langle Z_{l'm'}\Big|-\alpha\widehat{L}_z^{*}\mathbf{e}_{r_{\mathbf{R}}}\widehat{x}\widehat{z}-i\widehat{L}_z^{*}\mathbf{e}_{r_{\mathbf{R}}}\widehat{y}\widehat{z}+\alpha\Big(\widehat{L}^{-\alpha}\Big)^{*}\mathbf{e}_{r_{\mathbf{R}}}\widehat{z}^2\Big|Z_{lm}\Big\rangle\Big\}\\
&=-\langle\phi|\Delta|\gamma\rangle\,\mathbf{n}^{\mathbf{R}}_{\mathbf{q}\lambda}\sum_{m_0,m_1}K^{*}_{l'm'm_1}K_{lmm_0}\cdot\\
&\quad\Big\{\delta_{\alpha\alpha'}\Big[\sqrt{\frac{4\pi}{15}}\hbar S^{+\alpha}_{l'm_1}\left(\left\langle Y_{l'(m_1+\alpha)}\left|\mathbf{e}_{r_{\mathbf{R}}}Z_{21}\right|Y_{lm_0}\right\rangle\right.\\
&\qquad\left.+i\alpha\left\langle Y_{l'(m_1+\alpha)}\left|\mathbf{e}_{r_{\mathbf{R}}}Z_{2-1}\right|Y_{lm_0}\right\rangle\right)\\
&\qquad+\frac{1}{3}\hbar m_1\left(\sqrt{\frac{16\pi}{5}}\left\langle Y_{l'm_1}\left|\mathbf{e}_{r_{\mathbf{R}}}Z_{20}\right|Y_{lm_0}\right\rangle+\left\langle Y_{l'm_1}\left|\mathbf{e}_{r_{\mathbf{R}}}\right|Y_{lm_0}\right\rangle\right)\Big]\\
&\quad+\delta_{-\alpha\alpha'}\Big[\sqrt{\frac{4\pi}{15}}\hbar m_1\left(-\alpha\left\langle Y_{l'm_1}\left|\mathbf{e}_{r_{\mathbf{R}}}Z_{21}\right|Y_{lm_0}\right\rangle\right.\\
&\qquad\left.-i\left\langle Y_{l'm_1}\left|\mathbf{e}_{r_{\mathbf{R}}}Z_{2-1}\right|Y_{lm_0}\right\rangle\right)+\alpha\frac{1}{3}\hbar S^{-\alpha}_{l'm_1}\cdot\\
&\qquad\left(\sqrt{\frac{16\pi}{5}}\left\langle Y_{l'(m_1-\alpha)}\left|\mathbf{e}_{r_{\mathbf{R}}}Z_{20}\right|Y_{lm_0}\right\rangle+\left\langle Y_{l'(m_1-\alpha)}\left|\mathbf{e}_{r_{\mathbf{R}}}\right|Y_{lm_0}\right\rangle\right)\Big]\Big\}\\
&=-\langle\phi|\Delta|\gamma\rangle\,\mathbf{n}^{\mathbf{R}}_{\mathbf{q}\lambda}\sum_{m_0,m_1,LM}K^{*}_{l'm'm_1}K_{lmm_0}\cdot\\
&\quad\Big\{\delta_{\alpha\alpha'}\Big[\sqrt{\frac{4\pi}{15}}\hbar S^{+\alpha}_{l'm_1}\left(\widetilde{\mathbf{G}}^{21}_{LM}\left\langle Y_{l'(m_1+\alpha)}\left|Z_{LM}\right|Y_{lm_0}\right\rangle\right.\\
&\qquad\left.+i\alpha\widetilde{\mathbf{G}}^{2-1}_{LM}\left\langle Y_{l'(m_1+\alpha)}\left|Z_{LM}\right|Y_{lm_0}\right\rangle\right)\\
&\qquad+\frac{1}{3}\hbar m_1\left(\sqrt{\frac{16\pi}{5}}\widetilde{\mathbf{G}}^{20}_{LM}\left\langle Y_{l'm_1}\left|Z_{LM}\right|Y_{lm_0}\right\rangle+\mathbf{C}^{lm_0}_{l'm_1}\right)\Big]\\
&\quad+\delta_{-\alpha\alpha'}\Big[\sqrt{\frac{4\pi}{15}}\hbar m_1\left(-\alpha\widetilde{\mathbf{G}}^{21}_{LM}\left\langle Y_{l'm_1}\left|Z_{LM}\right|Y_{lm_0}\right\rangle\right.\\
&\qquad\left.-i\widetilde{\mathbf{G}}^{2-1}_{LM}\left\langle Y_{l'm_1}\left|Z_{LM}\right|Y_{lm_0}\right\rangle\right)\\
&\quad+\alpha\frac{1}{3}\hbar S^{-\alpha}_{l'm_1}\left(\sqrt{\frac{16\pi}{5}}\widetilde{\mathbf{G}}^{20}_{LM}\left\langle Y_{l'(m_1-\alpha)}\left|Z_{LM}\right|Y_{lm_0}\right\rangle+\mathbf{C}^{lm_0}_{l'(m_1-\alpha)}\right)\Big]\Big\}
\end{aligned}
$$

$$
\begin{aligned}
&= - \langle\phi|\Delta|\gamma\rangle\, \mathbf{n}^{\mathbf{R}}_{\mathbf{q}\lambda} \sum_{m_0,m_1,LM} K^*_{l'm'm_1} K_{lmm_0} \cdot \\
&\Big\{ \delta_{\alpha\alpha'} \Big[\sqrt{\frac{4\pi}{15}} \hbar S^{+\alpha}_{l'm_1} C_{l'(m_1+\alpha),LM,lm_0} \left(\widetilde{\mathbf{G}}^{21}_{LM} + i\alpha \widetilde{\mathbf{G}}^{2-1}_{LM} \right) \\
&\qquad + \frac{1}{3}\hbar m_1 \left(\sqrt{\frac{16\pi}{5}} \widetilde{\mathbf{G}}^{20}_{LM} C_{l'm_1,LM,lm_0} + \mathbf{C}^{lm_0}_{l'm_1} \right) \Big] \\
&+ \delta_{-\alpha\alpha'} \Big[\sqrt{\frac{4\pi}{15}} \hbar m_1 C_{l'm_1,LM,lm_0} \left(-\alpha \widetilde{\mathbf{G}}^{21}_{LM} - i \widetilde{\mathbf{G}}^{2-1}_{LM} \right) \\
&\quad + \alpha \frac{1}{3} \hbar S^{-\alpha}_{l'm_1} \left(\sqrt{\frac{16\pi}{5}} \widetilde{\mathbf{G}}^{20}_{LM} C_{l'(m_1-\alpha),LM,lm_0} + \mathbf{C}^{lm_0}_{l'(m_1-\alpha)} \right) \Big] \Big\}.
\end{aligned}
\tag{A.37}
$$

3. The third line of eq. (A.32) is quite similar to the second line (again with eqs. (A.29), (A.16) and the short notation of eq. (A.27)):

$$
\begin{aligned}
&- \langle\gamma|\Delta|\phi\rangle\, \mathbf{n}^{\mathbf{R}}_{\mathbf{q}\lambda} \; \{ \langle Z_{l'm'} | \mathbf{e}_{r_{\mathbf{R}}} (\widehat{x}\widehat{z}\delta_{\alpha\alpha'} - \widehat{y}\widehat{z} i\alpha \delta_{\alpha\alpha'} - \widehat{z}^2 \alpha \delta_{-\alpha\alpha'}) \widehat{L}_x + \\
&\qquad\qquad \mathbf{e}_{r_{\mathbf{R}}} (\widehat{x}\widehat{z} i\alpha \delta_{\alpha\alpha'} + \widehat{y}\widehat{z}\delta_{\alpha\alpha'} + \widehat{z}^2 (-i) \delta_{-\alpha\alpha'}) \widehat{L}_y + \\
&\qquad\qquad \mathbf{e}_{r_{\mathbf{R}}} (\widehat{x}\widehat{z}\alpha\delta_{-\alpha\alpha'} + \widehat{y}\widehat{z} i \delta_{-\alpha\alpha'} + \widehat{z}^2 \delta_{\alpha\alpha'}) \widehat{L}_z | Z_{lm} \rangle \} \\
&= - \langle\gamma|\Delta|\phi\rangle\, \mathbf{n}^{\mathbf{R}}_{\mathbf{q}\lambda} \; \cdot \\
&\Big\{ \delta_{\alpha\alpha'} \left\langle Z_{l'm'} \left| \mathbf{e}_{r_{\mathbf{R}}} \widehat{x}\widehat{z} \widehat{L}^{\alpha} - i\alpha \mathbf{e}_{r_{\mathbf{R}}} \widehat{y}\widehat{z} \widehat{L}^{\alpha} + \mathbf{e}_{r_{\mathbf{R}}} \widehat{z}^2 \widehat{L}_z \right| Z_{lm} \right\rangle \\
&+ \delta_{-\alpha\alpha'} \left\langle Z_{l'm'} \left| \alpha \mathbf{e}_{r_{\mathbf{R}}} \widehat{x}\widehat{z} \widehat{L}_z + i \mathbf{e}_{r_{\mathbf{R}}} \widehat{y}\widehat{z} \widehat{L}_z - \alpha \mathbf{e}_{r_{\mathbf{R}}} \widehat{z}^2 \widehat{L}^{\alpha} \right| Z_{lm} \right\rangle \Big\} \\
&= - \langle\gamma|\Delta|\phi\rangle\, \mathbf{n}^{\mathbf{R}}_{\mathbf{q}\lambda} \sum_{m_0,m_1} K^*_{l'm'm_1} K_{lmm_0} \cdot \\
&\Big\{ \delta_{\alpha\alpha'} \Big[\sqrt{\frac{4\pi}{15}} \hbar S^{+\alpha}_{lm_0} \left(\left\langle Y_{l'm_1} \left| \mathbf{e}_{r_{\mathbf{R}}} Z_{21} \right| Y_{l(m_0+\alpha)} \right\rangle \right. \\
&\qquad \left. - i\alpha \left\langle Y_{l'm_1} \left| \mathbf{e}_{r_{\mathbf{R}}} Z_{2-1} \right| Y_{l(m_0+\alpha)} \right\rangle \right) \\
&+ \frac{1}{3} \hbar m_0 \left(\sqrt{\frac{16\pi}{5}} \left\langle Y_{l'm_1} \left| \mathbf{e}_{r_{\mathbf{R}}} Z_{20} \right| Y_{lm_0} \right\rangle + \left\langle Y_{l'm_1} \left| \mathbf{e}_{r_{\mathbf{R}}} \right| Y_{lm_0} \right\rangle \right) \Big]
\end{aligned}
$$

$$
\begin{aligned}
&+\delta_{-\alpha\alpha'}\Bigg[\sqrt{\frac{4\pi}{15}}\hbar m_0\,(\alpha\,\langle Y_{l'm_1}\,|\mathbf{e}_{r_\mathbf{R}}Z_{21}|\,Y_{lm_0}\rangle \\
&\qquad\qquad +i\,\langle Y_{l'm_1}\,|\mathbf{e}_{r_\mathbf{R}}Z_{2-1}|\,Y_{lm_0}\rangle) - \alpha\frac{1}{3}\hbar S^{+\alpha}_{lm_0}\cdot \\
&\left(\sqrt{\frac{16\pi}{5}}\,\langle Y_{l'm_1}\,|\mathbf{e}_{r_\mathbf{R}}Z_{20}|\,Y_{l(m_0+\alpha)}\rangle + \langle Y_{l'm_1}\,|\mathbf{e}_{r_\mathbf{R}}|\,Y_{l(m_0+\alpha)}\rangle\right)\Bigg]\Bigg\} \\
&= -\,\langle\gamma|\Delta|\phi\rangle\,\mathbf{n}^{\mathbf{R}}_{\mathbf{q}\lambda}\sum_{m_0,m_1,LM}K^*_{l'm'm_1}K_{lmm_0}\cdot \\
&\Bigg\{\delta_{\alpha\alpha'}\Bigg[\sqrt{\frac{4\pi}{15}}\hbar S^{+\alpha}_{lm_0}\Big(\widetilde{\mathbf{G}}^{21}_{LM}\,\langle Y_{l'm_1}\,|Z_{LM}|\,Y_{l(m_0+\alpha)}\rangle \\
&\qquad\qquad -i\alpha\widetilde{\mathbf{G}}^{2-1}_{LM}\,\langle Y_{l'm_1}\,|Z_{LM}|\,Y_{l(m_0+\alpha)}\rangle\Big) \\
&\qquad +\frac{1}{3}\hbar m_0\left(\sqrt{\frac{16\pi}{5}}\widetilde{\mathbf{G}}^{20}_{LM}\,\langle Y_{l'm_1}\,|Z_{LM}|\,Y_{lm_0}\rangle + \mathbf{C}^{lm_0}_{l'm_1}\right)\Bigg] \\
&+\delta_{-\alpha\alpha'}\Bigg[\sqrt{\frac{4\pi}{15}}\hbar m_0\Big(\alpha\widetilde{\mathbf{G}}^{21}_{LM}\,\langle Y_{l'm_1}\,|Z_{LM}|\,Y_{lm_0}\rangle \\
&\qquad\qquad +i\widetilde{\mathbf{G}}^{2-1}_{LM}\,\langle Y_{l'm_1}\,|Z_{LM}|\,Y_{lm_0}\rangle\Big) \\
&-\alpha\frac{1}{3}\hbar S^{+\alpha}_{lm_0}\left(\sqrt{\frac{16\pi}{5}}\widetilde{\mathbf{G}}^{20}_{LM}\,\langle Y_{l'm_1}\,|Z_{LM}|\,Y_{l(m_0+\alpha)}\rangle + \mathbf{C}^{l(m_0+\alpha)}_{l'm_1}\right)\Bigg]\Bigg\} \\
&= -\,\langle\gamma|\Delta|\phi\rangle\,\mathbf{n}^{\mathbf{R}}_{\mathbf{q}\lambda}\sum_{m_0,m_1,LM}K^*_{l'm'm_1}K_{lmm_0}\cdot \\
&\Bigg\{\delta_{\alpha\alpha'}\Bigg[\sqrt{\frac{4\pi}{15}}\hbar S^{+\alpha}_{lm_0}C_{l'm_1,LM,l(m_0+\alpha)}\left(\widetilde{\mathbf{G}}^{21}_{LM} - i\alpha\widetilde{\mathbf{G}}^{2-1}_{LM}\right) \\
&\qquad +\frac{1}{3}\hbar m_0\left(\sqrt{\frac{16\pi}{5}}\widetilde{\mathbf{G}}^{20}_{LM}C_{l'm_1,LM,lm_0} + \mathbf{C}^{lm_0}_{l'm_1}\right)\Bigg] \\
&+\delta_{-\alpha\alpha'}\Bigg[\sqrt{\frac{4\pi}{15}}\hbar m_0 C_{l'm_1,LM,lm_0}\left(\alpha\widetilde{\mathbf{G}}^{21}_{LM} + i\widetilde{\mathbf{G}}^{2-1}_{LM}\right) \\
&\qquad -\alpha\frac{1}{3}\hbar S^{+\alpha}_{lm_0}\left(\sqrt{\frac{16\pi}{5}}\widetilde{\mathbf{G}}^{20}_{LM}C_{l'm_1,LM,l(m_0+\alpha)} + \mathbf{C}^{l(m_0+\alpha)}_{l'm_1}\right)\Bigg]\Bigg\}.
\end{aligned}
\tag{A.38}
$$

4. And finally the last line of eq. (A.32) (again with eqs. (A.16), (A.29) and the short notation of eq. (A.27)):

$$
\begin{aligned}
&\langle\phi|\Delta|\phi\rangle\, \mathbf{n}^{\mathbf{R}}_{\mathbf{q}\lambda}\ \langle Z_{l'm'}\chi_{\alpha'}|\widehat{L}^*_x\mathbf{e}_{r_{\mathbf{R}}}\big[\widehat{x}\widehat{z}\underline{\widehat{\sigma}}_x\widehat{L}_x+\widehat{y}\widehat{z}i^2\underline{\widehat{\sigma}}_y\widehat{L}_x+\widehat{z}^2(-i)^2\underline{\widehat{\sigma}}_z\widehat{L}_x\\
&\qquad+\widehat{x}\widehat{z}\underline{\widehat{\sigma}}_y\widehat{L}_y+\widehat{y}\widehat{z}(-i^2)\underline{\widehat{\sigma}}_x\widehat{L}_y+\widehat{z}^2(-i)\underline{1}\widehat{L}_y\\
&\qquad+\widehat{x}\widehat{z}\underline{\widehat{\sigma}}_z\widehat{L}_z+\widehat{y}\widehat{z}i\underline{1}\widehat{L}_z+\widehat{z}^2(-i^2)\underline{\widehat{\sigma}}_x\widehat{L}_z\big]\\
&\quad+\widehat{L}^*_y\mathbf{e}_{r_{\mathbf{R}}}\big[\widehat{x}\widehat{z}(-i^2)\underline{\widehat{\sigma}}_y\widehat{L}_x+\widehat{y}\widehat{z}\underline{\widehat{\sigma}}_x\widehat{L}_x+\widehat{z}^2i\underline{1}\widehat{L}_x\\
&\qquad+\widehat{x}\widehat{z}(-i)^2\underline{\widehat{\sigma}}_x\widehat{L}_y+\widehat{y}\widehat{z}\underline{\widehat{\sigma}}_y\widehat{L}_y+\widehat{z}^2i^2\underline{\widehat{\sigma}}_z\widehat{L}_y\\
&\qquad+\widehat{x}\widehat{z}(-i)\underline{1}\widehat{L}_z+\widehat{y}\widehat{z}\underline{\widehat{\sigma}}_z\widehat{L}_z+\widehat{z}^2(-i^2)\underline{\widehat{\sigma}}_y\widehat{L}_z\big]\\
&\quad+\widehat{L}^*_z\mathbf{e}_{r_{\mathbf{R}}}\big[\widehat{x}\widehat{z}(-i^2)\underline{\widehat{\sigma}}_z\widehat{L}_x+\widehat{y}\widehat{z}(-i)\underline{1}\widehat{L}_x+\widehat{z}^2\underline{\widehat{\sigma}}_x\widehat{L}_x\\
&\qquad+\widehat{x}\widehat{z}i\underline{1}\widehat{L}_y+\widehat{y}\widehat{z}(-i^2)\underline{\widehat{\sigma}}_z\widehat{L}_y+\widehat{z}^2\underline{\widehat{\sigma}}_y\widehat{L}_y\\
&\qquad+\widehat{x}\widehat{z}i^2\underline{\widehat{\sigma}}_x\widehat{L}_z+\widehat{y}\widehat{z}(-i)^2\underline{\widehat{\sigma}}_y\widehat{L}_z+\widehat{z}^2\underline{\widehat{\sigma}}_z\widehat{L}_z\big]|Z_{lm}\chi_\alpha\rangle\\
&=\langle\phi|\Delta|\phi\rangle\, \mathbf{n}^{\mathbf{R}}_{\mathbf{q}\lambda}\ \Big\{\delta_{-\alpha\alpha'}\cdot\\
&\quad\langle Z_{l'm'}|\widehat{L}^*_x\mathbf{e}_{r_{\mathbf{R}}}\big[\widehat{x}\widehat{z}\widehat{L}_x+\widehat{y}\widehat{z}(-i\alpha)\widehat{L}_x+\widehat{x}\widehat{z}i\alpha\widehat{L}_y+\widehat{y}\widehat{z}\widehat{L}_y+\widehat{z}^2\widehat{L}_z\big]\\
&\quad+\widehat{L}^*_y\mathbf{e}_{r_{\mathbf{R}}}\big[\widehat{x}\widehat{z}i\alpha\widehat{L}_x+\widehat{y}\widehat{z}\widehat{L}_x+\widehat{x}\widehat{z}(-1)\widehat{L}_y+\widehat{y}\widehat{z}i\alpha\widehat{L}_y+\widehat{z}^2i\alpha\widehat{L}_z\big]\\
&\quad+\widehat{L}^*_z\mathbf{e}_{r_{\mathbf{R}}}\big[\widehat{z}^2\widehat{L}_x+\widehat{z}^2i\alpha\widehat{L}_y+\widehat{x}\widehat{z}(-1)\widehat{L}_z+\widehat{y}\widehat{z}(-i\alpha)\widehat{L}_z\big]|Z_{lm}\rangle\\
&\quad+\delta_{\alpha\alpha'}\cdot\\
&\quad\langle Z_{l'm'}|\widehat{L}^*_x\mathbf{e}_{r_{\mathbf{R}}}\big[\widehat{z}^2(-\alpha)\widehat{L}_x+\widehat{z}^2(-i)\widehat{L}_y+\widehat{x}\widehat{z}\alpha\widehat{L}_z+\widehat{y}\widehat{z}i\widehat{L}_z\big]\\
&\quad+\widehat{L}^*_y\mathbf{e}_{r_{\mathbf{R}}}\big[\widehat{z}^2i\widehat{L}_x+\widehat{z}^2(-\alpha)\widehat{L}_y+\widehat{x}\widehat{z}(-i)\widehat{L}_z+\widehat{y}\widehat{z}\alpha\widehat{L}_z\big]\\
&\quad+\widehat{L}^*_z\mathbf{e}_{r_{\mathbf{R}}}\big[\widehat{x}\widehat{z}\alpha\widehat{L}_x+\widehat{y}\widehat{z}(-i)\widehat{L}_x+\widehat{x}\widehat{z}i\widehat{L}_y+\widehat{y}\widehat{z}\alpha\widehat{L}_y+\widehat{z}^2\alpha\widehat{L}_z\big]|Z_{lm}\rangle\Big\}\\
&=\langle\phi|\Delta|\phi\rangle\, \mathbf{n}^{\mathbf{R}}_{\mathbf{q}\lambda}\ \Big\{\delta_{-\alpha\alpha'}\cdot\langle Z_{l'm'}|\widehat{L}^*_x\mathbf{e}_{r_{\mathbf{R}}}\big[\widehat{x}\widehat{z}\widehat{L}^\alpha+\widehat{y}\widehat{z}(-i\alpha)\widehat{L}^\alpha+\widehat{z}^2\widehat{L}_z\big]\\
&\qquad+\widehat{L}^*_y\mathbf{e}_{r_{\mathbf{R}}}\big[\widehat{x}\widehat{z}i\alpha\widehat{L}^\alpha+\widehat{y}\widehat{z}\widehat{L}^\alpha+\widehat{z}^2i\alpha\widehat{L}_z\big]\\
&\qquad+\widehat{L}^*_z\mathbf{e}_{r_{\mathbf{R}}}\big[\widehat{z}^2\widehat{L}^\alpha+\widehat{x}\widehat{z}(-1)\widehat{L}_z+\widehat{y}\widehat{z}(-i\alpha)\widehat{L}_z\big]|Z_{lm}\rangle\\
&\quad+\delta_{\alpha\alpha'}\cdot\langle Z_{l'm'}|\widehat{L}^*_x\mathbf{e}_{r_{\mathbf{R}}}\big[\widehat{z}^2(-\alpha)\widehat{L}^\alpha+\widehat{x}\widehat{z}\alpha\widehat{L}_z+\widehat{y}\widehat{z}i\widehat{L}_z\big]\\
&\qquad+\widehat{L}^*_y\mathbf{e}_{r_{\mathbf{R}}}\big[\widehat{z}^2i\widehat{L}^\alpha+\widehat{x}\widehat{z}(-i)\widehat{L}_z+\widehat{y}\widehat{z}\alpha\widehat{L}_z\big]
\end{aligned}
$$

$$
\begin{aligned}
&\qquad + \widehat{L}_z^* \mathbf{e}_{r_\mathbf{R}} \left[\widehat{x}\widehat{z}\alpha \widehat{L}^\alpha + \widehat{y}\widehat{z}(-i)\widehat{L}^\alpha + \widehat{z}^2 \alpha \widehat{L}_z \right] |Z_{lm}\rangle \Big\} \\
&= \langle\phi|\Delta|\phi\rangle \, \mathbf{n}_{\mathbf{q}\lambda}^{\mathbf{R}} \ \cdot \\
&\Big\{ \delta_{-\alpha\alpha'} \cdot \langle Z_{l'm'}| \left(\widehat{L}^{-\alpha}\right)^* \mathbf{e}_{r_\mathbf{R}} \widehat{x}\widehat{z}\widehat{L}^\alpha + (-i\alpha) \left(\widehat{L}^{-\alpha}\right)^* \mathbf{e}_{r_\mathbf{R}} \widehat{y}\widehat{z}\widehat{L}^\alpha \\
&\qquad + \left(\widehat{L}^{-\alpha}\right)^* \mathbf{e}_{r_\mathbf{R}} \widehat{z}^2 \widehat{L}_z + \widehat{L}_z^* \mathbf{e}_{r_\mathbf{R}} \widehat{z}^2 \widehat{L}^\alpha + (-1) \widehat{L}_z^* \mathbf{e}_{r_\mathbf{R}} \widehat{x}\widehat{z}\widehat{L}_z \\
&\qquad + (-i\alpha) \widehat{L}_z^* \mathbf{e}_{r_\mathbf{R}} \widehat{y}\widehat{z}\widehat{L}_z |Z_{lm}\rangle \\
&+ \delta_{\alpha\alpha'} \cdot \langle Z_{l'm'}| (-\alpha) \left(\widehat{L}^{\alpha}\right)^* \mathbf{e}_{r_\mathbf{R}} \widehat{z}^2 \widehat{L}^\alpha + \alpha \left(\widehat{L}^{\alpha}\right)^* \mathbf{e}_{r_\mathbf{R}} \widehat{x}\widehat{z}\widehat{L}_z \\
&\qquad + i \left(\widehat{L}^{\alpha}\right)^* \mathbf{e}_{r_\mathbf{R}} \widehat{y}\widehat{z}\widehat{L}_z + \alpha \widehat{L}_z^* \mathbf{e}_{r_\mathbf{R}} \widehat{x}\widehat{z}\widehat{L}^\alpha + (-i) \widehat{L}_z^* \mathbf{e}_{r_\mathbf{R}} \widehat{y}\widehat{z}\widehat{L}^\alpha \\
&\qquad + \alpha \widehat{L}_z^* \mathbf{e}_{r_\mathbf{R}} \widehat{z}^2 \widehat{L}_z |Z_{lm}\rangle \Big\} \\
&= \langle\phi|\Delta|\phi\rangle \, \mathbf{n}_{\mathbf{q}\lambda}^{\mathbf{R}} \sum_{m_0, m_1, LM} K^*_{l'm'm_1} K_{lmm_0} \cdot \\
&\quad \Big\{ \delta_{-\alpha\alpha'} \cdot \hbar^2 \Big[S^{-\alpha}_{l'm_1} S^{+\alpha}_{lm_0} \sqrt{\frac{4\pi}{15}} \ \Big(\widetilde{\mathbf{G}}^{21}_{LM} \left\langle Y_{l'(m_1-\alpha)} | Z_{LM} | Y_{l(m_0+\alpha)} \right\rangle \\
&\qquad\qquad - i\alpha \widetilde{\mathbf{G}}^{2-1}_{LM} \left\langle Y_{l'(m_1-\alpha)} | Z_{LM} | Y_{l(m_0+\alpha)} \right\rangle \Big) \\
&\quad + S^{-\alpha}_{l'm_1} m_0 \frac{1}{3} \left(\sqrt{\frac{16\pi}{5}} \ \widetilde{\mathbf{G}}^{20}_{LM} \left\langle Y_{l'(m_1-\alpha)} | Z_{LM} | Y_{lm_0} \right\rangle + \mathbf{C}^{lm_0}_{l'(m_1-\alpha)} \right) \\
&\quad - m_1 m_0 \sqrt{\frac{4\pi}{15}} \ \Big(\widetilde{\mathbf{G}}^{21}_{LM} \left\langle Y_{l'm_1} | Z_{LM} | Y_{lm_0} \right\rangle + i\alpha \widetilde{\mathbf{G}}^{2-1}_{LM} \left\langle Y_{l'm_1} | Z_{LM} | Y_{lm_0} \right\rangle \Big) \\
&\quad + m_1 S^{+\alpha}_{lm_0} \frac{1}{3} \left(\sqrt{\frac{16\pi}{5}} \ \widetilde{\mathbf{G}}^{20}_{LM} \left\langle Y_{l'm_1} | Z_{LM} | Y_{l(m_0+\alpha)} \right\rangle + \mathbf{C}^{l(m_0+\alpha)}_{l'm_1} \right) \Big] \\
&\quad + \delta_{\alpha\alpha'} \cdot \hbar^2 \Big[S^{+\alpha}_{l'm_1} m_0 \sqrt{\frac{4\pi}{15}} \ \Big(\alpha \widetilde{\mathbf{G}}^{21}_{LM} \left\langle Y_{l'(m_1+\alpha)} | Z_{LM} | Y_{lm_0} \right\rangle \\
&\qquad\qquad + i \widetilde{\mathbf{G}}^{2-1}_{LM} \left\langle Y_{l'(m_1+\alpha)} | Z_{LM} | Y_{lm_0} \right\rangle \Big) \\
&\quad - \frac{\alpha}{3} S^{+\alpha}_{l'm_1} S^{+\alpha}_{lm_0} \left(\sqrt{\frac{16\pi}{5}} \ \widetilde{\mathbf{G}}^{20}_{LM} \left\langle Y_{l'(m_1+\alpha)} | Z_{LM} | Y_{l(m_0+\alpha)} \right\rangle + \mathbf{C}^{l(m_0+\alpha)}_{l'(m_1+\alpha)} \right)
\end{aligned}
$$

$$
\begin{aligned}
&+ m_1 S^{+\alpha}_{lm_0}\sqrt{\frac{4\pi}{15}}\ \Big(\alpha\widetilde{\mathbf{G}}^{21}_{LM}\left\langle Y_{l'm_1}|Z_{LM}|Y_{l(m_0+\alpha)}\right\rangle \\
&\qquad\qquad -i\widetilde{\mathbf{G}}^{2-1}_{LM}\left\langle Y_{l'm_1}|Z_{LM}|Y_{l(m_0+\alpha)}\right\rangle\Big) \\
&+ \frac{\alpha}{3}m_1m_0\left(\sqrt{\frac{16\pi}{5}}\ \widetilde{\mathbf{G}}^{20}_{LM}\left\langle Y_{l'm_1}|Z_{LM}|Y_{lm_0}\right\rangle + \mathbf{C}^{lm_0}_{l'm_1}\right)\Big]\Big\} \\
&= \langle\phi|\Delta|\phi\rangle\,\mathbf{n}^{\mathbf{R}}_{\mathbf{q}\lambda}\sum_{m_0,m_1,LM} K^*_{l'm'm_1}K_{lmm_0}\hbar^2\cdot \\
&\Big\{\delta_{-\alpha\alpha'}\cdot\Big[S^{-\alpha}_{l'm_1}S^{+\alpha}_{lm_0}\sqrt{\frac{4\pi}{15}}\ C_{l'(m_1-\alpha),LM,l(m_0+\alpha)}\left(\widetilde{\mathbf{G}}^{21}_{LM} - i\alpha\widetilde{\mathbf{G}}^{2-1}_{LM}\right) \\
&\quad + S^{-\alpha}_{l'm_1}m_0\frac{1}{3}\left(\sqrt{\frac{16\pi}{5}}\ \widetilde{\mathbf{G}}^{20}_{LM}C_{l'(m_1-\alpha),LM,lm_0} + \mathbf{C}^{lm_0}_{l'(m_1-\alpha)}\right) \\
&\quad - m_1m_0\sqrt{\frac{4\pi}{15}}\ C_{l'm_1,LM,lm_0}\left(\widetilde{\mathbf{G}}^{21}_{LM} + i\alpha\widetilde{\mathbf{G}}^{2-1}_{LM}\right) \\
&\quad + m_1S^{+\alpha}_{lm_0}\frac{1}{3}\left(\sqrt{\frac{16\pi}{5}}\ \widetilde{\mathbf{G}}^{20}_{LM}C_{l'm_1,LM,l(m_0+\alpha)} + \mathbf{C}^{l(m_0+\alpha)}_{l'm_1}\right)\Big] \\
&+ \delta_{\alpha\alpha'}\cdot\Big[S^{+\alpha}_{l'm_1}m_0\sqrt{\frac{4\pi}{15}}\ C_{l'(m_1+\alpha),LM,lm_0}\left(\alpha\widetilde{\mathbf{G}}^{21}_{LM} + i\widetilde{\mathbf{G}}^{2-1}_{LM}\right) \\
&\quad - \frac{\alpha}{3}S^{+\alpha}_{l'm_1}S^{+\alpha}_{lm_0}\left(\sqrt{\frac{16\pi}{5}}\ \widetilde{\mathbf{G}}^{20}_{LM}C_{l'(m_1+\alpha),LM,l(m_0+\alpha)} + \mathbf{C}^{l(m_0+\alpha)}_{l'(m_1+\alpha)}\right) \\
&\quad + m_1S^{+\alpha}_{lm_0}\sqrt{\frac{4\pi}{15}}\ C_{l'm_1,LM,l(m_0+\alpha)}\left(\alpha\widetilde{\mathbf{G}}^{21}_{LM} - i\widetilde{\mathbf{G}}^{2-1}_{LM}\right) \\
&\quad + \frac{\alpha}{3}m_1m_0\left(\sqrt{\frac{16\pi}{5}}\ \widetilde{\mathbf{G}}^{20}_{LM}C_{l'm_1,LM,lm_0} + \mathbf{C}^{lm_0}_{l'm_1}\right)\Big]\Big\}. \qquad \text{(A.39)}
\end{aligned}
$$

B Non-spin-diagonal matrix element (Yafet part)

The non-spin-diagonal matrix element $\langle \Phi_{\mathbf{R}l'm'\alpha'} | \widetilde{W}'^{nsd}_{\lambda,\mathbf{R}} | \Phi_{\mathbf{R}lm\alpha} \rangle$ is calculated in this chapter. The scattering operator only applies to the large component and reads (see eq. (6.29))

$$\widetilde{W}'_{\lambda,\mathbf{R}} = \sum_i \mathbf{n}^{\mathbf{R}}_{\mathbf{q}\lambda} \left\{ \mathbf{e}_{r_\mathbf{R}} \frac{1}{r_\mathbf{R}} \frac{\partial \xi(r_\mathbf{R})}{\partial r_\mathbf{R}} (\widehat{\mathbf{L}}_\mathbf{R})_i \, \underline{\underline{\widehat{\sigma}}}_i + \mathbf{e}_{\vartheta_\mathbf{R}} \frac{\xi(r_\mathbf{R})}{r_\mathbf{R}} (\mathbf{e}_{\vartheta_\mathbf{R}} \times \widehat{\mathbf{p}})_i \, \underline{\underline{\widehat{\sigma}}}_i + \mathbf{e}_{\phi_\mathbf{R}} \frac{\xi(r_\mathbf{R})}{r_\mathbf{R}} (\mathbf{e}_{\phi_\mathbf{R}} \times \widehat{\mathbf{p}})_i \, \underline{\underline{\widehat{\sigma}}}_i \right\}. \tag{B.1}$$

In the following the representation of the momentum operator and of the angular momentum operator in spherical coordinates is used (see eq. (6.11))

$$\widehat{\mathbf{p}} = -i\hbar \nabla_\mathbf{r} = -i\hbar \left(\mathbf{e}_r \frac{\partial}{\partial r} + \mathbf{e}_\vartheta \frac{1}{r} \frac{\partial}{\partial \vartheta} + \mathbf{e}_\phi \frac{1}{r \sin\vartheta} \frac{\partial}{\partial \phi} \right) \tag{B.2}$$

$$\widehat{\mathbf{L}} = -i\hbar (\mathbf{r} \times \nabla_\mathbf{r}) = -i\hbar r (\mathbf{e}_r \times \nabla_\mathbf{r}) = -i\hbar r \left(\mathbf{e}_\phi \frac{1}{r} \frac{\partial}{\partial \vartheta} - \mathbf{e}_\vartheta \frac{1}{r \sin\vartheta} \frac{\partial}{\partial \phi} \right) \tag{B.3}$$

and the index $\mathbf{R}$ is omitted for a better readability:

$$\begin{aligned} \widetilde{W}'_\lambda = \sum_i \mathbf{n}_{\mathbf{q}\lambda} \Bigg\{ & \mathbf{e}_r \frac{1}{r} \frac{\partial \xi(r)}{\partial r} \widehat{\mathbf{L}}_i \, \underline{\underline{\widehat{\sigma}}}_i \\ & - i\hbar \, \mathbf{e}_\vartheta \frac{\xi(r)}{r} \left(\mathbf{e}_\vartheta \times \mathbf{e}_r \frac{\partial}{\partial r} + \mathbf{e}_\vartheta \times \mathbf{e}_\phi \frac{1}{r \sin\vartheta} \frac{\partial}{\partial \phi} \right)_i \underline{\underline{\widehat{\sigma}}}_i \\ & - i\hbar \, \mathbf{e}_\phi \frac{\xi(r)}{r} \left(\mathbf{e}_\phi \times \mathbf{e}_r \frac{\partial}{\partial r} + \mathbf{e}_\phi \times \mathbf{e}_\vartheta \frac{1}{r} \frac{\partial}{\partial \vartheta} \right)_i \underline{\underline{\widehat{\sigma}}}_i \Bigg\} \end{aligned}$$

$$
\begin{aligned}
=&\sum_i \mathbf{n}_{\mathbf{q}\lambda}\,\Big\{\mathbf{e}_r\;\frac{1}{r}\frac{\partial\xi(r)}{\partial r}\widehat{\mathbf{L}}_i\;\underline{\widehat{\sigma}}_i\\
&-i\hbar\;\mathbf{e}_\vartheta\;\frac{\xi(r)}{r}\left(-\mathbf{e}_\phi\frac{\partial}{\partial r}+\mathbf{e}_r\;\frac{1}{r\sin\vartheta}\frac{\partial}{\partial\phi}\right)_i\underline{\widehat{\sigma}}_i\\
&-i\hbar\;\mathbf{e}_\phi\;\frac{\xi(r)}{r}\left(\mathbf{e}_\vartheta\frac{\partial}{\partial r}-\mathbf{e}_r\;\frac{1}{r}\frac{\partial}{\partial\vartheta}\right)_i\underline{\widehat{\sigma}}_i\Big\}\\
=&\sum_i \mathbf{n}_{\mathbf{q}\lambda}\,\Big\{\mathbf{e}_r\;\frac{1}{r}\frac{\partial\xi(r)}{\partial r}\widehat{\mathbf{L}}_i\;\underline{\widehat{\sigma}}_i\\
&-i\hbar\;\frac{\xi(r)}{r}\Big(-\mathbf{e}_\vartheta\;(\mathbf{e}_\phi)_i\frac{\partial}{\partial r}+\mathbf{e}_\phi\;(\mathbf{e}_\vartheta)_i\frac{\partial}{\partial r}\Big)\underline{\widehat{\sigma}}_i\\
&-i\hbar\;\frac{\xi(r)}{r}(\mathbf{e}_r)_i\;\underbrace{\left(\mathbf{e}_\vartheta\;\frac{1}{r\sin\vartheta}\frac{\partial}{\partial\phi}-\mathbf{e}_\phi\;\;\frac{1}{r}\frac{\partial}{\partial\vartheta}\right)}_{\widehat{\mathbf{L}}/(i\hbar r)}\underline{\widehat{\sigma}}_i\Big\}\\
=&\sum_i \mathbf{n}_{\mathbf{q}\lambda}\,\Big\{\mathbf{e}_r\;\frac{1}{r}\frac{\partial\xi(r)}{\partial r}\widehat{\mathbf{L}}_i\;\underline{\widehat{\sigma}}_i\\
&-i\hbar\;\frac{\xi(r)}{r}\frac{\partial}{\partial r}\Big[\Big(-\mathbf{e}_\vartheta\;(\mathbf{e}_\phi)_i+\mathbf{e}_\phi\;(\mathbf{e}_\vartheta)_i\Big)\underline{\widehat{\sigma}}_i\Big]-i\hbar\;\frac{\xi(r)}{r}(\mathbf{e}_r)_i\;\frac{1}{i\hbar r}\widehat{\mathbf{L}}\;\underline{\widehat{\sigma}}_i\Big\}\\
=&\mathbf{n}_{\mathbf{q}\lambda}\,\Big\{\mathbf{e}_r\;\frac{1}{r}\frac{\partial\xi(r)}{\partial r}\sum_i\widehat{\mathbf{L}}_i\;\underline{\widehat{\sigma}}_i\\
&-i\hbar\;\frac{\xi(r)}{r}\frac{\partial}{\partial r}\Big[\Big\{\begin{pmatrix}\cos\vartheta\cos\phi\\ \cos\vartheta\sin\phi\\ -\sin\vartheta\end{pmatrix}\cdot\sin\phi+\begin{pmatrix}-\sin\phi\\ \cos\phi\\ 0\end{pmatrix}\cdot\cos\vartheta\cos\phi\Big\}\underline{\widehat{\sigma}}_x\\
&\qquad+\Big\{-\begin{pmatrix}\cos\vartheta\cos\phi\\ \cos\vartheta\sin\phi\\ -\sin\vartheta\end{pmatrix}\cdot\cos\phi+\begin{pmatrix}-\sin\phi\\ \cos\phi\\ 0\end{pmatrix}\cdot\cos\vartheta\sin\phi\Big\}\underline{\widehat{\sigma}}_y\\
&\qquad+\Big\{-\begin{pmatrix}\cos\vartheta\cos\phi\\ \cos\vartheta\sin\phi\\ -\sin\vartheta\end{pmatrix}\cdot 0+\begin{pmatrix}-\sin\phi\\ \cos\phi\\ 0\end{pmatrix}\cdot(-\sin\vartheta)\Big\}\underline{\widehat{\sigma}}_z\Big]\\
&-\frac{\xi(r)}{r^2}\sum_i(\mathbf{e}_r)_i\;\underline{\widehat{\sigma}}_i\;\widehat{\mathbf{L}}\Big\}
\end{aligned}
$$

$$
\begin{aligned}
=&\mathbf{n}_{\mathbf{q}\lambda}\,\Big\{\mathbf{e}_r\;\frac{1}{r}\frac{\partial\xi(r)}{\partial r}\sum_i \widehat{\mathbf{L}}_i\;\underline{\underline{\widehat{\sigma}}}_i \\
&-i\hbar\;\frac{\xi(r)}{r}\frac{\partial}{\partial r}\Big[\begin{pmatrix}0\\ \cos\vartheta\\ -\sin\vartheta\sin\phi\end{pmatrix}\underline{\underline{\widehat{\sigma}}}_x+\begin{pmatrix}-\cos\vartheta\\ 0\\ \sin\vartheta\cos\phi\end{pmatrix}\underline{\underline{\widehat{\sigma}}}_y \\
&\qquad\qquad+\begin{pmatrix}\sin\vartheta\sin\phi\\ -\sin\vartheta\cos\phi\\ 0\end{pmatrix}\underline{\underline{\widehat{\sigma}}}_z\Big] \\
&-\frac{\xi(r)}{r^2}\big\{\sin\vartheta\cos\phi\;\underline{\underline{\widehat{\sigma}}}_x+\sin\vartheta\sin\phi\;\underline{\underline{\widehat{\sigma}}}_y+\cos\vartheta\;\underline{\underline{\widehat{\sigma}}}_z\big\}\widehat{\mathbf{L}}\Big\}. \qquad \text{(B.4)}
\end{aligned}
$$

The non-spin-diagonal matrix element reads

$\langle\Phi_{l'm'\alpha'}|\widetilde{W'}_\lambda^{nsd}|\Phi_{lm\alpha}\rangle$

$$
\begin{aligned}
=\mathbf{n}_{\mathbf{q}\lambda}\;&\Big\{\Big\langle\phi_{l'\alpha'}\Big|\frac{1}{r}\frac{\partial\xi(r)}{\partial r}\Big|\phi_{l\alpha}\Big\rangle\sum_i\langle Z_{l'm'}|\mathbf{e}_r\;\widehat{\mathbf{L}}_i\;|Z_{lm}\rangle\langle\chi_{\alpha'}|\underline{\underline{\widehat{\sigma}}}_i|\chi_\alpha\rangle \qquad \text{(B.5)}\\
&-i\hbar\;\Big\langle\phi_{l'\alpha'}\Big|\frac{\xi(r)}{r}\frac{\partial}{\partial r}\Big|\phi_{l\alpha}\Big\rangle\cdot \\
&\quad\Big[\langle Z_{l'm'}|\begin{pmatrix}0\\ \cos\vartheta\\ -\sin\vartheta\sin\phi\end{pmatrix}|Z_{lm}\rangle\langle\chi_{\alpha'}|\underline{\underline{\widehat{\sigma}}}_x|\chi_\alpha\rangle \\
&\quad+\langle Z_{l'm'}|\begin{pmatrix}-\cos\vartheta\\ 0\\ \sin\vartheta\cos\phi\end{pmatrix}|Z_{lm}\rangle\langle\chi_{\alpha'}|\underline{\underline{\widehat{\sigma}}}_y|\chi_\alpha\rangle \\
&\quad+\langle Z_{l'm'}|\begin{pmatrix}\sin\vartheta\sin\phi\\ -\sin\vartheta\cos\phi\\ 0\end{pmatrix}|Z_{lm}\rangle\langle\chi_{\alpha'}|\underline{\underline{\widehat{\sigma}}}_z|\chi_\alpha\rangle\Big] \qquad \text{(B.6)}\\
&-\Big\langle\phi_{l'\alpha'}\Big|\frac{\xi(r)}{r^2}\Big|\phi_{l\alpha}\Big\rangle\cdot\big\{\langle Z_{l'm'}|\sin\vartheta\cos\phi\;\widehat{\mathbf{L}}|Z_{lm}\rangle\langle\chi_{\alpha'}|\underline{\underline{\widehat{\sigma}}}_x|\chi_\alpha\rangle \\
&\qquad\qquad+\langle Z_{l'm'}|\sin\vartheta\sin\phi\;\widehat{\mathbf{L}}|Z_{lm}\rangle\langle\chi_{\alpha'}|\underline{\underline{\widehat{\sigma}}}_y|\chi_\alpha\rangle \\
&\qquad\qquad+\langle Z_{l'm'}|\cos\vartheta\;\widehat{\mathbf{L}}|Z_{lm}\rangle\langle\chi_{\alpha'}|\underline{\underline{\widehat{\sigma}}}_z|\chi_\alpha\rangle\big\}\qquad\Big\}. \qquad \text{(B.7)}
\end{aligned}
$$

All radial integrals have to calculated numerically whereas the angular and spin integrals are calculated analytically: The spin integrals are evaluated with eq. (A.16). The angular integral of equation-part (B.5) can be calculated analogously to the third line of eq. (A.13). The angular integrals of equation-part (B.6) are represented as Gaunt coefficients, eq. (A.6). The angular integrals of equation-part (B.7) are calculated with Maple. Finally, the matrix element reads

$$\langle \Phi_{l'm'\alpha'} | \widetilde{W'}_{\lambda}^{nsd} | \Phi_{lm\alpha} \rangle$$

$$\begin{aligned}
= \mathbf{n}_{\mathbf{q}\lambda} \Bigg\{ & \left\langle \phi_{l'\alpha'} \left| \frac{1}{r} \frac{\partial \xi(r)}{\partial r} \right| \phi_{l\alpha} \right\rangle \sum_{\substack{m_0=-l \\ m_1=-l'}}^{\substack{m_1=l' \\ m_0=l}} K^*_{l'm'm_1} K_{lmm_0} \hbar \cdot \\
& \qquad \left[\delta_{-\alpha\alpha'} S^{+\alpha}_{lm_0} \mathbf{C}^{l(m_0+\alpha)}_{l'm_1} + \delta_{\alpha\alpha'} \alpha m_0 \mathbf{C}^{lm_0}_{l'm_1} \right] \\
& - i\hbar \left\langle \phi_{l'\alpha'} \left| \frac{\xi(r)}{r} \frac{\partial}{\partial r} \right| \phi_{l\alpha} \right\rangle \cdot \sqrt{\frac{4\pi}{3}} \cdot \\
& \quad \Bigg[\begin{pmatrix} 0 \\ \widetilde{G}_{l'm',10,lm} \\ -\widetilde{G}_{l'm',1-1,lm} \end{pmatrix} \delta_{-\alpha\alpha'} + \begin{pmatrix} -\widetilde{G}_{l'm',10,lm} \\ 0 \\ \widetilde{G}_{l'm',11,lm} \end{pmatrix} i\alpha\delta_{-\alpha\alpha'} \\
& \quad + \begin{pmatrix} \widetilde{G}_{l'm',1-1,lm} \\ -\widetilde{G}_{l'm',11,lm} \\ 0 \end{pmatrix} \alpha\delta_{\alpha\alpha'} \Bigg] \\
& - \left\langle \phi_{l'\alpha'} \left| \frac{\xi(r)}{r^2} \right| \phi_{l\alpha} \right\rangle \cdot \Big\{ \langle Z_{l'm'} | \sin\vartheta \cos\phi \ \widehat{\mathbf{L}} | Z_{lm} \rangle \ \delta_{-\alpha\alpha'} \\
& \qquad + \langle Z_{l'm'} | \sin\vartheta \sin\phi \ \widehat{\mathbf{L}} | Z_{lm} \rangle \ i\alpha\delta_{-\alpha\alpha'} \\
& \qquad + \langle Z_{l'm'} | \cos\vartheta \ \widehat{\mathbf{L}} | Z_{lm} \rangle \ \alpha\delta_{\alpha\alpha'} \Big\} \qquad \Bigg\}. \qquad \text{(B.8)}
\end{aligned}$$

Bibliography

[1] E. Beaurepaire, J. C. Merle, A. Daunois, and J.-Y. Bigot, Phys. Rev. Lett. **76**, 4250 (1996)

[2] M. Agranat, S. Ashikov, A. Granovskii, and G. Rukman, Sov. Phys. JETP **59**, 804 (1984)

[3] A. Vaterlaus, T. Beutler, and F. Meier, Phys. Rev. Lett. **67**, 3314 (1991)

[4] A. Vaterlaus, T. Beutler, D. Guarisco, M. Lutz, and F. Meier, Phys. Rev. B **46**, 5280 (1992)

[5] C. D. Stanciu, F. Hansteen, A. V. Kimel, A. Kirilyuk, A. Tsukamoto, A. Itoh, and T. Rasing, Phys. Rev. Lett. **99**, 047601 (2007)

[6] I. Radu, K. Vahaplar, C. Stamm, T. Kachel, N. Pontius, H. A. Dürr, T. A. Ostler, J. Barker, R. F. L. Evans, R. W. Chantrell, A. Tsukamoto, A. Itoh, A. Kirilyuk, T. Rasing, and A. V. Kimel, Nature **472**, 205 (2011)

[7] U. Bovensiepen, J. Phys.: Condens. Matter **19**, 083201 (2007)

[8] M. Fähnle and C. Illg, J. Phys.: Condens. Matter **23**, 493201 (2011)

[9] O. Grotheer, *Ab-initio Berechnungen der Spinwellenspektren von Eisen, Kobalt und Nickel*, Ph.D. thesis, Max Planck Institute for Metals Research and University of Stuttgart (2001)

[10] C. Ederer, *Theorie magneto-optischer Effekte im Röntgenbereich und Anwendungen auf niedrigdimensionale magnetische Systeme*, Ph.D. thesis, Max Planck Institute for Metals Research and University of Stuttgart (2003)

[11] B. Meyer, *Entwicklung eines neuen ab-initio "mixed basis"- Pseudopotentialprogramms und Untersuchung atomarer Fehlstellen in Molybdän und intermetallischen Verbindungen*, Ph.D. thesis, Max Planck Institute for Metals Research and University of Stuttgart (1998)

[12] C. Illg, *Ab-initio Elliott-Yafet modeling of ultrafast demagnetization after laser irradiation*, Diploma thesis, Max Planck Institute for Metals Research and University of Stuttgart (2009)

[13] J. P. Perdew, K. Burke, and M. Ernzerhof, Phys. Rev. Lett. **77**, 3865 (1996)

[14] D. Vanderbilt, Phys. Rev. B **41**, 7892 (1990)

[15] P. Giannozzi, S. Baroni, N. Bonini, M. Calandra, R. Car, C. Cavazzoni, D. Ceresoli, G. L. Chiarotti, M. Cococcioni, I. Dabo, A. D. Corso, S. de Gironcoli, S. Fabris, G. Fratesi, R. Gebauer, U. Gerstmann, C. Gougoussis, A. Kokalj, M. Lazzeri, L. Martin-Samos, N. Marzari, F. Mauri, R. Mazzarello, S. Paolini, A. Pasquarello, L. Paulatto, C. Sbraccia, S. Scandolo, G. Sclauzero, A. P. Seitsonen, A. Smogunov, P. Umari, and R. M. Wentzcovitch, J. Phys.: Condens. Matter **21**, 395502 (2009)

[16] V. López-Flores, J. Arabski, C. Stamm, V. Halté, N. Pontius, E. Beaurepaire, and C. Boeglin, Phys. Rev. B **86**, 014424 (2012)

[17] C. Boeglin, E. Beaurepaire, V. Halté, V. López-Flores, C. Stamm, N. Pontius, H. A. Dürr, and J.-Y. Bigot, Nature **465**, 458 (2010)

[18] B. Koopmans, G. Malinowski, F. Dalla Longa, D. Steiauf, M. Fähnle, T. Roth, M. Cinchetti, and M. Aeschlimann, Nat. Mater. **9**, 259 (2010)

[19] N. W. Ashcroft and N. D. Mermin, *Solid State Physics*, 1st ed. (Brooks Cole, 1976)

[20] Y. S. Touloukian, R. K. Kirby, R. E. Taylor, and P. D. Desai, *Thermal Expansion: Metallic Elements and Alloys*, 1st ed. (IFI/Plenum, 1975)

[21] E. Fawcett, R. Griessen, W. Joss, and W. Kress, in *Landolt-Börnstein*, Vol. 13, edited by K.-H. Hellwege and J. L. Olsen (Springer, Berlin, 1983)

[22] D. Steiauf, C. Illg, and M. Fähnle, J. Phys.: Conf. Ser. **200**, 042024 (2010)

[23] D. Steiauf and M. Fähnle, Phys. Rev. B **79**, 140401(R) (2009)

[24] P. Brüesch, *Phonons: Theory and Experiments I*, 1st ed. (Springer, 1982)

[25] G. L. Squires, Ark. Fys. **25**, 21 (1962)

[26] C. Illg, B. Meyer, and M. Fähnle, Phys. Rev. B **86**, 174309 (2012)

[27] H. Kohl, phys. status solidi b **130**, 151 (1985)

[28] H. Spalt, A. Zounek, B. N. Dev, and G. Materlik, Phys. Rev. Lett. **60**, 1868 (1988)

[29] A. Zounek, H. Spalt, and G. Materlik, Z. Phys. B **92**, 21 (1993)

[30] R. J. Birgeneau, J. Cordes, G. Dolling, and A. D. B. Woods, Phys. Rev. **136**, A1359 (1964)

[31] M. Kresch, O. Delaire, R. Stevens, J. Y. Y. Lin, and B. Fultz, Phys. Rev. B **75**, 104301 (2007)

[32] A. J. E. Foreman and W. M. Lomer, Proc. Phys. Soc. London B **70**, 1143 (1957)

[33] R. S. Leigh, B. Szigeti, and V. K. Tewary, Proc. Roy. Soc. London A **320**, 505 (1971)

[34] W. Cochran, Acta Cryst. A **27**, 556 (1971)

[35] S. Baroni, S. de Gironcoli, A. Dal Corso, and P. Giannozzi, Rev. Mod. Phys. **73**, 515 (2001)

[36] A. Dal Corso and S. de Gironcoli, Phys. Rev. B **62**, 273 (2000)

[37] B. Meyer, V. Schott, and M. Fähnle, Phys. Rev. B **58**, R14673 (1998)

[38] H. J. Monkhorst and J. D. Pack, Phys. Rev. B **13**, 5188 (1976)

[39] M. Kresch, M. Lucas, O. Delaire, J. Y. Y. Lin, and B. Fultz, Phys. Rev. B **77**, 024301 (2008)

[40] M. Kresch, *Temperature dependence of phonons in elemental cubic metals studied by inelastic scattering of neutrons and x-rays*, Ph.D. thesis, California Institute of Technology (2009)

[41] S. I. Anisimov, B. L. Kopeliovich, and T. L. Perelman, Sov. Phys. JETP **39**, 375 (1974)

[42] A. Scholl, L. Baumgarten, R. Jacquemin, and W. Eberhardt, Phys. Rev. Lett. **79**, 5146 (1997)

[43] B. Koopmans, M. van Kampen, J. T. Kohlhepp, and W. J. M. de Jonge, Phys. Rev. Lett. **85**, 844 (2000)

[44] G. P. Zhang and W. Hübner, Phys. Rev. Lett. **85**, 3025 (2000)

[45] B. Koopmans, M. van Kampen, and W. J. M. de Jonge, J. Phys.: Condens. Matter **15**, S723 (2003)

[46] B. Koopmans, "Laser-induced magnetization dynamics," in *Spin dynamics in confined magnetic structures II*, edited by B. Hillebrands and K. Ounadjela (Springer, 2002) p. 253

[47] C. Stamm, T. Kachel, N. Pontius, R. Mitzner, T. Quast, K. Holldack, S. Khan, C. Lupulescu, E. F. Aziz, M. Wietstruk, H. A. Dürr, and W. Eberhardt, Nat. Mater. **6**, 740 (2007)

[48] T. Kachel, N. Pontius, C. Stamm, M. Wietstruk, E. F. Aziz, H. A. Dürr, W. Eberhardt, and F. M. F. de Groot, Phys. Rev. B **80**, 092404 (2009)

[49] M. van Kampen, J. T. Kohlhepp, W. J. M. de Jonge, B. Koopmans, and R. Coehoorn, J. Phys.: Condens. Matter **17**, 6823 (2005)

[50] H.-S. Rhie, H. A. Dürr, and W. Eberhardt, Phys. Rev. Lett. **90**, 247201 (2003)

[51] X. Wang, S. Nie, J. Li, R. Clinite, J. E. Clark, and J. Cao, Phys. Rev. B **81**, 220301 (2010)

[52] B. Koopmans, J. J. M. Ruigrok, F. Dalla Longa, and W. J. M. de Jonge, Phys. Rev. Lett. **95**, 267207 (2005)

[53] M. Djordjevic, M. Lüttich, P. Moschkau, P. Guderian, T. Kampfrath, R. G. Ulbrich, M. Münzenberg, W. Felsch, and J. S. Moodera, phys. status solidi c **3**, 1347 (2006)

[54] J.-Y. Bigot, M. Vomir, and E. Beaurepaire, Nat. Phys. **5**, 515 (2009)

[55] G. P. Zhang, W. Hübner, G. Lefkidis, Y. Bai, and T. F. George, Nat. Phys. **5**, 499 (2009)

[56] M. S. Si and G. P. Zhang, J. Phys.: Condens. Matter **22**, 076005 (2010)

[57] K. Carva, M. Battiato, and P. M. Oppeneer, Nat. Phys. **7**, 665 (2011)

[58] F. Dalla Longa, J. T. Kohlhepp, W. J. M. de Jonge, and B. Koopmans, Phys. Rev. B **75**, 224431 (2007)

[59] A. Eschenlohr, M. Battiato, P. Maldonado, N. Pontius, T. Kachel, K. Holldack, R. Mitznerand, A. Föhlisch, P. M. Oppeneer, and C. Stamm, Nat. Mater. **12**, 332 (2013)

[60] T. Roth, A. J. Schellekens, S. Alebrand, O. Schmitt, D. Steil, B. Koopmans, M. Cinchetti, and M. Aeschlimann, Phys. Rev. X **2**, 021006 (2012)

[61] E. Beaurepaire, G. M. Turner, S. M. Harrel, M. C. Beard, J.-Y. Bigot, and C. A. Schmuttenmaer, Appl. Phys. Lett. **84**, 3465 (2004)

[62] D. J. Hilton, R. D. Averitt, C. A. Meserole, G. L. Fisher, D. J. Funk, J. D. Thompson, and A. J. Taylor, Opt. Lett. **29**, 1805 (2004)

[63] R. J. Elliott, Phys. Rev. **96**, 266 (1954)

[64] Y. Yafet, in *Solid State Physics*, Vol. 14, edited by F. Seitz and D. Turnbull (Academic, New York, 1963)

[65] F. Beuneu and P. Monod, Phys. Rev. B **18**, 2422 (1978)

[66] B. Koopmans, H. H. J. E. Kicken, M. van Kampen, and W. J. M. de Jonge, J. Magn. Magn. Mater. **286**, 271 (2005)

[67] M. Krauß, T. Roth, S. Alebrand, D. Steil, M. Cinchetti, M. Aeschlimann, and H. C. Schneider, Phys. Rev. B **80**, 180407(R) (2009)

[68] S. Essert and H. C. Schneider, Phys. Rev. B **84**, 224405 (2011)

[69] E. Carpene, E. Mancini, C. Dallera, M. Brenna, E. Puppin, and S. D. Silvestri, Phys. Rev. B **78**, 174422 (2008)

[70] A. B. Schmidt, M. Pickel, M. Donath, P. Buczek, A. Ernst, V. P. Zhukov, P. M. Echenique, L. M. Sandratskii, E. V. Chulkov, and M. Weinelt, Phys. Rev. Lett. **105**, 197401 (2010)

[71] K. Carva, M. Battiato, and P. M. Oppeneer, Phys. Rev. Lett. **107**, 207201 (2011)

[72] K. Carva, M. Battiato, D. Legut, and P. M. Oppeneer, Phys. Rev. B **87**, 184425 (2013)

[73] S. Essert and H. C. Schneider, J. Appl. Phys. **111**, 07C514 (2012)

[74] C. Stamm, N. Pontius, T. Kachel, M. Wietstruk, and H. A. Dürr, Phys. Rev. B **81**, 104425 (2010)

[75] A. J. Schellekens and B. Koopmans, Phys. Rev. Lett. **110**, 217204 (2013)

[76] J. Stöhr and H. C. Siegmann, *Magnetism — From Fundamentals to Nanoscale Dynamics*, 1st ed. (Springer, 2006)

[77] M. Battiato, K. Carva, and P. M. Oppeneer, Phys. Rev. Lett. **105**, 027203 (2010)

[78] M. Haag, C. Illg, and M. Fähnle, Phys. Rev. B **87**, 214427 (2013)

[79] U. Atxitia, O. Chubykalo-Fesenko, J. Walowski, A. Mann, and M. Münzenberg, Phys. Rev. B **81**, 174401 (2010)

[80] M. Battiato, K. Carva, and P. M. Oppeneer, Phys. Rev. B **86**, 024404 (2012)

[81] A. Melnikov, I. Razdolski, T. O. Wehling, E. T. Papaioannou, V. Roddatis, P. Fumagalli, O. Aktsipetrov, A. I. Lichtenstein, and U. Bovensiepen, Phys. Rev. Lett. **107**, 076601 (2011)

[82] D. Rudolf, C. La-O-Vorakiat, M. Battiato, R. Adam, J. M. Shaw, E. Turgut, P. Maldonado, S. Mathias, P. Grychtol, H. T. Nembach, T. J. Silva, M. Aeschlimann, H. C. Kapteyn, M. M. Murnane, C. M. Schneider, and P. M. Oppeneer, Nat. Commun. **3**, 1037 (2012)

[83] B. Pfau, S. Schaffert, L. Mueller, C. Gutt, A. Al-Shemmary, F. Buettner, R. Delaunay, S. Duesterer, S. Flewett, R. Froemter, J. Geilhufe, E. Guehrs, C. M. Guenther, R. Hawaldar, M. Hille, N. Jaouen, A. Kobs, K. Li, J. Mohanty, H. Redlin, W. F. Schlotter, D. Stickler, R. Treusch, B. Vodungbo, M. Klaeui, H. P. Oepen, J. Luening, G. Gruebel, and S. Eisebitt, Nat. Commun. **3**, 1100 (2012)

[84] B. Vodungbo, J. Gautier, G. Lambert, A. B. Sardinha, M. Lozano, S. Sebban, M. Ducousso, W. Boutu, K. Li, B. Tudu, M. Tortarolo, R. Hawaldar, R. Delaunay, V. Lopez-Flores, J. Arabski, C. Boeglin, H. Merdji, P. Zeitoun, and J. Luening, Nat. Commun. **3**, 999 (2012)

[85] A. J. Schellekens, W. Verhoeven, T. N. Vader, and B. Koopmans, Appl. Phys. Lett. **102**, 252408 (2013)

[86] E. Turgut, C. La-O-Vorakiat, J. M. Shaw, P. Grychtol, H. T. Nembach, D. Rudolf, R. Adam, M. Aeschlimann, C. M. Schneider, T. J. Silva, M. M. Murnane, H. C. Kapteyn, and S. Mathias, Phys. Rev. Lett. **110**, 197201 (2013)

[87] M. Fähnle, M. Haag, and C. Illg, J. Magn. Magn. Mater. **347**, 45 (2013)

[88] A. Einstein and W. J. de Haas, Verhandl. Deuts. Phys. Ges. **17**, 152 (1915)

[89] B. Koopmans, "Time-resolved Kerr-effect and Spin Dynamics in Itinerant Ferromagnets," in *Handbook of Magnetism and Advanced Magnetic Materials*, edited by H. Kronmüller and S. Parkin (Wiley, 2007) p. 1589

[90] G. P. Zhang and T. F. George, Phys. Rev. B **78**, 052407 (2008)

[91] L. Chaput, A. Togo, I. Tanaka, and G. Hug, Phys. Rev. B **84**, 094302 (2011)

[92] N. Teeny, *Quantum kinetic theory for demagnetization after femtosecond laser pulses*, Master's thesis, Max Planck Institute for Intelligent Systems and University of Stuttgart (2013)

[93] N. Teeny and M. Fähnle, J. Phys. A: Math. Theor. **46**, 385302 (2013)

[94] J. Schilp, T. Kuhn, and G. Mahler, Phys. Rev. B **50**, 5435 (1994)

[95] A. G. McLellan, J. Phys. C: Solid State Phys. **21**, 1177 (1988)

[96] C. Grimaldi and P. Fulde, Phys. Rev. B **55**, 15523 (1997)

[97] A. K. Rajagopal and M. Mochena, Phys. Rev. B **57**, 11582 (1998)

[98] B. Y. Mueller, T. Roth, M. Cinchetti, M. Aeschlimann, and B. Rethfeld, New J. Phys. **13**, 123010 (2011)

[99] B. Y. Mueller and B. Rethfeld, Phys. Rev. B **87**, 035139 (2013)

[100] D. Steiauf, C. Illg, and M. Fähnle, J. Magn. Magn. Mater. **322**, L5 (2010)

[101] J. Fabian and S. Das Sarma, Phys. Rev. Lett. **81**, 5624 (1998)

[102] L. Nordheim, Ann. Phys. **401**, 607 (1931)

[103] W. H. Butler, in *Physics of Transition Metals* (AIP, New York, 1980) p. 505

[104] P. B. Allen, T. P. Beaulac, F. S. Khan, W. H. Butler, F. J. Pinski, and J. C. Swihart, Mat. Res. Soc. Symp. Proc. **63**, 259 (1985)

[105] A. Al-Lehaibi, J. C. Swihart, W. H. Butler, and F. J. Pinski, Phys. Rev. B **36**, 4103 (1987)

[106] D. Glötzel, D. Rainer, and H. R. Schober, Z. Phys. B **35**, 317 (1979)

[107] W. H. Butler, J. J. Olson, J. S. Faulkner, and B. L. Gyorffy, Phys. Rev. B **14**, 3823 (1976)

[108] W. H. Butler, Can. J. Phys. **60**, 735 (1982)

[109] W. H. Press, S. Teukolsky, W. T. Vetterling, and B. P. Flannery, *Numerical Recipes*, 3rd ed. (Cambridge University Press, 2007)

[110] C. Illg, M. Haag, and M. Fähnle, Phys. Rev. B **88**, 214404 (2013)

[111] J. L. Cheng, M. W. Wu, and J. Fabian, Phys. Rev. Lett. **104**, 016601 (2010)

[112] V. F. Gantmakher and Y. B. Levinson, "Carrier scattering in metals and semiconductors," in *Modern Problems in Condensed Matter Sciences*, Vol. 19, edited by V. M. Agranovich and A. A. Maradudin (North-Holland, Amsterdam, 1987)

[113] J. Fabian and M. W. Wu, "Spin relaxation and spin dynamics in semiconductors," in *Handbook of Spin Transport and Magnetism*, Vol. 1, edited by E. Y. Tsymbal and I. Žutić (Chapman and Hall/CRC Press, Boca Raton, 2012)

List of publications

1. D. Steiauf, C. Illg, and M. Fähnle, *Demagnetization on the fs timescale by the Elliott-Yafet mechanism*, Journal of Physics: Conference Series **200**, 042024 (2010)

2. D. Steiauf, C. Illg, and M. Fähnle, *Extension of Yafet's theory of spin relaxation to ferromagnets*, Journal of Magnetism and Magnetic Materials **322**, L5 (2010)

3. M. Fähnle, J. Seib, and C. Illg, *Relating Gilbert damping and ultrafast laser-induced demagnetization*, Physical Review B **82**, 144405 (2010)

4. M. Fähnle, D. Steiauf, and C. Illg, *Generalized Gilbert equation including inertial damping: Derivation from an extended breathing Fermi surface model*, Physical Review B **84**, 172403 (2011)

5. M. Fähnle and C. Illg, *Electron theory of fast and ultrafast dissipative magnetization dynamics*, Journal of Physics: Condensed Matter **23**, 493201 (2011)

6. M. Kammerer, H. Stoll, M. Noske, M. Sproll, M. Weigand, C. Illg, G. Woltersdorf, M. Fähnle, C. Back, and G. Schütz, *Fast spin-wave-mediated magnetic vortex core reversal*, Physical Review B **86**, 134426 (2012)

7. C. Illg, B. Meyer, and M. Fähnle, *Frequencies and polarization vectors of phonons: Results from force constants which are fitted to experimental data or calculated ab initio*, Physical Review B **86**, 174309 (2012)

8. M. Kammerer, M. Sproll, H. Stoll, M. Noske, M. Weigand, C. Illg, M. Fähnle, and G. Schütz, *Delayed magnetic vortex core reversal*, Applied Physics Letters **102**, 012404 (2013)

9. M. Haag, C. Illg, and M. Fähnle, *Theory of scattering of crystal electrons at magnons*, Physical Review B **87**, 214427 (2013)

10. M. Fähnle, M. Haag, and C. Illg, *Is the angular momentum of a ferromagnetic sample after exposure to a fs laser pulse conserved?*, Journal of Magnetism and Magnetic Materials **347**, 45 (2013)

11. C. Illg, M. Haag, and M. Fähnle, *Ultrafast demagnetization after laser irradiation in transition metals: ab-initio calculations of the spin-flip electron-phonon scattering with reduced exchange splitting*, Physical Review B **88**, 214404 (2013)

12. M. Fähnle, D. Steiauf, and C. Illg, *Erratum: Generalized Gilbert equation including inertial damping: Derivation from an extended breathing Fermi surface model*, Physical Review B **88**, 219905(E) (2013)

13. C. Illg, M. Haag, and M. Fähnle, *Ultrafast demagnetization after laser pulse irradiation in Ni: Ab-initio electron-phonon scattering and phase space calculations*, Proceedings of the Ultrafast Magnetism Conference Strasbourg, in press (2014)

Danksagung

Ich bedanke mich bei allen, die mir beim Gelingen dieser Arbeit geholfen haben:

- Prof. Dr. Manfred Fähnle für die Möglichkeit in seiner Gruppe zu promovieren, für die vielen wissenschaftlichen und nicht-wissenschaftlichen Diskussionen und für seine fachliche Begeisterung und Neugierde.
- Prof. Dr. Günter Wunner für die freundliche Übernahme des Mitberichts.
- Dr. Lothar Schimmele für die vorübergehende Betreuung und für viele lange Diskussionen, die meinen Horizont erweitert haben.
- Dr. Sergej Subkow für seine Hilfsbereitschaft und seinen Optimismus.
- Michael Haag, Michael Kopp und Nicolas Teeny für die tolle, kollegiale Zusammenarbeit und für viele Diskussionen über ultraschnelle Entmagnetisierung, Numerik und Modellierung.
- Franz-Werner Gergen und Heinz Schühle für die Hilfe bei der Administration des Abteilungsservers.
- Abteilung Schütz für die tolle, kollegiale Arbeitsatmosphäre.
- meinen Eltern, die mich stets unterstützt haben.
- meiner Schwester, Schwager und Nichten, die mir während der Promotionszeit sehr viel Freude bereitet haben.